Mechanisms contributing to RNA localization and translation: study of neuronal zipcodes in primary cortical neurons, and translational changes in neurodegeneration

Inaugural-Dissertation

to obtain the academic degree

Doctor rerum naturalium (Dr. rer. nat.)

submitted to the Department of Biology, Chemistry, Pharmacy

of Freie Universität Berlin

by

Samantha Annamarie Mendonsa

February 2023, Berlin

The research mentioned in this thesis was carried out and published between September 2017 and January 2023 under the supervision of Dr. Marina Chekulaeva at the Berlin Institute for Medical Systems Biology (BIMSB), Max-Delbrück-Centrum für Molekulare Medizin, Hannoversche Str. 28, 10115 Berlin-Mitte.

1st reviewer: Dr. Marina Chekulaeva
Berlin Institute for Medical Systems Biology (BIMSB)
Max-Delbrück-Centrum für Molekulare Medizin
Hannoversche Str. 28, 10115 Berlin

2nd reviewer: Prof. Dr. Florian Heyd
Freie Universität Berlin
Takustr. 6, 14195 Berlin

Date of defense: 08 June 2023

Declaration of Independence

I, Samantha Annamarie Mendonsa, herewith declare that this thesis titled, “Mechanisms contributing to RNA localization and translation: study of neuronal zipcodes in primary cortical neurons, and translational changes in neurodegeneration” and the work presented in it, are my own. This dissertation has been independently written by me, and has not been submitted in the same or similar form in any previous doctoral procedure.

Acknowledgements

My PhD journey was filled with the contributions and guidance of many.

To begin, my supervisor, Marina Chekulaeva. Thank you for giving me the opportunity to work in your lab, and for all your guidance and support during these last few years. Without your constant push and dedication, especially when the science did not work, I would not be the scientist that I am today.

I would like to acknowledge the members of my thesis advisory committee, Florian Heyd, Erich Wanker, and Andrew Woehler, for their additional guidance, and scientific discussions of my research. Thank you, Andrew, for patiently answering my countless emails regarding microscopy; learning from you was fun.

I want to thank all members of the Chekulaeva lab, past and present, who constantly spared their time to discuss science, failure, and solutions with me. A special thank you to Alessandra Zappulo, Camilla Ciolli Mattioli, Nicolai von Kügelgen, Sayaka Dantsuji, Artem Baranovskii, Erik Becher, Inga Lödige, Katarzyna 'Kasia' Ludwik, Guli-Nuer Imincan, Lucija Bujanic, and David van den Bruck. I have learnt a lot from all of you. An extra thank you to Nicolai von Kügelgen for all the analysis to my data.

A huge thank you to amazing collaborators, Igor Ulitsky, Maya Ron, and Laura Breimann. My papers would not be complete without your help and scientific input. Thank you to the MDC and BIMSB community, you contributed to a wonderful scientific environment during my PhD.

Thank you to Ana Veloso, Ana Luisa, Hazel Quinn, Liene Astica, and Anna Monaco, for all the laughs, travels, and wine. This PhD would have been less fun without your support and hugs, inside and outside the lab. To all my friends who additionally contributed to my life outside the lab, Max, Matt, Anna, Mudit, Jess, Teddy, Lucy, Chris, Rita, Eoin, Rovina, Aakriti, Saad, Suhail, Simo, and Rahul; thank you all for the long nights after equally long working days. A special thank you to Max for the late-night drives to the lab, allowing me to complete experiments I should have finished earlier, and for the emotional support when these experiments still did not succeed.

Finally, my family. Words would never be able to express the gratidue I have for all of you. Thank you to my parents, whose daily calls were a constant reminder of their support and belief in me. To all my siblings and their families; thank you for the constant flow of love and support. Riyan, Alisha, Franz, and Shaun, you set the bar so high, but thank you for also pulling me up with you. Alisha, I followed in your footsteps; thanks for making your PhD look so easy that I was completely caught off guard when I started mine. Mum, Dad, Shaun, and Franz, thank you for visiting me and making Berlin feel more like home.

Foreword

This dissertation is cumulative, and includes two manuscripts that have been published in peer-reviewed journals (Chapters 3 and 4). Three additional chapters provide a general introduction (Chapter 1), aims of the thesis (Chapter 2), and a general discussion (Chapter 5). All references cited in chapters 1, 2, and 5 have been merged in a common bibliography at the end of the dissertation.

I. **Samantha Mendonsa*,** Nicolai von Kügelgen*, Sayaka Dantsuji*, Maya Ron*, Laura Breimann, Artem Baranovskii, Inga Lödige, Marieluise Kirchner, Meret Fischer, Nadja Zerna, Lucija Bujanic, Philipp Mertins, Igor Ulitsky & Marina Chekulaeva, Massively parallel identification of mRNA localization elements in primary cortical neurons, Nature Neuroscience, 16 January 2023, https://doi.org/10.1038/s41593-022-01243-x
   * These authors contributed equally

The published version is reproduced in Chapter 3 of this thesis.

II. **Samantha Mendonsa**, Nicolai von Kuegelgen, Lucija Bujanic, Marina Chekulaeva, Charcot–Marie–Tooth mutation in glycyl-tRNA synthetase stalls ribosomes in a pre-accommodation state and activates integrated stress response, Nucleic Acids Research, Volume 49, Issue 17, 27 September 2021, Pages 10007–10017, https://doi.org/10.1093/nar/gkab730

The published version is reproduced in Chapter 4 of this thesis.

Summary

The regulation of gene expression in terms of space and time is governed by the distribution of RNA and proteins within a cell. This tightly controlled regulation is necessary for mediating cellular development and function. The localization of RNA is also a highly controlled process that is influenced by specific *cis*- and *trans*-acting elements. In polarized cells, such as neurons, the localization of transcripts towards axons and dendrites (neurites) enables the immediate and efficient local synthesis of proteins in response to external stimuli. This thesis focuses on the examination of the *cis*-elements, or "zipcodes," that contribute to the localization of RNA towards the neurites and the translational defects that result in the peripheral neuropathy Charcot-Marie-Tooth (CMT) disease.

The first part of this thesis details the development and validation of a novel neuronal zipcode identification protocol (N-zip) by my colleagues and myself. Using N-zip, we identified the *let-7* binding site and $(AU)_n$ motif as *de novo* zipcodes in the 3' UTRs of transcripts in mouse primary cortical neurons. To our knowledge, this methodology represents the first demonstration of the regulation of RNA localization via a microRNA.

In the second part, I investigate the mechanisms that lead to the repression of translation observed in CMT disease when glycyl-tRNA synthetase is mutated (CMT-GARS). High-resolution ribosome profiling analysis showed how mutations in GARS cause ribosomes to pause at glycine codons in a pre-accommodation state. We discovered that this pausing was due to the sequestration of glycyl-$tRNA^{Gly}$ by mutant CMT-GARS, reducing its availability for translation and disrupting elongation. We also identified a secondary mechanism of translation repression resulting from the activation of the integrated stress response (ISR), which affects translation initiation.

This thesis summarizes the above findings, which have been published in Nature Neuroscience and Nucleic Acids Research, respectively. These results significantly advance our understanding of how RNA localization and translation are regulated.

Zusammenfassung

Die räumliche und zeitliche Regulierung der Genexpression wird durch die Verteilung von RNA und Proteinen in einer Zelle bestimmt. Diese streng kontrollierte Regulierung ist notwendig, um die Entwicklung und Funktion von Zellen zu vermitteln. Die Lokalisierung von RNA ist ebenfalls ein hoch kontrollierter Prozess, der durch spezifische *cis*- und *trans*-wirkende Elemente beeinflusst wird. In polarisierten Zellen, wie z. B. Neuronen, ermöglicht die Lokalisierung von Transkripten in Axonen und Dendriten (Neuriten) eine schnelle und effiziente lokale Synthese von Proteinen als Reaktion auf äußere Reize. Diese Arbeit beschäftigt sich mit der Untersuchung der cis-Elemente oder "Zipcodes", die zur Lokalisierung von RNA in Neuriten beitragen, sowie der Translationsdefekte, die zur peripheren Neuropathie Charcot-Marie-Tooth (CMT) führen.

Der erste Teil dieser Arbeit beschreibt die Entwicklung und Validierung eines neuen Protokolls zur Identifizierung neuronaler Zipcodes (N-zip) durch meine Kollegen und mich. Mit Hilfe von N-zip haben wir die Bindestelle der microRNA let-7 und das $(AU)_n$-Motiv als de novo-Zipcodes in den 3'-UTRs von Transkripten in primären kortikalen Neuronen der Maus identifiziert. Dies ist der erste Nachweis der Regulierung der RNA-Lokalisierung durch eine microRNA.

Im zweiten Teil meiner Arbeit untersuche ich die Mechanismen, die zu der bei der CMT-Krankheit beobachteten Unterdrückung der Translation führen, wenn die Glycyl-tRNA-Synthetase mutiert ist (CMT-GARS). Hochauflösende Ribosomen-Profiling-Analysen haben gezeigt, dass Mutationen in GARS dazu führen, dass Ribosomen an Glycin-Codons in einem Prä-Akommodationszustand pausieren. Wir haben entdeckt, dass dieses Innehalten auf die Sequestrierung von Glycyl-$tRNA^{Gly}$ durch mutiertes CMT-GARS zurückzuführen ist. Hierdurch wird die Verfügbarkeit von Glycyl-$tRNA^{Gly}$ für die Translation verringert und die Elongation gestört. Außerdem haben wir einen sekundären Mechanismus der Translationsunterdrückung identifiziert, der aus der Aktivierung der integrierten Stressreaktion (ISR) resultiert und die Translationsinitiation beeinflusst.

Die vorliegende Arbeit fasst die oben genannten Ergebnisse zusammen, die in Nature Neuroscience und Nucleic Acids Research veröffentlicht worden sind. Meine Ergebnisse leisten einen wesentlichen Beitrag zu einem besseren Verständnis der Regulierung von RNA-Lokalisierung und Translation.

Contents

List of Figures

List of Tables

List of Abbreviations

Anxa2	Annexin A2
APC	Adenomatous Polyposis Coli
Atf4	Activating Transcription Factor 4
ATP	Adenosine 5’-TriPhosphate
CAF1	Chromatin Assembly Factor 1
Cdc42	Cell Division Cycle 42
CNOT7	carbon catabolite repression 4 (CCR4)–negative on TATA-less (NOT) complex subunit 7
CPEB	Cytoplasmic Polyadenylation Element Binding protein
CRISPR	Clustered Regularly Interspaced Short Palindromic Repeats
CSB	Cockayne Syndrome B
dsDNA	double stranded DNA
DSIF	DRB Sensitivity Inducing Factor
ELAVL4	(Embryonic Lethal, Abnormal Vision, *Drosophila)*-Like 4
ELL	RNA polymerase II ELongation factor
ED	Extended Data
FCP1	F-Cell Production 1
GCN2	General Control Nonderepressible 2
GTP	Guanosine-5'-TriPhosphate
GTPBP2	GTP Binding Protein 2
HBS1L	HBS1 Like Translational GTPase
hnRNP	heterogeneous nuclear RiboNucleoProteins
IGF2BP1	Insulin like Growth Factor 2 mRNA Binding Protein 1
Ilf3	InterLeukin enhancer-binding Factor 3
lncRNA	long non-coding RNA
m7G cap	7-methylguanosine cap
MARTA2	MAP2-RNA *Trans*-Acting protein
mGluR	metabotropic Glutamate Receptor
miRNA	micro RNA
mRNA	messenger RNA
mRNP	messenger RiboNucleoProtein
NELF	Negative ELongation Factor
NF90	Nuclear Factor 90
NGS	Next Generation Sequencing
NMDA	N-methyl-D-aspartate
Nrn1	Neuritin 1

RNA pol	RNA polymerase
rRNA	ribosomal RNA
Sen1	Splicing ENdonuclease 1
snRNA	small nuclear RNA
TNRC6	TriNucleotide Repeat-Containing gene 6 protein
TRBP	Transactivation Response element RNA-Binding Protein
tRNA	transfer RNA

To my family, and closest friends…

1. General Introduction

1.1 The birth of RNA: Transcription

To fully comprehend how living cells function, one needs to understand the most fundamental biological process: the expression and transfer of hereditary information. Simplistically, this flow of cellular information is based on the central dogma, wherein, with the use of complex cellular machinery, DNA proceeds to protein through an RNA intermediate. Out of the several highly controlled steps during gene expression, I will focus on RNA and the complex and highly regulated process of its creation: transcription.

Chapter 1.1 describes the different phases observed during RNA transcription, followed by the different post-transcriptional modifications. This provides the basic information necessary for the following chapters, which contributed to the development of my research questions.

1.1.1 Transcription: An overview

Eukaryotic transcription is a complex process separated into initiation, elongation and termination phases (Figure 1.1). The three polymerase enzymes, RNA pol I, RNA pol II, and RNA pol III, are each responsible for the transcription of different RNA classes. While all their structures are homologous, RNA pol I is responsible for the transcription of most rRNAs (28S, 18S and 5.8S rRNAs); RNA pol II for the transcription of mRNAs and some snRNAs and regulatory RNAs including miRNAs and lncRNAs; and RNA pol III for the transcription of 5S rRNA and tRNAs (Cramer et al., 2001).

mRNA synthesis

Initiation. Initiation requires the association of RNA pol II along with several general transcription factors (GTFs); TFIIB, TFIID, TFIIE, TFIIF, and TFIIH. These GTFs interact with the gene promoters that are a combination of basal or core promoter elements, promoter proximal elements, and distal enhancer elements, to form the preinitiation complex (PIC). Two major types of core promoters exist: focused and dispersed. The most-extensively studied focused core promoter element found in ~10-15% of mammalian genes is the TATA box, an AT-rich sequence located 25bp upstream of the transcription start site that is bound by TBP (TATA box-binding protein). In addition, other focused core promoters that contain different sequence motifs include the (i) BRE, a TFIIB recognition element; (ii) DPE (Downstream core Promoter Element), a downstream TFIID recognition element necessary for basal transcription activity; (iii) MTE (Motif Ten Element); (iv) DCE (downstream core element) that occurs frequently with the TATA

box; and (v) Inr (The Initiator), a motif that encompasses the transcription start site and occurs the most in focused promoters. CpG islands usually contain dispersed core promoters that have several start sites (Juven-Gershon et al., 2008; Nikolov & Burley, 1997).

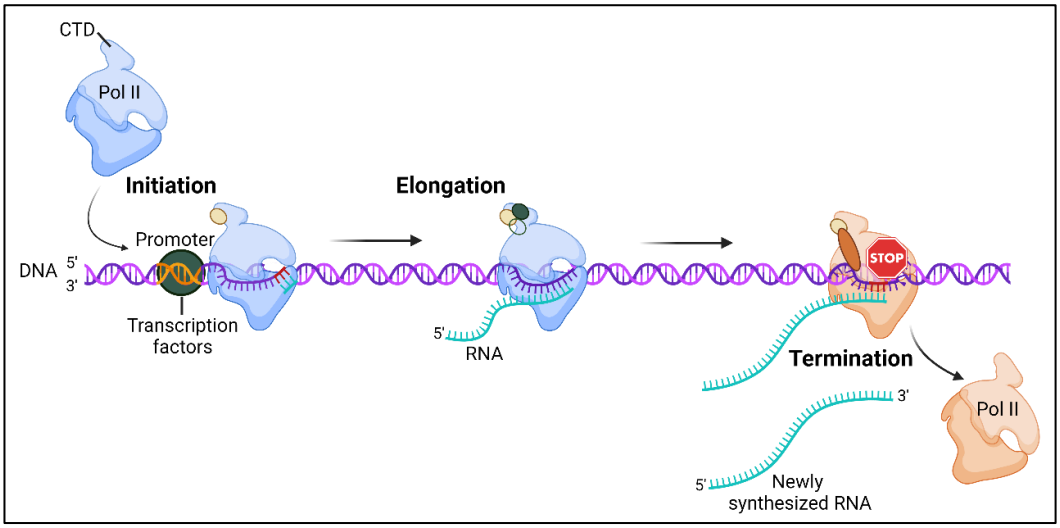

Figure 1.1: Schematic representation of different phases of RNA Polymerase II (Pol II) transcription in Eukaryotes. Initiation: Pol II is recruited by transcription factors to the gene promoter, the DNA is opened to expose the template strand, and the first few RNA nucleotides are synthesised. Elongation: An RNA-DNA hybrid is formed and Pol II extends the transcript. Termination: Pol II stops RNA synthesis in preparation for termination (indicated by change in colour from blue to orange), and Pol II along with the nascent RNA are released from the DNA template. Protein factors involved in elongation (yellow ovals), RNA processing (green ovals), and termination (orange ovals) co-transcriptionally associate with Pol II C-terminal domain (CTD). Adapted from (Kuehner et al., 2011). Created with BioRender.com.

In general, mRNA production starts with the assembly of the PIC via the recognition and binding of the TATA element by TFIID, an interaction mediated by TFIID subunit TBP. This is followed by the addition of TFIIB, RNA pol IIA, the other GTFs TFIIF, TFIIE, and TFIIH, along with transcriptional activators and coactivators. ATP hydrolysis at TFIIH enables the separation of the dsDNA, allowing RNA pol II access to the transcription start site on the DNA strand. Transcription is regulated via the activators (or repressors) and coactivators (or corepressors), whereas basal or general transcription is driven solely by the PIC (Nikolov & Burley, 1997).

Elongation. Elongation is conducted in 3 phases: promoter clearance, promoter-proximal pausing, and productive elongation. During promoter clearance, the C-terminal domain (CTD) of RNA polymerase II subunit 1 (Rbp1), the largest subunit of RNA pol II, is phosphorylated. Phosphorylation of CTD generates a stable interaction between RNA pol II and the DNA template strand, transitioning the transcription complex into an early elongation complex (EEC). This process is usually accompanied by transcriptional stalling near the promoter (promoter-proximal stalling). As an important step in the regulation of elongation, RNA pol II pauses at the 5' region of the complex, progressing into productive elongation only on the influence of numerous factors that alleviate (TFIIF, Elongins, ELL, CSB, FCP1, and DSIF) or exploit

this pause (NELF). After these two main rate-limiting stages of elongation, P-TEFb (positive transcription elongation factor b) kinase activity stimulates the final phase, productive elongation. TFIIS activity also helps RNA pol II efficiently escape from this pausing (Reines et al., 1996; Saunders et al., 2006; Sims et al., 2004).

Termination. Termination of transcription by RNA pol II is generally initiated by the nascent transcript 3'-end processing signals and termination factors, leading to the release of both RNA pol II and the nascent transcript from the DNA template. Most eukaryotes lack a determined termination sequence, instead poly(A)-dependent and Sen1-dependent termination pathways are most common (Kuehner et al., 2011).

Nascent transcripts produced by RNA polymerases further undergo splicing and post-transcriptional modifications that dictate their destiny within a cell.

1.1.2 Post-transcriptional modifications

The processing or modification of nascent mRNA is necessary to determine their features, such as stability, location, or interactions. The CTD of RNA pol II stimulates the processing events of 5' capping, splicing of introns, and 3' cleavage/polyadenylation to generate a mature mRNA (Fong & Bentley, 2001; Ramanathan et al., 2016).

Capping

The first modification of mRNA takes place co-transcriptionally in the nucleus via a mechanism known as capping. The mRNA 5' end is modified by the addition of a m7G cap via sequential enzymatic steps: (i) removal of γ-phosphate from the 5' triphosphate terminated RNA via RNA triphosphatase (TPase), (ii) transfer of GMP to the 5' diphosphate end via RNA guanylyltransferase (GTase), forming a G cap, and, (iii) methylation of the G cap at the N7 amine via guanine-N7 methyltransferase (guanine-N7 MTase) (Fong & Bentley, 2001).

The m7G cap plays important roles during the mRNA life cycle in the nucleus and cytoplasm due to its interacting protein factors, nuclear cap-binding complex (CBC) and cytoplasmic eukaryotic transcription initiation factor 4E (eIF4E) (Fong & Bentley, 2001; Ramanathan et al., 2016). The m7G cap in mammalian systems (Inoue et al., 1989; Ohno et al., 1987) was shown to mediate efficient pre-mRNA splicing by recruiting and binding the CBC, leading to events such as spliceosome assembly, 3' processing, RNA export, and miRNA biogenesis (Pabis et al., 2013; Topisirovic et al., 2011). Cap-dependent translation initiation also occurs for the majority of cellular mRNA via CBC recruitment of eIF4E and eIF4A to the 5' end of mRNA (Choe et al., 2012).

Interestingly, eukaryotic cells have been reported to maintain a cytoplasmic pool of uncapped mRNA in processing-bodies (P-bodies) as messenger ribonucleoproteins (mRNPs) (Erwin van Dijk et al., 2002). P-bodies are cytoplasmic foci containing proteins involved in post-transcriptional processes, formed due to phase separation. This allows uncapped mRNA in P-bodies to re-enter the polysome for translation (Brengues et al., 2005). Cytoplasmic (re)-capping might be a mechanism to regulate protein synthesis via mRNA inactivation and reactivation (Mukherjee et al., 2012).

Splicing & Alternative Splicing

Eukaryotic genomes contain introns and exons in the precursor mRNA (pre-mRNA) that need to undergo splicing to generate a mature mRNA. Constitutive splicing, wherein introns are removed and exons are ligated, is an important step during gene expression in eukaryotes. Non-continuous exon-intron genetic structure allows for alternative splicing, wherein alternative mRNA isoforms are generated, accounting for the discrepancy between the number of protein coding genes (~25,000) and number of actual proteins produced (>90,000) in humans (Y. Wang et al., 2015). Alternative splicing (AS) is an important mechanism to increase transcriptomic and proteomic diversity within a cell, as well as regulate mRNA expression post-transcriptionally (Gehring & Roignant, 2021; Y. Wang et al., 2015).

Splicing is carried out by the spliceosome, a large ribonucleoprotein complex containing small nuclear ribonucleoproteins (snRNPs) that assemble on the pre-mRNA. snRNPs consist of 1 or 2 snRNAs (U1, U2, U4/U6, or U5), and variable complex-specific proteins. Splicing is a 2-step transesterification reaction (Figure 1.2A). The first step forms the pre-spliceosome or A complex, starting with the U1 snRNP binding to the 5’ splice site of an exon, followed by U2 snRNP binding just upstream of the 3’ splice site of the downstream exon. This complex becomes the precatalytic spliceosome or B-complex when tri-RNP U4/U6.U5 heterodimer join U1 and U2. After unwinding and release of U4 and U1 snRNPs from the complex, U6 of the active spliceosome (B*) base pairs with the 5’ splice site and the branch point sequence (BPS), completing the first transesterification splicing reaction. This results in cleavage of the 5’ splice site followed by a free 3’ OH-group upstream, and an intron lariat downstream. The resulting C-complex catalyses the second step, wherein U5 pairs with both 5’ and 3’ sequences of the splice site, bringing the ends together, while the upstream 3’OH-group fuses with the 3’ intron-exon junction, excising the intron lariat and ligating the exons. The spliceosome disassembles and can be recycled for more splicing reactions (Gehring & Roignant, 2021; Kornblihtt et al., 2013; van den Hoogenhof et al., 2016).

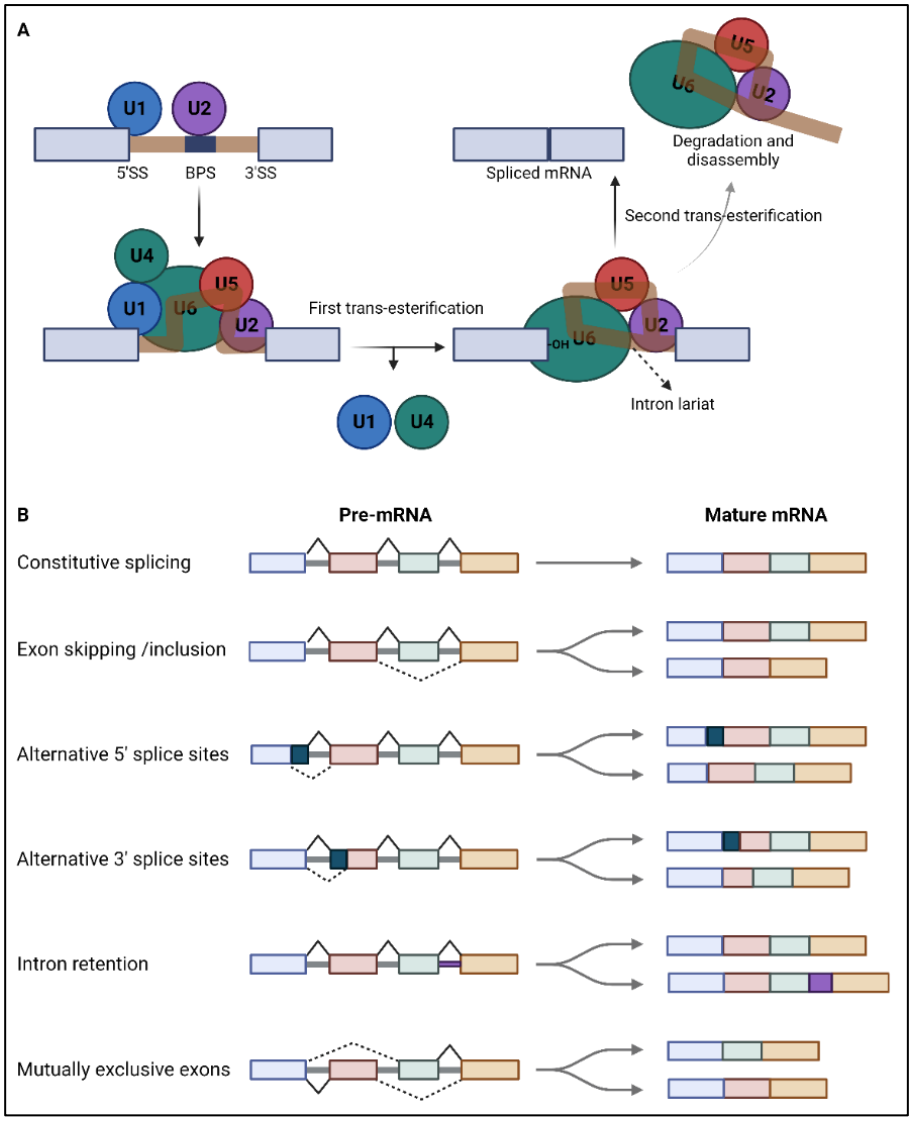

Figure 1.2: Splicing and Alternative Splicing. (A) The two-step splicing reaction. Initially, U1 snRNP assembles at the exon 5' splice site (5' SS), and U2 snRNP at the BPS (branch point sequence) upstream of the downstream exons 3' splice site (3' SS) to form the pre-spliceosome. Next, U5 and U4-U6 complexes join to form the precatalytic spliceosome. The U4-U6 complexes then unwind to release U4 and U1 from the pre-spliceosomal complex, allowing the base pairing of U6, 5' SS, and BPS. Following cleavage of the 5' SS, a 3' OH-group is freed at the upstream exon, and the intronic region at the downstream exon is branched to form the intron lariat. Next, the upstream exons 3' OH-group fuses with the 3' intron-exon junction, merging the two exons, while excising the intron as a lariat that gets degraded. The spliceosome disassembles and individual components recycled for another splicing reaction. **(B) Different types of alternative splicing.** The different types of alternative splicing are illustrated, with the coloured boxes representing exons, and lines representing introns. Constitutive splicing is the process of excising introns and joining exons. The inclusion or exclusion of one or more (cassette) exons is termed exon skipping. Alternative 5' or 3' SS selection produces shorter or longer exons. The inclusion of part of an intron within a mature mRNA is classified as intron retention. Cassette exons can also be mutually exclusive. Adapted from (van den Hoogenhof et al., 2016). Created with BioRender.com.

AS deviates from this process, while selectively skipping certain exons, resulting in multiple mature mRNA isoforms from the same gene. Apart from exon skipping, multiple patterns of AS can occur via mutually

exclusive exon usage, alternative splice site selection, or intron retention (Figure 1.2B) (Li et al., 2007; van den Hoogenhof et al., 2016). To a lesser extent, lncRNAs are also subjected to AS. *Cis* regulatory sequences (exonic splicing enhancers (ESEs), exonic splicing silencers (ESSs), intronic splicing enhancers (ISEs) and intronic splicing silencers (ISSs)), and *trans* acting regulatory proteins (Ser/Arg-rich proteins (SRs) and hnRNPs) target the spliceosome and enhance or repress its assembly, regulating AS (Gehring & Roignant, 2021; Kornblihtt et al., 2013; van den Hoogenhof et al., 2016; Y. Wang et al., 2015).

Interestingly, AS plays an important role in expanding the mammalian nervous system transcriptome, and regulating gene function during neuronal differentiation and development. Failures in splicing can alter the mRNA, thereby affecting the function of the protein product. Another aspect of AS that is fascinating, is the subcellular localization and local translation of the different RNA splice isoforms, and their role in the cellular system – Do different isoforms have different functions at different subcellular locations in the same or different cell types?

In morphologically complex cells like neurons that require compartmentalized expression, the post-transcriptional processing of mRNA is very important to drive the necessary transcriptome diversity (Andreassi et al., 2018). Zheng et al. showed that AS of postsynaptic density protein 95 (PSD-95), an excitatory postsynaptic protein, is responsible for its neural-specific versus non-neuronal expression. Exon 18 of PSD-95 mRNA is included only in neurons, enabling its expression before synaptogenesis, contributing to time-dependent synapse formation; whereas exon 18 excluded PSD-95 transcripts in non-neuronal cells are targeted for non-sense mediated decay (NMD) (Soto et al., 2019; S. Zheng, 2016; S. Zheng et al., 2012). Many molecules involved in axon guidance, neurite outgrowth, and synaptogenesis, like cell-adhesion molecules (DIng et al., 2017; Graf et al., 2004), cytoskeletal components, kinases, etc., are also regulated by AS (Holmberg et al., 2000; Walsh & Doherty, 1997). RNA binding proteins (RBPs) also interact with *cis*-sequences in retained introns that influence RNA localization and translation. As an example, RBP Staufen2 affects the localization of *Calmodulin 3* (*Calm3*) (Sharangdhar et al., 2017) and *α subunit of calcium/calmodulin-dependent protein kinase II* (*CamKIIα*) (Ortiz et al., 2017) in neurons via interaction with a retained intron in the splice isoforms of the respective transcripts. Sharangdhar et al. showed that the 3' untranslated region (3' UTR) of *Calm3* contains a retained intron that is targeted by Staufen2, and regulates its localization to the dendrites in rat hippocampal neurons (Sharangdhar et al., 2017).

AS of untranslated regions (UTRs: 5' and 3') also plays an important role in transcript localization and translation regulation, especially in neurons as they express transcripts with the longest and most varied 3' ends (Andreassi et al., 2018; Tushev et al., 2018). Alternative 3' UTR analysis of transcripts in different neuronal compartments led to the discovery of a huge neuronal mRNA 3' UTR diversity, accounting for differences in transcript isoform localization, function, and stability (Shigeoka et al., 2016; Tushev et al.,

2018). The importance of 3' UTRs and their role in mRNA localization in neurons is further elaborated in chapter 1.2.2.

Polyadenylation & alternative polyadenylation

In eukaryotes, the termination of transcription of nearly every mRNA occurs alongside endonucleolytic cleavage at the 3' end and addition of a poly(A) tail (polyadenylation tail) to the pre-mRNA. This processing of the 3' end during maturation of the pre-mRNA is crucial for mRNA nuclear export, function and stability (Colgan & Manley, 1997; Lutz & Moreira, 2011). The addition of a poly(A) tail and control of its length is controlled by a poly(A) polymerase (PAP) and specific factors (Balbo & Bohm, 2007).

Endonucleolytic cleavage and polyadenylation of the nascent transcript occur at specific sites, such as the hexanucleotide polyadenylation signal (PAS), located within 3' UTR, introns, or exons. Nearly every PAS in eukaryotes contain a core upstream element; the hexanucleotide AAUAAA, which is usually located approximately 10-35 nucleotides upstream of the PAS (Proudfoot NJ & Brownlee GG, 1976). A further 20-40 nucleotides downstream of the cleavage site is a second core element, a GU-rich motif.

The main 3' end processing machinery contains 4 complexes: cleavage and polyadenylation specificity factor (CPSF), cleavage factor I (CFIm), cleavage factor II (CFIIm), and cleavage stimulation factor (CstF). The CPSF recognises the core upstream element, followed by assembly of the complex on the pre-mRNA and the recruitment of PAP via nuclear Poly(A) binding protein (PABP) leading to cleavage and polyadenylation (Tian & Manley, 2016). The exact site for endonucleolytic attack depends on the distance between the two core elements, and the site can be shifted by changing this distance (Colgan & Manley, 1997; Lutz & Moreira, 2011).

Aside from AS, alternative polyadenylation (APA) is another way the cell increases transcriptomic and proteomic diversity, via the generation of multiple transcripts with differing 3' ends from a single gene (Tian et al., 2005). As mentioned above, PASs can be present at different locations, generating distinct isoforms that can be categorised into two subtypes. Tandem 3' UTR-APAs occur when the 3' UTR contains two or more PASs (Figure 1.3A). 3'UTR APA generates multiple transcripts differing in the length of the 3'UTR. On the other hand, when APA affects the protein coding region by occurring upstream of the last exon, it is an upstream region APA (UR-APA). UR-APA is separated into: (i) alternative last exon APA, (ii) intronic APA, and (iii) internal exon APA (Figure 1.3B) (Y. Zhang et al., 2021).

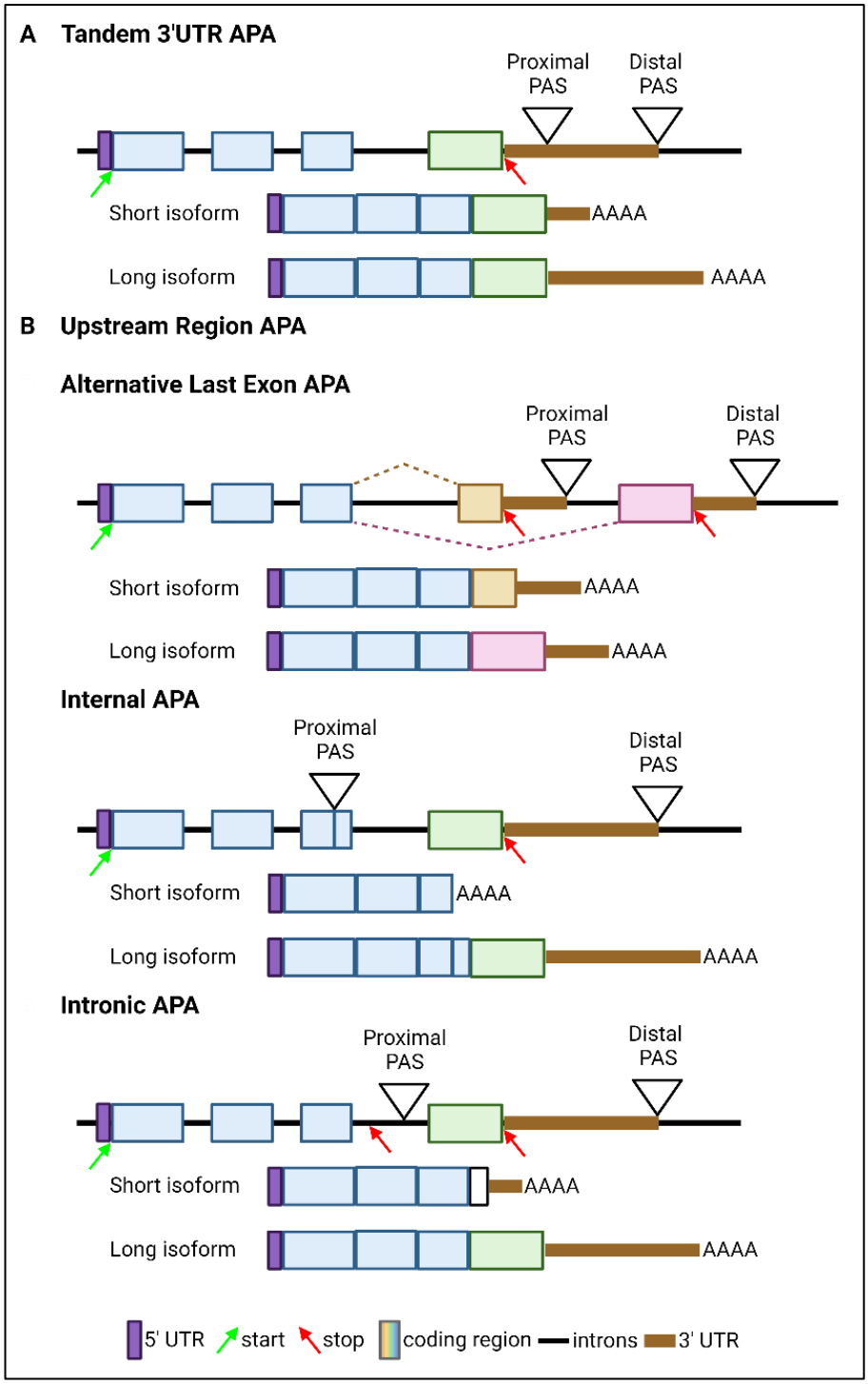

Figure 1.3: Schematic representation of different forms of alternative polyadenylation (APA). (A) Tandem 3'UTR APA. The most common APA containing two or more poly(A) sites (PASs) within the same terminal exon, resulting in multiple isoforms differing in 3'UTR lengths but encoding the same protein. **(B) Upstream Region APA.** APA events occurring upstream of the last exon, that can result in alternative last exons that potentially affect the coding sequences as well as 3'UTR length. Alternative last exon (ALE) APA results in isoforms differing in their last exon due to internal exon skipping; internal APA results in premature polyadenylation within the coding region, generating an isoform lacking the 3'UTR; and intronic APA wherein the cryptic intronic PAS is cleaved, extending an internal exon into the terminal exon. Adapted from (Bae & Miura, 2020; and Y. Zhang et al., 2021). Created with BioRender.com.

APA patterns have been found to be tissue specific, playing an important role in different cellular processes (Andreassi et al., 2018). Similar to AS, APA has been shown to play an essential role in neuronal function, more specifically, dendritic and axonal localization of transcripts. In 2012, Perry et al. showed that *importin $\beta 1$*, a core component of the injury-signalling complex in axons, exists as two 3'UTR variants (Perry et al., 2012). Depending on which PAS is used, a short isoform (proximal PAS) or a long isoform (distal PAS) is produced. They found that depletion of the distal isoform decreased axonal RNA localization, leading to a delay in injury recovery (Perry et al., 2012). Since many APA sites are found in the 3'UTRs and they often regulate RNA localization, apart from regulating RNA stability, translation, and neural plasticity (Andreassi et al., 2018; Y. Zhang et al., 2021), the function of APA has been recently explored in the context of RNA localization (Mattioli et al., 2019; Tushev et al., 2018).

1.2 Post-transcriptional Regulation

Chapter 1.2 describes the different mechanisms of post-transcriptional regulation, and how the disruption of these mechanisms causes diseases. The sub-chapter on RNA localization, along with gene regulation modulated by miRNAs, provide a detailed basis for my research described in chapter 3. The sub-chapter on RNA translation provides details of the molecular mechanisms of translation, creating a basis for my research described in chapter 4.

1.2.1 The localization of RNA: Transport

It was originally thought that proteins are sorted and localized post-translationally. However, our understanding of localization within a cell changed in 1978, when Jeffrey et al. first reported that mRNA was asymmetrically distributed in the ascidian embryo, during the early stages of its development (Jeffery & Capco, 1978). In 1986, Lawrence and Singer first reported the occurrence of subcellular mRNA localization using *in situ* hybridization targeting cytoskeletal protein β-actin mRNAs in chicken fibroblasts (Lawrence & Singer, 1986). Over the last 30+ years, scientists have increased our understanding of mRNA localization, and continue learning about why and how it happens.

1.2.1.1 Why RNA is localized: From embryo to neuron

Spatial organization within a cell and tissue is necessary to maintain biological processes that depend on cellular polarity, such as asymmetric cell division, migration, neuronal maturation, and embryonic patterning. Localization of mRNA within the cytoplasm provides a basis for this cellular polarity.

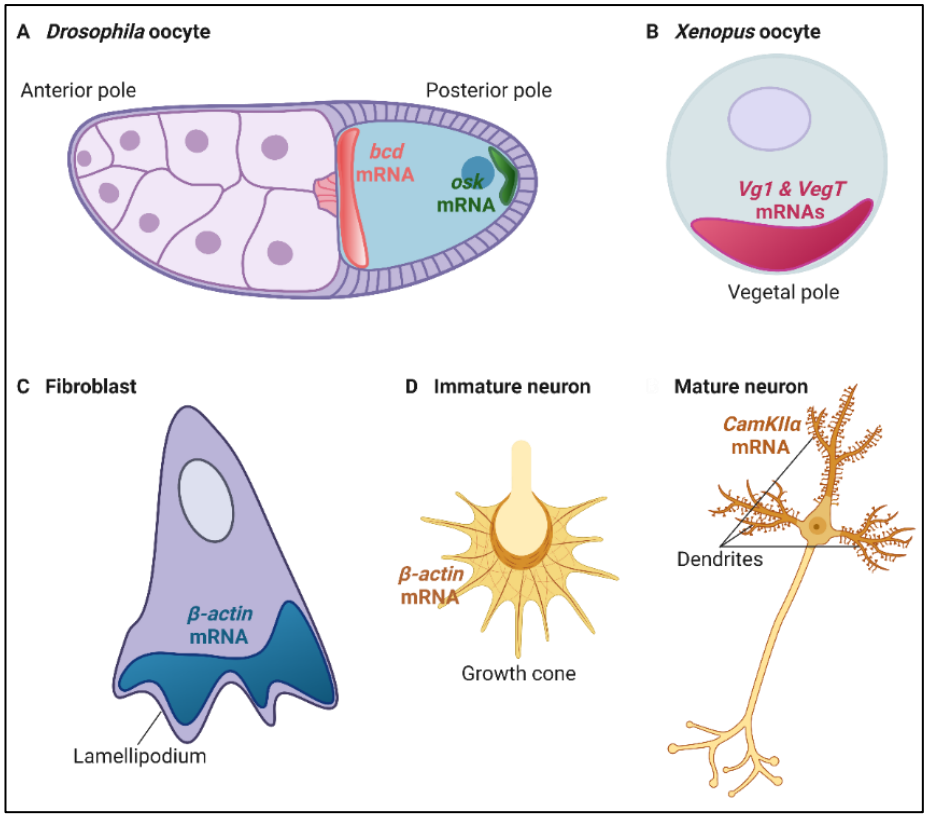

Figure 1.4: Examples of localized mRNAs. (A) In *Drosophila* oocytes, the maternal *bicoid* (*bcd* – red) and *oskar* (*osk* – green) mRNAs are localized to the anterior and posterior of the oocyte, respectively, necessary for the embryo anteroposterior patterning. **(B)** In *Xenopus* oocytes, *Vg1* and *VegT* mRNAs are localized to the vegetal pole, important for endoderm and mesoderm germ layer specification. **(C)** Migrating cells, like fibroblasts in chick and mammals, localize *β-actin* mRNA to lamellipodia, where its local translation helps in actin filament assembly, necessary for cell motility. **(D)** In developing neurons, *β-actin* mRNA is localized to the distal growth cones; while mature neurons localize transcripts such as *CamKIIα* to the dendrites, important for regulating synaptic plasticity. Adapted from (Martin & Ephrussi, 2009). Created with BioRender.com.

Asymmetric localization of organelles and cytoplasmic molecules has long been recognised for spatial organization through oogenesis and early embryogenesis, but the molecular nature of these organizational cues was not understood. In 1983, Jeffery et al. observed the asymmetric localization of *β-actin* mRNA in ascidian eggs and embryos (Jeffery et al., 1983), after which Rebagliati et al. found a special class of maternal mRNAs localized to the different hemispheres of *Xenopus* eggs (Rebagliati et al., 1985) (Figure 1.4B), and Berleth et al. showed that the *Drosophila* embryo anterior pattern is mediated via the localization of the bicoid transcript towards the anterior cortex of the oocyte (Berleth et al., 1988) (Figure 1.4A). With the development of technologies to visualise mRNAs *in vivo* via cloning and *in situ* hybridization, localization and local translation became the basis for proper embryonic patterning, characterized in the eggs of a wide range of organisms from zebrafish, to ascidians, arthropods and more (Cody et al., 2013; Medioni et al., 2012).

Once Lawrence and Singer demonstrated the intracellular trafficking of *β-actin* mRNA in chicken fibroblasts (Lawrence & Singer, 1986) (Figure 1.4C), the broader importance of mRNA localization was explored. Asymmetric distribution of mRNAs was soon identified within other differentiated cells like oligodendrocytes (Trapp et al., 1987), and neurons (Bassell et al., 1998; Burgin et al., 1990; Garner et al., 1988; Kuhl & Skehelt, 1998) (Figure 1.4D), wherein the mRNA was colocalized with their translated protein, suggesting mRNA transport as a mechanism to target proteins to specific locations. Significant developments in RNA detection techniques has led us to our current understanding that: mRNA localization and its localized translation provide a controlled mechanism to spatially and temporally regulate gene expression, essential for responding to intracellular and environmental cues.

Studies in polarized cells like neurons and fibroblasts have shown that protrusions from migrating cells and neuronal processes utilize mRNA localization and local translation to accumulate proteins necessary to sense and respond to external cues that regulate motility and directionality. (Lin & Holt, 2007). Campbell and Holt showed that axonal growth cone directional decisions require mRNA to be locally translated at the tip of the growing axon in *Xenopus* retinal neurons (Campbell & Holt, 2001). Utilizing microarray analysis, hundreds of mRNAs were identified in the axons of vertebrate sensory neurons in culture. (Zivraj et al., 2010). This led to the identification of localized transcripts that are translated into proteins necessary for polarized axon outgrowth (polarity proteins) (Hengst et al., 2009), axon guidance (actin cytoskeleton regulators) (K. Y. Wu et al., 2005), and transcription factor signalling for neuronal maintenance and regeneration (Cox et al., 2008). Utilizing rat hippocampal neurons, Baj et al. hypothesized a 'spatial code hypothesis', wherein the differential localization of *brain-derived neurotrophic factor* (*Bdnf)* splice variants in the dendrites led to the selective targeting of BDNF, allowing spatially restricted control on dendritic architecture and plasticity in neurons (Baj et al., 2011). Sutton and Schuman also showed that in mature neurons, localized transcripts encode proteins necessary for synaptic activity, such as ion channels, signal transduction enzymes, and neurotransmitter receptors (Sutton et al., 2006).

However, to address the biological question of "Why?" in a more basic sense; mRNA localization has several mechanistic benefits compared to protein localization, some of which are: (i) economy: mRNA can be used as a template for multiple rounds of translation compared to the trafficking of individual protein molecules, thereby being a more energy efficient method. (ii) rapid production of local pools of proteins in response to external cues, controlling gene expression in specific regions. (iii) subcellular autonomy within polarized cells, such that local translation of proteins allows for protection of other subcellular compartments wherein the protein might be toxic or deleterious. (iv) efficient mRNA targeting to different subcellular locations based on regulatory elements in their UTRs, that do not affect structure or function of the encoded protein (Cody et al., 2013; Martin & Ephrussi, 2009; Turner-Bridger et al., 2020). In order to localize mRNA within the cell and utilize these advantages, multiple cellular mechanisms underly this transport, elaborated in chapter 1.2.2.

1.2.1.2 What drives RNA localization in neurons: Spatial and temporal mechanisms

In structurally complex and highly compartmentalized cells like neurons, localization and local translation of mRNAs are extremely beneficial as they allow for rapid and dynamic well-regulated spatial control. As neurons can span huge distances in the body, the trafficking of mRNA to the distal dendrites and axons hundreds of microns away from the soma allows for an immediate response to environmental cues modulating dendritic and axonal growth, structure, and synaptic plasticity.

Multiple steps are involved in the subcellular trafficking of mRNAs. But first, how is the mRNA identified to be localized? Most frequently, the 3'UTRs of mRNAs contain a "cellular address" that is encoded by *cis*-acting elements called "zipcodes". In a few cases, these localization elements can be present in the 5'UTR or the coding sequence. Zipcode sequences are generally recognized and then bound by specific RBPs that often function in both transcript localization as well as translational regulation. The RBP-bound mRNAs, called mRNPs, can then form a part of a larger RNA transport granule, that can be transported along the cytoskeleton towards its destination in the cell. During this process, the transported mRNA is generally maintained in a translationally-repressed state, allowing for its translation at the final destination at the correct time.

The three proposed mechanisms enabling transcript localization post nuclear export include: (i) active, directed transport along a polarized cytoskeleton, (Bullock, 2011; Long et al., 1997) (ii) protection from degradation coupled to local stabilisation of transcripts, (Ding et al., 1993) and (iii) transcript diffusion-coupled local entrapment (Forrest & Gavis, 2003) (Figure 1.5). In the following sub-chapters, I have elaborated on these mechanisms, with a focus on understanding the *cis*- and *trans*- elements that are required to facilitate these mechanisms directly, or indirectly.

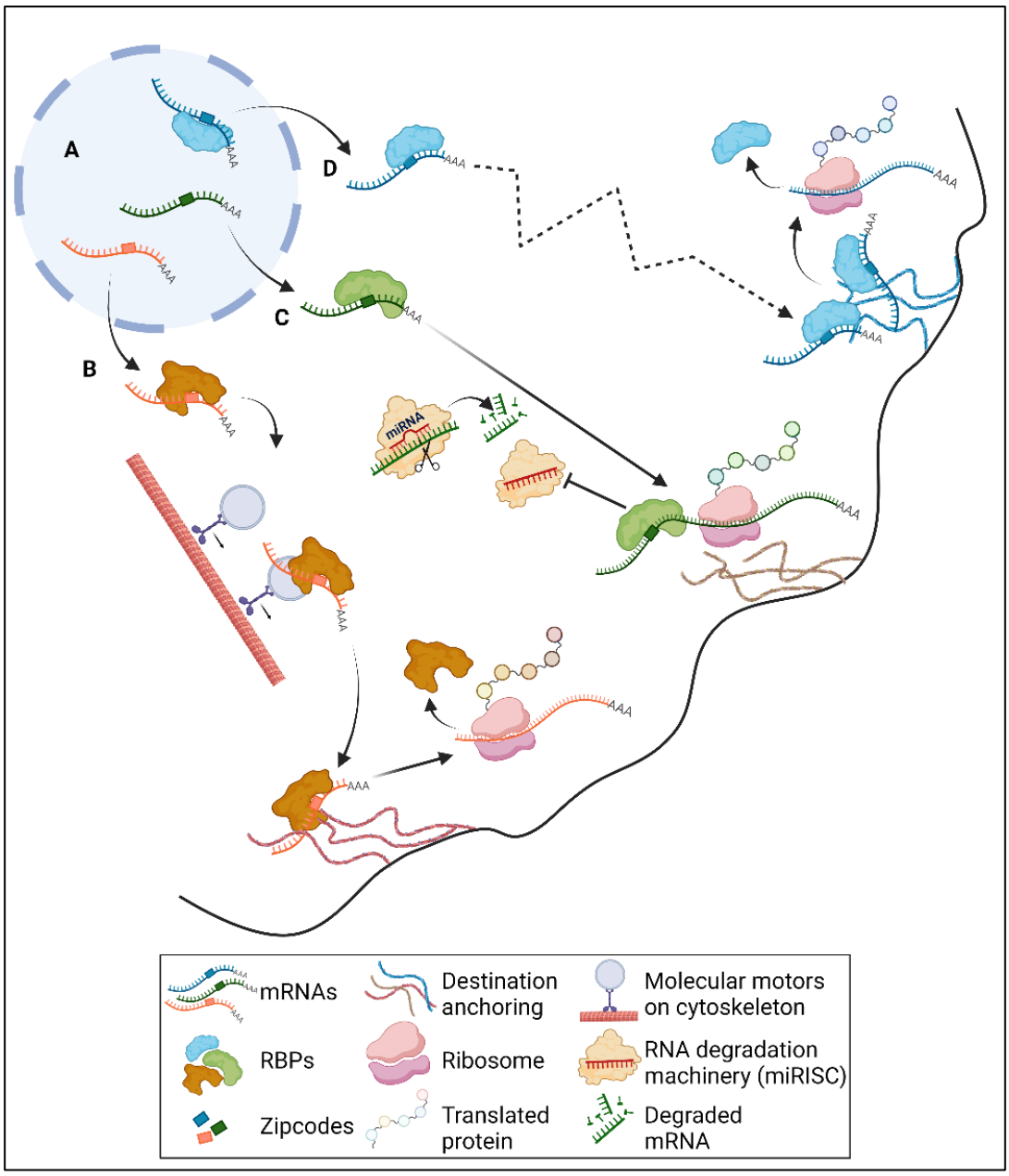

Figure 1.5: General model depicting the different mechanisms underlying mRNA localization. (A) Nuclear mRNAs contain zipcode elements recognised by specific RBPs either directly in the nucleus, or in the cytoplasm post mRNA nuclear export, to form RNPs that modulate mRNA trafficking to different subcellular regions. **(B)** RNPs can couple with molecular motors in the cytoplasm to promote directed transport along the cytoskeleton. **(C)** Some mRNAs become localized due to protection from degradation, as the non-localized mRNAs are targeted by the degradation machinery. **(D)** RNPs can also undergo diffusion, coupled with their local entrapment at a specific region of the cell. At their final destination, these mRNAs are anchored and can locally synthesise protein. Adapted from (Cody et al., 2013; and Medioni et al., 2012). Created with BioRender.com.

Cis-acting sequences: Zipcodes present on RNA

Table 1.1: Examples of mRNA zipcodes and their interacting RNA binding proteins in neurons

mRNA	RBP	Localization element	Length (nt)	Subcellular destination	Reference
β-actin	ZBP1	3' UTR, 5'-GGACU-3' (4-8) and 5'-ACA-3' (22-24)	54	axon	(Bassell et al., 1998; Kislauskis et al., 1994)
β-actin	APC	3' UTR G-rich sequence	87	axon	(Preitner et al., 2014)
annexin A2	SMN	near 3' UTR, G-rich motif, primary sequence	18	axon	(Rihan et al., 2017)
Gap43	HuD-ZBP1 complex	3' UTR AU-rich regulatory element	40	axon	(Chung et al., 1997; Yoo et al., 2013)
tau	HuD, Ilf3, NF90	3' UTR U-rich sequence	91	axon	(Behar et al., 1995; Larcher et al., 2004; Litman et al., 1993)
CamKIIa	CPEB	3' UTR cytoplasmic polyadenylation element (CPE)	170	dendrites	(Blichenberg et al., 2001; Y. S. Huang et al., 2003; Mori et al., 2000)
CamKIIa	FMRP	3' UTR G-quadruplex		dendrites	(Bassell & Warren, 2008; Muddashetty et al., 2007)
CamKIIa	Staufen	3' UTR	30	dendrites	(Mori et al., 2000)
neurogranin	CPEB	3' UTR CPE	170	dendrites	(Y. S. Huang et al., 2003; Mori et al., 2000)
Map2	MARTA2	3' UTR	≤ 640	dendrites	(Blichenberg et al., 1999; Zivraj et al., 2013)
Map1b	FMRP	5' UTR G-quadruplex		dendrites	(Bassell & Warren, 2008; Darnell et al., 2001)
PSD95	FMRP	3' UTR G-quadruplex		dendrites	(Bassell & Warren, 2008; Muddashetty et al., 2007)
BC1	hnRNP A2	5' UTR stem-loop GA kink-turn (KT) motif	62	dendrites	(Muslimov et al., 1997, 2006)

In the early 1990s, Rob Singer and colleagues coined the term "zipcode" for specific targeting regions usually found in the 3' UTR of *β-actin*. These RNA zipcodes serve as a recruitment interface for *trans*-acting factors that specify the required cellular transport machinery. Zipcodes can be different shapes, based on (i) primary sequence, (ii) secondary/tertiary structural features, or (iii) a combination of sequence and structure (Jambhekar & Derisi, 2007). These *cis*-elements can also be different sizes, ranging from short segments with a defined sequence (25nt localization element FVLE1 in *Xenopus*

oocyte; Agnes P. Chan et al., 1999) to short repeating sequences (*β-actin*; Kislauskis et al., 1994), and can direct localization independently to the sequences adjacent to them.

As mentioned earlier, the localization of RNAs is often a multistep process, wherein its transport occurs in multiple steps that are spatially or temporally distinct. Specific *cis*-acting signals within individual transcripts may direct each of these steps, although multiple elements need to work together to effect localization. Recent analysis of available high-throughput data revealed that hundreds to thousands of mRNAs are localized to the neurites, however, our knowledge is restricted to only a few examples of zicodes, some of which are summarised in table 1.1 (von Kügelgen & Chekulaeva, 2020).

Map2 (Microtubule-associated protein 2) mRNA, a dendritically localized transcript, contains a 640nt *cis*-element in its 3'UTR shown to be essential and sufficient for its transport in rat hippocampal and sympathetic neurons (Blichenberg et al., 1999). Blichenberg et al. also predicted that this 640nt region folds into multiple stem-loop structures, although, without a deeper understanding of the sequence/structure influence on *Map2* localization.

The 3'UTR of the *CaMKIIα* mRNA was found to contain more than one *cis*-element. Utilizing reporter assays, Blichenberg et al. identified an ~1200nt fragment sufficient for localization (Blichenberg et al., 2001). Huang et al. mapped another zipcode to the distal 170nt of its UTR, containing cytoplasmic polyadenylation elements (CPEs), also identified in *Map2* (Y. S. Huang et al., 2003). The CPE is a nucleotide sequence (UUUUUAU) identified as important for the transport of *Map2* and *CaMKIIα* to the dendrites of rat hippocampal neurons (Blichenberg et al., 2001; Y. S. Huang et al., 2003). A third zipcode was identified within the first 94nt of the *CaMKIIα* 3'UTR due to its high homology with the 30nt dendritic targeting element in the 3'UTR of *neurogranin* mRNA (Mori et al., 2000).

Short AU-rich elements are an important example of *cis*-acting elements found in axonal transcripts. In the mRNAs encoding Mapt (Microtubule-associated protein tau) (Litman et al., 1993), Neuritin (Gomes et al., 2017), and GAP43 (Growth Associated Protein 43) (Chung et al., 1997), all three AU-rich elements were recognized by the same *trans*-acting factor (HuD) and capable of driving localization to the axon.

Multiple *cis*-elements can also act synergistically towards a common goal. Kislauskis et al. in 1994 characterized the multiple motif containing 54nt zipcode present at the 3'UTR of β-actin mRNA in chicken fibroblast. (Jambhekar & Derisi, 2007). The 54nt zipcode as well as a separate 43nt region both contain the two motifs, GGACT and AATGC, that along with an AC-rich region between these two motifs act synergistically to direct *β -actin* localization (Jambhekar & Derisi, 2007). A few years later, *β -actin* was observed to be localized to the neurite growth cones in cultured rat and chicken neurons, necessary to enrich the β-actin protein aiding the movement of neuronal growth cones (Kislauskis et al., 1994).

Cis-acting elements can also be present in the 5'UTR of the RNA as well as in noncoding RNA, nicely illustrated by the neuronal *brain cytoplasmic* (*BC1*) RNA. Muslimov et al. identified a 62nt zipcode in its 5'UTR that was sufficient to transport a reporter to the dendrites of rat sympathetic neurons at levels comparative to full-length *BC1* RNA (Muslimov et al., 1997, 2006).

All these examples highlight the use of single or multiple zicpcode elements to enable subcellular targeting of mRNAs. These zipcodes are found in a range of sizes and structures, that may be separated along the mRNA sequence. However, RNA localization is not necessarily a "one-man" job, and barring a few examples, zipcodes generally function constitutively. An interaction of zipcodes with *trans*-acting factors has been extensively studied, and binding of these *trans*-acting factors is usually necessary to enable efficient RNA localization.

In the following chapter, I describe these *trans*-acting factors, and provide examples of their interaction with zipcodes to mediate RNA transport.

Trans-acting factors: RNA Binding Proteins

Multiple studies have shown that mRNAs do not travel alone within a cell, but are usually accompanied by a "travel-buddy" that guide their journey. "Travel-buddies", also known as *trans*-acting factors, primarily consist of RBPs. These RBPs recognise and bind *cis*-elements on their target mRNAs, and traffic them within a complex or granule called a "messenger ribonucleoprotein particle" or mRNP.

With more than 1500 proteins identified to directly bind mRNAs, RBPs comprise a large family of proteins that regulate all aspects of RNA metabolism, as well as RNA localization (Castello et al., 2012). The specificity of an RBP is linked to its RNA Binding Domain (RBD), which exist in multiple structurally unique forms. The most canonical domains include the RNA recognition motif (RRM), K homology (KH) domain, zinc finger domains (Znf), and DEAD-box motif, that recognize and bind to short sequences within an mRNA transcript (Auweter et al., 2006; Cook et al., 2011; Lunde et al., 2007). Single or multiple of these domains can exist on an RBP, affecting its binding affinity with its target mRNA or interactions with multiple targets at the same time (Helder et al., 2016; Lunde et al., 2007). Additionally, RBPs can interact with mRNAs through non-canonical RBDs that recognize RNA secondary structures, or sequence motifs within structured regions (Lunde et al., 2007). However, the precise molecular interplay between different RBPs and mRNAs that regulate the mRNP localization is still unclear.

One of the first RBPs identified to bind and regulate the localization of axonal transcripts was Zipcode binding protein 1 (ZBP1/IGF2BP1). Two separate KH domains of ZBP1 recognize the bipartite *β-actin* zipcode, regulating its localization in neuronal axons (Donlin-Asp et al., 2021; Leung et al., 2006; Tiruchinapalli et al., 2003; H. L. Zhang et al., 1999). Interestingly, *cis*-elements on transcripts can also be

recognized and interact with multiple RBPs. Such is the case for *β-actin*; as it is also recognised by other axonal RBPs such as human antigen D (HuD, also known as ELAVL4) (Kim et al., 2015) and, heterogeneous nuclear (hn)RNP R (Glinka et al., 2010). To demonstrate the complexity of these interactions, Kim et al. showed that although ZBP1 and HuD both bind to the *β-actin* zipcode, they have different binding preferences. HuD shows a preference for the U-rich sequence, while ZBP1 binding depends more on the structure of the site, requiring a specific stem-loop spatial organization within the motif (Kim et al., 2015).

HuD has been shown to interact with a number of different mRNA and RBPs. Tau, a family of well-studied microtubule associated proteins present in the axon hillock and growth cones of neurons, has a U-rich *cis*-acting signal located on the 3' UTR of its mRNA that is recognized by HuD. This interaction is necessary to localize *tau* to the proximal portion of the axon, explaining the localized Tau protein expression and its implications in neuronal plasticity (Litman et al., 1993).

Alternatively, RBPs can also cooperatively regulate localization, with RBP-RBP interactions being important for modulating localization of axonal mRNAs. For example, the localization of GAP-43 mRNA has been reported to be cooperatively regulated into axons via a HuD-ZBP1 RNP complex (Yoo et al., 2013). HuD interacts with another RBP, survival motor neuron (SMN). Using time-lapse microscopy, they showed that SMN and HuD were co-transported in mouse motor neurons, whereby this binding facilitates the localization of mRNAs into axons (Fallini et al., 2011). Other examples of RBPs or RBP-RBP complexes directly binding specific mRNAs, and their binding zipcodes (if known), are summarized in table 1.1.

Sometimes RBPs can exclude mRNAs from being localized to the axon, and instead retain them in the neuronal cell body. Pumillo 2 (Pum2) RBP is restricted in expression to the soma of developing rat dorsal root ganglia (DRG) neurons. In the soma, Pum2 binds to transcripts containing Pumilio-binding elements (PBEs), retaining this subset of mRNAs in the soma, and developmentally controlling intra-axonal protein synthesis necessary for regulating axonal outgrowth and regeneration (Martnez et al., 2019).

Localization is accomplished by the synergistic activity of *cis*- and *trans*- acting elements, however, our understanding of these interactions are just a minute part of the vast unknown. As we start building on known examples of RNA-RBP interactions, we are faced with accepting that there are many factors at play *in vivo* that cannot be recapitulated for ease of study. As highlighted with the above examples, RBPs show different affinities that depend not only on the specific zipcodes, but also on zipcode structure and interactions with other proteins. In contrast, zipcodes can be bound by different RBPs, affecting their destination and function. The complexity of this interplay is far from understood, however, utilizing available molecular tools, the following mechanisms have been proposed with respect to RNA localization.

Motor protein directed cytoskeletal transport

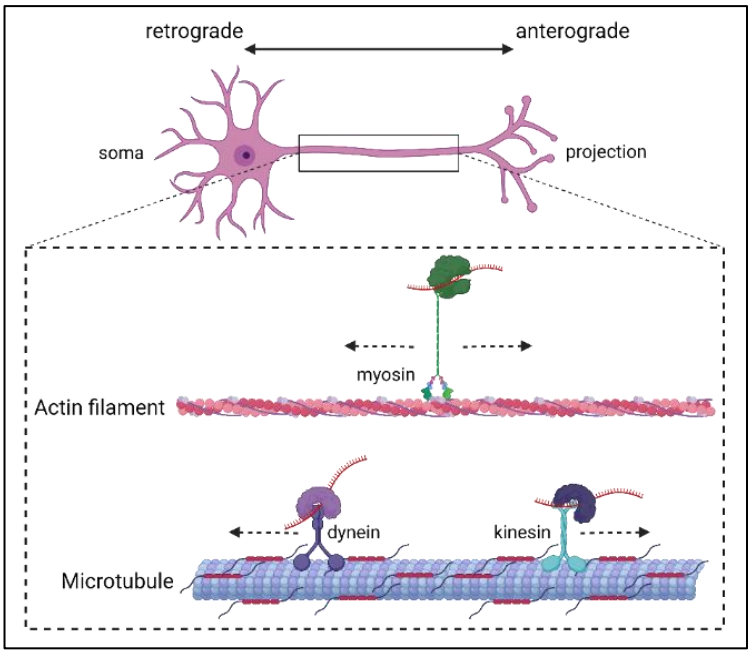

Figure 1.6: Illustration of active RNA transport along the neuronal cytoskeleton. Actin filament with myosin motor protein mediate short-range transport of mRNPs, enabling both, retrograde and anterograde movement. Microtubules stabilised with Tau protein mediate long-range transport of mRNPs, enabling retrograde movement with dynein, and anterograde movement with kinesin motor proteins in neurons. Adapted directly from (Engel et al., 2020). Created with BioRender.com.

mRNAs can be actively transported along the neuronal cytoskeleton within mRNP complexes, with long-range and short-range transport utilising different machinery (Figure 1.6). This directed transport via motor proteins utilizes ATP hydrolysis to change their conformation, generating processive movement along the different cytoskeletal tracks. The speed and direction of these cytoskeleton-associated RNPs is usually regulated based on its exact composition. Different motor proteins exhibit different kinetic properties with the speed of transport ranging from 0.2 – 60 µm/sec for myosins and 0.02 - 2 µm/sec for kinesins, compared to mRNA diffusion with a lower range of 0.1 - 0.4 μm^2/sec (Alberts B et al., 2002; Milo & Phillips, 2015; Mitsumori et al., 2017; Park et al., 2014b). In fact, Fusco et al. showed that an mRNA transported at 1.5 µm/sec via a molecular motor can travel the same distance 60x faster than via diffusion (Fusco et al., 2003).

Kinesins and dyneins mediate uni- or bi-directional long-range transport on microtubules, with plus end (axon) directed kinesin motors driving anterograde axonal transport, and minus end (cell body) directed dynein motors mediating retrograde axonal transport. This elaborate network of microtubules formed via α- and β-tubulin heterodimer polymerization radiates from the soma into the axon and dendrites (Cai & Sheng, 2009). In contrast, smaller cellular compartments such as the presynaptic terminals and dendritic spines mostly require bi-directional short-distance transport mediated via actin filament

associated motors, myosins. The neuronal actin cytoskeleton is composed of filamentous (F-actin) bundles and networks (Bridgman, 2004).

Most anterograde transport is performed by the kinesin superfamily proteins (KIFs), primarily by kinesin-1 (KIF5), a heterotetrameric kinesin with two heavy chains (KHCs) and two light chains (KLCs) (Rodrigues et al., 2021). Kanai et al. isolated a large KIF5 binding Rnase-sensitive granule (~1000S) from the mouse brain that contained a total of 42 proteins, including a number of RBPs (PURα/β, Staufen, FMRPs) as well as the mRNAs *CaMKIIα* and *activity-regulated cytoskeleton-associated protein* (*Arc*), providing evidence for association of KIF5 and an RNA-transporting granule (Kanai et al., 2004). Other kinesins, like KIF3A, were also found to localize the above-mentioned *tau*-HuD mRNP complex towards the axon (Aranda-Abreu et al., 2005).

The active transport of mRNP granules in neurons has also been reported to exhibit a bidirectional or oscillatory movement in neurites, suggesting a "tug-of-war" between the microtubule motor proteins (Buxbaum et al., 2015; Kanai et al., 2004). Single RBPs can direct this bidirectionality, as they associate with both motor proteins, dynein and kinesin. The *Drosophila* homologue of Fragile X mental retardation protein (dFMR) is one such protein that can associate with both, kinesin-1 and cytoplasmic dynein, to transport its associated mRNP granules (S.-C. Ling et al., 2004). Similarly, using imaging and molecular approaches, Chu et al. showed co-operative RBP-RBP interactions to regulate directionality of *Rac1* mRNPs in mouse neuronal dendrites. TAR DNA Binding Protein 43 (TDP-43) co-operates with Staufen1 to regulate retrograde transport of *Rac1* via binding with cytoplasmic dynein, while TDP-43 and FMRP co-regulate the anterograde transport of *Rac1* via binding with KIF5 (Chu et al., 2019).

Alternatively, the myosin superfamily can be divided into 15-18 structurally distinct classes, with only myosin classes I, II, V, VI and XI clearly present in vertebrate neurons, where they contribute essentially to the regulation of synaptic plasticity (Bridgman & Elkin, 2000; Kneussel & Wagner, 2013). In rat cortical neurons, Myosin Va and actin filaments are responsible for the dendritic localization of the RNP containing Staufen1 RBP and *Map2* (Balasanyan & Arnold, 2014).

There are also known instances of multiple RNAs being transported to the dendrites via the same pathway. Gao et al. showed that in oligodendrocytes, *Neurogranin*, *CaMKIIα*, and *Arc* mRNAs are dendritically targeted within the same hnRNP A2 containing RNP granule (Gao et al., 2008). Another aspect to consider is the change in directionality and speed of these granules during different states of neuronal activity (Donlin-Asp et al., 2021). Neuronal activity via depolarization and NMDA receptor activation was shown to increase the frequency of anterograde movements for *CaMKIIα* and *β-actin* containing mRNPs towards the dendrites, highlighting the multiple layers of active cytoskeletal transport (Das et al., 2019).

Diffusion-coupled local entrapment model

The asymmetric localization of mRNA can also be achieved via facilitated diffusion in combination with the entrapment of mRNA to previously localized anchors at specific sites in a cell. This mechanism has been clearly illustrated during late phase oogenesis in *Drosophila* for transcripts such as *nanos* (*nos*) mRNA. During this late phase, the microtubule cytoskeleton is reorganized into cortical bundles and does not show any anterior-posterior polarity. A study by Forrest et al. confirmed the diffusion and entrapment model for *nos* localization by using microtubule-depolymerising drugs that did not abolish *nos* localization to the posterior pole of the oocyte (Forrest & Gavis, 2003). They identified that strong cytoplasmic flows swiftly moved *nos* throughout the oocyte so that it encountered previously localized germ plasm proteins that locally trapped *nos* via a cortical actin-dependent association (Forrest & Gavis, 2003). Earlier studies in *Xenopus* oocytes also revealed an actin-dependent anchoring of the maternal mRNA *Vg1* at the vegetal cortex (Yisraeli et al., 1990).

The diffusion-coupled entrapment model is not very defined in neurons. However, bidirectional directed transport via motor proteins can also be coupled to local entrapment creating local RNA enrichment. Using a Halo-tagged *β-actin* reporter, Yoon et al. showed that on activation of a synapse in dendrites, *β-actin* mRNA granules containing ZBP1 and ribosomes are localized to the activated spine where they are locally anchored and undergo multiple rounds of translation (Yoon et al., 2016).

Selective degradation or stabilisation

Another mechanism that does not directly affect transport, rather controls the local transcriptome, is via mRNA decay. Selective degradation or protection from degradation in specific subcellular regions is a less studied mechanism that has been observed in very few cell types, but is an important method by which mRNA is patterned within a cell. This process was first described in the *Drosophila* embryo, wherein the posterior localization of *Heat Shock Protein 83* (*Hsp83*) mRNAs was accomplished via its protection from degradation at the posterior pole, largely regulated via its 3'UTR *cis*-element binding to the destabilising RBP Smaug (Ding et al., 1993; Semotok et al., 2008). A study by Aronov et al. looked at the stability of *tau* mRNA on binding to HuD RBP to promote its axonal localization. Due to HuDs ability to stabilise RNA, they hypothesised that in the absence of HuD, *tau* mRNA is degraded before it is transported (Aronov et al., 2002).

Canonical RNA degradation pathways like the miRNA pathway have also been characterized to spatially regulate RNA abundance. The role of miRNAs in regulation of transcript localization is elaborated in chapter 1.2.3.2. In this chapter, I will focus on noncanonical degradation pathways such as the NMD pathway, that regulates the degradation of improperly translated mRNAs. Initially, NMD was described to degrade mRNAs carrying premature termination codons. However, recent findings suggest that the

NMD pathway also regulates abundance of other mRNAs in axons (Colak et al., 2013) and dendrites (Notaras et al., 2020), influencing growth cone formation and axon guidance, and synaptic plasticity, respectively. NMD targets could instead contain 3'UTR introns or alternative splicing events resulting in stop codons followed by an exon-junction complex, as shown by the *roundabout guidance receptor 3.2* (*Robo3.2*) isoform compared to *Robo3.1* (Colak et al., 2013; Weischenfeldt et al., 2012). In the axons of mouse commissural neurons, *Robo3.2* mRNA synthesis is regulated via NMD by inducing degradation of *Robo3.2* mRNA in axons that encounter the floorplate of the spinal cord. As ROBO3.2 is a guidance cue receptor, this process influences axonal pathfinding and is fundamental for the correct axon positioning at the spinal cord midline (Colak et al., 2013). Neuron-specific functions of the NMD pathway can be further illustrated via modulation of Glutamate Receptor 1 (GLUR1) surface levels in mouse hippocampal dendrites via regulator of nonsense transcripts 2 (UPF2) degradation of *Arc* and *5'-AMP-activated protein kinase subunit gamma-3* (*Prkag3*) mRNAs, thereby regulating synaptic plasticity and cognitive function (Notaras et al., 2020). RNA degradation is a well-regulated method that creates specific localized transcriptomes in an effective manner.

1.2.2 The generation of protein from RNA: Translation

1.2.2.1 Translation: An overview

Protein synthesis in eukaryotes is a cyclical process during which the ribosomal subunits are recycled from the post-termination ribosome complexes (post-TCs) of the previous round of translation, to initiate a new round. The ribosome then reads the genetic code on the mRNA one codon at a time using aminoacyl-tRNAs. This whole process can be divided into 4 phases of translation: initiation, elongation, termination, and ribosome recycling. In brief, the eukaryotic translation initiation factors (eIFs) promote 80S ribosome assembly at the AUG start codon, along with the initiator methionyl-tRNA (Met-tRNA$_i^{Met}$) bound to the P site. Next, through the coordinated efforts of aminoacyl-tRNAs and the eukaryotic translation elongation factors (eEFs), the 80S ribosome processively moves along the mRNA, synthesising the encoded protein. Once the ribosome encounters a termination codon at the end of the open reading frame (ORF), the eukaryotic release factors (eRFs) promote the release of the nascent protein. Finally, the ribosome complex is recycled to its 40S and 60S subunits, followed by a new round of translation (Blanchet et al., 2022). In the following paragraphs, I will describe the genetic code and aminoacylation of tRNAs, along with these phases in more detail.

The instructions for building a polypeptide are the groups of three RNA nucleotides (A, C, G, U) called codons. 61 codons exist that code for the 20 common amino acids found in proteins. AUG acts as the translation start codon, coding the amino acid methionine. Three other codons, UAA, UAG, and UGA are

the translation stop codons that do not code for any amino acid, and signal the termination of translation. This relationship between the RNA codon and polypeptide amino acids is the genetic code, a universal, unambiguous, and redundant code (Crick et al., 1961; Yanofsky, 2007).

Apart from the mRNA, ribosomes and tRNAs are an essential part of the translational machinery. Ribosomes, made up of the 40S and 60S subunits in eukaryotes, contain around one-third protein and two-thirds rRNA. The rRNA is responsible for the structure of the ribosome, while the proteins bind to translation factors and help tune the ribosomal properties such as translation fidelity. The ribosome contains three sites wherein tRNAs can bind: A site, P site, and E sites; enabling them to deliver the amino acid that is added to the synthesising protein chain. This addition is done via the complimentary binding of the tRNA anticodon to the mRNA codon that encodes the delivered amino acid. However, according to the Wobble-Hypothesis, the pairing of the third codon base is less stringent than the first two, allowing a single tRNA to recognise more than one codon, such that fewer tRNAs cover all the codons. The attachment of a tRNA with its respective amino acid is catalysed via enzymes called aminoacyl-tRNA synthetases (aaRS) during a two-step process called aminoacylation. During the first step of activation, aminoacyl-adenylate (aminoacyl-AMP) Is formed on the synthetase enzyme through ATP (adenosine triphosphate) hydrolysis. This is followed by tRNA "charging", the transfer of the activated amino acid residue from the aminoacyl-AMP to its cognate tRNA. A different synthetase enzyme exists for each amino acid, recognising the cognate amino acid with the appropriate uncharged tRNA (Blanchet et al., 2022; J. Ling et al., 2009).

Initiation. Translation initiation is comprised of two major steps, resulting in the formation of the 80S ribosome with the Met-tRNA$_i^{Met}$ anticodon binding the start codon at the P site (Figure 1.7). During the first step, Met-tRNA$_i^{Met}$ binds to the start codon in the 40S subunit P site to generate the 48S initiation complex. The second step joins the ribosome 60S subunit and 48S complex, resulting in the 80S initiation complex required for elongation. Formation of the 48S initiation complex is a complex process requiring a lot of eukaryotic initiation factors (eIFs). It starts with the formation of a ternary complex containing Met-tRNA$_i^{Met}$, eIF2, and GTP. This complex binds to the 40S subunit along with eIF1, eIF1A, eIF3, and eIF5 to form the 43S pre-initiation complexes (PICs). Binding of the 40S subunit with eIF1 and eIF1A induces conformational changes resulting in the "open" conformation of the mRNA entry channel. Association of mRNAs with the PIC requires the eIF4F protein complex to unwind the mRNA 5' cap-proximal region. Once the mRNA is attached, the PIC scans along the 5' end, downstream of the mRNA cap, to find the AUG initiation codon. While scanning, the 5' UTR secondary structure unwinds, allowing the PIC to move in a 5' to 3' direction until it recognises the initiation codon. A discriminatory mechanism promotes recognition of the actual initiation codon, preventing premature Met-tRNA$_i^{Met}$ binding to similar triplets in the 5' UTR.

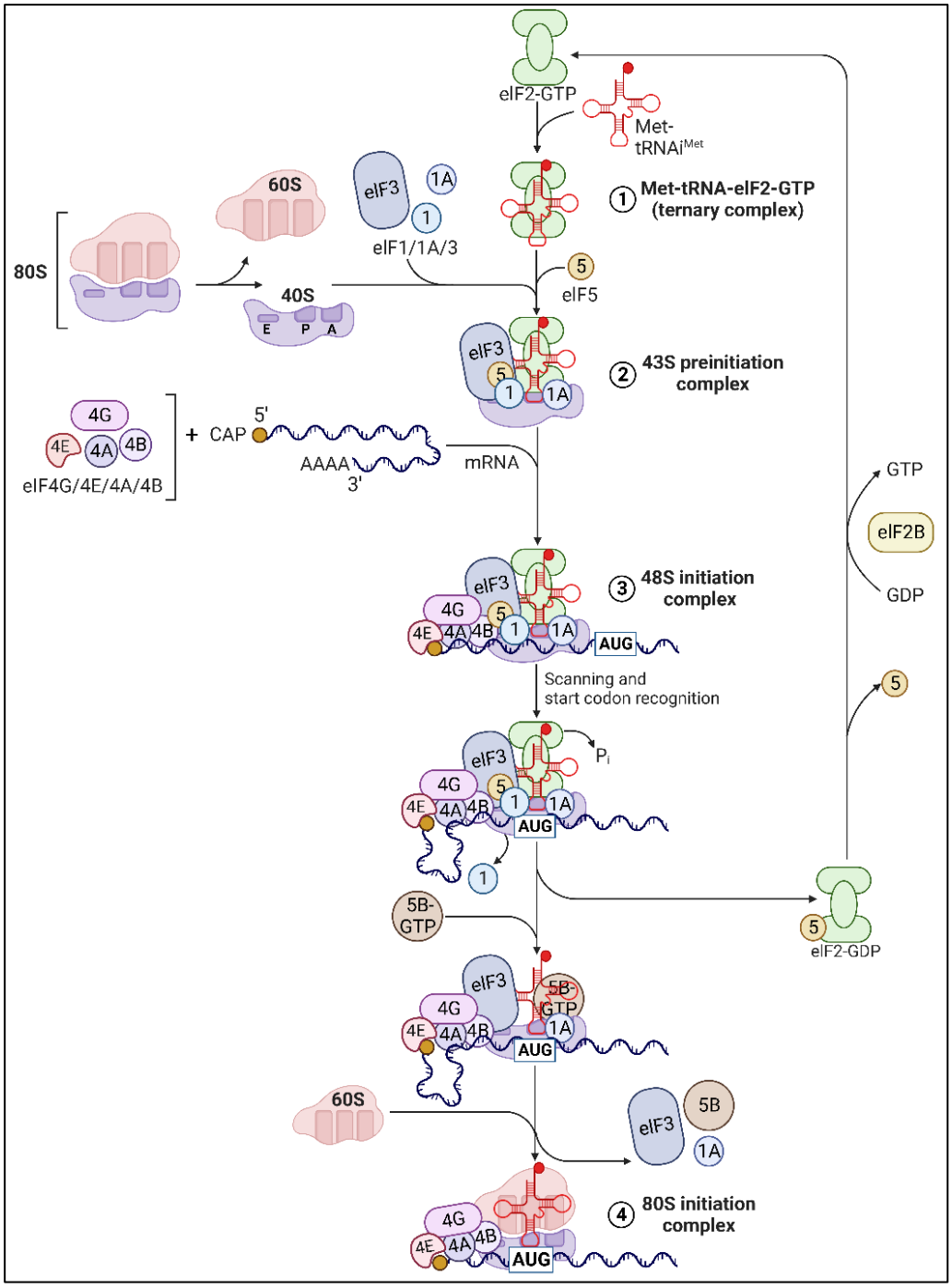

Figure 1.7: Steps in eukaryotic translation initiation. The ternary complex (eIF2–GTP–Met-tRNAi^{Met}) along with the 40S ribosome and eIF1,1A,3,5 form the 43S pre-initiation complex (PIC). The 43S PIC along with the mRNA recruited with the help of the eIF4F complex then form the 48S PIC. Post mRNA scanning and recognition of the AUG start codon, eIF5B helps the 60S subunit join, formaing the 80S initiation complex (IC). Adapted from (Blanchet et al., 2022). Created with BioRender.com using a template by Valeria Yartseva, Ph.D.

The bona fide start site is generally the first AUG triplet in the optimum GCC(**A/G**)CCAUG**G** nucleotide context, having a purine at the -3 and G at the +4 position relative to the A of the AUG codon, also known as the Kozak sequence (Kozak, 1991; Pisarev et al., 2008). eIF1 enables the PIC to choose the correct AUG,

preventing the aberrant assembly of ribosomal complexes at the near-cognate 5' UTR triplets. Once the start codon is recognised, eIF1 is released from the ribosome followed by eIF2-GTP hydrolysis via the GTPase-activating eIF5. These events trigger the "closed" conformation of the 48S PIC, stabilising its interaction with Met-tRNA$_i^{Met}$ and mRNA, and stopping ribosome scanning. After eIF2-GDP and eIF5 dissociate, the ribosome associated GTPase, eIF5B, along with eIF1A facilitate 60S joining. Once the 60S joins and eIF5B and eIF1A are dissociated, the 80S initiation complex containing the Met-tRNA$_i^{Met}$ in the P site base paired with the AUG start codon is formed and ready to enter the elongation phase (Aitken & Lorsch, 2012; Blanchet et al., 2022).

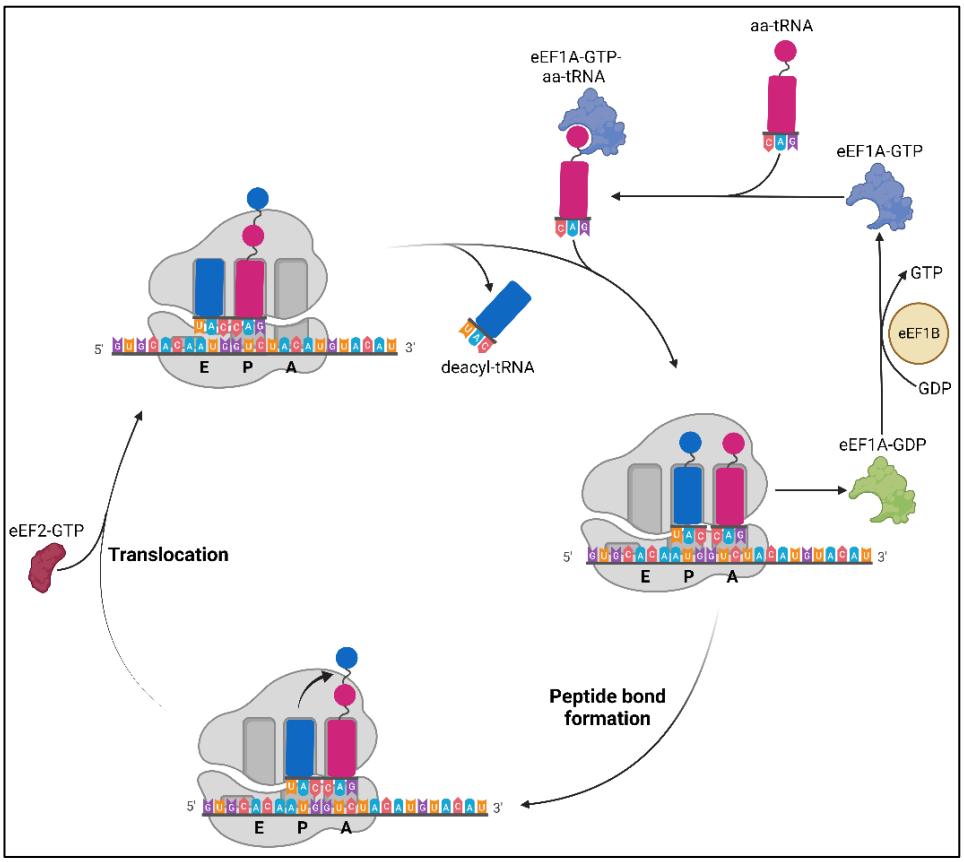

Figure 1.8: Steps in eukaryotic translation elongation. During elongation, eEF1A delivers the aa-tRNA to the A site. Once the peptide is formed between the amino acids, eEF2 helps with the translocation of the peptidyl-tRNA from the A site and the P site tRNA to the P and E sites, respectively. Finally, the deacylated tRNA is released from the E site, and the elongation cycle is repeated until a stop codon. Adapted from (Blanchet et al., 2022). Created with BioRender.com.

Elongation. Elongation can be separated into three phases: mRNA decoding via cognate aminoacyl-tRNAs, peptide bond formation, and translocation of the tRNA-mRNA complex (Figure 1.8). The eukaryotic elongation factor eEF1A, a member of the GTPase superfamily, binds the aminoacyl-tRNA (aa-tRNA) utilising GTP, delivering the aa-tRNA to the ribosome A-site. Recognition of the codon by the aa-tRNA results in GTP hydrolysis by eEF1A, releasing eEF1A and allowing accommodation of the aa-tRNA in the A site. eEF1B, a guanine nucleotide exchange factor (GEF), accelerates GDP dissociation from eEF1A.

Once the aa-tRNA is accommodated in the A-site, the peptide bond is rapidly formed with the P-site peptidyl-tRNA in the peptidyl transferase center (PTC), resulting in the formation of the pre-translocation complex. (Moazed & Noller, 1989) This complex is dynamic and has the ability to fluctuate between several conformations. The ribosomal subunits change conformation to a rotated state, triggering the adoption of hybrid states by tRNAs. In this state, the tRNA anticodon ends remain in the P and A sites of the 40S subunit, while the acceptor ends are in the E and P sites of the 60S subunit. eEF2 facilitates the translocation of the mRNA-tRNA in the ribosome, returning the tRNAs from the hybrid to the classical state. GTP-bound eEF2 stabilises the earlier hybrid state, while eEF2 conformational changes upon GTP hydrolysis unlock the ribosome, causing movement of mRNA and tRNA, and locking of the ribosome subunits in a post-translocation state. In this state, the E site in occupies by a deacylated tRNA, and the P site with a peptidyl-tRNA, vacating the A site to allow for binding of the next eEF1A bound aa-tRNA (Blanchet et al., 2022; Ferguson et al., 2015). Elongation is repeated until the complete protein is synthesised and the ribosome encounters a stop codon

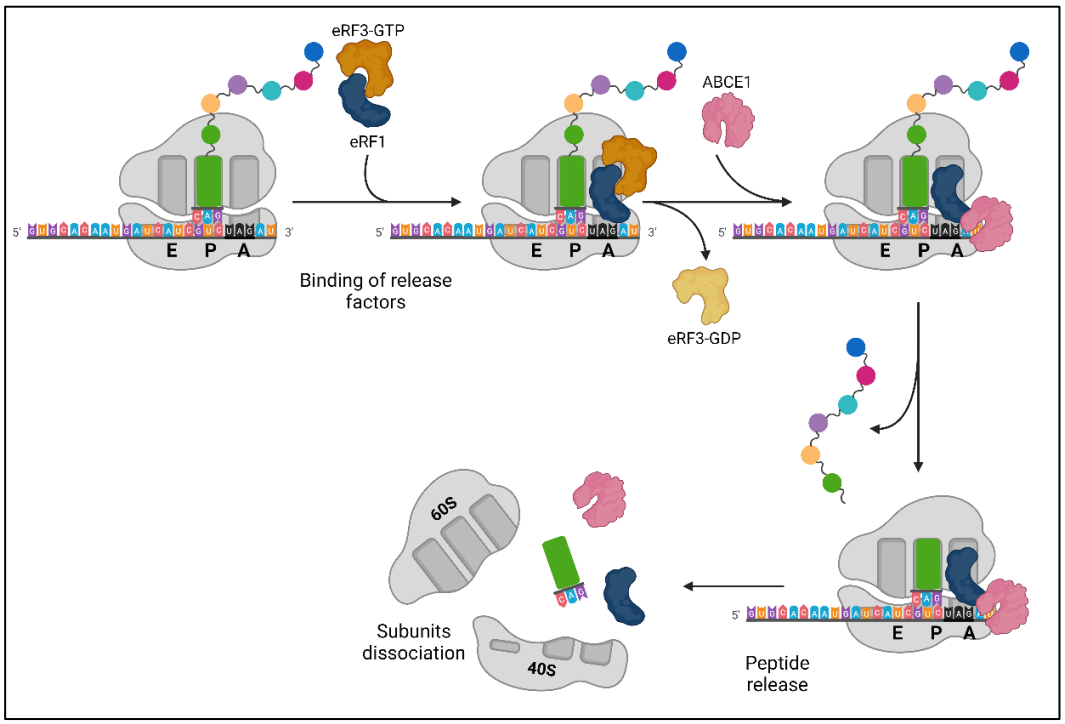

Figure 1.9: Steps in eukaryotic translation termination and ribosome recycling. Once a stop codon enters the A site of the ribosome, termination occurs and is catalysed by eRF1 and eRF3. ABCE1 promotes the release of the peptide, along with inducing ribosomal subunit dissociation. Adapted from (Blanchet et al., 2022. Created with BioRender.com.

Termination. Once the ribosome encounters a stop codon (UAA, UGA, or UAG), termination starts. Translation termination is catalysed by eRF1, which recognises the three stop codons, and a GTPase eRF3, which enables termination via GTP hydrolysis (Figure 1.9). eRF1 contains a structural NIKS (Asn-Ile-Lys-Ser) motif along with several other elements that help recognise the termination codons. The eRF1 central

domain also contains a GGQ (Gly-Gly-Gln) motif that extends into the PTC to promote peptidyl-tRNA GTP hydrolysis by eRF3 and release of the nascent peptide (Blanchet et al., 2022).

Recycling of ribosomal subunits. After termination, the ribosomal subunits dissociate and the mRNA and deacylated tRNA are released, freeing the components for subsequent translation rounds. Ribosome recycling is facilitated by the ATPase ABCE1. Upon ABCE1 binding and ATP hydrolysis, the Fe-S (iron-sulfur) cluster at its amino-terminal undergoes a conformational change, pushing eRF1 between the ribosome subunits, resulting in dissociation of the post-termination ribosomes into their 40S and 60S subunits. mRNA and deacylated tRNA are finally released from the 40S subunit via eIF2D, as well as eIF1, eIF1A, and eIF3j *in vitro* (Pisarev et al., 2010).

1.2.2.2 Local translation in neurons and why it is necessary

The complexity of the neuron reinforces the importance of spatial and temporal gene regulation, necessary for the creation of structural and functional neuronal networks (Figure 1.10). Some neurons can extend their axons up to a meter from the cell body while a neuron with an axon of ~200 cm can form about 50,000 synapses (Ishizuka et al., 1990). A typical excitatory neuron can also receive information from 1-10,000 neurons while transmitting to 50-100.000 neurons through their synapses (Holt et al., 2019). With such a complex morphology, it is understandable that the ability to precisely and rapidly respond to a stimulus poses some logistical challenges that can be overcome via a local system in place to synthesise new proteins on-demand. Neurons control their local translatome by transporting translationally silent mRNAs, followed by their local translation, necessary to regulate correct wiring of the nervous system during development, and proper function and synaptic plasticity during adulthood (Holt et al., 2019).

During development of the nervous system, the axons of neurons extend and navigate towards their postsynaptic targets using their growth cones. Growth cones are specialised tips of the axon that detect and react to guidance cues to guide their movement towards their destination, where they form the synapse. The dendritic spines of dendrites form excitatory synapses that contain many proteins, including neurotransmitter receptors, and other molecules for scaffolding, signalling, and adhesion. Protein copy numbers for the pre- and post-synaptic compartments have been quantified to an extent, with the axon terminal of the pre-synaptic neuron containing ~100-10,000 copies of various proteins (Richter et al., 2018). Specific proteins from the post-synapse have also being quantified containing a range of 10-1,000 copies, with CamKIIα having 5,000 copies, and PSD-95 having 300 copies (Sheng & Hoogenraad, 2007). We also need to consider the half-life of neuronal proteins so that we understand how often a protein needs to be synthesised. Dörrbaum et al. measured a half-life of ~5.5 days for neuronal proteins *in vitro* (Dörrbaum et al., 2018), while proteins *in vivo*, in the mouse brain, exhibited half-lives of ~10 days, as

measured by Fornasiero et al. (Fornasiero et al., 2018). Finally, in order to comprehend the necessity for local translation, we need to compare the speed of protein transport through the axon until it reaches the synapse. As compiled by Maday et al., the fastest transport of a protein in axons was measured at 1µm/sec (Maday et al., 2014). This suggests that the time needed to traffic a protein from the neuronal cell body to an axon terminal ~1m away would require 11.6 days! As neuronal processes have the ability to adapt their synaptic number, size and strength through the process of synaptic plasticity, they require a mechanism to fulfil local protein demands in response to external cues within minutes rather than hours. This is where local translation plays a huge role, providing subcellular functions necessary for neuronal development, synaptogenesis, plasticity, and survival (Holt et al., 2019).

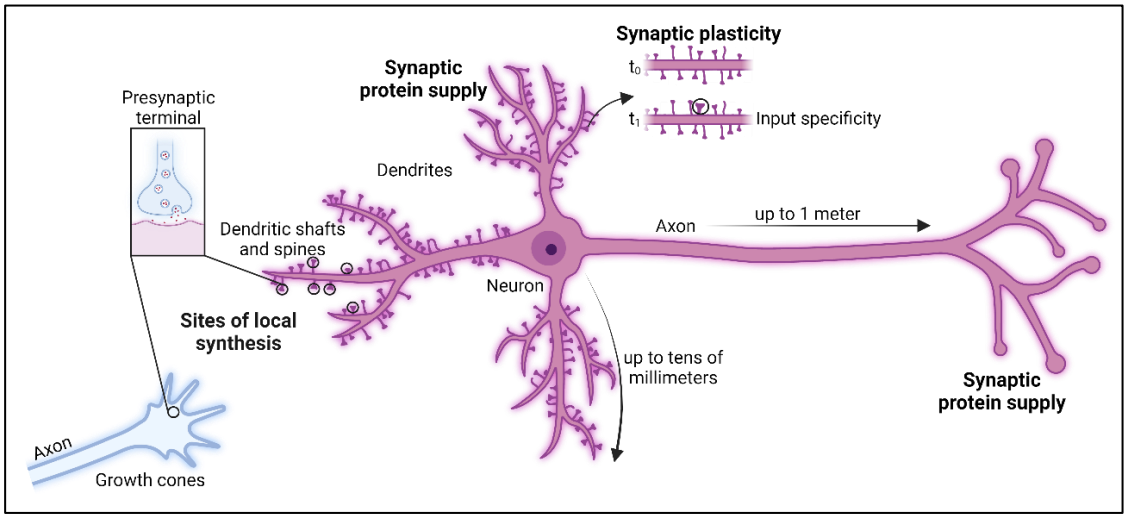

Figure 1.10: Neuron depicting the sites of local protein synthesis and local translation dependent neuronal functions. Due to the size of a neuron, local protein synthesis occurs in the axons and dendrites, aiding neuronal functions. The axon terminals and the dendritic spines form the pre- and post-synaptic terminals, respectively, where local translation occurs. Synaptic plasticity at the spines is a specific and time dependent process that also depends on external stimulus and local protein synthesis. Adapted from (Holt et al., 2019). Created with BioRender.com.

Since 1965, when ribosomes were first identified in primate spinal cord motor neuron dendrites (Bodian, 1965), followed by Steward and Levys 1982 discovery of polyribosomes at the dendritic spine of hippocampal neurons (Steward & Levy, 1982), a lot of research has established the importance of mRNA localization and local translation in the developing and adult nervous system. One of the first evidences of local protein synthesis was in the axon of the giant squid by Giuditta et al., where they demonstrated metabolic incorporation of amino acids in axonal proteins (Giuditta et al., 1968). In 1993, Feig and Lipton demonstrated the first evidence for *de novo* protein synthesis in dendrites in response to neuronal stimulation (Feig & Lipton, 1993). Using applied electrical stimulation along with carbachol, a muscarinic acetylcholine agonist, in hippocampal slices exposed to [^{3}H]leucine, they detected an increase in [^{3}H]leucine incorporation in the dendrites, with no effect in the cell body (Feig & Lipton, 1993). Kang and Schuman then went on to discover the importance of local protein synthesis in BDNF or Neurotropin-3

(NT-3) facilitated synaptic plasticity. Using rat hippocampal slices, they isolated the CA3 or CA1 synaptic regions from the cell bodies using a microlesion, and still observed synaptic transmission in response to external BDNF or NT-3 application (Kang & Schuman, 1996). As BDNF and NT-3 induced synaptic potentiation requires new protein to be synthesised, this experiment confirmed local synaptic translation away from the cell body. (Kang & Schuman, 1996)

For protein synthesis to occur, the translation machinery is also locally required. Apart from the localization of the protein template: mRNA, mentioned in chapter 1.2.1.2, the presence of ribosomes, tRNAs, and regulatory elements is also of importance. Ostroff et al. compared the ultrastructure of dendritic spines and synapses in hippocampal slices before and after long term potentiation (LTP) induction, and found an increased percentage of polyribosomes in spines post stimulation. Interestingly, they also noticed an increase in the postsynaptic density (PSD) of spines containing polyribosomes, suggesting that stimulation-dependent local translation stabilizes spine PSD and is an indicator for spines expressing LTP (Ostroff et al., 2002). On the other hand, Bingol and Schuman demonstrated the recruitment and sequestration of proteasomes on activation of the NMDA receptor, suggesting a coupling of translation and degradation to remodel the local synaptic protein composition, enabling rapid protein turnover (Bingol & Schuman, 2006). Getting back to the ribosome, ribosomes are usually transported in mRNPs or transporting granules (Fernandopulle et al., 2021). As ribosomal protein (RP) mRNAs have also been identified in dendrites and axons, there is evidence supporting local synthesis of RPs, and their incorporation into pre-existing axonal ribosomes (Shigeoka et al., 2019).

As tRNA availability influences the speed of mRNA decoding during translation, local translation would require a readily available local pool of tRNAs. In 1996, Tiedge and Brosius detected the presence of tRNAs in neuronal dendrites (Tiedge & Rgen Brosius, 1996). A recent study by Koltun et al. looked at the dynamics of these tRNAs in the neuron (Koltun et al., 2020). They observed tRNA puncta that were bidirectionally transported in dendrites, with some of them participating in active translation due to their destabilization with puromycin, a translation inhibitor (Koltun et al., 2020). As mentioned earlier, regulatory elements such as the co- and post-translational processing machinery is also required to process integral membrane and secretory proteins. Membrane and secretory proteins require the endoplasmic reticulum (ER), the ER–Golgi intermediate compartment (ERGIC), the Golgi apparatus, as well as the *trans*-Golgi network to fold, assemble, and glycosylate them before plasma membrane delivery. Organelles staining for the ER, ERGIC, and Golgi complex have been identified in dendrites and axons, suggesting the presence of a functional ER and Golgi equivalent, necessary to locally synthesise membrane and secretory proteins (Gardiol et al., 1998; Merianda et al., 2009). This evidence along with the abundance of membrane proteins in the transcriptomes of dendrites and axons, indicate the presence of all the necessary machinery to locally synthesis the different proteins identified in neuronal dendrites and axons (Holt et al., 2019).

To directly observe protein translation, scientists initially used synaptosomes, the detached synaptic spines with their presynaptic terminals, and synaptoneurosomes, subcellular structure containing presynaptic structures along with the postsynaptic densities. Using these preparations, they demonstrated the stimulation-dependent translation of CamKIIα (Bagni et al., 2000), PSD95 (Muddashetty et al., 2007), and Arc (Yin et al., 2002). To directly link neuronal synaptic plasticity and local translation, Miller et al. mutated the endogenous CamKIIα gene in a mouse, such that the 3' UTR mRNA zipcode for dendritic localization was disrupted (Miller et al., 2002). In this way, the CamKIIα protein region was intact, but its mRNA was restricted to the soma. They found a dramatic 85% reduction of CamKIIα in PSDs, along with deficits in LTP and impairments in memory processes, directly demonstrating the importance of local translation of a specific protein in neuronal function (Mayford et al., 1996; Miller et al., 2002). Similarly, Perry et al. perturbed the endogenous axonal localization of importin β1 mRNA by altering its mRNA zipcode (Perry et al., 2012). Normally, importin β1 is locally upregulated in the axon in response to axonal injury and coordinates the transport of an injury signaling complex to the cell body. Axonal importin β1 knockout mice had reduced axonal expression and delayed recovery, without altering its functions in the cell body and nucleus (Perry et al., 2012). These results further add to the mounting evidence that local translation is necessary for axonal function and repair.

To address another aspect of local translation: activation of translation of translationally silent localized mRNAs, Muddashetty et al. described the use of phosphorylation of translational repressors as a molecular mechanism for the spatial and temporal control of translation (Muddashetty et al., 2011). Phosphorylation of the RBP FMRP promotes the miRNA-induced silencing complex (miRISC) formation, a translation repression complex (further elaborated in chapter 1.2.3), that represses the translation of PSD-95 in dendrites. However, on FMRP dephosphorylation, the miRISC is released, thereby activating translation of PSD-95 (Muddashetty et al., 2011). The RBP ZBP1 is another example of phosphorylation regulated translation. Hüttelmaier et al. described how unphosphorylated ZBP1 is required for the localization of *β-actin* mRNA to the synapse in a translationally repressed form (Hüttelmaier et al., 2005). However, ZBP1 phosphorylation at the synapse via Src protein kinase reduces its binding to *β-actin* mRNA, activating its local translation (Hüttelmaier et al., 2005).

The local synthesis of proteins in neurons is a process that regulates neuronal function, from axonal guidance and growth during development, to synaptic plasticity and neuronal repair and survival during maturity. The fine balance of translation regulation at spatial and temporal scales is what determines the health of a neuron. With the continuous development of new tools to study local translation, we can further explore this well-regulated process in neurons and deeper understand this complex process in these complex cells.

1.2.3 miRNA dependent regulation

1.2.3.1 miRNA biogenesis

miRNAs are small non-coding RNAs, ~21 nucleotides in length, transcribed by RNA pol II. miRNA biogenesis starts with DNA sequences that are transcribed by RNA pol II into primary miRNAs (pri-miRNAs), long transcripts with a local hairpin structure wherein the miRNA sequence is embedded. They are then processed via canonical or non-canonical pathways into precursor miRNAs (pre-miRNAs) and finally into mature miRNAs that mostly interact with the 3'UTR of their target mRNAs to regulate expression (Figure 1.11).

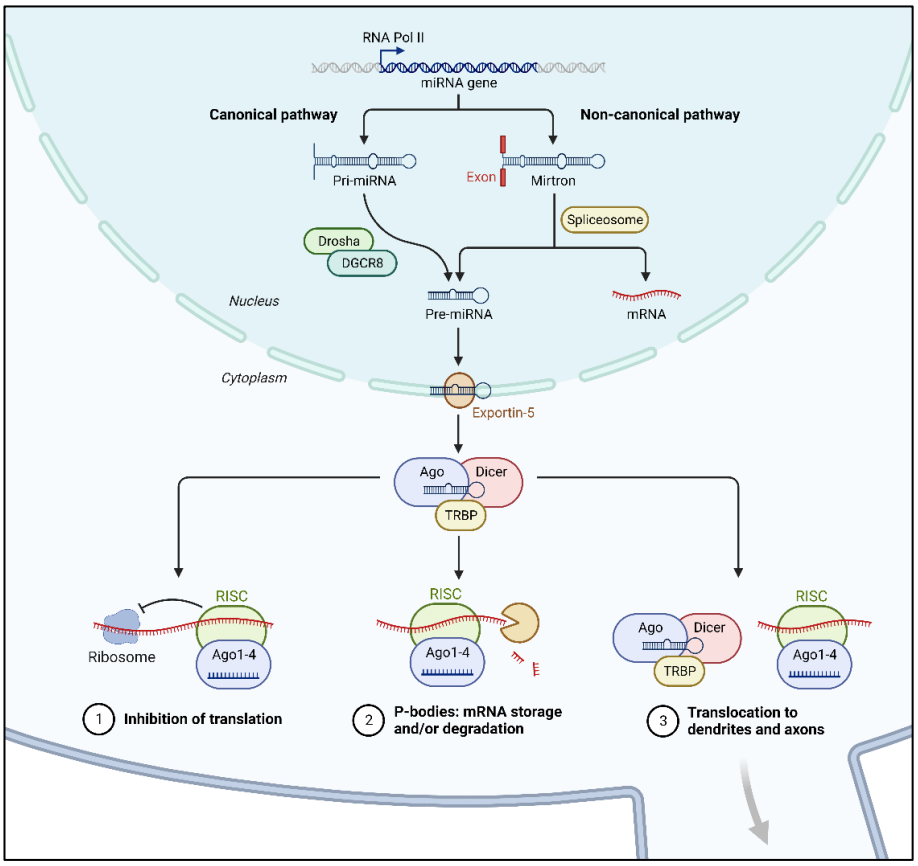

Figure 1.11: Overview of miRNA biogenesis and mechanism of action in the neuron. During the canonical pathway, pri-mRNAs are produced from miRNA genes encoded in either exonic, intronic, or intergenic regions. Drosha/DGCR8 processes pri-mRNA into pre-mRNAs. During the non-canonical mirtron pathway, intronic pre-miRNA hairpins are produced via splicing of short introns independent of Drosha processing. Pre-miRNAs generated via both pathways are exported to the cytoplasm via Exportin 5, followed by Dicer cleavage within the RLC, unwinding of the miRNA/miRNA* duplex via Argonaute, and loading into the miRISC via TRBP. mRNAs bound by miRNAs in the miRISC results in **(1)** inhibition of translation, and/or **(2)** degradation of mRNA in cytoplasmic P-bodies. **(3)** miRISC can also be transported in protein complexes through the entire neuron for local regulation. Adapted from (O'Carroll & Schaefer, 2013). Created with BioRender.com using a template by Eunice Huang.

Majority of the canonical miRNAs identified are intragenic and encoded by introns of non-coding or coding transcripts, and relatively few exonic regions, while the remaining are intergenic. Sometimes, several miRNA loci are clustered and transcribed as one long transcript, constituting a polycistronic transcription unit, that may have similar seed regions forming a family (eg. *lethal-7* (*let-7*) miRNA family).

During the canonical miRNA biogenesis pathway, long pri-miRNAs (> 1kb) containing a local stem–loop structure are processed into pre-miRNAs (~65 nucleotides) via a microprocessor complex, comprising of the nuclear RNase III Drosha (Pasha in *D. melanogaster* and PASH-1 in *C. elegans*) together with its essential cofactor DGCR8 (DiGeorge syndrome critical region 8). Following processing, pre-miRNAs are exported to the cytoplasm via a transport complex containing exportin 5 (XPO5) and Ran-GTP. In the cytoplasm, it is further cleaved by Dicer RNase III endonuclease near the terminal loop within the RISC locading complex (RLC), generating an ~22 bp mature miRNA/miRNA* duplex. This processing is usually coupled with the formation of the miRISC. The miRISC basically consists of the "guide strand" of the miRNA, loaded onto the Argonaute family of proteins (AGO1-4 in humans) and GW182 (glycine-tryptophan (GW) repeat-containing protein of 182 kDa) family proteins. This complex interacts with its target RNAs to repress their expression, while the other miRNA* strand (the "passenger strand") is usually destroyed (G. C. Shukla et al., 2011).

Various alternative mechanisms have been discovered to generate a minority of miRNAs, utilizing Drosha/DGCR8-independent and Dicer-independent pathways. Mirtrons, produced from mRNA introns during splicing, and 7-methylguanosine (m7G)-capped pre-miRNA are produced via the microprocessor complex independent pathway, wherein they are directly exported to the cytoplasm using exportin 1 without Drosha cleavage. Some small RNAs derived from tRNAs, snoRNAs, or small nuclear viral RNAs also bypass the microprocessor complex. On the other hand, short hairpin RNA (shRNA) transcripts are processed by Drosha and require the catalytic activity of AGO2 for miRNA maturation due to their insufficient length for Dicer cleavage (Ha & Kim, 2014; O'Brien et al., 2018).

1.2.3.2 miRNA regulation of RNA localization and translation in neurons

The discovery of miRNAs unearthed a new layer of gene regulation. miRNAs play an important role in silencing RNA, and extensively regulate gene expression post-transcriptionally. Generally, miRNAs bind to the 3' UTR of target mRNAs and inhibit protein synthesis either by destabilization of their target mRNAs and/or repressing translation. miRNA-repressed mRNAs are usually deadenylated, followed by their degradation (Cannell et al., 2008). However, in a study using *miR-125b* and *let-7* miRNAs, Wu et al. revealed that miRNA translational repression does not necessarily require a poly(A) tail, and can instead use a 3' histone stem-loop to target other RNAs (L. Wu et al., 2006).

The spatiotemporal regulation of mRNA translation in the mammalian nervous system plays a vital role in neuronal development and synaptic plasticity. The nervous system is a source of an abundance of miRNAs, where they are linked to the regulation of transport and translation of neuronal mRNAs (Kosik, 2006; Sempere et al., 2004). One of the first studies to characterise the localized function of a brain specific miRNA, *miR-134*, was conducted by Schratt et al. (Schratt et al., 2006). They showed that *miR-134* localized to the synapto-dendritic compartment in rat hippocampal neurons, where it negatively regulates the dendritic spine structure through translational repression of *LIM-domain kinase 1* (*Limk1*) mRNA, a protein kinase encoding mRNA that regulates spine development (Schratt et al., 2006). Synaptic input via an external stimulus such as BDNF relieves this inhibition, allowing Limk1 to contribute to synaptic development and maturation (Schratt et al., 2006). *miR-9*, expressed in the axons of primary cortical neurons, was found to control axonal growth and branching via a BDNF-dependent regulation of *microtubule associated protein 1B* (*Map1b*) mRNA translation (Dajas-Bailador et al., 2012). This regulation by *miR-134* and *miR-9* highlight the complex interplay between subcellular localization, translation, and an additional level of extrinsic stimulation, contributing to the changes in neuronal gene regulation (B. Wang & Bao, 2017).

miRNAs can also cooperatively regulate neuronal processes like axon growth, by targeting different mRNAs. For example, axon elongation is positively regulated by *miR-132* via the local targeting of *Rasal1* mRNA (Hancock et al., 2014). On the other hand, *miR-181d* negatively regulates axon growth via translational repression of *Map1B* and *Calm1* mRNAs in the axon (B. Wang et al., 2015).

Remarkably, RBPs can mediate the delivery of miRNAs, and even their target mRNAs, to specific subcellular compartments. *miR-181d*, mentioned above, is localized to the axons of rat DRG neurons via a granule containing the RBP fragile X mental retardation protein (FMRP) (B. Wang et al., 2015). FMRP also mediates the axonal delivery of *Map1b* and *Calm1* (B. Wang et al., 2015). Several other miRNAs have been identified to associate with FMRP in the mouse brain. In hippocampal neurons, *miR-125b* along with FMRP and AGO1 negatively regulate NR2A expression, an NMDA receptor subunit, regulating synaptic structure and plasticity (Edbauer et al., 2010).

Interestingly, when the copy number of miRNAs was quantified by Bissels et al. and compared to the abundance of mRNA targets, most miRNA copy numbers were relatively low (Bissels et al., 2009; Schwanhüusser et al., 2011). This posed an important question: How can miRNAs effectively regulate their mRNA targets? Sambandan et al. recently elucidated this with their discovery that pre-miRNAs can be spatially and temporally regulated in neurons, leading to a precise increase in miRNA expression and their mediated translational repression (Sambandan et al., 2017). Using high-resolution *in situ* hybridization in rat neuronal dendrites, they visualized the activity dependent maturation of an inducible pre-miRNA probe that exhibited an increase in florescence on maturation (Sambandan et al., 2017). In

association with this result, protein synthesis of the target mRNA at the synapse was reduced on synaptic-stimulation-dependent maturation of the pre-miRNA probe (Sambandan et al., 2017).

Therefore, research on miRNAs has revealed the complexity and importance of their role in gene regulation, especially their significant contribution to local RNA expression levels and translation in neurons.

1.2.4 Localization and translation in neuronal and neuromuscular diseases

Table 1.2: Summary of proteins and mRNAs involved in abnormal local translation in different neuronal pathologies

Compiled from (Gamarra et al., 2021; and Turner-Bridger et al., 2020).

Disease	Experimental model	Local translation alterations	References
fragile X syndrome (FXS)	**FMRP** knockdown in mouse embryonic DRG neurons	Reduced axonal transport of granules containing ***miR-181d***, ***Map1b***, and ***Calm1***	(B. Wang et al., 2015)
amyotrophic lateral sclerosis (ALS)	*Drosophila* model of ALS; *Drosophila* and human-derived **TDP-43 mutant** (M337V, A315T) motor neurons	Abnormal ***futsch/Map1b*** mRNA trafficking to neurites causing cytoskeletal defects; impaired anterograde axonal transport of ***Nefl* mRNP** granule	(Alami et al., 2014; Coyne et al., 2014)
	Mutant FUS (R521H, R521C) mouse hippocampal neurons	Inhibition of intra-axonal translation	(López-Erauskin et al., 2018)
spinal muscular atrophy (SMA)	**SMN knockdown** in mouse motor neurons, chick forebrain, and rat hippocampal cultures	Reduction in axonal **poly(A)-positive RNAs**; mislocalization of ***β-actin***, ***Nrn1***, ***Anxa2***, and ***GAP43*** affecting neurite growth and presynaptic function	(Fallini et al., 2011, 2014; Rihan et al., 2017; Saal et al., 2014)
Huntington's Disease (HD)	**HTT knockdown** in U2OS cell line; rat cortical neurons and rat cortex sections	HTT regulates post-transcriptional processes via Ago2 association; impaired levels of ***β-Actin*** mRNA in dendrites; altered ***bdnf*** mRNA axonal transport	(Ma et al., 2010; Savas et al., 2008, 2010)
Alzheimer's disease (AD)	Synthetic **Aβ1-42 peptide** application in rat embryonic hippocampal axons	Altered axonal transcriptome, including ***Atf4*** *mRNA* localization to axons resulting in neuronal death	(Baleriola et al., 2014)

As mentioned above, dendritic and axonal RNA localization and local translation is important for maintaining the healthy state of a neuron. Only in 2001, when Zheng et al. described the activation of intra-axonal RNA translation in response to nerve injury, did we link the deregulation of local translation

with neuronal pathologies (J.-Q. Zheng et al., 2001). Growing evidence suggests the association of defects in mRNA localization and local translation with an increasing number of neurological disorders that affect different areas of the brain. In this chapter, I have highlighted a few key findings relating RNA transport and translation with diseases such as fragile X syndrome (FXS), amyotrophic lateral sclerosis (ALS), and spinal muscular atrophy (SMA), along with a summary in table 1.2.

One of the best characterised developmental neurological disorder linked to altered mRNA transport is FXS, an X-linked disorder caused by loss of expression of the RBP FMRP. FXS is an inherited genetic disorder, wherein expansion of CGG repeats in the 5' UTR of *Fragile X Messenger Ribonucleoprotein 1* (*FMR1*) results in its transcriptional silencing, and loss of its encoded protein, FMRP (Bassell & Warren, 2008). Multiple studies have described the association of FMRP with a vast number of mRNAs (such as *Map1b*, *PSD95*, *Fmr1*, and *CaMKIIα*), and other RBPs to form RNPs or granules, and its role in regulating mRNA transport and translation; functions that are disrupted in FXS (Darnell et al., 2011; Darnell & Klann, 2013). Loss of FMRP causes dysregulation of neuronal RNA transport, resulting in slower localization of RNP granules and mis-localization of mRNAs, for example, disruption of *Map1b* and *Calm1* FMRP axonal targeting in DRG axons (B. Wang et al., 2015). Kao et al. also illustrated FMRPs role in local protein synthesis by looking at *CamKIIα* mRNA movement in *Fmr1* KO and WT mouse cortical neurons upon I mGluR stimulation (Kao et al., 2010). On comparison with *Fmr1* KO neurons, *CamKIIα* mRNA and protein synthesis was enriched only in the WT dendrite spines. These results suggest a lack of local plasticity-dependent translation in *Fmr1* KO neurons, due to aberrant mRNA targeting in the absence of FMRP (Kao et al., 2010). Although we are closer to understanding FMRPs physiological function and the defects due to its depletion, the direct functional implications of axonal mRNA mis-localization in FXS is yet to be determined.

In recent years, the connection between neurodegenerative disorders and aberrant axonal mRNA localization is gaining a lot of traction. Mutations in RBPs exhibit frequent phenotypes associated with motor neuron diseases. ALS is one such neurodegenerative disease that is characterized by motor neuron loss due to mutations in genes implicated to affect RNA metabolism, including defects in alternative splicing, stabilisation, and localization. Apart from superoxide dismutase 1 (SOD1) and chromosome 9 open reading frame 72 (C9orf72), mutations in the RBPs TDP-43 and Fused in Sarcoma (FUS) are strongly linked to ALS (Fiesel & Kahle, 2011; Gamarra et al., 2021). TDP-43 and FUS are both RBPs that under healthy conditions, are localized in the nucleus where they regulate transcription and splicing of pre-mRNAs. They also shuttle between the nucleus and cytoplasm, regulating mRNA export and transport to the cytoplasm (Ederle & Dormann, 2017). Apart from mRNA transport, both these RBPs are also components of stress granules, which regulate mRNA translation (Aulas & Velde, 2015). In ALS as well as another neurodegenerative disease, frontotemporal lobar degeneration (FTLD), TDP-43 positive aggregates are identified in most sporadic as well as familial cases, and are used as a marker for the disease. As mentioned earlier, TDP-43 is a well-studied RBP that is involved in mRNA splicing, localization,

and translation in neurons. Under normal conditions, TDP-43 associates with its target mRNAs in RNP granules, transporting them to their subcellular destinations within a neuron, where they can be locally translated (Alami et al., 2014). Several ALS-causing mutations impair TDP-43s role in axonal mRNA trafficking. Mutations in its prion-like C terminal domain affect TDP-43 and possibly affect its phase separation and ability to form mRNPs. For example, TDP-43 was reported to transport *neurofilament-L* (*NEFL*) (Alami et al., 2014) and *Map1b* to the axons (Coyne et al., 2014). In *Drosophila*, Coyne et al. described how mutant TDP-43 altered *futsch* mRNA (*Map1b* in mammals) localization to the neuromuscular junction (NMJ), and also affected its translation by shifting the mRNA from actively translating polysomes to non-translating RNP particles (Coyne et al., 2014). Similarly, *Map1b* localization was also altered in ALS spinal cords, similar to their observations in *Drosophila* (Coyne et al., 2014). FUS is also identified in cytoplasmic aggregations, altering RNP granule formation and local translation in neurons. FUS has also been observed at translational sites in axons. When FUS is mutated, some target mRNAs are abnormally expressed, for example, in mutant FUS motor neurons, *Fos-B* was upregulated in axons causing increased axonal branching (Akiyama et al., 2019). Although tremendous progress has been made to elucidate the pathogenesis of TDP-43 and FUS proteinopathies, future research is required to comprehensively dissect the key mechanisms underlying ALS.

Interestingly, FUS has also been shown to interact with SMN protein, an RBP responsible for SMA development (Gamarra et al., 2021; Turner-Bridger et al., 2020). SMA is another neurodegenerative disease associated with the degeneration of spinal motor neurons, followed by the progressive loss of muscle function and paralysis (Fallini et al., 2012). SMA is usually caused by mutations in the SMN1 gene that encodes the SMN protein, resulting in insufficient levels of SMN. The main function of the ubiquitously expressed RBP is the assembly of snRNPs for mRNA splicing. However, neuronal SMN also helps in the assembly of RNP complexes used for axonal mRNA transport where they can be locally translated. Similar to TDP-43, reduced SMN levels result in impaired trafficking and reduced translation of various axonal transcripts, such as *growth-associated protein 43* (*GAP43*), *ActB*, and *neuritin/cpg15* (Fallini et al., 2012, 2016). Curiously, reduced SMN expression can be compensated via overexpression of other RBPs required for RNP granule assembly and transport, such as HuD (Akten et al., 2011) and ZBP1 (Fallini et al., 2016), implicating the role of SMN as an RNA transport regulator (Fallini et al., 2016). As mentioned above, FUS was also identified to interact with SMN in a study by Groen et al., with mutant FUS influencing this association, leading to SMN redistribution to FUS aggregates, and the following impairment in SMN axonal localization (Groen et al., 2013). This link between ALS and SMA supports the theory that different motor neuron disorders might be caused by defects in shared pathways (Groen et al., 2013). The above studies relating to ALS and SMN provide evidence that RBP dysfunction, and the consequent mis-localization of target mRNAs lead to alterations in local translation that underly the pathophysiological features of these diseases.

Sometimes, alterations in the axonal transcriptome can contribute to the pathophysiology of a disease, even though the disease is not directly associated with mutated genes coding for regulators of RNA processing. For example, mutations in the KIF5A gene have been linked to Charcot–Marie–Tooth disease type 2D (CMT2D) and ALS (Crimella et al., 2012; Nicolas et al., 2018). CMT is a group of hereditary peripheral neuropathies that cause loss of sensation and fine motor control at the extremities. More than 100 genes have been identified to cause CMT, with CMT1 being a demyelinating neuropathy, and CMT2 an axonal neuropathy (Markworth et al., 2021). CMT2B, caused by mutations in Ras-related protein 7 (Rab7), a lysosomal motor adaptor, shows a phenotype of significantly decreased axonal translation, dysfunctional axonal mitochondria, and widespread degeneration (Cioni et al., 2019). Targeted experimental models have helped identify the specific proteins whose translation is affected. During CMT4D neurodegeneration in DRG sensory neurons, Fukuda et al. showed that the splicing factor proline/glutamine-rich (SPFQ) RBP bound mRNA *Bclw* required for axon survival, was not transported to the axon, preventing its local translation (Fukuda et al., 2020). However, this effect was rescued by the axonal application of a Bclw peptide mimic, supporting the causal relationship between aberrant local translation and neurodegenerative diseases (Fukuda et al., 2020).

To summarise, different RBP or RNA-assembly protein abnormalities have been linked to different neurodegenerative disorders. As a lot of the identified interacting mRNAs are required for axonal functions, especially at the growth cones and synapses, we can agree that the axonal transport and local protein synthesis of these target transcripts is necessary for a healthy neuronal morphology, and synaptic and growth cone function. Dysfunction in these processes lead to degeneration of the axon terminals, disconnecting the neural network, leading to a diseased pathophysiology. It is important to appreciate the recent advances in understanding these neuronal diseases, however, we still need to dig further to understand the exact molecular mechanisms regulating RNA metabolism in neurons.

1.3 Experimental techniques to study RNA localization and translation

In this chapter I have described the experimental techniques used in my research, as well as additional methods and their advancements developed to study RNA localization and translation.

1.3.1 Imaging-based methods for RNA localization

Hybridization-based methods

In the early 1980s, when protein localization was connected to local mRNA translation, only one method was available to visualise RNA: ***in situ* hybridisation (ISH)** (Jeffery et al., 1983; Singer & Wardt, 1982). ISH is a method in which short DNA or RNA labelled probes with a complementary sequence are hybridised to the endogenous RNA sequence of interest in fixed cells or tissues. The first visualisation of asymmetric mRNA distribution in chicken muscle cells and ascidian eggs was for *actin* mRNA using biotinylated or radioactive probes (Jeffery et al., 1983; Singer & Wardt, 1982).

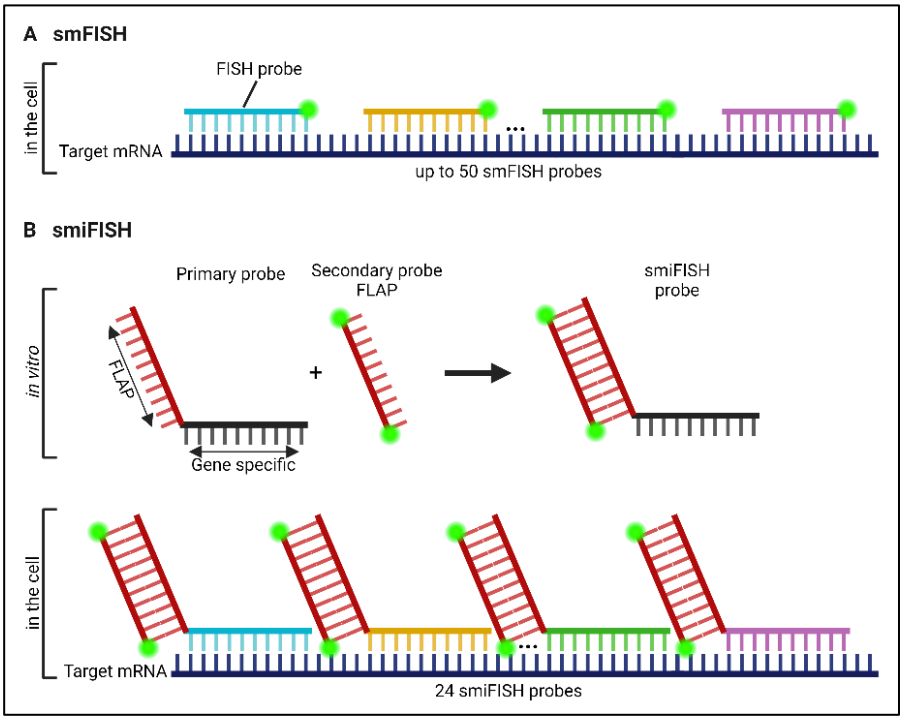

Figure 1.12: Single RNA detection using *in situ* hybridisation in fixed cells. (A) smFISH probes (~20 bases) labelled with a single fluorophore hybridise to the target gene sequence. Multiple probes on a single transcript produce a detectable fluorescence signal. **(B)** smiFISH probes indirectly label the transcript of interest. A secondary probe labelled with two fluorophores is pre-hybridised to 24 primary probes, resulting in hybridisation of these duplexes to the RNA. Adapted from (Pichon et al., 2018; and Tsanov et al., 2016). Created with BioRender.com.

With the development of fluorescence technologies, **fluorescence *in situ* hybridisation (FISH)** was developed utilising fluorescently labelled probes. As FISH is highly sequence specific and can distinguish RNAs that differ only by a single base, it allows for the specific detection of a single mRNA sequence. Along with the development of brighter fluorescence labels and more sensitive image detection we can

easily detect a single mRNA molecule. **Single-molecule FISH (smFISH)** utilises multiple fluorescent probes that hybridise to single mRNAs, enabling bright single-molecular detection (Figure 1.12A). Recent developments to this method have made it fast, multiplexed, and even high throughput (Battich et al., 2013; Levsky et al., 2002; Shaffer et al., 2013).

In 2016, Tsanov et al. made this method more affordable by developing **single molecule inexpensive FISH (smiFISH)**, a method that uses unlabelled primary probes along with a secondary detector oligonucleotide that is fluorescently labelled (Figure 1.12B) (Tsanov et al., 2016). As the gene-specific probes are unlabelled, they can be synthesised at a low cost, increasing the number of probes that can be used, resulting in an increased detection efficiency. The detector oligonucleotide is also labelled on both ends, doubling the detection intensity. smiFISH can also be used to visualise different targets simultaneously based on the fluorophore label of the secondary detector oligonucleotides (Tsanov et al., 2016).

Live-cell RNA tracking

Over the years, multiple methods have been developed for better visualisation and tracking of RNA movements in living cells. These genetic-based strategies usually involve an RNA of interest engineered with a genetic tag insertion that can be recognised by fluorescently labelled RBPs or small molecules.

The **MS2 system** was the first method published and successfully used to track single mRNA molecules in multiple organisms and cell types (Figure 1.13A) (Bertrand et al., 1998; Park et al., 2014). It is based on a high-affinity interaction of the MS2 coat protein (MCP) from bacteriophages with a specific 19nt MS2 RNA hairpin. A transgene is generated containing multimerised MS2 hairpins derived from a MS2 phage genome regulatory element and inserted into the 3' UTR of the mRNA of interest. These hairpins have multiple MS2-binding sites (MBS) that can be recognised by a green fluorescent protein (GFP)-fused MCP RBP expressed from another transgene (Bertrand et al., 1998). One advantage of this system is the capability to endogenously express both, the tagged mRNA target and the fluorescent marker protein binder, allowing for a more physiological experimental context. However, multiple drawbacks also exist, such as the time-consuming nature of generating a transgenic system, as well as the size of the MS2-fusion tag along with the hairpins on the RNA interfering with the normal functioning and localization of the mRNA.

Due to high background produced in this system by the unbound protein, modifications have been made to the binder RBPs, utilising fused **photoactivatable GFP** or fluorescence complementation approaches by using a **split-GFP** which only on dimerisation can fluoresce (Cody et al., 2013; B. Wu et al., 2014).

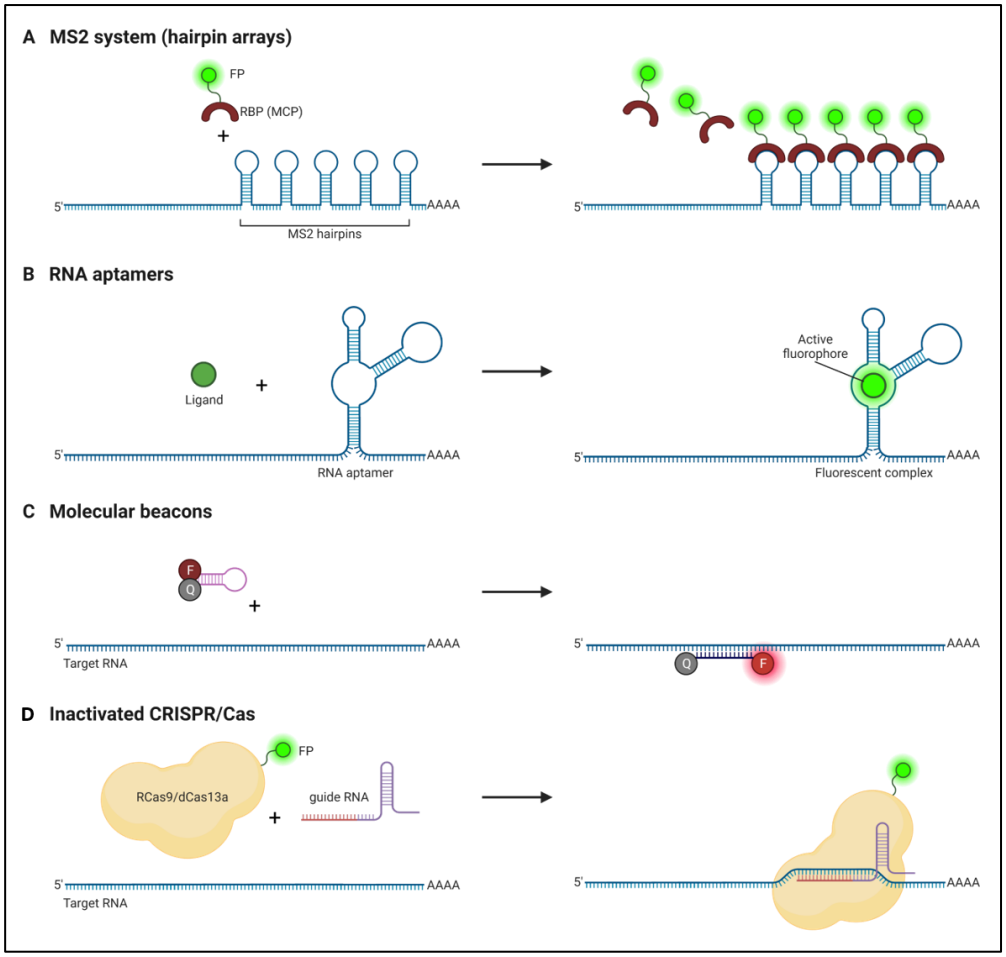

Figure 1.13: RNA visualisation methods in living cells. **(A)** An RBP/coat protein fused to a fluorescent protein (FP) binds to hairpin arrays engineered into the 3' UTRs of transcripts. **(B)** RNA aptamers are added to an RNA of interest, and small molecules on binding to the aptamers emit fluorescence. **(C)** Unbound probes exist as a hairpin with a fluorophore (F) in the vicinity of a quencher molecule (Q). On binding to target RNAs, the quencher moves away, releasing the fluorophore and enabling its fluorescence. **(D)** Inactivated CRISPR/Cas fused to a fluorescent protein (FP) can recognise target transcripts via the guide RNA, enabling fluorescence of the transcript. Adapted from (Pichon et al., 2018; and Taliaferro, 2019). Created with BioRender.com.

RNA aptamers, another form of nucleotide-base probes, are short, single stranded oligonucleotides that can also bind specific target molecules (Figure 1.13B). Paige et al. identified an aptamer named Spinach which emits a fluorescence similar to GFP only on binding of a specific small-molecule fluorophore (Paige et al., 2011). In this system, the reporter and probe are present on the same oligonucleotide that can be added to the mRNA of interest (Paige et al., 2011). Several RNA aptamers are currently available with a variety of spectral emissions, ranging from blue to red, that have been further enhanced for binding efficiency as well as strength of fluorescence, allowing the possibility for multiplexing mRNA targets for simultaneous visualisation (Dolgosheina et al., 2014; Paige et al., 2011). Similar to the MS2 system, RNA aptamers could potentially impede mRNA function or localization.

Molecular beacon (MB)-based imaging of single mRNA in living cells was first described in 2003 by Bratu et al. where they labelled *oskar* mRNA in *Drosophila* oocytes (Figure 1.13C) (Bratu et al., 2003). This method reduces background signal as the MB is a DNA probe with one end linked to a fluorophore, and the opposite end to a quencher. The unbound probe is folded into a hairpin structure, inhibiting fluorescence due to the interaction of the fluorophore and quencher. However, upon recognition of the target mRNA, the probe stretches out while annealing, enabling fluorescence due to the separation of the fluorophore and quencher. Initially, MB-based imaging utilised the genetic modification of an mRNA target to add an MB-tag. This tag contains multiple copies of one sequence that are recognised by the MBs, unquenching the fluorophore, thereby enabling fluorescence (Vargas et al., 2005). Alternatively, distinct MBs can be used to label different parts of an unmodified endogenous mRNA, directly labelling the mRNA without the need of genetic modification (Mao et al., 2020; Turner-Bridger et al., 2018).

In 2016, Nelles et al. described an **RNA-targeting Cas9 (RCas9)** to recognize unmodified endogenous mRNAs for live cell tracking (Figure 1.13D) (Nelles et al., 2016). As most RNA targeting methods, like those mentioned above, rely on the incorporation of an exogenous tag, the use of a nuclease-inactive CRISPR/Cas9 to bind specific RNAs in a nucleic-acid-programmed manner, allows for endogenous RNA tracking without genetic engineering of a cell. Utilising a nuclear-localized RCas9 along with guide RNAs targeting different mRNAs, they observed endogenous RCas9-GFP-mRNA localization outside the nucleus, that was comparable to the FISH signal for that specific mRNA (Nelles et al., 2016). This method allows for the live cell tracking of mRNA without interfering with normal RNA metabolism, and reduced background signal as unbound RCas9 is restricted to the nucleus (Nelles et al., 2016). Similarly, Abudayyeh et al. described the use of a catalytically inactive **Cas13a (dCas13a)** fused to a fluorescent protein that targets an mRNA of interest using specific guide RNAs (Abudayyeh et al., 2017).

1.3.2 NGS-based and high-throughput methods

Classically, researchers explored only one transcript at a time, investigating the mechanisms regulating its localization within a cell. These approaches included systematically testing the 3’ UTR sequences of the target mRNAs for the ability to localize a reporter transcript. This was followed by progressively decreasing the length of the 3’ UTR to identify a minimal element sufficient for localization. The sequence of this minimal element could provide information regarding the secondary structure, and potential RBPs that can bind to it. However, regardless of the success of this approach, it only revealed the zipcode or localization mechanisms for single transcripts, and could not be generalised to a larger group. Hence, high-throughput methods were developed that could assess RNA localization on a global scale. Similarly, high-throughput methods were also developed to identify the subcellular translatome, to investigate local translation. A few methods have been briefly described in the following sub-chapters.

Cellular separation-based systems for local transcriptome analysis

In order to understand RNA localization mechanisms and their local functions, we first need to elucidate the local transcriptome of a cell. Multiple techniques have been developed to isolate and analyse the subcellular transcriptomes, most of which utilise different variations of cellular fractionation coupled with RNA sequencing. Sequencing is followed by analysis to identify the enrichment and localization of specific transcripts between the different subcellular compartments.

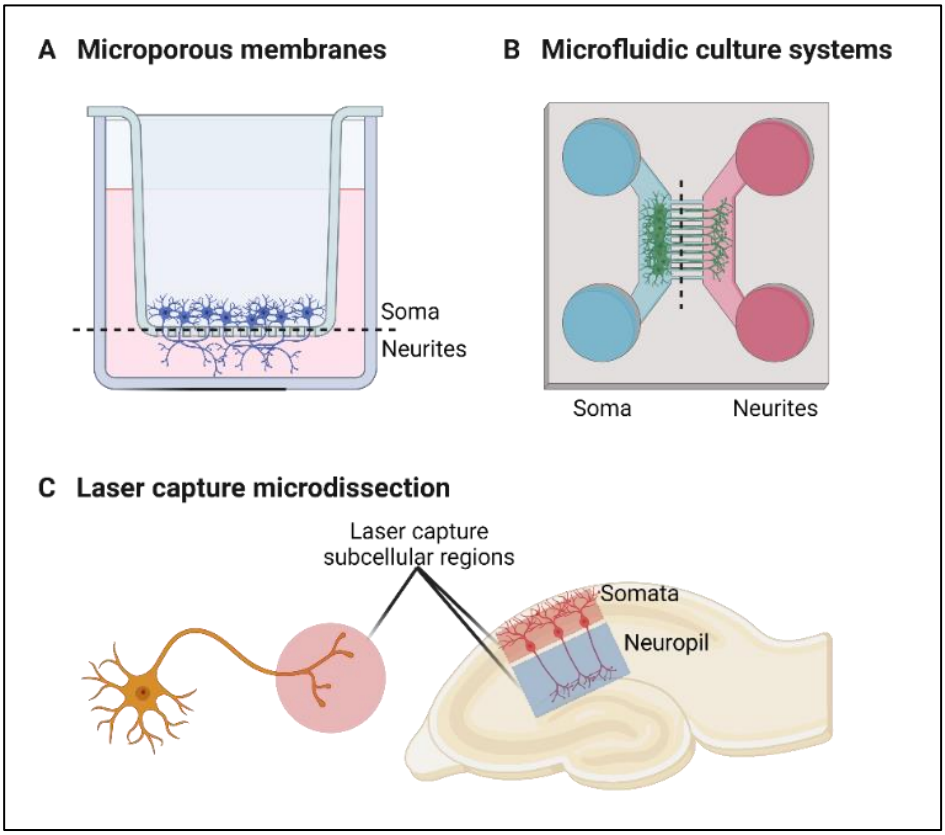

Figure 1.14: Cellular separation methods for local transcriptome analysis. (A) Cells like neurons, that have long and thin projections, can be grown on microporous membranes, such that the soma remains on the top, while the projections grow through the pores. The soma and neurites can be mechanically separated from the top and bottom of the membrane. **(B)** Neurons can also be grown on microfluidic devices, such that the axons grow through the narrow channels to the opposite side, hydrostatically separating them from the soma. The soma and axon compartments can be isolated separately for downstream analysis. **(C)** Laser capture microdissection can be used to dissect out subcellular compartments of cells, such as neuronal growth cones; or dissect out cellular compartments from a tissue section, such as the somata and neuropil of neurons in hippocampal slices. Adapted from (Glock et al., 3032; and Taliaferro, 2022)**.** Created with BioRender.com.

Microporous membranes. Taliaferro et al. in 2016, and Zappulo et al. in 2017, were the first to use microporous membranes for cellular fractionation of neurons (Figure 1.14A) (Taliaferro et al., 2016; Zappulo et al., 2017). The neurons can be mechanically separated into the cell body (soma) and neurite

fractions, followed by RNA extraction from both compartments. This RNA can then be analysed via high-throughput sequencing, resulting in a list of transcripts that are significantly enriched or more abundant in either compartment.

Depending on the size of the cells, they can be grown on membranes with pores usually between 1 to 3 µm in diameter. As the neurons develop, the pores are just big enough to allow the neurites to grow through, while the soma is restricted to the top of the membrane. Via pipetting or scraping the soma on the top, the soma can be mechanically removed, while the neurites remain on the bottom of the membrane. RNA is then extracted from the separated soma and neurite compartments (Ludwik et al., 2019).

Microfluidic culture systems. In microporous membranes, both axons and dendrites can grow through the pores, making it impossible to differentiate the transcripts from either structure. In order to provide a better spatial resolution of axonally localized transcripts, microfluidic culture systems were developed (Figure 1.14B).

Taylor et al. in 2005 described a microfluidic culture platform to polarize the growth of neuronal axons, hydrostatically separating the soma and dendrites, from the axon (Taylor et al., 2005). As this method allows for exact measurement of axonal growth, the distances can be adjusted to allow for precise separation of the axons at a specific distance from the soma (Taylor et al., 2005). This system has been used to identify localized transcripts in different mouse and human neurons (Briese et al., 2015; Taylor et al., 2009).

Laser capture microdissection. If culturing of cells is not an option, tissue sections of a region of interest have been utilised. When the cellular region of interest can be easily identified via microscopy, laser capture microdissection can be used to directly dissect this region out of a cell or tissue (Figure 1.14C). During this method, a targeted laser is used to remove the region of interest, followed by RNA extraction and analysis.

Zivraj et al. used laser capture microdissection to study the transcriptome of the neuronal growth cone (Zivraj et al., 2010). Cajigas et al. elucidated the local transcriptome of the synaptic neuropil via dissection of the soma and neuropil segments from mouse hippocampal slices, followed by RNA analysis (Cajigas et al., 2012). Although this is a precise technique that also allows for subcellular transcriptomic analysis within tissue sections, the amounts of RNA recovered are small, requiring specialized library and sequencing protocols.

Subcellular Transcriptomics via Proximity Labelling

Since cellular fractionation methods include all RNAs in a spatially specific compartment, regardless of their actual interaction, multiple proximity labelling techniques have been developed that specifically label RNA populations within a spatially defined region within a living cell. These labels can be used as handles to purify and analyse these specific RNAs. As described in earlier chapters, RNA localization is tightly linked to the RBPs that bind and transport them. Proximity labelling methods utilise this interaction of RNAs and proteins.

Proximity labelling methods were first developed to identify protein-protein interactions at a specific site, for example, newly translated transcripts at the ER surface via an *Escherichia coli*-derived BirA biotin ligase (Jan et al., 2014). Similarly, the **APEX system**, an engineered ascorbate peroxidase from soybean, catalyses the biotinylation of biomolecules in the vicinity of the APEX enzyme, with a radius of approximately 20nm. It was used by Rhee et al. to map the proteomic composition of the mitochondria (Rhee et al., 2013). However, to study the transcriptomic composition of subcellular regions, Kaewsapsak et al. combined the APEX labelling system with RNA-protein crosslinking, called **APEX-RIP** (Kaewsapsak et al., 2017). **APEX2**, the improved derivative, was fused to proteins that very specifically localize to the mitochondria or ER. After APEX-catalysed biotinylation on addition of hydrogen peroxide, followed by chemical crosslinking, the crosslinked proteins and RNAs can be affinity purified via a streptavidin pulldown, and the transcripts analysed via high-throughput sequencing (Kaewsapsak et al., 2017). Although APEX-catalysed activated biotin-phenol biotinylates proteins, it also directly labels RNA on guanosine residues. So, Fazal et al. utilised this property to obviate the need for crosslinking (**APEX-Seq**), and identified local transcriptomes at or near multiple organelles (Fazal et al., 2019).

CAP-seq is another proximity-labelling technique that is instead optically controlled via the miniSOG2 enzyme (P. Wang et al., 2019). Similar to APEX, miniSOG2 localization to subcellular regions is controlled via specific marker proteins that are genetically fused to it. On light-activation, transcripts in proximity to miniSOG2 had their guanosine nucleobases converted into products of photo-oxidation that could crosslink with propargylamine, resulting in their alkylation. These transcripts were extracted and then biotinylated *in vitro* via click chemistry, and finally analysed by high-throughput sequencing (P. Wang et al., 2019). Although CAP-seq is similar to the APEX2 system, CAP-seq requires longer labelling times (20 minutes) compared to APEX2 (1 minute), suggesting APEX2 as the method of choice for studying fast biological processes.

A recent proximity-labelling technique, **Halo-Seq**, was developed by Engel et al. (Engel et al., 2022). Following irradiation of a small molecule dibromofluorescein (DBF), reactive species are produced that label proximal RNA. Incorporation of DBF into a Halo ligand controls its location within the cell. Utilising

a spatially restricted protein genetically fused with the Halo Tag, DBF localization is restricted. On activation of DBF, the labelled transcripts are also alkylated and then biotinylated *in vitro* (Engel et al., 2022).

Although these techniques have expanded our ability to profile local transcriptomes, some regions are still inaccessible due to lack of a bait protein that is specifically localized to one region.

Spatial transcriptomics

Most methods for local transcriptomics lose spatial resolution, including positional information within a tissue. In 2016, Ståhl et al. described a new method of using a tissue section on reverse transcription primers containing unique positional barcodes to map the spatial distribution of RNA expression within the tissue section, allowing for reconstruction of the tissue morphology along with the transcriptomic patterns (Ståhl PL et al., 2016).

Spatial transcriptomic methods can be categorized into Next Generation Sequencing (NGS)-based, as described by Ståhl et al., and sequencing combined imaging-based methods such as *in situ* sequencing (ISS) using patterned DNA-barcoded arrays to which transcripts are amplified and sequenced in a tissue section (Rodriques et al., 2019), and global *in situ* hybridization (ISH) in which imaging probes are hybridized sequentially in a tissue section (K. H. Chen et al., 2015; Lubeck et al., 2014). Chen et al. even developed Stereo-seq, an approach combining DNA nanoball-patterned arrays and *in situ* RNA capture and library generation, allowing up to a 400 unique barcode combination within a cell (A. Chen et al., 2022). Using this method, they mapped the spatiotemporal transcriptomic patterns during mouse organogenesis (A. Chen et al., 2022).

Identification of RNA localization regulatory elements

All the above techniques can be used to identify the different transcripts localized to subcellular compartments, but do not give us direct information on which regulatory elements helped them get there.

As explained in chapter 1.2.1.2, RNA localization regulatory elements are usually present within the mRNA 3’ UTR, and regulated via binding of RBPs. Due to their short, degenerate sequence that usually require certain secondary structures for RBP recognition and binding, it is difficult to computationally predict and validate *cis*-elements. To identify RNA binding sequences *in vivo*, many methods combining

crosslinking with RBP immunoprecipitation followed by high-throughput sequencing were developed, such as **RIP-Seq** (RNA immunoprecipitation), **HITS-CLIP** (High-throughput sequencing of RNA isolated by crosslinking immunoprecipitation), and **PAR-CLIP** (Photoactivatable-Ribonucleoside-Enhanced CLIP).

The **perturbation of specific RBPs** followed by analysis of the local transcriptome was also used to identify mislocalized transcripts. These transcripts might contain a common sequence bound by the perturbed RBP, suggesting the presence of a localization element. This approach was used for a few RBPs, elucidating the transcripts whose localization is affected by them. For example, analysis of the local transcriptome in neurons of FMRP-null mouse, resulted in the identification transcripts that require FMRP for neuritic transport (Goering et al., 2020). Further analysis of these transcripts showed an enrichment of 3' UTR G-quadruplex sequences, identifying a localization regulatory element (Goering et al., 2020).

However, all these methods are labour intensive and/or require prior knowledge of specific RBPs.

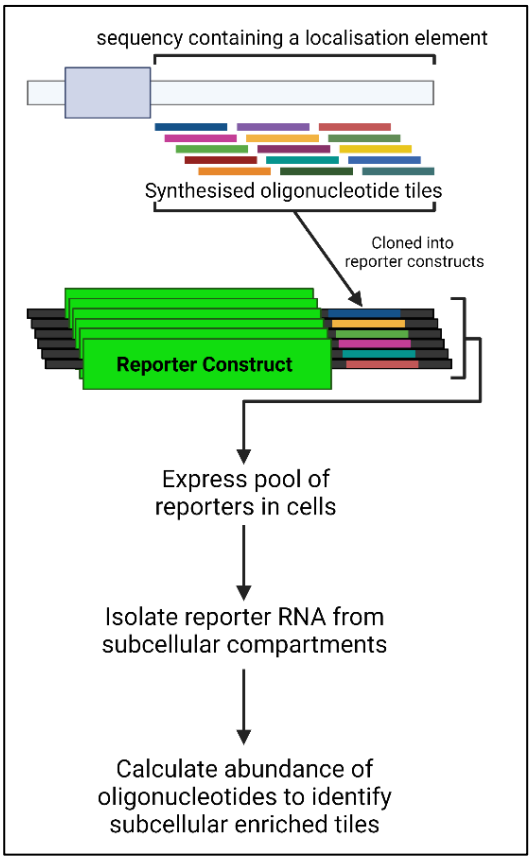

Figure 1.15: MRPA design and application. Fragments tiled across the 3' UTRs of transcripts of interest are synthesised and cloned into reporter constructs. This generates a library of reporter constructs differing only by the inserted tile sequence. This library is expressed in a cellular system, followed by separation into different subcellular compartments. The reporter RNA is extracted from both compartments, and analysed via RNA-Seq. Localized tiles from each 3' UTR showing enrichment in one compartment in comparison to the other tiles from the same transcript, suggest the presence of a localization element within those tiles whose sequence can be identified and validated. Adapted from (Mendonsa et al., 2023; and Taliaferro, 2022). Created with BioRender.com.

High-throughput or **massively parallel reporter assays (MPRAs)** were initially developed to identify regulatory elements that affect transcript stability and translation (Elemento et al., 2007; Lubelsky & Ulitsky, 2018; Rabani et al., 2017; Yartseva et al., 2017), and recently to study the localization of linear and circular RNAs due to sequence elements (Ron & Ulitsky, 2022). These assays allow for the dissection of RNA metabolism for thousands of sequences in parallel. Generally, a library is generated that contains a base construct that is varied to contain one of thousands of sequences. Any differences observed can therefore be linked to the inserted sequence, suggesting the presence of a regulatory element.

MPRAs have recently been developed for the purpose of RNA localization element identification (Figure 1.15). Three studies, including my research, utilised this method in neuronal systems (Arora et al., 2022; Mendonsa et al., 2023; Mikl et al., 2022). 3'UTRs from a pool of transcripts were fragmented and inserted into a reporter construct to generate a library of reporter transcripts. This library was expressed in neuronal cells, followed by their separation into soma and neurites from microporous membranes. RNA-Seq analysis elucidated fragments that were more abundant in a specific compartment, containing putative localization regulatory elements that were validated using different methods. I will further elaborate on the design and use of MPRAs to identify RNA localization elements in the general discussion.

Global analysis of translation via NGS

Many studies that used quantitative proteomics and transcriptomics on a global scale highlight the low correlation between mRNA and protein levels in different biological systems, suggesting post-transcriptional regulation of gene expression (Dermit et al., 2017). Multiple methods have been developed to quantify translation, using mRNA association with translating ribosomes as a proxy to estimate the rates of translation. A few methods to study global translation are described below.

Ribosome profile (Ribo-Seq), developed by Ingolia et al. in 2009, captures a snapshot of translation on a genome-wide scale, with position sensitive nucleotide resolution (Figure 1.16A) (Ingolia et al., 2009). In this method, translation is stopped with the use of cycloheximide, an inhibitor of ribosome translocation, rapid detergent-based lysis, or flash-freezing. The mRNA-ribosome complexes are subjected to nuclease footprinting, resulting in a monosome population containing 20-30nt ribosome protected mRNA fragments (RPFs). Once these RPF containing monosomes are recovered via sedimentation, the RPFs are purified and analysed via RNA-Seq. These RFP sequences can be identified and quantified, providing us with the exact identity of all translating open reading frames (ORFs) at a global level (Ingolia et al., 2012).

Ribo-Seq has also revealed the translation of noncanonical ORFs, including translation from non-AUG start codons or alternative start sites, overlapping ORFs, and instances where the stop codon is bypassed; as

well as translation of upstream ORFs (uORFs) and short ORFs (sORFs) present in previously assumed non-coding RNAs (Dunn et al., 2013; Ingolia et al., 2011, 2019). As Ribo-Seq combined with RNA-Seq captures an instant snapshot of translation with extreme sensitivity and range, this method is ideal for quantification of temporal translation changes. Ribo-Seq has also been adapted over the years to resolve the different ribosome functional states observed during translation elongation (C. C. C. Wu et al., 2019).

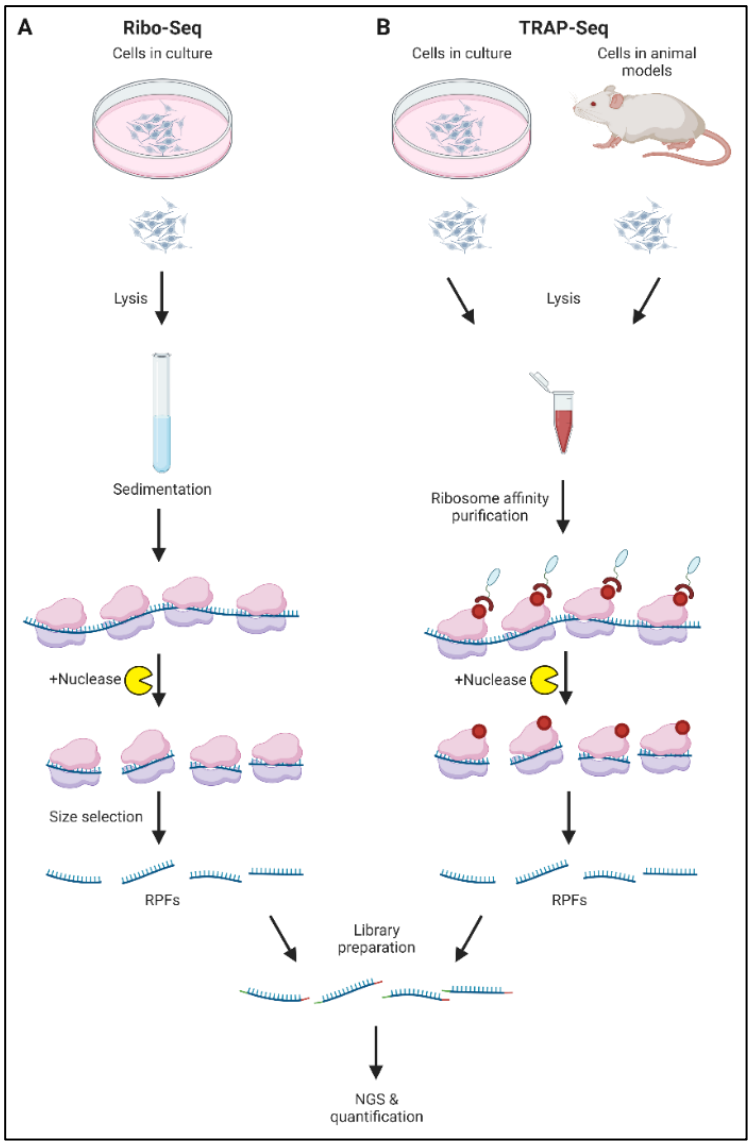

Figure 1.16: Methods for global analysis of translation via NGS. (A) In Ribo-Seq, cells are lysed and translating ribosomes are purified via sedimentation. Unprotected RNA regions are degraded via nuclease treatment, resulting in 20-30nt ribosome protected fragments (RPFs) called ribosome footprints. These footprints are used to generate a library, followed by RNA-Seq and analysis. The read densities obtained after sequencing, can be used to identify individual ORFs, and quantify translation rates. These footprint reads have a distinctive three nucleotide periodicity, indicative of translocation of the ribosome throughout the ORF length. **(B)** TRAP-Seq allows for ribosome purification via immunoprecipitation of epitope tagged ribosomal proteins stably expressed in cells *in vitro* or transgenically in a specific cell-type *in vivo*. These purified ribosomes then follow a similar protocol as in Ribo-Seq, including nuclease treatment, library preparation, and RNA-Seq**.** Adapted from (Dermit et al., 2017)**.** Created with BioRender.com.

Heiman et al. developed **translating ribosome affinity purification-sequencing (TRAP-Seq)** as an alternative to ribosome sedimentation as in Ribo-Seq (Figure 1.16B) (Heiman et al., 2014). TRAP-Seq uses ribosome proteins that are epitope tagged, enabling translating ribosome purification via immunoprecipitation (Heiman et al., 2014). An interesting use of this method is the ability to transgenically express epitope tagged ribosomal proteins in specific cell types *in vivo*, allowing us to monitor cell-specific translation from an animal model (Thomas et al., 2012).

Recently, the labs of Oudenaarden and Cenik have taken Ribo-Seq a step further, adapting the method for the quantification of translational dynamics at the single cell level (**Single-cell Ribo-seq**), enabling scientists the technology to elucidate the contribution of translation to cellular diversity in an organism without the need for genetic engineering (Tonna et al., 2021; VanInsberghe et al., 2021).

Along with cellular separation, Zappulo et al. also used Ribo-Seq to identify local translational changes in mouse embryonic stem cell derived neurons, to elucidate the relationship between the local transcriptome and proteome (Zappulo et al., 2017). Similarly, other labs have utilised a combination of different cellular separation methods (microdissection or microfluidic devices) with Ribo-Seq, to identify the local translatome (Glock et al., 2017, 2021). On the other hand, Jan et al. also adapted Ribo-Seq to study the local translatome by adding a proximity-specific adaptation - **proximity-specific Ribo-Seq** (Jan et al., 2014). Rather than the use of an epitope tag as in TRAP-Seq, they tagged ribosomal proteins with a biotin acceptor peptide, called the Avi Tag. Along with the targeting of a biotin ligase, BirA, to a specific subcellular compartment, specific ribosomes in the vicinity can be biotinylated through a biotin pulse, followed by a streptavidin purification and Ribo-Seq (Jan et al., 2014).

Regardless of how brilliant these methods are, the low starting materials combined with their cost, and long experimental and analysis times, add to its drawbacks. Nevertheless, these methods have added enormously to our knowledge of RNA metabolism and the proteome.

Proteomics-based analysis of translation

As mentioned above, Ribo-Seq and its adaptations use mRNA association with ribosome as a proxy for translation. Alternatively, proteomics-based methods have been developed to assess translation via the direct identification and quantification of nascent peptides. These methods include the labelling of nascent proteins combined with their purification and quantification via mass spectrometry (MS).

Pulsed-SILAC (p-SILAC) developed by Selbach et al. utilised the stable isotope labelling of amino acids in culture (SILAC) to metabolically label newly synthesised proteins (Figure 1.17A) (Selbach et al., 2008). As p-SILAC uses a pulse of stable isotopologues of arginine (Arg) and lysine (Lys), the newly synthesised

proteins are labelled at the time of the pulse. The cells are initially cultured in media containing unlabelled 'light' Arg and Lys. For the duration of the pulse, the media is changed to include 'medium' (Arg^6 and Lys^4) or 'heavy' (Arg^{10} and Lys^8) labelled SILAC amino acids. The samples can then be harvested, combined and processed together, followed by peptide analysis using liquid chromatography and tandem MS (LC-MS/MS) (Selbach et al., 2008). The proteins containing the labelled amino acids are then identified and quantified, providing information regarding translation rates in mammalian cell cultures, and how protein translation contributed towards cellular protein steady-state levels (Schwanhüusser et al., 2011). Since the uptake of pulsed amino acids takes hours as they need to be conjugated to tRNAs before incorporation into nascent peptides, p-SILAC cannot be used for temporal resolution of translation dynamics. However, the biggest advantages of this approach are the low sample required, and minimal sample processing without any biochemical purification, enabling quantification of translation dynamics in subcellular fractionations (Dermit et al., 2017).

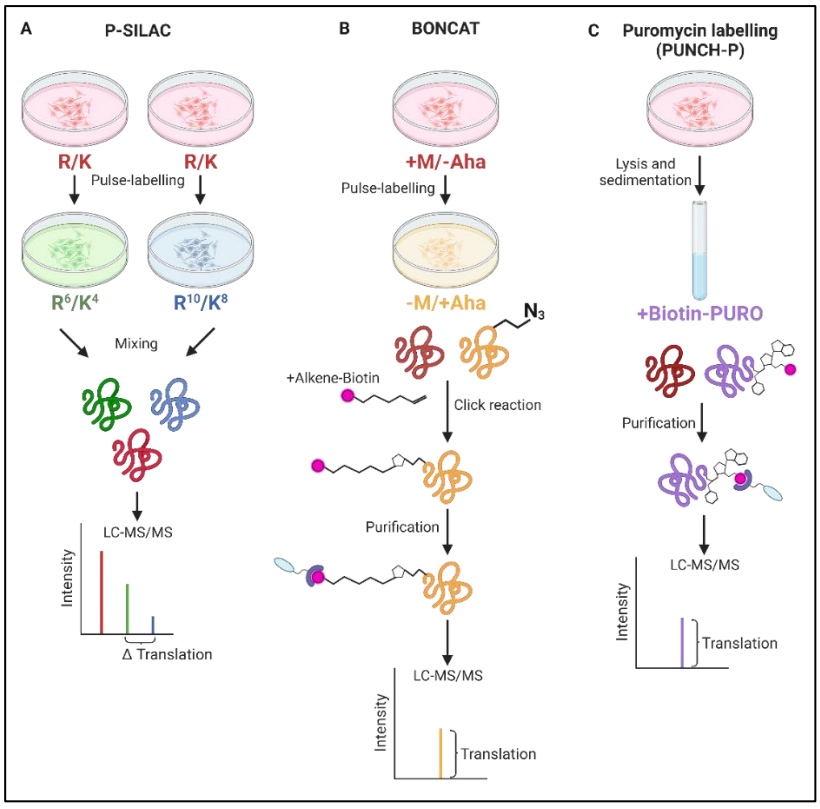

Figure 1.17: Methods for proteomics-based global analysis of translation. (A) P-SILAC directly quantifies the differences in rates of newly synthesised proteins via LC-MS/MS by comparing intensity ratios of the SILAC pulsed labelled nascent proteins, K^4/R^6 vs. K^8/R^{10}. The unlabelled proteins (K^0/R^0) are not analysed. **(B)** BONCAT uses a similar concept as p-SILAC, instead using non-canonical amino acids – the methionine analogue azidohomoalanine (Aha), containing an active azide (N^3) moiety. Pulse labelled Aha proteins are covalently bound to a tag, like biotin, using click chemistry, enabling streptavidin pulldown of the proteins followed by identification via LC-MS/MS. **(C)** Variants of the puromycin antibiotic can be used for labelling and purification of newly synthesised proteins. In PUNCH-P, post lysis, the translating ribosomes are purified via sedimentation, followed by labelling of the newly synthesised proteins *in vitro*, using a Biotin-PURO conjugate. The labelled nascent proteins are purified using streptavidin, and identified via LC-MS/MS. Adapted from (Dermit et al., 2017; and Gamarra et al., 2021). Created with BioRender.com.

Another metabolic labelling method to assess global translation is **bio-orthogonal non-canonical amino acid tagging (BONCAT)** (Figure 1.17B) (Dieterich et al., 2010). Instead of using stable isotopologues, BONCAT labels nascent proteins with pulses of non-canonical amino acids. Dieterich et al. used a methionine analogue containing an active azide moiety, azidohomoalanine (Aha), that incorporates into nascent proteins instead of the canonical counterpart Methionine, due to some aa-tRNA synthetases having a permissive nature (Dieterich et al., 2006). The incorporated amino acids can also be coupled to affinity tags like biotin via Click chemistry, or to fluorescent compounds as used in fluorescent non-canonical amino acid tagging (FUNCAT), allowing the visualization of protein translation (Dieterich et al., 2010). The biotin labelled proteins can then be purified and quantified via LC-MS/MS. A major limitation of these methods is the low affinity of non-canonical amino acids to aa-tRNA synthetases.

The antibiotic **puromycin** is an alternative method to label nascent proteins. Produced by the bacterium *Streptomyces*, Puromycin in an aminonucleoside that inhibits translation elongation. Puromycin strongly resembles the 3' terminal end of the conjugate of tyrosyl-tRNA, providing it with the ability to occupy the ribosome A-site during translation elongation, and incorporating non-selectively into the nascent peptide chain via the peptidyl-transferase enzyme. Since the peptidyl chain containing puromycin cannot incorporate more amino acids, translation is prematurely terminated, releasing the puromycinylated peptide from the translating ribosome (Yarmolinsky & de La Haba, 1959). These puromycinylated newly synthesized protein can be directly visualised or detected via microscopy (Puro-PLA (Tom Dieck et al., 2015)), western-blotting, or fluorescence-activated cell sorting (FACS) with an anti-puromycin antibody (Schmidt et al., 2009). Alternatively, for global profiling and quantification of newly synthesized proteins, **puromycin-associated nascent chain proteomics (PUNCH-P)** uses Biotin-PURO, a biotinylated variant of puromycin, followed by LC-MS/MS (Figure 1.17C) (Aviner et al., 2013). As low concentrations of puromycin can be rapidly incorporated into nascent peptides in a timescale of minutes, this method can be used for temporal resolution of translation dynamics (Dermit et al., 2017).

2. Aims

The present thesis is focused on investigating two crucial questions in the field of neurodegeneration and RNA localization in neurons.

Cis-regulatory elements in mRNAs mediating localization

In the early 1990s, Rob Singer proposed that RNA localization in cells is regulated by *cis*-acting elements in the 3' UTR, referred to as "RNA zipcodes". These zipcodes recruit RNA Binding Proteins (RBPs) to facilitate localization of mRNA molecules. Decades of research have shown that mRNAs are localized and translated in the distal compartments of neurons such as dendrites and axons, providing an effective system to study RNA localization. However, very few zipcodes have been identified, regardless of the localization of hundreds of mRNAs to the neurites.

Therefore, I aimed to characterise neuronal zipcodes that were identified utilising high-throughput assays. Our lab developed a novel neuronal zipcode identification protocol (N-zip) to identify zipcodes across hundreds of 3' UTRs all at once. The combination of this protocol and spatial transcriptomics of mouse primary cortical neurons led to the identification of the *let-7* binding site and $(AU)_n$ motif as novel zipcodes. My main goal was to understand the functional mechanisms of these zipcode-containing transcripts. The resulting analysis revealed the involvement of *trans*-acting factors (i) *let-7*, a miRNA involved in the miRISC degradation complex, and (ii) HBS1L, an RBP involved in mRNA quality control pathways, and showed that *let-7* miRNA and HBS1L RBP mediated localization by destabilizing target mRNAs in the soma, leading to increased transcripts in the distal neurites.

Role of mutations in aminoacyl-tRNA synthetases in Charcot-Marie-Tooth disease

In many neurological disorders, localization and local translation of specific transcripts is affected, contributing to the onset and progression of the disease. The study focused on investigating Charcot-Marie-Tooth (CMT) disease type 2D, caused by mutations in the glycyl-tRNA synthetase (GARS) gene.

My main aim was to understand the mechanisms by which translation is affected in CMT2D. Using Ribo-Seq and other molecular biology assays, I explored the effects of $tRNA^{Gly}$ sequestration by mutant GARS. Further analysis also revealed a secondary mechanism of translational repression via the activation of the Integrated Stress Response (ISR).

3. Massively parallel identification of mRNA localization elements in primary cortical neurons

Samantha Mendonsa*, Nicolai von Kügelgen*, Sayaka Dantsuji*, Maya Ron*, Laura Breimann, Artem Baranovskii, Inga Lödige, Marieluise Kirchner, Meret Fischer, Nadja Zerna, Lucija Bujanic, Philipp Mertins, Igor Ulitsky & Marina Chekulaeva

* These authors contributed equally

This chapter was published on 16 January 2023:

Nature Neuroscience (2023)

Volume 26 Issue 3, pages 394–405

DOI: 10.1038/s41593-022-01243-x

Link: https://doi.org/10.1038/s41593-022-01243-x

Extended data for this publication is detailed in Appendix I.

nature neuroscience

Article

https://doi.org/10.1038/s41593-022-01243-x

Massively parallel identification of mRNA localization elements in primary cortical neurons

Received: 14 December 2021

Accepted: 1 December 2022

Published online: 16 January 2023

Check for updates

Samantha Mendonsa[1,2,6], Nicolai von Kügelgen[1,2,6], Sayaka Dantsuji[1,6], Maya Ron[3,6], Laura Breimann[1,4], Artem Baranovskii[1], Inga Lödige[1], Marieluise Kirchner[5], Meret Fischer[1], Nadja Zerna[1], Lucija Bujanic[1], Philipp Mertins[5], Igor Ulitsky[3] ✉ & Marina Chekulaeva[1] ✉

Cells adopt highly polarized shapes and form distinct subcellular compartments in many cases due to the localization of many mRNAs to specific areas, where they are translated into proteins with local functions. This mRNA localization is mediated by specific *cis*-regulatory elements in mRNAs, commonly called 'zipcodes'. Although there are hundreds of localized mRNAs, only a few zipcodes have been characterized. Here we describe a novel neuronal zipcode identification protocol (N-zip) that can identify zipcodes across hundreds of 3′ untranslated regions. This approach combines a method of separating the principal subcellular compartments of neurons—cell bodies and neurites—with a massively parallel reporter assay. N-zip identifies the let-7 binding site and $(AU)_n$ motif as de novo zipcodes in mouse primary cortical neurons. Our analysis also provides, to our knowledge, the first demonstration of an miRNA affecting mRNA localization and suggests a strategy for detecting many more zipcodes.

Delivery of mRNAs to specific subcellular locations is a key mechanism to produce localized pools of proteins. This process occurs in organisms as diverse as yeast, plants, insects and vertebrates (reviewed in ref. [1]). It is particularly prominent in highly polarized cells, such as oocytes, migrating cells and neurons. For example, the development of the embryonic body axes in the *Drosophila* oocyte relies on the asymmetric localization of four maternal mRNAs: *gurken*, *bicoid*, *oskar* and *nanos* (reviewed in ref. [1]). Neuronal functions also depend on specific patterns of mRNA localization to cell bodies (soma) and extensions (neurites). For example, in developing neurons, localization of β-actin mRNA to growth cones plays an essential role in axon guidance[2,3].

The localization is thought to be mediated by *cis*-regulatory elements ('zipcodes') that are usually found in mRNA 3′ untranslated regions (UTRs)[4]. Zipcodes are bound by specific RNA-binding proteins (RBPs) that link their targets to transport machinery or regulators of mRNA stability and direct mRNAs to the sites of function. A few zipcodes and their bound RBPs have been described so far. Localization of β-actin is mediated by a 54-nucleotide (nt) zipcode, which targets mRNA to the cell periphery[5]. Zipcode-binding protein 1 (ZBP1) was identified as a binder of the *β-actin* zipcode, playing a role in both localization and translational control[6,7]. The cytoplasmic polyadenylation element (CPE) and its binding protein CPEB also facilitate transport to dendrites of several mRNAs, including *Map2* (microtubule-associated

[1]Max-Delbrück-Center for Molecular Medicine in the Helmholtz Association (MDC), Berlin Institute for Medical Systems Biology (BIMSB), Berlin, Germany. [2]Free University Berlin, Berlin, Germany. [3]Department of Immunology and Regenerative Biology and Department of Molecular Neuroscience, Weizmann Institute of Science, Rehovot, Israel. [4]Department of Genetics, Harvard Medical School, Boston, MA, USA. [5]Core Unit Proteomics, Berlin Institute of Health at Charite-Universitätsmedizin Berlin and Max-Delbrück-Center for Molecular Medicine in the Helmholtz Association (MDC), Berlin, Germany. [6]These authors contributed equally: Samantha Mendonsa, Nicolai von Kügelgen, Sayaka Dantsuji, Maya Ron. ✉e-mail: igor.ulitsky@weizmann.ac.il; marina.chekulaeva@mdc-berlin.de

protein 2)[8] and *Bdnf* (brain-derived neurotrophic factor)[9]. Localization of other transcripts with essential functions in neurites, such as *CaMKIIa* (Ca^{2+}/calmodulin-dependent protein kinase II subunit α)[10], *Arc* (activity-regulated cytoskeleton-associated protein)[11] and *Mapt* (microtubule-associated protein tau)[8], was also reported to depend on sequences in their 3′ UTRs.

High-throughput analyses have demonstrated specific localization patterns for hundreds to thousands of mRNAs in diverse organisms and cell types[12–25]. Presumably, many of these events rely on a similar mechanism, but, to date, only a few zipcodes have been characterized. Here we report the development of a method to systematically map neuronal zipcodes transcriptome-wide. Our approach combines a massively parallel reporter assay (MRPA) with the isolation of neuronal subcellular compartments: soma and neurites. We identify the let-7 binding site and $(AU)_n$ motif as de novo zipcodes in mouse primary cortical neurons (PCNs). To our knowledge, our work provides the first demonstration of an miRNA affecting mRNA localization.

Results

Development of the neuronal zipcode identification protocol

To perform an unbiased transcriptome-wide analysis of zipcodes, we developed the neuronal zipcode identification protocol (N-zip). This combines MPRA[26] with a neurite/soma fractionation scheme established previously[24,25,27] (Fig. 1a). As the input for N-zip, we selected 99 transcripts localized to neurites in mouse PCNs (Extended Data Fig. 1a) and at least one other published dataset generated from primary neurons: dorsal root ganglia, cortical, hippocampal or motor neurons[20–22,28–31]. To narrow down regions containing potential zipcodes, we designed a pool of 4,813 oligos, 75–110 nt in length, tiled across 3′ UTRs of selected neurite-enriched transcripts with 15–25-nt offset (Supplementary Table 1). The oligos were cloned into the 3′ UTR of GFP reporter, and the resulting pooled lentiviral library was delivered into PCNs. Infected neurons were cultured on a microporous membrane so that soma stayed on top of the membrane, and neurites grew through the pores on the lower side[25]. We isolated neurites and soma, carried out RT–PCR and prepared amplicon sequencing libraries, referred to as N-zip libraries. Western blotting confirmed the separation efficiency between neurites and soma (Extended Data Fig. 1b).

The term 'mRNA localization' has been used in two different ways: to signify the mere presence of mRNA in neurites and as an enrichment of mRNA in neurites versus soma. Because enrichment points to active localization, we focus on transcripts enriched in neurites. Our analysis of triplicate N-zip libraries identified 65 neurite-localized tiled fragments or tiles (Supplementary Table 1 and Fig. 1b). These tiles mapped to 33 out of 99 transcripts included in the library. For example, we detected a neurite localization of tiles 7–10 from *Mcf2l* (*Mcf2l*-7–10), which encodes the guanine nucleotide exchange factor for CDC42 and RHOA. This protein mediates the formation and stabilization of the glutamatergic synapses and is associated with intellectual disability and autism[32]. Similarly, we observed a neuritic enrichment of *Utrn*-61, which encodes a component of a dystrophin glycoprotein complex. This complex links the actin cytoskeleton to the extracellular matrix and plays a role in forming neuromuscular junctions[33]. Among other transcripts with a neurite-localized tile were cell growth and survival regulators *Rassf3* (ref. [34]) and *Cflar*[35] as well as *Cox5b*, which encodes a mitochondrial enzyme.

Neural stimulation was reported to enhance localization of certain mRNAs (reviewed in ref. [1]). Such stimulation modulates the depolarization of neurons; therefore, we decided to analyze how depolarization affects localization of the N-zip reporter library. For that, we treated PCNs, grown on a microporous filter, with potassium chloride (KCl) (Extended Data Fig. 2a). As a proof that cells responded to the depolarizing stimulus, we showed an increase in levels of *c-Fos* and *Egr1*, whose expression is triggered by depolarization[36] (Extended Data Fig. 2b). We then prepared N-zip libraries from such depolarized and control non-depolarized neurons. Depolarization affected localization of 123 tiles from 51 transcripts (DESeq2 adjusted $P < 0.05$ for difference in neurites/soma ratios), out of which 55 became more neurite-enriched and 68 became more soma-enriched. Curiously, among them were transcripts encoding ribosomal proteins and *Adcy1* (adenylyl cyclase type 1), which plays an essential role in synaptic plasticity[37] (Extended Data Fig. 2c).

We performed a comprehensive motif analysis on neurite-localized tiles using the XSTREME tool from the MEME suite[38]. Among identified motifs, there were UYCUACCUCAGA (Y: pyrimidine, C or U), AU-rich, GU-rich and C-rich motifs (Extended Data Fig. 3a). Further sequence analysis showed that neurite-localized tiles have no bias in GC content and a low tendency to form secondary structures (Extended Data Fig. 3b). Curiously, Gene Ontology (GO) term analysis showed that transcripts with neurite-localized tiles are linked with local neuronal structures and processes, such as synapse, actin cytoskeleton and cell polarity (Extended Data Fig. 3c).

To fine-map the sequences that mediate localization, we performed extensive mutagenesis of 16 neurite-localized fragments. We generated a secondary N-zip library with 6,266 sequences (Fig. 1a). In these cases, we (1) introduced every possible single point mutation; and (2) mutated G ↔ C and A ↔ U within 2-nt, 5-nt and 10-nt windows (Supplementary Table 2). This analysis identified two specific motifs required for localization to neurites: CUACCUC and $(AU)_n$ (Fig. 2). Notably, both motifs were also identified in our motif analysis of the tiled library (Extended Data Fig. 3a).

Mutations in CUACCUC shifted the localization of *Cflar*-14, *Mcf2l*-7 and *Utrn*-61 toward soma. Any mutation of $(AU)_8$ in *Rassf3-91* markedly reduced neurite enrichment. Similarly, the *Cox5b-6* $(AU)_6$ motif was essential for localization, with contributions from flanking U and A bases and from an additional $(U)_{11}$ stretch. This latter region could tolerate mutations to A but not to G or C. The results of single point mutations were confirmed by mutagenesis of 2-nt, 5-nt and 10-nt windows (Extended Data Fig. 4a).

In both the original and the secondary library, $(AU)_n$ was associated with neurite localization for $n \geq 6$. In the original library, these motifs were also found in *Map2*-29–32, *Ppp1r9b*-56–59, *Shank3*-58–60 and *Tmcc2*-36–39 tiles, and some showed conservation in other mammals (Extended Data Fig. 4b). Curiously, in some cases, our mutagenesis introduced CUACCUC and $(AU)_n$ stretches into heterologous sequences (Extended Data Fig. 5). These artificially created motifs resulted in neuritic localization of the fragment, showing that these motifs are not only necessary but also sufficient for localization to neurites.

Let-7 directs localization of its target mRNAs to neurites

Analysis of miRbase[39] showed that the CUACCUC motif, which we identified as a de novo zipcode in N-zip (Fig. 2), represents the binding site for the seed of the let-7 miRNA family (Fig. 3a, top). miRNAs regulate gene expression by pairing with complementary sites in their target mRNAs; this recruits a complex of proteins that destabilizes the mRNAs[40]. The miRNA seed is a conserved sequence at positions 2–7 from the miRNA 5′ end, which binds to target mRNAs via a perfect base-pairing. Indeed, every point mutation in CUACCUC affected localization of tiles containing this motif (Fig. 2b). This is to be expected from an miRNA seed site but not from a consensus RBP motif. Furthermore, in mouse brain, the position of CUACCUC in *Utrn-61* matched the summit of a cross-linking immunoprecipitation (CLIP) peak for AGO2 (ref. [41]), which is the core component of the miRNA repression complex (Fig. 3a, bottom).

To confirm that the let-7 binding sites in *Cflar*-14, *Mcf2l*-7 and *Utrn*-61 are functional, we performed a luciferase reporter assay (Fig. 3b). As a positive control, we used a reporter bearing the *Hmga2* 3′ UTR (Hmga2-wt), a validated let-7 target[42]. Endogenously produced in HeLa cells, let-7 repressed Hmga2-wt >5-fold compared to a mutant version lacking let-7 sites (Hmga2-mut). We generated analogous luciferase reporters bearing the tested tiles in their 3′ UTRs (Mcf2l-wt,

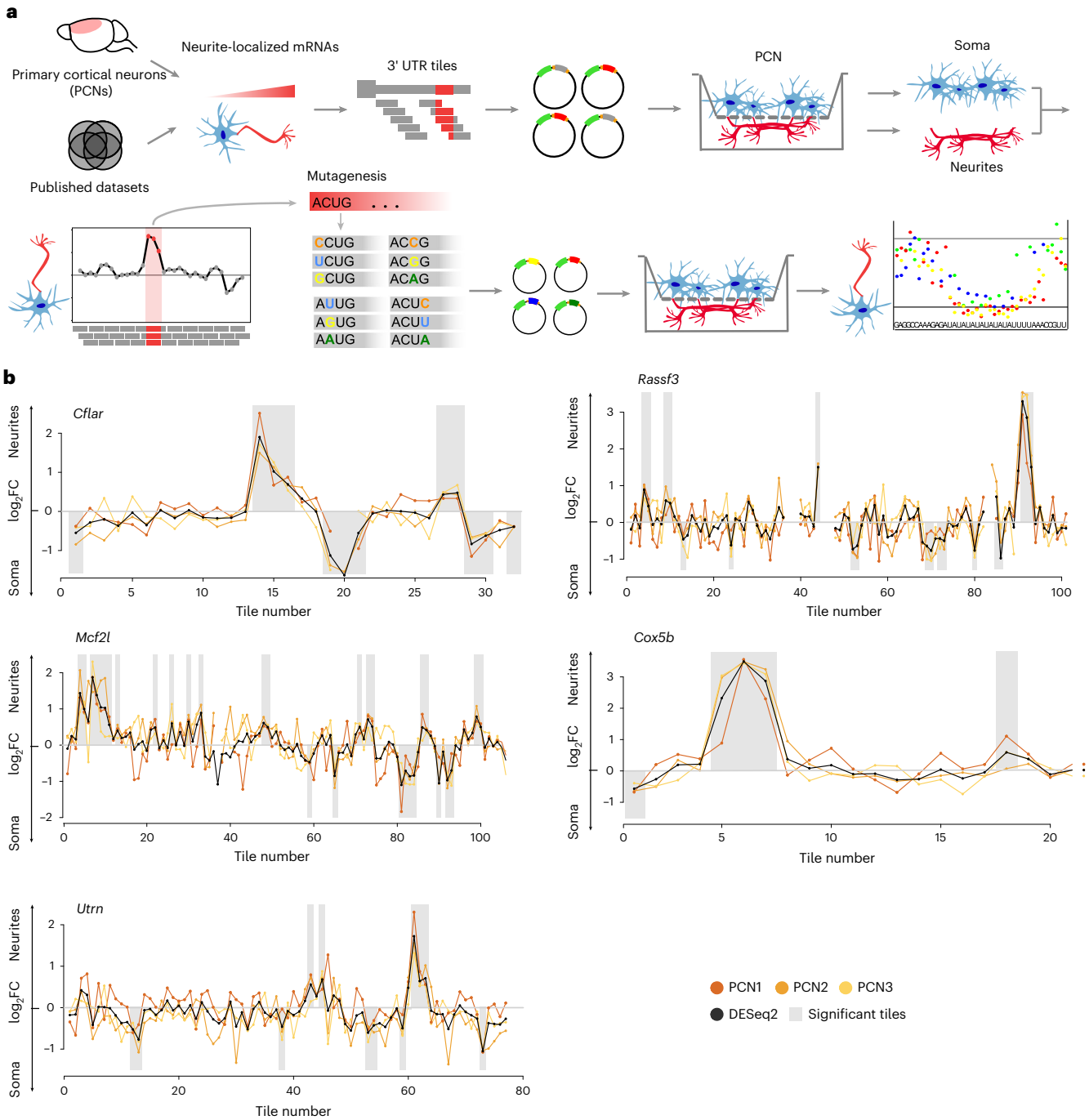

Fig. 1 | N-zip identifies neuronal zipcodes in PCNs. a, Scheme of N-zip. The method involves the following steps. (1) Integrative analysis is used to identify a group of transcripts localized to neurites in at least two neuronal localization datasets; fragments tiled across 3′ UTRs of these transcripts (tiles) are generated. (2) Tiles are cloned in 3′ UTRs of lentiviral vector, between adapter sequences, to generate a pooled reporter library; to restrict the expression of the library to neurons, a neuron-specific synapsin promoter is used. (3) The resulting library is delivered into PCNs grown on a microporous filter, separating soma from neurites. (4) Soma and neurites are isolated, and RNA-seq libraries are prepared from RNA fragments flanked by adapters. (5) Tiles that are sufficient for the localization of RNAs to neurites are identified. (6) An extensive mutagenesis of these tiles is performed, and steps 2–5 are repeated to map the specific sequences that serve as zipcodes. **b**, N-zip identifies 3′ UTR fragments driving RNA localization to neurites of PCNs. Specific examples of identified tiled fragments that mediate localization to neurites are shown. Enrichment of a given tile ($\log_2$-transformed fold change neurites/soma ($\log_2$FC) ≥ 1, adjusted $P < 0.1$) (y) is plotted against tiled fragment number (x). Neurite/soma ratios for individual biological replicates (shades of yellow: PCN1, PCN2 and PCN3) and ratios computed by DESeq2 based on all replicates (black line) are shown. Shaded regions indicate tiles with significant enrichment ($P < 0.05$) in one of the subcellular compartments. The gene name is shown above each plot.

https://doi.org/10.1038/s41593-022-01243-x

Fig. 2 | N-zip combined with mutagenesis maps motifs driving mRNA localization to neurites of PCNs. Selected localized tiled fragments were mutagenized and used for the secondary N-zip in PCNs as shown in Fig. 1a (step 'Mutagenesis'). Specific examples of mutated motifs that mediate localization to neurites are shown. The data are presented as in Fig. 1b. The initial sequence of mutagenized fragment is shown above the *x* axis, and introduced point mutations are indicated with green (A), orange (C), yellow (G) and blue (U) dots. The gene name and tile number are shown above the plot.

Cflar-wt and Urtn-wt). As negative controls, we mutated let-7 seeds in the tested regions (Mcf2l-mut, Cflar-mut and Utrn-mut). Compared to the mutated versions, the Mcf2l-wt with three let-7 sites was repressed about five-fold, the Cflar-wt with two let-7 sites about four-fold and the Utrn-wt with a single let-7 site about 1.7-fold. These data confirmed that the let-7 sites in the analyzed tiles are functional.

We next wondered whether other let-7 targets localize to neurites. To test this, we examined the frequency of let-7 sites across differentially localized transcripts in our N-zip libraries. Consistent with the role of let-7 binding sites in mRNA localization, we observed an enrichment of transcripts bearing let-7 7mer seeds in neurites (black line, Fig. 3c) compared to transcripts without let-7 seeds (gray line). The effect was even stronger for extended 8mer seeds (red line).

Next, we examined if let-7 sites also contribute to the localization of endogenous mRNAs. We detected an enrichment of let-7 site-bearing endogenous transcripts in neurites, the degree of which depended on the number of let-7 sites (gray line: no sites, yellow line: one site, red line >1 site; Fig. 3d and Supplementary Table 3). This let-7 site-dependent shift in localization was less profound for endogenous mRNAs than for N-zip reporters, probably because other regions in endogenous full-length 3′ UTRs contribute to their localization.

Our global analysis of miRNA seeds in N-zip libraries revealed that let-7 sites were enriched compared to sites of other miRNAs in neurites (Fig. 3e). To investigate the potential underpinnings of this specificity, we analyzed miRNA expression levels by small RNA sequencing (RNA-seq). We found that let-7 is the most abundant miRNA in PCNs (>30% of all miRNA reads; Fig. 4a and Supplementary Table 4), explaining the preferential influence of let-7 on the neurite-enriched transcriptome. Given the role of miRNAs in mRNA stability, we compared levels of N-zip reporters with let-7 sites with those in which let-7 sites had been mutated. Mutations of let-7 sites stabilized N-zip reporters, and this effect was stronger in soma than in neurites (Fig. 4b, compare blue and green boxes). These data suggest that let-7 promotes the enrichment of its targets in neurites by destabilizing them more potently in soma. To experimentally test this hypothesis, we perturbed mRNA degradation by expressing a dominant negative mutant of deadenylase CAF1 (dnCAF1)[43]. Expression of dnCAF1 led to stabilization of let-7 targets, compared with control GFP-expressing PCNs (Extended Data Fig. 6a, compare white and red boxes). We then isolated soma and neurites and analyzed changes in mRNA localization upon dnCAF1 expression by RNA-seq. Consistently with our model that let-7 promotes the enrichment of its targets in neurites through regulation of their stability, let-7 targets shifted to soma, compared with transcripts lacking let-7 sites (Extended Data Fig. 6b).

Because levels of let-7 were similar in neurites and soma, we next used proteomics to examine the levels of proteins involved in

https://doi.org/10.1038/s41593-022-01243-x

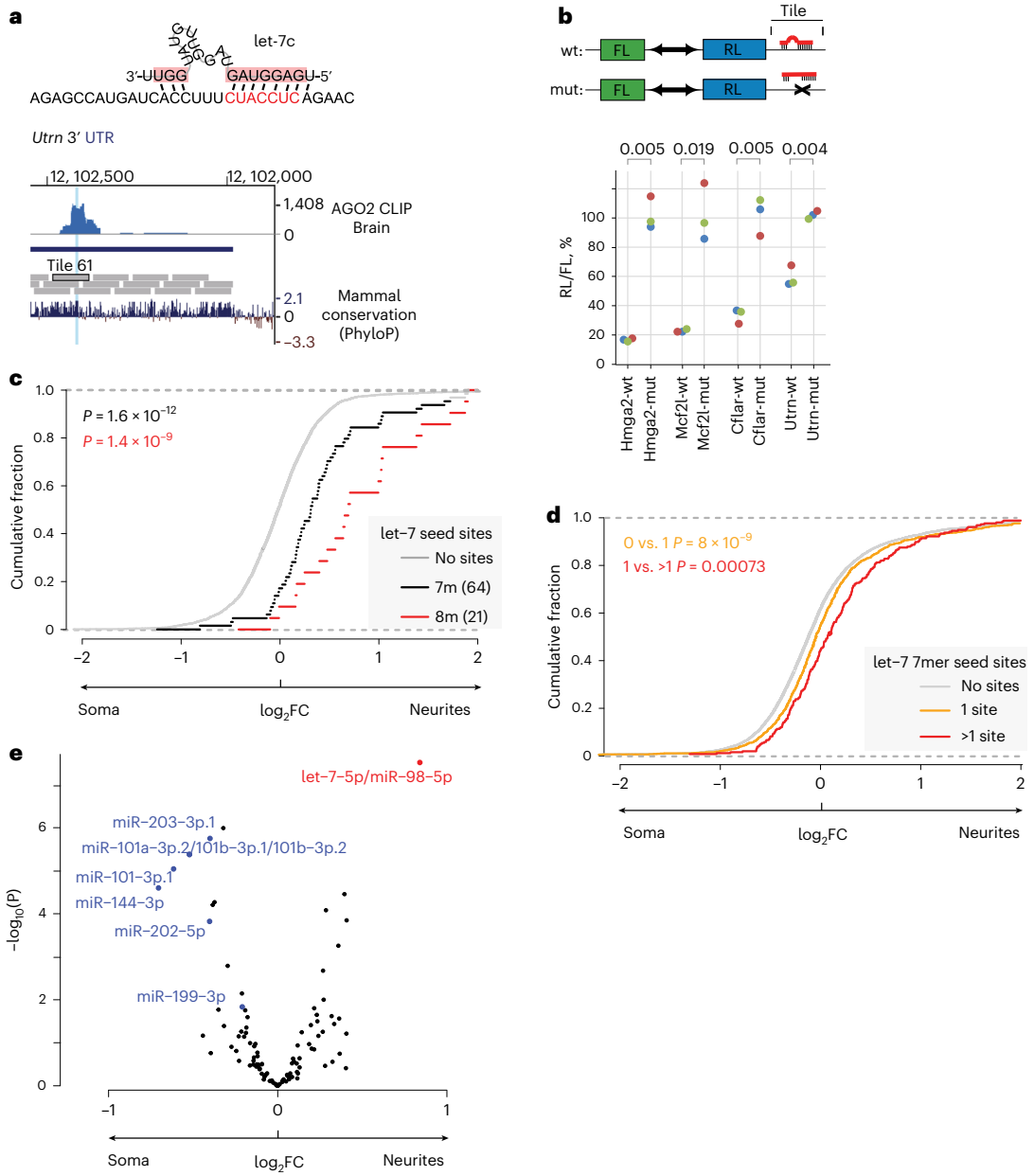

Fig. 3 | Let-7 binding sites direct mRNA localization to neurites in PCNs. **a**, Neurite-localized motif CUACCUC is a binding site for let-7. Top: base-paring between let-7c and *Utrn*-61 tile predicted by mfold[80]. Bottom: UCSC genome browser view showing coverage of AGO2 HITS-CLIP reads in mouse brain[41] (upper track) around let-7 seed in *Utrn*-61 (highlighted in blue). Lower track shows sequence conservation (PholyP). **b**, Validation of functionality of let-7 sites in *Cflar*-14, *Mcf2l*-7 and *Utrn*-61 in luciferase reporter assay. Indicated reporters were transfected in HeLa-rtTA cells: *Renilla* luciferase (RL) and firefly luciferase (FL) are produced from the same vector, with indicated N-zip tiles, either with wild-type (wt) or with mutated (mut) let-7 sites, inserted downstream of RL. As a positive control, analogous reporters with *Hmga2* 3′ UTR (hmga2-wt and hmga2-mut) were used. For each reporter pair, RL activity was normalized to that of FL and presented as a percentage of luciferase activity produced by mutated reporter. Individual biological triplicates (colored dots, $n = 3$) are plotted. Statistical significance of differences between wild-type and mutated reporters were computed by two-sided *t*-test and shown on the plot. **c**, N-zip mRNAs with let-7 sites are enriched in neurites of PCNs. Cumulative distribution function (CDF) showing fractions of mRNAs (y) plotted against neurite/soma enrichment (x) for transcripts with no let-7 sites (gray), at least one 7mer (black) or 8mer let-7 site (red). The number of detected tiles with indicated let-7 sites is shown in the legend. *P* values were computed with two-sided Wilcoxon rank-sum test. **d**, Endogenous mRNAs with let-7 sites are enriched in neurites of PCNs. The data are plotted, and *P* values were computed as in **c** for transcripts with no (gray), one (yellow) or more than one (red) let-7 sites. **e**, Let-7 sites are enriched in neurite-localized mRNAs in PCNs. Volcano plot showing the mean neurite/soma enrichment of tiles containing 7mer matches to the seeds of individual miRNA families in N-zip mRNAs. miRNAs with statistically significant enrichment in one of the compartments ($P < 0.05$, two-sided *t*-test) are labeled in red (neurite-enriched) and blue (soma-enriched).

https://doi.org/10.1038/s41593-022-01243-x

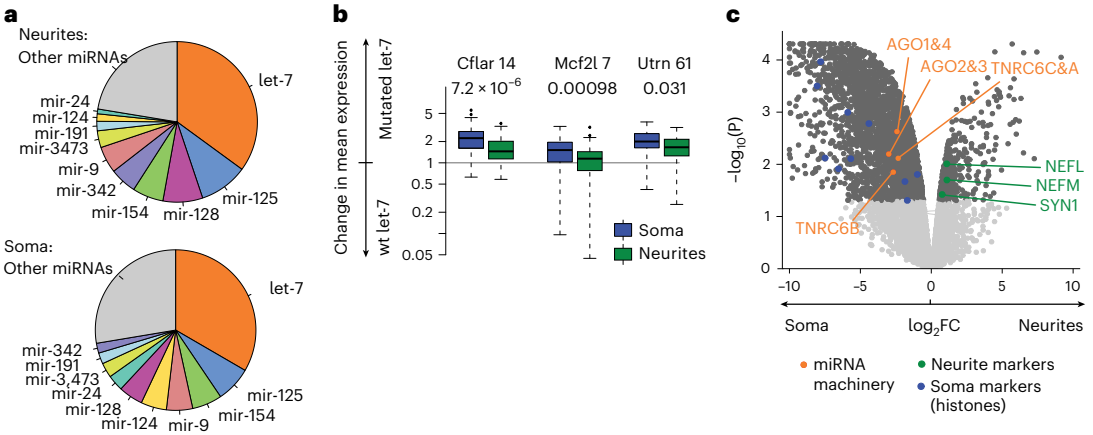

Fig. 4 | Let-7 functions by preferentially destabilizing its target mRNAs in soma of PCNs. a, Let-7 is the most abundant miRNA in PCNs. Pie charts showing the percentage of different miRNAs in neurites and soma of PCNs, determined by small RNA-seq. **b**, Mutations of let-7 binding sites lead to a stronger increase of N-zip mRNA reporter levels in soma. Box plots showing changes in the normalized expression levels between tiles that contain intact let-7 seed sites (wt let-7) and tiles in which let-7 seeds were mutated (mutated let-7). In the mutated tiles, at least one let-7 seed site was lost. The data are shown separately for each tile (as indicated on *x*) and each subcellular compartment (green: neurite, blue: soma). *P* values, computed with two-sided Wilcoxon rank-sum test, are shown above the plots ($n = 3$ independent biological replicates). Box plot elements, here and further, unless otherwise specified: center line, medium; box limits, upper and lower quartiles; whiskers, 1.5× interquartile range; points, outliers. **c**, Proteomic analysis of isolated soma and neurites indicates somatic enrichment of the core components of the miRNA repression complex (AGO1, 2, 3 and 4; TNRC6A, B and C, orange). Volcano plot showing $-\log_{10}$ *P* values (*y*) plotted against $\log_2$FC of iBAQ values, normalized to GAPDH in each compartment. *P* values were computed with limma's eBayes function (Methods) and adjusted for multiple testing using the Benjamini–Hochberg method. Significant values (FDR < 5%) are shown in dark gray and non-significant in light gray. Neurofilaments (NEFL and NEFM) and synapsin (SYN1) were used as neurite markers (green) and histones as soma markers (blue) to confirm the efficiency of the separation of soma and neurites.

miRNA-mediated regulation. This analysis showed that the core components of the miRNA repression complex (AGO and TNRC6 family members) are enriched in soma (Fig. 4c, orange, and Supplementary Table 5). These data explain a higher let-7 activity in soma and the enrichment of let-7 targets in neurites.

To experimentally confirm the role of the miRNA pathway in mRNA localization, we combined N-zip with *Ago2* depletion using short hairpin RNA (shRNA). RT–qPCR and western blot confirmed a ~70% depletion of *Ago2* (Fig. 5a and Supplementary Table 3). We next analyzed how the enrichment of let-7 targets in neurites changes upon *Ago2* depletion. Compared to N-zip tiles without let-7 sites (zero let-7 sites; Fig. 5b), let-7 targets shifted toward soma, an effect whose degree depended on the number of sites (compare zero with one, two and three let-7 sites).

We then decided to analyze the effect of *Ago2* deletion on the localization of endogenous mRNAs, using mRNA-seq analysis of neurites and soma. Compared with mRNAs that did not contain let-7 sites (gray line, Fig. 5c), let-7 targets shifted their localization toward the soma upon *Ago2* depletion (yellow line: one let-7 7mer seed match; red line: two or more let-7 7mer seed matches).

To validate the effect of *Ago2* depletion on the localization of let-7 targets, we constructed GFP reporters with one of the tiles bearing let-7 binding sites in their 3′ UTR: *Cflar*-14, *Mcf2l*-7 or *Utrn*-61. We used a GFP mRNA without tile sequences (GFP) as a negative control. Upon *Ago2* depletion or treatment with a scrambled shRNA, we transduced these reporters into PCNs and performed single molecule inexpensive FISH (smiFISH)[44] with GFP-specific probes. Primary cortical cultures are heterogenous and show high variability in reporter expression levels; therefore, to quantify mRNA localization, we compared the signal in the proximal part and in the distal part of neurites within individual neurons (Fig. 5d and Extended Data Fig. 7). Reporter localization in smiFISH recapitulated the results of N-zip. In particular, the incorporation of let-7-bearing tiles in GFP reporters shifted their localization toward distal neurites (Fig. 5d, compare GFP with Cflar, Mcf2l and Utrn, gray boxes). Moreover, *Ago2* depletion reduced localization of let-7 reporters to neurites, supported by significantly higher proximal versus distal signal in *Ago2*-depleted neurons (red) than in scrambled control (gray). Notably, the GFP reporter without let-7 binding sites ('GFP') was not significantly affected by *Ago2* depletion.

Given the enrichment of the protein components of the mRNA repression complex in soma (Fig. 4b), we decided to explore if other miRNAs might also affect mRNA localization. We analyzed the frequency of miRNA seeds across differentially localized N-zip reporters and endogenous mRNAs. Consistently with our finding that let-7 is the most abundant miRNA in PCNs (Fig. 4a), the let-7 seed was the only one with statistically significant enrichment in neurite-localized mRNAs (Extended Data Fig. 6c). However, we also detected a modest effect for a few other abundant miRNAs, including miR-154, miR-342 and miR-24 (Extended Data Fig. 6c,d and Supplementary Table 4). These data suggest that other miRNAs have the potential to contribute to mRNA localization, and the ultimate effect may depend on the miRNA expression profiles in individual cell types.

$(AU)_n$-containing mRNAs recruit HSB1L protein to localize to neurites

Our N-zip analysis identified $(AU)_n$ as a de novo zipcode. We next analyzed how the length of $(AU)_n$ affected mRNA localization. We found that N-zip reporters with ≥6 AU repeats were enriched in neurites (Fig. 6a). Similarly, endogenous mRNAs with ≥6 AU repeats in their 3′ UTRs (red line, Fig. 6b) were shifted to neurites compared to transcripts with fewer or no AU repeats (gray line). The effect was weaker for endogenous transcripts than for N-zip reporters, presumably due to other regulatory sequences in the full-length 3′ UTRs. Strikingly, transcripts with ≥5 AU repeats were enriched also in neurites of neuroblastoma lines[45] (Extended Data Fig. 8a), suggesting that the role of this motif in mRNA localization is conserved in multiple cell types.

We next examined how $(AU)_n$ affects transcript levels in soma and neurites. Mutations of $(AU)_n$ stabilized N-zip reporters, and this effect was stronger in soma than in neurites (Extended Data Fig. 8b,

https://doi.org/10.1038/s41593-022-01243-x

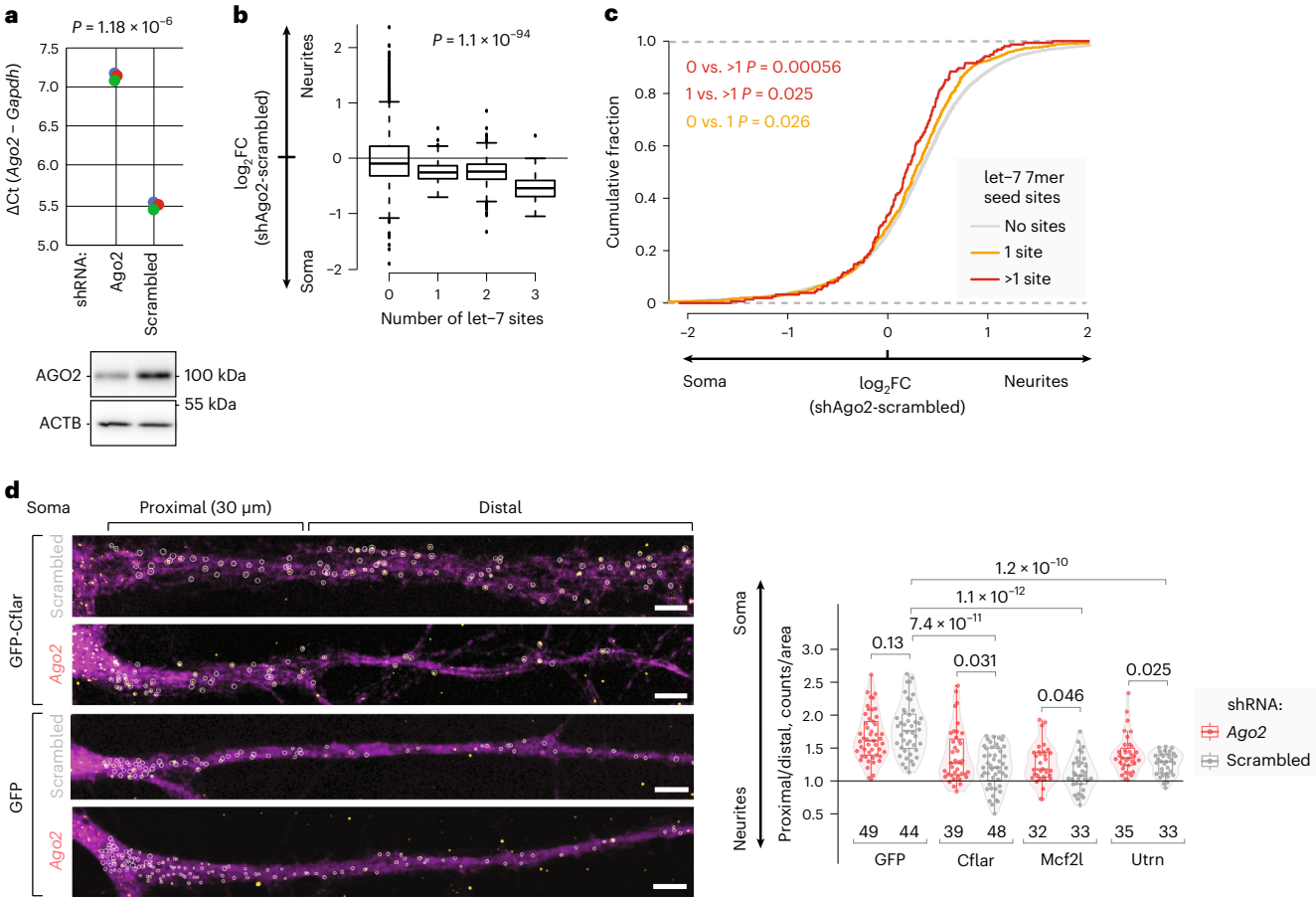

Fig. 5 | Localization of let-7 targets to neurites requires AGO2. a, Efficient AGO2 depletion in PCNs. *Ago2* expression levels in *Ago2*-depleted and control scrambled shRNA samples were quantified by RT–qPCR, normalized to *Gapdh*, and plotted on *y* as individual biological triplicates (colored dots, $n = 3$). *P* value was computed by two-sided *t*-test. Western blotting against AGO2 and ACTB (loading control) is shown below the plot. **b**, *Ago2* knockdown shifts N-zip reporters with let-7 sites toward soma. Box plots showing changes in neurite/soma enrichment between *Ago2*-depleted and scrambled samples (*y*) as a function of the number of let-7 sites in the N-zip reporter tiles (*x*). *P* values were computed using two-sided Wilcoxon rank-sum test ($n = 3$ independent biological replicates). **c**, *Ago2* knockdown in PCNs shifts endogenous let-7 targets toward soma. Cumulative distribution functions (CDFs) showing fractions of endogenous mRNAs with no let-7 sites (gray), one let-7 site (yellow) and more let-7 sites (red) (*y*), plotted against changes in neurite/soma enrichment upon *Ago2* knockdown (*x*). *P* values were computed using two-sided Wilcoxon rank-sum test. **d**, smiFISH validates the role of AGO2 in the localization of let-7 targets. PCNs were transduced with either *Ago2*-targeting (red) or scrambled shRNAs (gray) and one of the GFP-encoding reporters: let-7 reporter bearing *Cflar*-14, *Mcf2l*-7 or *Utrn*-61 tile downstream of GFP or a negative control without let-7 sites (GFP). Representative smiFISH images (left): *Gfp* RNA, yellow; GFP protein (serving to outline cell borders), magenta; scale bar, 5 µm. Circled are *Gfp* RNA spots quantified using the RS-FISH Fiji plugin[81]. Representative images for *Mcf2l* and *Utrn* reporters are shown in Extended Data Fig. 7. smiFISH quantification (right): the box plots show ratios of the *Gfp* signal in proximal (0–30 µm) versus distal part of neurites (30 µm up to 100 µm); points show ratios for individual neurons. The number of quantified neurons (biological replicates) is indicated below the box plots. *P* values were computed with Welch's adaptation of *t*-test (two-sided) at 95% confidence interval and adjusted for multiple comparisons using the Benjamini–Hochberg method.

compare blue and green boxes). As in the case of let-7 targets, expression of dnCAF1 led to stabilization of mRNAs containing ≥6 AU repeats (Extended Data Fig. 6a, compare white and red boxes; $P < 10^{-16}$ for both tiles). Moreover, transcripts with a long AU stretch shifted toward soma, when compared with mRNAs carrying short or no AU repeats (Extended Data Fig. 8c). These data suggest that, similarly to let-7 sites, $(AU)_n$ mediates enrichment of transcripts in neurites primarily by destabilizing them in soma.

Next, we decided to investigate the RBPs that are recruited by $(AU)_n$ and might mediate its localization. Analysis of known RBP motifs suggested that $(AU)_n$ could be bound by RBMS1 and RBMS3 (Extended Data Fig. 3a). However, the binding motif for these proteins contains only three AU repeats[46], which is insufficient for mRNA localization (Fig. 6a). To identify more plausible $(AU)_n$ interactors, we used RNA affinity capture[47] combined with proteomics (Extended Data Fig. 8d). This analysis identified 23 proteins as significantly enriched in complexes formed on $(AU)_8$ RNA, compared with a negative control with mutated $(AU)_8$ (false discovery rate (FDR) 5%; Fig. 7a and Supplementary Table 6). Among them were HBS1-like protein (HBS1L), critical for cerebellar neurogenesis[48], and neuronal members of the ELAV-like (nELAVL) family, with the roles in learning and memory[49].

HBS1L and nELAVLs were reported to have opposite effects on mRNA fate: HBS1L is an mRNA decay factor[50,51], whereas nELAVL proteins stabilize bound mRNAs by preventing their association with destabilizing proteins[52]. As localization of $(AU)_n$-containing mRNAs to neurites is due to their preferential destabilization in soma (Extended Data Fig. 8b,c), HBS1L is a plausible player in this mechanism. Thus, we depleted *Hbs1l* with an shRNA (Fig. 7b) and examined how this depletion affected localization of $(AU)_n$-containing transcripts by mRNA-seq of isolated neurites and soma. Remarkably, *Hbs1l* depletion shifted the

https://doi.org/10.1038/s41593-022-01243-x

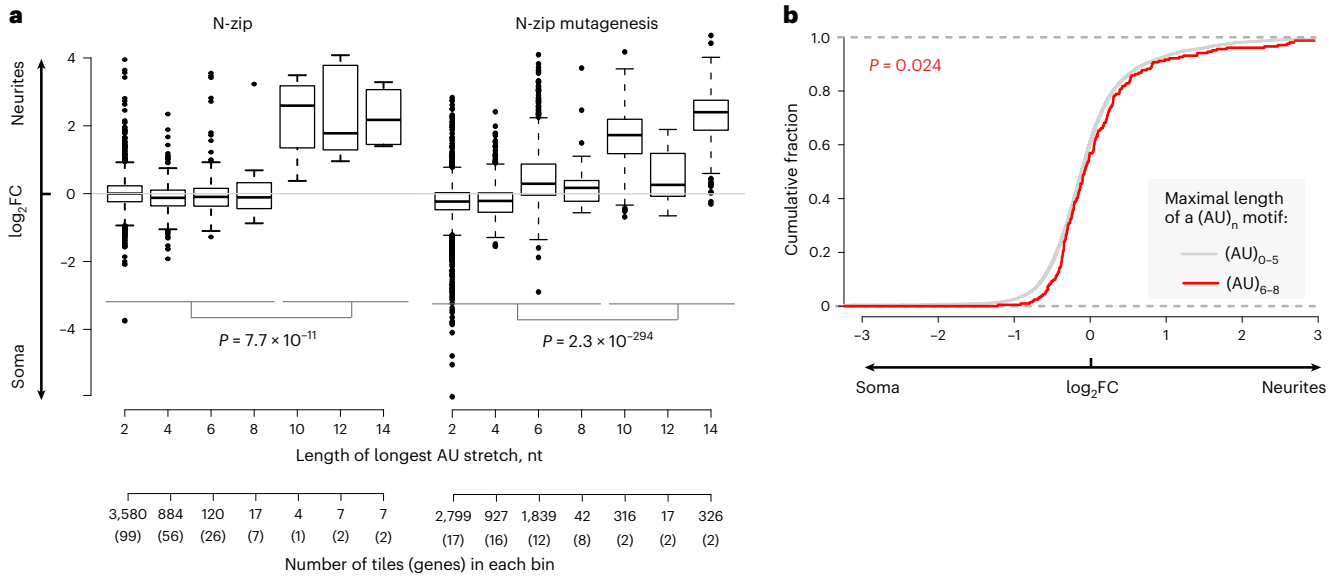

Fig. 6 | $(AU)_n$ motif-containing mRNAs localize to neurites of PCNs. **a**, Box plot showing neurite/soma enrichment (*y*) as a function of the maximal length of the $(AU)_n$ stretch length in the tiles in original N-zip (left plot) and mutated N-zip (right plot) mRNA libraries (*x*). The additional *x* axis shows the number of tiles and the number of genes that these tiles were derived from (in parentheses), in which AU stretches of the indicated length were found. *P* values were computed using two-sided Wilcoxon rank-sum test ($n = 3$ independent biological replicates). **b**, Cumulative distribution functions (CDFs) showing fractions of endogenous mRNAs with $(AU)_{0\text{-}5}$ (gray) and $(AU)_{6\text{-}8}$ stretches (red), as measured by mRNA-seq (*y*), plotted against neurite/soma enrichment. *P* value was computed using two-sided Wilcoxon rank-sum test.

localization of transcripts with a long $(AU)_n$ motif (red line, Fig. 7c, and Extended Data Fig. 8e) toward soma, compared with transcripts with a short or no $(AU)_n$ (gray line). In contrast, the same approach applied to nELAVL-depleted neurons (Extended Data Fig. 8f) showed no correlation between the length of $(AU)_n$ and changes in mRNA localization (Extended Data Fig. 8g). Depleting *Hbs1l* also changed the localization of N-zip reporters in a manner dependent on $(AU)_n$ length (Extended Data Fig. 8h). Thus, these data confirmed the role of HBS1L in localization of $(AU)_n$-containing transcripts in PCNs.

To validate the effect of *Hbs1l* depletion on localization of $(AU)_n$-containing transcripts by smiFISH[44], we generated GFP reporters with one of $(AU)_n$-carrying tiles in their 3′ UTR (Map2 and Rassf3, Fig. 7d, and Extended Data Fig. 9). As a negative control, we used a GFP construct without any tile in the 3′ UTR (GFP). Quantification of the signal from GFP-specific probes in the proximal and distal part of neurites showed that incorporation of $(AU)_n$-bearing tiles in GFP reporters shifted their localization toward distal neurites (Fig. 7d, compare GFP with Map2 and Rassf3, gray boxes); also, *Hbs1l* depletion reduced localization of $(AU)_n$ reporters to neurites (Fig. 7d). Indeed, proximal versus distal signal was significantly higher in *Hbs1l*-depleted neurons (red) than in the ones treated with scrambled control (gray). Consistently with the role of $(AU)_n$, such an effect was not observed for the control GFP reporter.

Discussion

Although hundreds to thousands of mRNAs localize to neurites[12–25], in most cases the mechanisms and biological functions of such localization remain to be understood. Here we present an MRPA[26,53]-based method, N-zip (Fig. 1a), to find zipcodes involved in mRNA localization in neurons. Identifying zipcodes makes it possible to manipulate the localization of specific mRNAs and test their biological roles. Using this method, we analyzed 99 neurite-localized transcripts. For one-third of them, we identified tiles localized to neurites of PCNs (Fig. 1b). Curiously, these transcripts with neurite-localized tiles are associated with local neuronal structures and processes, such as synapse and actin cytoskeleton organization (Extended Data Fig. 3c). Our further analysis of neurite-localized tiles identified several motifs (Extended Data Fig. 3a), two of which— let-7 binding site and $(AU)_n$—we characterized in detail and demonstrated their role in mRNA localization in PCNs. We found these two motifs in 15 of the 33 transcripts with a neurite-enriched tile, suggesting that additional mechanisms of localization remain to be characterized in future studies.

mRNA localization can be achieved via different mechanisms. First, mRNAs can be transported along cytoskeletal fibers with the help of motor proteins. In addition, localization can be attained by degrading mRNAs in other regions where they should not be on hand. Notably, whereas the first mechanism generates an mRNA localization pattern by increasing mRNA concentration in one subcellular compartment, the latter achieves the same outcome by decreasing mRNA concentration in another compartment. For example, localization-dependent mRNA degradation has been described for *Hsp83* and *nanos*. Their mRNAs are degraded throughout *Drosophila* eggs via the Smaug-mediated recruitment of deadenylation complex but remain stable at the posterior pole[54,55]. Previous studies reported local processing of miRNAs[56] and modification of the components of the miRNA pathway in response to synaptic activity[57–59]. However, to our knowledge, localization-dependent degradation of mRNAs by miRNAs has not been previously described. Given the known role of miRNAs in mRNA degradation (reviewed in ref. [40]), it seems highly likely that this could be used as a mechanism to establish pools of specific mRNAs in some areas of the cell by degrading them in others. N-zip identified the binding site for an miRNA—let-7—as a zipcode (Fig. 1b2). Let-7 is the most abundant miRNA in the mammalian brain[56,60,61] (Fig. 4a) and is involved in neuronal differentiation[62], regeneration[63,64] and synapse formation[65,66]. Our results point to a new neuronal function for let-7 in mediating mRNA localization.

Relatively moderate effects of miRNAs on their targets (~1.3-fold downregulation on average[67,68]) may enable many mRNA molecules to escape degradation by miRNAs in soma and localize to neurites. Intriguingly, let-7 was equally abundant in the neurites and soma of

https://doi.org/10.1038/s41593-022-01243-x

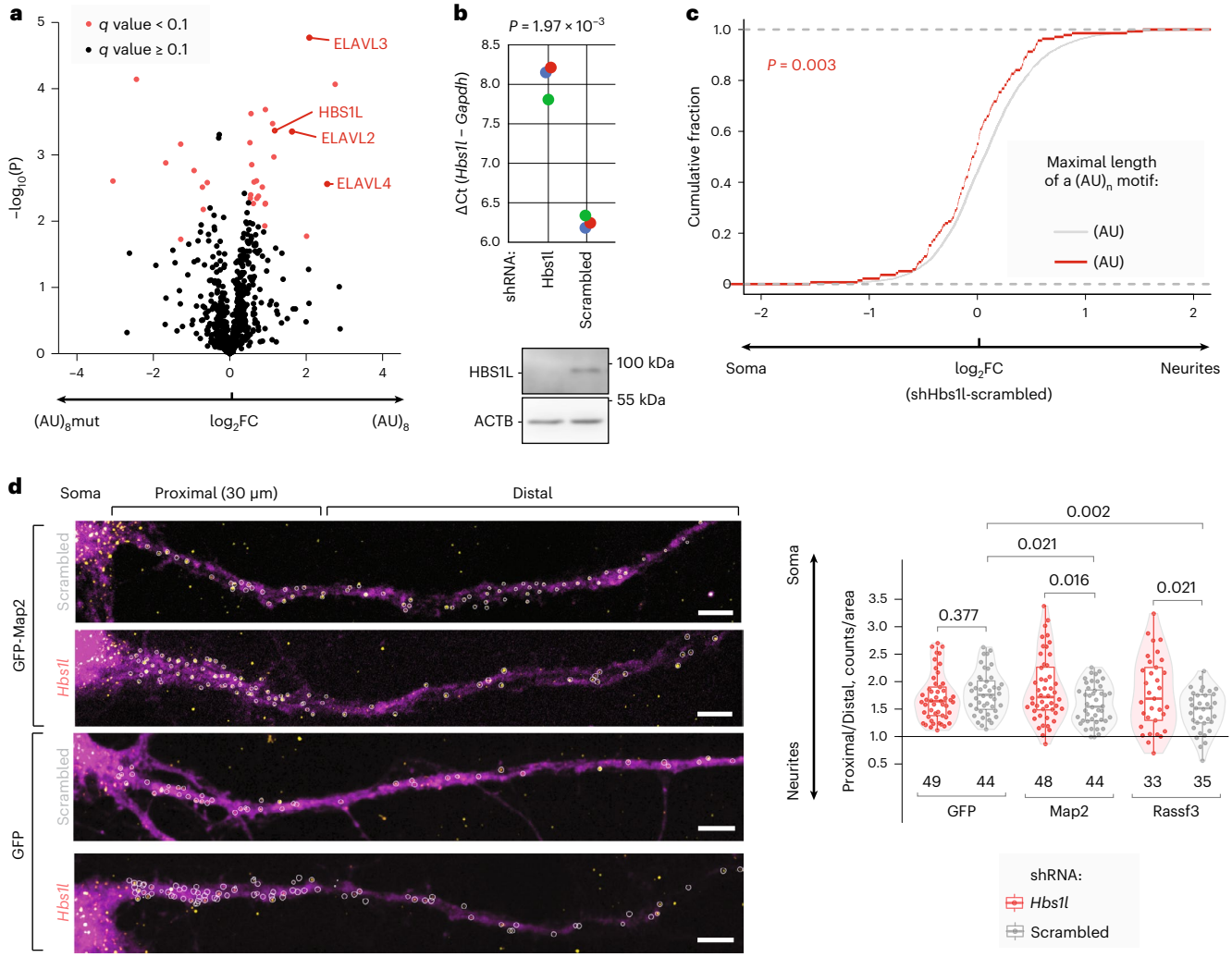

Fig. 7 | HBS1L binds $(AU)_n$ motif to direct mRNA localization to neurites of PCNs. a, $(AU)_n$ motif binds HBS1L and nELAVL proteins. Volcano plot showing proteins enriched in $(AU)_8$-GRNA chromatography. $-\log_{10} P$ values (y, two-sided t-test with equal variance) are plotted against $\log_2$FC of LFQ values between $(AU)_8$ and mutant RNA pulldowns (x). Proteins with significant q value (FDR < 5% using Benjamini–Hochberg correction) are marked in red. **b**, RT–qPCR (top) and western blotting (bottom) show an efficient HBS1L depletion with shRNA in PCNs. *Hbs1l* expression levels for *Hbs1l*-depleted and control scrambled shRNA samples, normalized to *Gapdh* (ΔC_t), are plotted on y as individual biological triplicates (colored dots, $n = 3$). P value was computed by two-sided t-test. Western blotting showing the expression of HBS1L protein in both samples is provided below the RT–qPCR plot. ACTB was used as a loading control in western blotting. **c**, Depletion of *Hbs1l* in PCNs shifts $(AU)_n$-containing mRNAs toward soma. Cumulative distribution functions (CDFs) showing fractions of endogenous mRNAs with no or short $(AU)_n$ stretch ($n = 0–5$, gray) and a long $(AU)_n$ stretch ($n > 5$, red), as measured by mRNA-seq (y), plotted against changes in neurite/soma enrichment upon *Hbs1l* depletion (x). P value was computed using two-sided Wilcoxon rank-sum test. **d**, smiFISH validates the role of HBS1L in the localization of $(AU)_n$-containing reporter. Representative smiFISH images (left) and quantification of smiFISH signal (right) are shown. PCNs were transduced with either *Hbs1l*-targeting (red) or scrambled shRNAs (gray) and one of the GFP-encoding reporters: $(AU)_n$ reporter bearing *Map2*-3′ or *Rassf3*-91 tile downstream of GFP or a negative control without $(AU)_n$ (GFP; Methods). The data were analyzed and presented as in Fig. 5d. The same set of neurons was used as a negative control (GFP reporter with scrambled shRNA) in both smiFISH panels. Representative images for *Rassf3* reporter are shown in Extended Data Fig. 9.

PCNs (Fig. 4a), raising the question about the mechanism underpinning the higher let-7 activity in soma. One explanation came from our proteomic analysis, which has shown that protein components of miRNA machinery are enriched in soma (Fig. 4c), leading to lower levels of let-7 targets in soma (Fig. 4b).

It remains to be understood how such mRNAs, regulated via differential stability, are transported into neurites. In long and thin neurites, diffusion seems unlikely to suffice in transporting mRNAs at hundreds of micrometers. It is tempting to speculate that they may be transported with the help of motor proteins. In the simplistic view of motor-dependent transport, RBPs recognize specific localization elements in mRNA and tether them to motor proteins for transport (reviewed in ref. [1]). However, in vivo, this process appears to be more complex, involving the formation of higher-order messenger ribonucleoprotein (mRNP) transport granules. Such granules can be formed through phase separation and contain numerous mRNAs and RBPs co-transported with a limited set of motor proteins (reviewed in ref. [69]). Non-selective inclusion of mRNA in such granules may facilitate their transport to neurites, whereas selective mRNA degradation would generate an mRNA gradient across the cell.

We identified $(AU)_n$ as another de novo zipcode in PCNs. $(AU)_n$ is found in important neuritically enriched mRNAs, including *Map2*

and *Shank3* (Supplementary Table 1 and Extended Data Fig. 4b). RNA affinity capture showed that $(AU)_n$ is bound by an mRNA decay factor HBS1L and nELAVL proteins (Fig. 7a), both having important functions in neuronal development[48,49]. Based on RIP-Chip and SELEX experiments[70], ELAVL proteins bind AU-rich elements (AREs), including UUUAUUU and its variations. AREs bear some resemblance to $(AU)_n$, which may explain detection of nELAVLs among $(AU)_n$ interactors. However, nELAVLs stabilize their bound mRNAs (reviewed in ref. [52]), whereas our analysis showed that localization of $(AU)_n$-containing transcripts is mediated by selective mRNA destabilization (Extended Data Fig. 8b,c). Indeed, depletion of nELAVLs did not decrease neurite enrichment of $(AU)_n$-containing transcripts (Extended Data Fig. 8f,g).

Our depletion experiments showed that HBS1L mediated localization of $(AU)_n$-containing mRNAs (Fig. 7b–d and Extended Data Fig. 8e,h). HBS1L is involved in mRNA quality control pathways, including No-Go and Nonstop decay, that degrade mRNAs with stalls in translation elongation (reviewed in ref. [71]). HBS1L belongs to the GTPases family and is homologous to translation elongation and termination factors eEF1 and eRF3. In this study, we uncovered the role of HBS1L in the localization of $(AU)_n$-containing transcripts via selective degradation in soma. It remains to be understood how it is recruited to $(AU)_n$ to trigger mRNA degradation.

Parallel studies[45,72] describe similar approaches to identifying zipcodes in neuroblastoma cell lines. We detected no overlap with the results of Arora et al.[72], most probably because their MRPA library included only eight neurite-localized transcripts. Our analysis of the Mikl et al.[45] data showed that the $(AU)_n$ motif is linked to mRNA localization not only in cortical neurons but also in neuroblastoma lines (Extended Data Fig. 8a). Moreover, binding motifs for CELF/BRUNOL and PCBP family members, identified among the binders of the neurite-localized synthetic sequence by Mikl et al.[45], were also overrepresented in neurite-localized N-zip tiles (Extended Data Fig. 3a). Both CELF/BRUNOL and PCBP protein families are broadly involved in RNA metabolism. Curiously, CELF/BRUNOL is involved in localized translation in *Drosophila* oocyte[73,74]. In contrast, let-7 binding sites function as zipcodes in PCNs (Fig. 3c,d) but not in neuroblastoma lines. This is likely due to differences in let-7 expression levels between primary neurons and neuronal cell lines[75]. This example illustrates the merits of using primary cells to identify functional elements with biological roles in vivo.

N-zip has also identified and refined several previously known zipcodes. For example, the CPE was reported to facilitate mRNA transport to dendrites and play a role in *Map2* (ref. [8]) and *Bdnf* (ref. [9]) localization. In line with that, CPE-containing tiles in *Map2* (tiles 4–6) and *Bdnf* (tile 1) were neurite-localized in N-zip (Extended Data Fig. 10). As a group, tiles containing CPE in the last 30 bases tended to become more neurite-enriched upon depolarization ($P = 7.7 \times 10^{-15}$). In contrast, no effect was observed when considering the whole tile ($P = 0.41$), suggesting that CPE is more functional when located closer to the polyadenylation signal, consistent with previous literature[76]. Moreover, we identified the second localization element in *Bdnf* (tile 56; Extended Data Fig. 10) within the region previously shown to contribute to dendritic localization of *Bdnf*[77]. We also found that tile 31 in the neuritically localized isoform of *Cdc42* (ref. [25]) is sufficient for localization.

Curiously, depolarization activated localization of tiles mapping to transcripts with essential functions in neurites, including mRNAs encoding ribosomal proteins (Extended Data Fig. 2). Localization of these transcripts to neurites is conserved across multiple types of neurons[31], hinting to their importance in local translation. Indeed, newly translated ribosomal proteins provide for ribosome maintenance in neurites[78,79]. Localization of mRNAs encoding for different ribosomal proteins may also generate specialized pools of ribosomes translating local transcriptome. In addition, depolarization stimulated localization of a tile from *Adcy1*, encoding an enzyme that catalyzes the formation of the signaling molecule cAMP and plays an essential role in memory and learning[37].

It should be noted that N-zip is limited to the detection of relatively short (≤150-nt) zipcodes. For example, the zipcode of *Arc*, containing a 350-nt region[11], is too long to be mapped by N-zip. Zipcodes consisting of multiple motifs residing in different 3′ UTR parts and those dependent on splicing are also not detectable in our current implementation of N-zip. A further limitation is that we are studying the activity of zipcodes in a fixed backbone, and different backbones, along with their length, GC content and splicing status, can have variable effects on the activity of individual tiles[53]. Our mutagenesis approach can detect zipcodes that are disrupted by mutations of single nucleotides or longer kmers, but it is limited in the detection of redundantly acting zipcodes. Lastly, the activity of individual zipcodes can depend on the developmental stage and neuronal activity.

Let-7 binding sites and $(AU)_n$ motifs help localize both exogenously introduced N-zip reporters and endogenous mRNAs, but the effect is stronger for N-zip reporters. The likely reason is that the full-length 3′ UTRs of endogenous mRNAs are longer and potentially carry additional regulatory elements that may exercise a finer control over mRNA localization. It can also affect the distance between the elements and the poly(A) tails. The ultimate localization of these mRNAs is a combinatorial result based on multiple regulatory sequences. In support of this, a single 3′ UTR often harbors sequences that promote and inhibit neurite enrichment (Fig. 1b). In summary, N-zip allows decoding the combinatorial effects that regulate mRNA localization by zooming in on shorter sequences with specific roles in localization. This is a crucial step toward unraveling how a finite number of patterns produce many types of polarized cells and help them adapt to challenges and changes.

Online content

Any methods, additional references, Nature Portfolio reporting summaries, source data, extended data, supplementary information, acknowledgements, peer review information; details of author contributions and competing interests; and statements of data and code availability are available at https://doi.org/10.1038/s41593-022-01243-x.

References

1. Martin, K. C. & Ephrussi, A. mRNA localization: gene expression in the spatial dimension. *Cell* **136**, 719–730 (2009).
2. Micheva, K. D., Vallee, A., Beaulieu, C., Herman, I. M. & Leclerc, N. β-Actin is confined to structures having high capacity of remodelling in developing and adult rat cerebellum. *Eur. J. Neurosci.* **10**, 3785–3798 (1998).
3. Bassell, G. J. et al. Sorting of β-actin mRNA and protein to neurites and growth cones in culture. *J. Neurosci.* **18**, 251–265 (1998).
4. Kislauskis, E. H. & Singer, R. H. Determinants of mRNA localization. *Curr. Opin. Cell Biol.* **4**, 975–978 (1992).
5. Kislauskis, E. H., Zhu, X. & Singer, R. H. Sequences responsible for intracellular localization of β-actin messenger RNA also affect cell phenotype. *J. Cell Biol.* **127**, 441–451 (1994).
6. Ross, A. F., Oleynikov, Y., Kislauskis, E. H., Taneja, K. L. & Singer, R. H. Characterization of a β-actin mRNA zipcode-binding protein. *Mol. Cell. Biol.* **17**, 2158–2165 (1997).
7. Farina, K. L., Huttelmaier, S., Musunuru, K., Darnell, R. & Singer, R. H. Two ZBP1 KH domains facilitate β-actin mRNA localization, granule formation, and cytoskeletal attachment. *J. Cell Biol.* **160**, 77–87 (2003).
8. Huang, Y. S., Carson, J. H., Barbarese, E. & Richter, J. D. Facilitation of dendritic mRNA transport by CPEB. *Genes Dev.* **17**, 638–653 (2003).
9. Oe, S. & Yoneda, Y. Cytoplasmic polyadenylation element-like sequences are involved in dendritic targeting of BDNF mRNA in hippocampal neurons. *FEBS Lett.* **584**, 3424–3430 (2010).

10. Rook, M. S., Lu, M. & Kosik, K. S. CaMKIIα 3′ untranslated region-directed mRNA translocation in living neurons: visualization by GFP linkage. *J. Neurosci.* **20**, 6385–6393 (2000).
11. Kobayashi, H., Yamamoto, S., Maruo, T. & Murakami, F. Identification of a *cis*-acting element required for dendritic targeting of activity-regulated cytoskeleton-associated protein mRNA. *Eur. J. Neurosci.* **22**, 2977–2984 (2005).
12. Poon, M. M., Choi, S. H., Jamieson, C. A., Geschwind, D. H. & Martin, K. C. Identification of process-localized mRNAs from cultured rodent hippocampal neurons. *J. Neurosci.* **26**, 13390–13399 (2006).
13. Zhong, J., Zhang, T. & Bloch, L. M. Dendritic mRNAs encode diversified functionalities in hippocampal pyramidal neurons. *BMC Neurosci.* **7**, 17 (2006).
14. Lecuyer, E. et al. Global analysis of mRNA localization reveals a prominent role in organizing cellular architecture and function. *Cell* **131**, 174–187 (2007).
15. Zivraj, K. H. et al. Subcellular profiling reveals distinct and developmentally regulated repertoire of growth cone mRNAs. *J. Neurosci.* **30**, 15464–15478 (2010).
16. Gumy, L. F. et al. Transcriptome analysis of embryonic and adult sensory axons reveals changes in mRNA repertoire localization. *RNA* **17**, 85–98 (2011).
17. Cajigas, I. J. et al. The local transcriptome in the synaptic neuropil revealed by deep sequencing and high-resolution imaging. *Neuron* **74**, 453–466 (2012).
18. Jambor, H. et al. Systematic imaging reveals features and changing localization of mRNAs in *Drosophila* development. *eLife* **4**, e05003 (2015).
19. Shigeoka, T. et al. Dynamic axonal translation in developing and mature visual circuits. *Cell* **166**, 181–192 (2016).
20. Taliaferro, J. M. et al. Distal alternative last exons localize mRNAs to neural projections. *Mol. Cell* **61**, 821–833 (2016).
21. Tushev, G. et al. Alternative 3′ UTRs modify the localization, regulatory potential, stability, and plasticity of mRNAs in neuronal compartments. *Neuron* **98**, 495–511 (2018).
22. Briese, M. et al. Whole transcriptome profiling reveals the RNA content of motor axons. *Nucleic Acids Res.* **44**, e33 (2016).
23. Maciel, R. et al. The human motor neuron axonal transcriptome is enriched for transcripts related to mitochondrial function and microtubule-based axonal transport. *Exp. Neurol.* **307**, 155–163 (2018).
24. Zappulo, A. et al. RNA localization is a key determinant of neurite-enriched proteome. *Nat. Commun.* **8**, 583 (2017).
25. Ciolli Mattioli, C. et al. Alternative 3′ UTRs direct localization of functionally diverse protein isoforms in neuronal compartments. *Nucleic Acids Res.* **47**, 2560–2573 (2019).
26. Lubelsky, Y. & Ulitsky, I. Sequences enriched in Alu repeats drive nuclear localization of long RNAs in human cells. *Nature* **555**, 107–111 (2018).
27. Ludwik, K. A., von Kuegelgen, N. & Chekulaeva, M. Genome-wide analysis of RNA and protein localization and local translation in mESC-derived neurons. *Methods* **161–162**, 31–41 (2019).
28. Rotem, N. et al. ALS along the axons—expression of coding and noncoding RNA differs in axons of ALS models. *Sci. Rep.* **7**, 44500 (2017).
29. Minis, A. et al. Subcellular transcriptomics-dissection of the mRNA composition in the axonal compartment of sensory neurons. *Dev. Neurobiol.* **74**, 365–381 (2014).
30. Middleton, S. A., Eberwine, J. & Kim, J. Comprehensive catalog of dendritically localized mRNA isoforms from sub-cellular sequencing of single mouse neurons. *BMC Biol.* **17**, 5 (2019).
31. von Kügelgen, N. & Chekulaeva, M. Conservation of a core neurite transcriptome across neuronal types and species. *Wiley Interdiscip. Rev. RNA* **11**, e1590 (2020).
32. Hayashi, T., Yoshida, T., Ra, M., Taguchi, R. & Mishina, M. IL1RAPL1 associated with mental retardation and autism regulates the formation and stabilization of glutamatergic synapses of cortical neurons through RhoA signaling pathway. *PLoS ONE* **8**, e66254 (2013).
33. Belhasan, D. C. & Akaaboune, M. The role of the dystrophin glycoprotein complex on the neuromuscular system. *Neurosci. Lett.* **722**, 134833 (2020).
34. Donninger, H., Schmidt, M. L., Mezzanotte, J., Barnoud, T. & Clark, G. J. Ras signaling through RASSF proteins. *Semin. Cell Dev. Biol.* **58**, 86–95 (2016).
35. He, M. X. & He, Y. W. CFLAR/c-FLIPL: a star in the autophagy, apoptosis and necroptosis alliance. *Autophagy* **9**, 791–793 (2013).
36. Tyssowski, K. M. et al. Different neuronal activity patterns induce different gene expression programs. *Neuron* **98**, 530–546 (2018).
37. Wu, Z. L. et al. Altered behavior and long-term potentiation in type I adenylyl cyclase mutant mice. *Proc. Natl Acad. Sci. USA* **92**, 220–224 (1995).
38. Grant, C. E. & Bailey, T. L. XSTREME: comprehensive motif analysis of biological sequence datasets. Preprint at https://www.biorxiv.org/content/10.1101/2021.09.02.458722v1 (2021).
39. Kozomara, A., Birgaoanu, M. & Griffiths-Jones, S. miRBase: from microRNA sequences to function. *Nucleic Acids Res.* **47**, D155–D162 (2019).
40. Chekulaeva, M. & Filipowicz, W. Mechanisms of miRNA-mediated post-transcriptional regulation in animal cells. *Curr. Opin. Cell Biol.* **21**, 452–460 (2009).
41. Chi, S. W., Zang, J. B., Mele, A. & Darnell, R. B. Argonaute HITS-CLIP decodes microRNA–mRNA interaction maps. *Nature* **460**, 479–486 (2009).
42. Chekulaeva, M. et al. miRNA repression involves GW182-mediated recruitment of CCR4-NOT through conserved W-containing motifs. *Nat. Struct. Mol. Biol.* **18**, 1218–1226 (2011).
43. Zheng, D. et al. Deadenylation is prerequisite for P-body formation and mRNA decay in mammalian cells. *J. Cell Biol.* **182**, 89–101 (2008).
44. Tsanov, N. et al. smiFISH and FISH-quant—a flexible single RNA detection approach with super-resolution capability. *Nucleic Acids Res.* **44**, e165 (2016).
45. Mikl, M. et al. A massively parallel reporter assay reveals focused and broadly encoded RNA localization signals in neurons. *Nucleic Acids Res.* **50**, 10643–10664 (*2022*).
46. Paz, I., Argoetti, A., Cohen, N., Even, N. & Mandel-Gutfreund, Y. RBPmap: a tool for mapping and predicting the binding sites of RNA-binding proteins considering the motif environment. *Methods Mol. Biol.* **2404**, 53–65 (2022).
47. Czaplinski, K. et al. Identification of 40LoVe, a *Xenopus* hnRNP D family protein involved in localizing a TGF-β-related mRNA during oogenesis. *Dev. Cell* **8**, 505–515 (2005).
48. Terrey, M., Adamson, S. I., Chuang, J. H. & Ackerman, S. L. Defects in translation-dependent quality control pathways lead to convergent molecular and neurodevelopmental pathology. *eLife* **10**, e66904 (2021).
49. Quattrone, A. et al. Posttranscriptional regulation of gene expression in learning by the neuronal ELAV-like mRNA-stabilizing proteins. *Proc. Natl Acad. Sci. USA* **98**, 11668–11673 (2001).
50. Kalisiak, K. et al. A short splicing isoform of HBS1L links the cytoplasmic exosome and SKI complexes in humans. *Nucleic Acids Res.* **45**, 2068–2080 (2017).
51. Simms, C. L., Thomas, E. N. & Zaher, H. S. Ribosome-based quality control of mRNA and nascent peptides. *Wiley Interdiscip. Rev. RNA* **8**, 10.1002/wrna.1366 (2017).
52. Mirisis, A. A. & Carew, T. J. The ELAV family of RNA-binding proteins in synaptic plasticity and long-term memory. *Neurobiol. Learn. Mem.* **161**, 143–148 (2019).

53. Ron, M. & Ulitsky, I. Context-specific effects of sequence elements on subcellular localization of linear and circular RNAs. *Nat. Commun.* **13**, 2481 (2022).
54. Semotok, J. L. et al. Smaug recruits the CCR4/POP2/NOT deadenylase complex to trigger maternal transcript localization in the early *Drosophila* embryo. *Curr. Biol.* **15**, 284–294 (2005).
55. Ding, D., Parkhurst, S. M., Halsell, S. R. & Lipshitz, H. D. Dynamic Hsp83 RNA localization during *Drosophila* oogenesis and embryogenesis. *Mol. Cell. Biol.* **13**, 3773–3781 (1993).
56. Sambandan, S. et al. Activity-dependent spatially localized miRNA maturation in neuronal dendrites. *Science* **355**, 634–637 (2017).
57. Ashraf, S. I., McLoon, A. L., Sclarsic, S. M. & Kunes, S. Synaptic protein synthesis associated with memory is regulated by the RISC pathway in *Drosophila*. *Cell* **124**, 191–205 (2006).
58. Banerjee, S., Neveu, P. & Kosik, K. S. A coordinated local translational control point at the synapse involving relief from silencing and MOV10 degradation. *Neuron* **64**, 871–884 (2009).
59. Muddashetty, R. S. et al. Reversible inhibition of PSD-95 mRNA translation by miR-125a, FMRP phosphorylation, and mGluR signaling. *Mol. Cell* **42**, 673–688 (2011).
60. Lagos-Quintana, M. et al. Identification of tissue-specific microRNAs from mouse. *Curr. Biol.* **12**, 735–739 (2002).
61. Petri, R. et al. let-7 regulates radial migration of new-born neurons through positive regulation of autophagy. *EMBO J.* **36**, 1379–1391 (2017).
62. Schwamborn, J. C., Berezikov, E. & Knoblich, J. A. The TRIM-NHL protein TRIM32 activates microRNAs and prevents self-renewal in mouse neural progenitors. *Cell* **136**, 913–925 (2009).
63. Zou, Y. et al. Developmental decline in neuronal regeneration by the progressive change of two intrinsic timers. *Science* **340**, 372–376 (2013).
64. Li, S. et al. Let-7 microRNAs regenerate peripheral nerve regeneration by targeting nerve growth factor. *Mol. Ther.* **23**, 423–433 (2015).
65. Caygill, E. E. & Johnston, L. A. Temporal regulation of metamorphic processes in *Drosophila* by the let-7 and miR-125 heterochronic microRNAs. *Curr. Biol.* **18**, 943–950 (2008).
66. Edbauer, D. et al. Regulation of synaptic structure and function by FMRP-associated microRNAs miR-125b and miR-132. *Neuron* **65**, 373–384 (2010).
67. Selbach, M. et al. Widespread changes in protein synthesis induced by microRNAs. *Nature* **455**, 58–63 (2008).
68. Baek, D. et al. The impact of microRNAs on protein output. *Nature* **455**, 64–71 (2008).
69. Pushpalatha, K. V. & Besse, F. Local translation in axons: when membraneless RNP granules meet membrane-bound organelles. *Front. Mol. Biosci.* **6**, 129 (2019).
70. Cook, K. B., Kazan, H., Zuberi, K., Morris, Q. & Hughes, T. R. RBPDB: a database of RNA-binding specificities. *Nucleic Acids Res.* **39**, D301–D308 (2011).
71. Doma, M. K. & Parker, R. RNA quality control in eukaryotes. *Cell* **131**, 660–668 (2007).
72. Arora, A. et al. High-throughput identification of RNA localization elements in neuronal cells. *Nucleic Acids Res.* **50**, 10626–10642 (2022).
73. Lie, Y. S. & Macdonald, P. M. Apontic binds the translational repressor Bruno and is implicated in regulation of oskar mRNA translation. *Development* **126**, 1129–1138 (1999).
74. Filardo, P. & Ephrussi, A. Bruno regulates *gurken* during *Drosophila* oogenesis. *Mech. Dev.* **120**, 289–297 (2003).
75. Cherone, J. M., Jorgji, V. & Burge, C. B. Cotargeting among microRNAs in the brain. *Genome Res.* **29**, 1791–1804 (2019).
76. Pique, M., Lopez, J. M., Foissac, S., Guigo, R. & Mendez, R. A combinatorial code for CPE-mediated translational control. *Cell* **132**, 434–448 (2008).
77. An, J. J. et al. Distinct role of long 3′ UTR BDNF mRNA in spine morphology and synaptic plasticity in hippocampal neurons. *Cell* **134**, 175–187 (2008).
78. Shigeoka, T. et al. On-Site ribosome remodeling by locally synthesized ribosomal proteins in axons. *Cell Rep.* **29**, 3605–3619 (2019).
79. Fusco, C. M. et al. Neuronal ribosomes exhibit dynamic and context-dependent exchange of ribosomal proteins. *Nat. Commun.* **12**, 6127 (2021).
80. Zuker, M. Mfold web server for nucleic acid folding and hybridization prediction. *Nucleic Acids Res.* **31**, 3406–3415 (2003).
81. Bahry, E. et al. RS-FISH: precise, interactive, fast, and scalable FISH spot detection. *Nat. Methods* **19**, 1563–1567 (2022).

Methods

Our research complies with all relevant ethical regulations and has been approved by the Max Delbrück Center (MDC) for Molecular Medicine and the German regulation authority: das Landesamt für Gesundheit und Soziales (LAGeSo).

Experimental models

The HeLa-rtTA cell line used for luciferase reporter assay was obtained from Kai Schoenig (ZI Mannheim)[82], and the 293T cell line used for lentivirus production was obtained from the MDC. Male and female *Mus musculus* embryos (embryonic day 14 (E14)) or neonatal pups (P0) of the C57BL/6J strain, obtained from the MDC mouse facility, were used to prepare cortical neuron cultures. The number of animals dissected for each experiment was defined by the number of neurons required for plating (see 'PCN culture and lentiviral transduction' subsection) and calculated based on the expected yield of 5×10^6 neurons per pup.

PCN culture and lentiviral transduction

PCN culture, separation on soma and neurites and lentivirus preparation were done as described previously[25]. In short, cortical neurons were isolated from E14 or P0 pups and co-cultured with astrocytes[83]. For separation on neurites and soma, 1×10^5 cells per cm^2 neurons were plated on double-coated (poly-D-lysine and laminin) cell inserts (Millicell six-well PISP30R48, Millipore). Soma was dissociated from the top of inserts by intensive washes with cold PBS and spinning at 5,000*g* and 4 °C for 1.5 minutes. For neurites isolation, cotton swabs were used to remove the remaining soma from the top of the insert, and the membrane with attached neurites was used for protein or RNA isolation. For protein lysates, neurites and soma were lysed in 8 M urea and 0.1 M Tris-HCl pH 7.5. TRIzol reagent (Thermo Fisher Scientific) was used for RNA isolation.

To prepare lentiviral particles, 293T cells growing in 10-cm dishes were transfected using polyethylenimine (PEI) with 10 µg of the envelope (Addgene, 12259), packaging (Addgene, 12260) and transfer plasmids in the ratio 1:1:2. The next day, the medium was exchanged to 10 ml of DMEM without FBS. Seventy-two hours after transfection, the lentivirus-containing medium was cleared from cell debris by centrifugation at 500*g* for 5 minutes and concentrated at 4 °C for 4–24 hours using 3 volumes of Lenti-X concentrator (631232, Takara Bio). Viral particles were collected by centrifugation at 1,500*g* and 4 °C for 45 minutes and resuspended in 200 µl of cold PBS. Virus was applied on cortical neurons between days in vitro 3 (DIV3) and DIV6, and cells were collected at DIV9. For N-zip experiments, 70 µl of the concentrated virus was added per 10^6 PCNs growing on a Millicell cell insert (six-well) at DIV5. Preparation of the shRNA depletion samples for RNA-seq of endogenous RNAs was performed similarly, with 30 µl of the concentrated virus transduced. For shRNA depletion experiments combined with N-zip libraries, 30 µl of shRNA virus was added to cells at DIV3; the medium was changed at DIV5; and 70 µl of viral N-zip library was added at DIV6.

For depolarization experiments, P0 PCNs were treated as described previously[36]. In brief, on DIV8, the cells were treated for 16 hours with 50 µM APV and 10 µM CNQX to block NMDA and AMPA receptors. Neurons were then stimulated with a final concentration of 55 mM KCl using 3× KCl depolarization solution (170 mM KCl, 10 mM HEPES pH 7.4, 1 mM $MgCl_2$ and 2 mM $CaCl_2$). RNA for RT–qPCR and N-zip library preparation was collected from cells before depolarization (control samples) and after sustained 3-hour depolarization. The experiment was performed in biological triplicates.

Luciferase reporter assays

Human HeLa-rtTA cells expressing reverse tetracycline-controlled transactivator[82] were grown in DMEM with GlutaMAX supplement (DMEM + GlutaMAX, Gibco) with 10% FBS and used in luciferase reporter assay. Transfections were done in 96-well plates with PEI using a 1:3 ratio of DNA:PEI. Cells were transfected with 1–3 ng of FL/RL doxycycline-inducible let-7 reporter per well. Increasing amounts of GFP-let-7 sponge (40, 60, 80, 100 and 125 ng per well) were co-transfected, where indicated. GFP-encoding plasmid was used as a filler, to top up each transfection to the same total amount of DNA. Expression of luciferase reporters was induced with doxycycline (1 µg ml^{-1}), and cells were lysed 24 hours after transfection. Luciferase activities were measured with a homemade luciferase reporter assay system as described previously[84]. More specifically, 45 µl of FLuc reagent (75 mM HEPES pH 8.0, 0.1 mM EDTA, 4 mM $MgSO_4$, 530 µM ATP, 270 µM coenzyme A, 470 µM DTT and 470 µM luciferin) and 45 µl of RLuc reagent (2.2 mM Na_2EDTA, 220 mM K_3PO_4 pH 5.1, 0.44 mg ml^{-1} of BSA, 1.1 M NaCl, 1.3 mM NaN_3 and 0.6 µg ml^{-1} of coelenterazine) reagents per sample were used to measure luciferase activities.

DNA constructs

FL/RL-hmga2-wt and FL/RL-hmga2-mut were previously described[42,85]. For other let-7 reporters, we modified the same backbone with bi-directional promoter for simultaneous expression of two genes, pSF2.GFPLuc[86]. First, *Renilla* luciferase (RL) was PCR-amplified and cloned into EcoRI/NotI-cut pSF2.GFPLuc, to substitute GFP with RL and produce pSF2-FL/RL. Next, a fragment containing the polyadenylation signal was cloned into NotI site downstream of RL, to generate pSF2-FL/RL-pA. Finally, synthetic oligos corresponding to Cflar-14, Mcf2l-7 and Utrn-61 tiles (Supplementary Table 1) or their mutated versions (CTACCTC → CCATCCC and CTACCTC → GATGGAG) were annealed and cloned between AgeI and NotI sites of pSF2-FL/RL-pA.

To generate a GFP-encoding plasmid, GFP open reading frame (ORF) was PCR-amplified and cloned between AgeI and EcoRI sites of the lentiviral vector with synapsin I promoter (Addgene, 20945). During this cloning, the AgeI site was destroyed, and a new AgeI was introduced on a PCR primer downstream of GFP. The resulting pLenti-GFP construct was used to produce pLenti-GFP-Map2, pLenti-GFP-Cflar, pLenti-GFP-Rassf3, pLenti-GFP-Mcf2l, pLenti-GFP-Utrn and pooled N-zip lentiviral libraries. To generate pLenti-GFP reporters with N-zip tiles in their 3′ UTR, the corresponding annealed oligonucleotides (Supplementary Table 7) were cloned between AgeI and EcoRI sites downstream of GFP.

To produce $(AU)_8$-boxB and $(AU)_8$mut-boxB constructs for GRNA chromatography, synthetic oligos corresponding to *Rassf3-91* tile or its mutated version (ATATATATATATATAT → GTACATACATGTACAT) were annealed and cloned between KpnI and NheI sites of pBS-Luc-boxB[87].

pLKO-shAgo2 and pLKO-shHbs1l were generated by cloning of annealed oligonucleotides (Supplementary Table 7; shAgo2-fw and shAgo2-rev, shHbs1l-fw and shHbs1l-rev, correspondingly) into AgeI and EcoRI-cut pLKO1-puro vector (Addgene, 8453).

Western blotting

Next, 5–10 µg of total protein was separated on a 10% Laemmli PAAG. Proteins were transferred to the PVDF membrane and analyzed by western blotting. The following primary antibodies were used: rabbit anti-histone H3 1:5,000 (ab1791, Abcam), mouse anti-actin 1:4,000 (Sigma-Aldrich, A2228), mouse anti-neurofilament SMI312 1:10,000 (837904, BioLegend), rabbit anti-Hbs1l 1:500 (H00010724-PW1, Abnova) and mouse anti-Ago2/eIF2C2 1:500 (H00027161-M01, Abnova). Western blot images shown in Figs. 5a and 7b and Extended Data Fig. 1b have been cropped for presentation. Full-size images are presented in Source Data.

smiFISH probe design and preparation

To assay RNA localization of GFP reporter constructs, complementary 18–20-nt DNA probes against the ORF of GFP (24 probes) were designed using the Biosearch Technologies Stellaris RNA FISH probe designer tool (https://biosearchtech.com). All probe sequences are provided in Supplementary Table 7. The reverse complement of the X FLAP[44] sequence was added to the 5′ end of each probe:

CCTCCTAAGTTTCGAGCTGGACTCAGTG. The X FLAP oligo (CACTGAGTCCAGCTCGAAACTTAGGAGG), 5′ and 3′ end-labeled with Quasar 570, was synthesized by Biosearch Technologies. X FLAP was hybridized with the probe set using the following conditions: 2 µl of the probe set (40 pmol in total), 0.5 µl of 100 µM X FLAP, 1 µl of 10× NEB 3 buffer and 6.5 µl of water were mixed and annealed in a thermal cycler as described previously[44]: 85 °C for 3 minutes, 65 °C for 3 minutes, 25 °C for 5 minutes and 4 °C hold. Annealed probes were stored at −20 °C.

smiFISH imaging

smiFISH was performed with *GFP* probes on mouse PCNs (P0 and DIV9) cultured on 15-mm glass coverslips as described previously[44], with some modifications. The media was aspirated, and cells were washed with 1× PBS. Cells were fixed with 4% paraformaldehyde (PFA) for 20 minutes at room temperature and then rinsed twice with 1× PBS. Permeabilization was done with 70% ethanol at 4 °C overnight. The cells were washed with 15% formamide freshly prepared in 1× SSC buffer for 15 minutes at room temperature. Then, 50 µl of hybridization mix (1 µl of FLAP hybridized probes in 2× SSC, 10% formamide and 10% w/v dextran sulfate) was added to each coverslip and incubated overnight at 37 °C in a humid chamber. The cells were washed twice for 30 minutes with freshly prepared 15% formamide/1× SSC at 37 °C in the dark. During the second wash, DAPI nuclear stain was added (5 ng µl^{-1}). The cells were washed twice more in 2× SSC, and the coverslips were mounted on a glass slide with 10 µl of ProLong Glass mounting medium (Thermo Fisher Scientific, P36980) without DAPI. Then, 3 × 3 tiled z-stack images were acquired using a Dragonfly 200 spinning disc confocal microscope with a ×63 oil objective and stitched using Fusion acquisition software. Consistent laser intensity and exposure times were used across samples to detect DAPI, EGFP protein and Quasar 570 (EGFP RNA).

smiFISH image analysis

The images were analyzed using radial symmetry-FISH (RS-FISH)[81]. In brief, maximum projections were performed using Fiji (ImageJ)[88] for EGFP and used to generate a mask for soma and neurites using ilastik[89] and manual curation using Fiji to generate masks for proximal neurite (up to 30 µm from the cell body/soma) and distal neurite (30 µm up to a maximum of 100 µm). The RNA foci were detected and quantified using the RS-FISH Fiji plugin as described in Bahry et al.[81]. The detections were subsequently filtered using either the distal neurite or proximal neurite masks using the mask filtering tool in RS-FISH. The RNA detections were normalized by area in their region. Scripts for smiFISH image analysis can be found at https://github.com/LauraBreimann/smFISH_neuron_analysis.

RNA extraction and qRT–PCR

For RT–qPCR analysis, RNA was isolated with TRIzol (Thermo Fisher Scientific), treated with RQ1 DNase I and reverse-transcribed using the Maxima first-strand cDNA synthesis kit (Thermo Fisher Scientific). *Ago2*, *Hbs1l* and *Gapdh* were quantified using sensiFAST SYBR No ROX qPCR kit (Bioline). *Homer and Snord15b* were used to estimate the efficiency of soma/neurite separation. See Supplementary Table 7 for primer sequences. Relative expression levels were calculated using the $\Delta\Delta C_t$ method with *Gapdh* as a reference gene.

In vitro transcription, GRNA chromatography and mass spectrometry

$(AU)_8$-boxB and $(AU)_8$mut-boxB RNAs were generated using a T3 MEGAscript in vitro transcription kit (Thermo Fisher Scientific, AM1338) according to the manufacturer's recommendations. The template plasmids were linearized with HindIII. RNA was purified using Agencourt RNAClean XP beads (Beckman Coulter, A63987).

GRNA chromatography was performed as described previously[87] with the following modifications. First, 30 µg ml^{-1} of GST-lambda N fusion peptide was immobilized on 20 µl of a 50% slurry of Glutathione Sepharose 4B (Amersham, 17075601) in binding buffer (BB: 20 mM Tris-HCl pH 7.5, 150 mM NaCl, 10% glycerol, 0.05% NP-40 and 0.4 mM) by incubating on an orbital rocker for 30 minutes at room temperature. Beads were washed twice in 1 ml of BB and incubated with 25 pmol of RNA ((AU)8-boxB and (AU)8mut-boxB) in 200 µl of BB for 1 hour at 4 °C. The beads were washed twice with 1 ml of BB and incubated with 3 mg of protein lysate prepared from P0 mouse brain (lysis buffer: BB with 0.5% NP-40) for 2 hours at 4 °C. The beads were washed three times with 1 ml of BB, and bound proteins were eluted with 0.15 µg of RNAse A in 60 µl of BB without NP-40 for 30 minutes at 30 °C on an orbital shaker. Eluates were supplemented with 70 µl of 2.5 M NaOAC pH 5.0, 1 µl of GlycoBlue (Ambion) and absolute EtOH up to 2 ml and incubated at 4 °C overnight. Proteins were recovered by centrifugation at 18,000*g* and 4 °C for 30 minutes. Total protein lysates from neurites and soma of PCNs were prepared as previously described[24]. Eluates and total lysates were subjected to in-solution digest using trypsin, and desalted peptides were subjected to liquid chromatography–tandem mass spectrometry (LC–MS/MS) using a Q Exactive HF-X mass spectrometer coupled to an Easy nLC1200 system (Thermo Fisher Scientific). MS data were processed with Max Quant software (1.6.3.4) with peptide FDR cutoff at 1%. The resulting text files were filtered to exclude reverse database hits, potential contaminants and proteins identified only by site. For eluate samples, label-free quantification (LFQ) intensity values were filtered for 'minimum value of 3' in at least one group. Missing values were imputed with random noise simulating the detection limit of the mass spectrometer. Differential proteins were defined using two-sample Student's *t*-test and FDR-based significance cutoff. The DEP R package (version 1.6.1)[90] was used to analyze iBAQ protein intensity values from total proteome data. Only proteins detected in at least half (three out of six) of samples and not marked as potential contaminant or reverse sequence were retained for analysis. Missing values were imputed using the 'MinProb' algorithm (random draws from a Gaussian distribution) with standard settings, and values from each compartment were then normalized to the median GAPDH intensity. Enrichment between compartments was calculated using a generalized linear model (limma), and *P* values were FDR-corrected with the Benjamini–Hochberg method.

mRNA-seq and total RNA-seq libraries preparation

mRNA-seq libraries were prepared with TruSeq Stranded mRNA library preparation kit (Illumina, 2002059) according to the manufacturer's recommendations. mRNA-seq was done in biological triplicates, using 100 ng of total RNA from neurites or soma per sample. RNA was supplemented with ERCC spike-ins (Thermo Fisher Scientific, 4456740) according to the manufacturer's recommendations. Based on the spike-ins, we estimate that ~4% of mRNA per PCN is contained in neurites and the rest in soma. SLAM-seq library preparation and data analysis are described elsewhere (E-MTAB-11572 and E-MTAB-11575, https://github.com/melonheader/Stability). Total RNA-seq libraries (Extended Data Fig. 1) were prepared using TruSeq Stranded total RNA library preparation kit (20020596, Illumina). Libraries were pooled and sequenced on Illumina NextSeq 500 or NovaSeq 6000 system with a single-end 75-cycle or 150-cycle run.

N-zip libraries preparation

To generate a pooled lentiviral library expressing fragments tiled across 3′ UTRs of neurite-localized transcripts, a pool of the corresponding oligos (Supplementary Tables 1 and 2) flanked by adapter sequences (TTCGATATCCGCATGCTAGC-tile-GATCGGAAGAGCACACGTCT) was synthesized (Twist Bioscience or Agilent Technologies). Fragments were PCR-amplified (see Supplementary Table 7 for primer sequences) and cloned via Gibson assembly into AgeI-cut pLenti-GFP downstream of GFP, using Endura ElectroCompetent Cells (Lucigen, 60242-1). Resulting pooled DNA libraries were used to produce lentiviral particles and infect PCNs.

RNA, isolated from neurites and soma of PCNs as previously described[25], was used to prepare N-zip libraries. In short, RNA was reverse-transcribed into cDNA with a primer complementary to the 3′ adapter flanking the tiles. Unique molecular identifiers (UMIs) were introduced during the second-strand synthesis with a pool of primers complementary to the 5′ adapter flanking the tiles. Residual primers were removed with an ExoI/rSAP mix. The resulting double-stranded DNA (dsDNA) was purified with AMPure beads, and the N-zip tiles were PCR-amplified and barcoded. Libraries were pooled and sequenced on Illumina NextSeq 500 or NovaSeq 6000 system with a single-end 75-cycle or 150-cycle run.

Analysis of published RNA-seq datasets

Several transcriptome datasets from compartments of primary neurons were acquired from published sources: raw datasets were downloaded from the Gene Expression Omnibus (GEO) database (GSE67828 (ref. [20]), GSE66230 (ref. [22]) and GSE51572 (ref. [29])) and analyzed using the PiGx RNA-seq pipeline[91] (version 0.0.3) with default settings using the Ensembl mouse genome assembly (GRCm38.p6, release 91); alternatively, counts were taken from supplementary tables of studies that either did not deposit raw data[28] or did not use a standard RNA-seq approach[21,30]. Differential expression analysis between neurite and soma compartments was performed using DESeq2 (ref. [92]). Additionally, counts were normalized to transcripts per million (TPM) and averaged for neurite and soma compartment within each dataset.

Analysis of PCN RNA-seq data

RNA-seq data from our PCNs were analyzed with the PiGx pipeline in the same way as published datasets. Because genomic and intronic reads were detected in the stranded library, a restricted set of genes was chosen for analysis: strand-specific counts (sense and antisense) as well as intron counts were generated using a custom ht-seq-based[93] Python script. Only genes with strong exon/intron and sense-strand/antisense-strand ratios ($\log_2$(exon/intron) > 2.5 and $\log_2$(sense/antisense) > 2) were used for further analysis.

Selection of zipcode candidate 3′ UTRs

To select sequences for the first N-zip library, only genes with significant enrichment (adjusted $P < 0.05$) in the analyzed primary neuronal datasets were considered as candidates to generate a list of genes with reliable neurite localization. This selection was further restricted to genes for which an enrichment value could be calculated in our PCN system ($\log_2$FC not NA). Then, genes with (1) a significant enrichment in at least four datasets; (2) median $\log_2$FC > 1; and (3) either mean $\log_2$FC > 1 or a positive $\log_2$FC value in all datasets were chosen. Additionally, genes with a significant enrichment value in at least five datasets and either median $\log_2$FC > 1 or mean $\log_2$FC > 1 or a positive $\log_2$FC value in all datasets were chosen as well.

This initial unbiased set of genes was then manually refined by (1) excluding genes encoded by the mitochondrial genome as well as some genes with the annotated nuclear or mitochondrial function (*Pola1*, *Ezh2*, *Smc4*, *Cenpb*, *Pink1* and *Ncl*); (2) adding genes with a known zipcode or neurite localization sequence (*Camk2a*[94], *Actb*[5], *Bdnf*[9], *Arc*[11,95], *Cdc42* (ref. [25]), *Map2* (ref. [96]) and *Bc1* (ref. [97])); (3) adding genes that showed localization in non-primary[31] and in-house datasets as well as our PCN and fewer other primary datasets (*Rab13*, *Net1*, *Hmgn5*, *2410006H16Rik*, *Pfdn5*, *Tagln2*, *Pfdn1* and *Cryab*); and (4) restricting the genes encoding for ribosomal proteins and translation factors to a smaller subset with sufficiently large 3′ UTRs (*Rplp2*, *Rpl12*, *Rpl39*, *Rpl37*, *Rpl14*, *Rps28*, *Rpsa*, *Rps24*, *Rps23*, *Rps18*, *Eef1b2*, *Eef1a1* and *Eef1g*).

Design of the 3′ UTR tile library

The 3′ UTR sequences for all transcript isoforms of the chosen genes were downloaded via Ensembl biomaRt. For each gene, the 3′ UTR sequences fully contained in another isoform were removed, leaving only the longest non-overlapping 3′ UTR sequences. For all genes with multiple unique 3′ UTR sequences, we manually decided which isoform sequence(s) to include in the final set of sequences, based on annotation and PCN genome browser tracks of the corresponding genes. For *Cflar* and *Cdc42*, both alternative 3′ UTRs were included (and named *Cflar*-1 and *Cflar*-2, respectively, for *Cdc42*). For *Hdac5* and *Arhgap11a*, the different but overlapping isoforms were manually merged into one sequence. This resulted in a final list of 99 3′ UTR sequences.

Each of these sequences was then cut into overlapping tiles covering the entire sequence. For sequences smaller than 500 nt, tiles with 75-nt size and 15-nt offset were designed. For sequences larger than 500 nt, tiles with 100-nt size with 25-nt offset were generated. In both cases, any remaining sequence was added to the last tile while keeping the maximum tile size below 80 nt or 110 nt, correspondingly. In addition, five control tiles with scrambled sequences were generated from the first tile of *Camk2a*, *Actb* and *Bc1* each. The final set of 4,813 tiles was ordered, including 3′ and 5′ adapter sequences (3′: TTCGATATCCGCATGCTAGC; 5′: GATCGGAAGAGCACACGTCT). The full sequences are provided in Supplementary Table 1.

N-zip data analysis

The sequenced reads were used to count individual library tiles. We considered only R1 reads that contained the TTCGATATCCGCATGCTAGC adaptor sequence and extracted the UMI sequence preceding the adaptor. Each read was then matched to the sequences in the library, without allowing insertions or deletions. The output from this step was a table of counts of reads mapping to each library sequence. The N-zip libraries had 4.8 million mapped reads on average, and the mutagenized N-zip had 1.9 million mapped reads on average. Only fragments with at least 20 reads on average were used in subsequent analysis. In the N-zip library, 4,745 tiles had at least three samples with at least 20 reads (98.5%). The mutagenized N-zip library had 6,266 tiles, and 5,679 (90.6%) had at least three samples with at least 20 reads. The reads were normalized to the total number of mapped reads. Counts within each compartment were highly correlated between replicates (Spearman R > 0.85). The normalized counts were used to compute neurite/soma ratios after adding a pseudocount of 0.5. Statistical significance for each tile was estimated with DESeq2's Wald test (default) and corrected for multiple testing using the Benjamini–Hochberg procedure. Ratios for groups of tiles were compared using two-sided Wilcoxon rank-sum test. The code for N-zip data analysis is available at https://github.com/IgorUlitsky/MPRNA.

Analysis of miRNA binding sites and $(AU)_n$ motif

Analysis of miRNA binding sites and $(AU)_n$ motif enrichment was performed on N-zip libraries and mRNA-seq libraries. Tile sequences and sequences of 3′ UTRs of protein-coding genes annotated in GENCODE were analyzed using the R 'stringr' package (version 1.4.0) for matches to the let-7 seed sequence and for the maximal match to the $(AU)_n$ motif. For obtaining neurites/soma ratios in mRNA-seq data, reads were mapped to the transcriptome using Salmon, and transcript abundance and enrichment was calculated using tximport and DESeq2 workflow[92]. Only the most abundant isoforms, with total TPM of at least 10 in the averaged soma and neurites samples were considered in all further analyses. For analysis of the shRNA-treated cells, we used RSEM and GENCODE vM21 to obtain isoform-specific expression levels quantified as TPM. These were used to compute $\log_2$-transformed ratios between the averages of the neurite and the soma samples using a pseudocount of 1.

Design of mutation tile library

From the first N-zip library, a subset of neurite-enriched tiles was chosen for extensive mutagenesis. In case of overlapping tiles forming one peak, the central tile was selected. More specifically, from the tiles with significant (adjusted $P < 0.1$) and high (mean $\log_2$FC > 1) enrichment in

neurites, we chose the following 16 tiles: *Ndufa2*, tiles 11 + 12 (for 75-nt tiles, two tiles were combined); *Camk2n1*, tile 12; *Msn*, tile 48; *Golim4*, tile 56; *Cdc42_2*, tile 31; *Bdnf*, tile 56; *Map2*, tile 5; *Cflar_2*, tile 52; *Rassf3*, tile 91; *Mcf2l*, tile 7; *Cflar_1*, tile 14; *Utrn*, tile 61; *Cald1*, tile 58; *Rps23*, tiles 11 + 12; *Cox5b*, tiles 6 + 7; and *Kif1c*, tile 80. For each of these tiles, we generated all possible single base substitutions as well as sets of A ⇄ T and C ⇄ G base transitions in 2mer, 5mer and 10mer stretches that together cover each tile. Additionally, the wild-type and three scrambled versions of each tile were added as controls. All tiles were ordered in one oligo pool from Agilent Technologies. The full list of sequences is provided in Supplementary Tables 1 and 2.

Motif enrichment and GO analyses

The sequences of all neurite-enriched tiles in N-zip (log_2FC neurites/soma ≥ 1, adjusted $P < 0.1$; Supplementary Table 1) were used as input for motif discovery and enrichment analysis using the XSTREME web interface[38]. Analysis for enriched functional terms was performed for all genes with a neurite-enriched peak in the N-zip library with gProfiler2 using the default settings[98]. Five top GO terms with the lowest *P* values for biological processes (BPs) and cellular compartments (CCs) domains were used for plotting.

Quantification and statistical data analysis

Details of exact statistical analyses, packages, tests and other procedures used can be found in the main text, figure legends and Methods. No statistical methods were used to pre-determine sample sizes, but our sample sizes are similar to those reported in previous publications[24–26,53]. Data collection and analysis were not performed blinded to the conditions of the experiments. No datapoint was excluded from the analyses. No randomization was performed. A-parametric tests that do not rely on the assumption of normal distributions were used unless indicated otherwise.

Reporting summary

Further information on research design is available in the Nature Portfolio Reporting Summary linked to this article.

Data availability

Next-generation sequencing data have been deposited at ArrayExpress (accession numbers E-MTAB-10902, E-MTAB-11572 and E-MTAB-11575). The mass spectrometry proteomics data have been deposited to the ProteomeXchange Consortium via the PRIDE[99] partner repository with the dataset identifiers PXD028300 and PXD026089. smiFISH images have been deposited to the figshare image repository (https://doi.org/10.6084/m9.figshare.21196765.v1). Source data are provided with this paper.

Code availability

The code for N-zip data analysis is available at https://github.com/IgorUlitsky/MPRNA, the code for the SLAM-seq at https://github.com/melonheader/Stability and the code for smiFISH analysis at https://github.com/LauraBreimann/smFISH_neuron_analysis.

References

82. Weidenfeld, I. et al. Inducible expression of coding and inhibitory RNAs from retargetable genomic loci. *Nucleic Acids Res.* **37**, e50 (2009).
83. Kaech, S. & Banker, G. Culturing hippocampal neurons. *Nat. Protoc.* **1**, 2406–2415 (2006).
84. Mauri, M. et al. Conservation of miRNA-mediated silencing mechanisms across 600 million years of animal evolution. *Nucleic Acids Res.* **45**, 938–950 (2016).
85. Bethune, J., Artus-Revel, C. G. & Filipowicz, W. Kinetic analysis reveals successive steps leading to miRNA-mediated silencing in mammalian cells. *EMBO Rep.* **13**, 716–723 (2012).
86. Loew, R., Vigna, E., Lindemann, D., Naldini, L. & Bujard, H. Retroviral vectors containing Tet-controlled bidirectional transcription units for simultaneous regulation of two gene activities. *J. Mol. Genet. Med.* **2**, 107–118 (2006).
87. Chekulaeva, M., Hentze, M. W. & Ephrussi, A. Bruno acts as a dual repressor of *oskar* translation, promoting mRNA oligomerization and formation of silencing particles. *Cell* **124**, 521–533 (2006).
88. Schindelin, J. et al. Fiji: an open-source platform for biological-image analysis. *Nat. Methods* **9**, 676–682 (2012).
89. Berg, S. et al. ilastik: interactive machine learning for (bio)image analysis. *Nat. Methods* **16**, 1226–1232 (2019).
90. Zhang, X. et al. Proteome-wide identification of ubiquitin interactions using UbIA-MS. *Nat. Protoc.* **13**, 530–550 (2018).
91. Wurmus, R. et al. PiGx: reproducible genomics analysis pipelines with GNU Guix. *Gigascience* **7**, giy123 (2018).
92. Love, M. I., Huber, W. & Anders, S. Moderated estimation of fold change and dispersion for RNA-seq data with DESeq2. *Genome Biol.* **15**, 550 (2014).
93. Anders, S., Pyl, P. T. & Huber, W. HTSeq—a Python framework to work with high-throughput sequencing data. *Bioinformatics* **31**, 166–169 (2015).
94. Mori, Y., Imaizumi, K., Katayama, T., Yoneda, T. & Tohyama, M. Two *cis*-acting elements in the 3′ untranslated region of α-CaMKII regulate its dendritic targeting. *Nat. Neurosci.* **3**, 1079–1084 (2000).
95. Ninomiya, K., Ohno, M. & Kataoka, N. Dendritic transport element of human arc mRNA confers RNA degradation activity in a translation-dependent manner. *Genes Cells* **21**, 1263–1269 (2016).
96. Blichenberg, A. et al. Identification of a *cis*-acting dendritic targeting element in MAP2 mRNAs. *J. Neurosci.* **19**, 8818–8829 (1999).
97. Muslimov, I. A., Iacoangeli, A., Brosius, J. & Tiedge, H. Spatial codes in dendritic BC1 RNA. *J. Cell Biol.* **175**, 427–439 (2006).
98. Raudvere, U. et al. g:Profiler: a web server for functional enrichment analysis and conversions of gene lists (2019 update). *Nucleic Acids Res.* **47**, W191–W198 (2019).
99. Perez-Riverol, Y. et al. The PRIDE database and related tools and resources in 2019: improving support for quantification data. *Nucleic Acids Res.* **47**, D442–D450 (2019).
100. Hofacker, I. L. Vienna RNA secondary structure server. *Nucleic Acids Res.* **31**, 3429–3431 (2003).

Acknowledgements

N.v.K. is supported by the MDC PhD fellowship; S.M. by the DAAD PhD fellowship; S.D. by the Honjo International PhD; and L. Breimann by the MDC, the Joachim Herz Foundation (850022) and the NIH/NHGRI (RM1HG011016). Work in the Igor Ulitsky laboratory was supported by Israeli Science Foundation grant ISF 852/19 and the Nella and Leon Benoziyo Center for Neurological Diseases. This work is supported by a grant from the German Israeli Foundation to I.U. and M.C. and a Deutsche Forschungsgemeinschaft (DFG) grant to M.C. We thank R. Hodge for comments on the manuscript. The funders had no role in study design, data collection and analysis, decision to publish or preparation of the manuscript.

Author contributions

Experiments were performed by S.M. (shRNA depletions and library preparations, smFISH imaging and quantification, cloning of GFP-let-7 sponge, pSf2-FL/RL-pA, Utrn-wt, Utrn-mut, Cflar-wt, pLKO-shAgo2, pLKO-shHbs1l, pLenti-GFP-Map2 and pLenti-GFP-Cflar); by S.D. (N-zip, secondary N-zip and small RNA library preparation); by L. Breimann (smFISH quantification pipeline); by I.L. (SLAM-seq);

by M.F. (smFISH quantification); by L. Bujanic (cloning of pSf2-FL/RL, Mcf2l-wt, Mcf2l-mut and Cflar); by N.Z. (cloning of boxB constructs and preparation of virus); by M.K. and P.M. (mass spectrometry); and by M.C. (GRNA chromatography, let-7 reporter assays, cloning of pLenti-GFP and Cflar-mut). A.B. performed SLAM-seq analysis. N.v.K. designed the N-zip libraries. N.v.K., M.R. and I.U. performed computational data analysis. I.U. and M.C. conceptualized and supervised the work. M.C. wrote the paper, with feedback from all authors.

Funding
Open access funding provided by Max-Delbrück-Centrum für Molekulare Medizin in der Helmholtz-Gemeinschaft (MDC).

Competing interests
The authors declare no competing interests.

Additional information
Extended data is available for this paper at https://doi.org/10.1038/s41593-022-01243-x.

Supplementary information The online version contains supplementary material available at https://doi.org/10.1038/s41593-022-01243-x.

Correspondence and requests for materials should be addressed to Igor Ulitsky or Marina Chekulaeva.

Peer review information *Nature Neuroscience* thanks the anonymous reviewers for their contribution to the peer review of this work.

4. Charcot–Marie–Tooth mutation in glycyl-tRNA synthetase stalls ribosomes in a pre-accommodation state and activates integrated stress response

Samantha Mendonsa, Nicolai von Kuegelgen, Lucija Bujanic, Marina Chekulaeva

This chapter was published on 17 August 2021:

Nucleic Acids Research (2021)

Volume 49, Issue 17, Pages 10007–10017

DOI: 10.1093/nar/gkab730

Link: https://doi.org/10.1093/nar/gkab730

Supplementary data for this publication is detailed in Appendix II.

Published online 17 August 2021 *Nucleic Acids Research, 2021, Vol. 49, No. 17* ***10007–10017***
https://doi.org/10.1093/nar/gkab730

Charcot–Marie–Tooth mutation in glycyl-tRNA synthetase stalls ribosomes in a pre-accommodation state and activates integrated stress response

Samantha Mendonsa[1,2], Nicolai von Kuegelgen[1,2], Lucija Bujanic[1] and Marina Chekulaeva[1,*]

[1]Berlin Institute for Medical Systems Biology, Max Delbrück Center for Molecular Medicine in the Helmholtz Association, Berlin, Germany and [2]Free University, Berlin, Germany

Received August 04, 2021; Editorial Decision August 09, 2021; Accepted August 12, 2021

ABSTRACT

Toxic gain-of-function mutations in aminoacyl-tRNA synthetases cause a degeneration of peripheral motor and sensory axons, known as Charcot–Marie–Tooth (CMT) disease. While these mutations do not disrupt overall aminoacylation activity, they interfere with translation via an unknown mechanism. Here, we dissect the mechanism of function of CMT mutant glycyl-tRNA synthetase (CMT-GARS), using high-resolution ribosome profiling and reporter assays. We find that CMT-GARS mutants deplete the pool of glycyl-tRNA^{Gly} available for translation and inhibit the first stage of elongation, the accommodation of glycyl-tRNA into the ribosomal A-site, which causes ribosomes to pause at glycine codons. Moreover, ribosome pausing activates a secondary repression mechanism at the level of translation initiation, by inducing the phosphorylation of the alpha subunit of eIF2 and the integrated stress response. Thus, CMT-GARS mutant triggers translational repression via two interconnected mechanisms, affecting both elongation and initiation of translation.

INTRODUCTION

Defects in translational regulation have been identified as common features in multiple neurodegenerative disorders (reviewed in (1)). Yet in some cases the precise mechanisms by which they disrupt translation have to be clarified. For protein synthesis, amino acids are ligated to their cognate tRNAs by aminoacyl-tRNA synthetases (aaRSs), and mutations in six of these enzymes cause a degeneration of peripheral motor and sensory axons, known as Charcot–Marie–Tooth (CMT) disease (reviewed in (2)). A subtype of this disease, CMT type 2D (CMT2D), is caused by dominant mutations in the gene encoding glycyl-tRNA synthetase (*GARS*). Curiously, although overall aminoacylation activity is not disrupted by CMT2D-causing mutations, global translation is inhibited (3–7). This raises the question about the mechanisms of translational repression in this disease.

Translation cycles through three stages: initiation, elongation and termination. Because initiation is the rate-limiting stage of translation, it has been considered the main stage at which translational control occurs (reviewed in (8)). Eukaryotic translational initiation is a multi-step process that requires many proteins, the so called eukaryotic initiation factors (eIFs). It involves the formation of the 43S pre-initiation complex, which consists of the small (40S) ribosomal subunit, ternary complex (the initiator Met-tRNAi and eIF2 in its GTP-bound form, hereafter referred to as eIF2:GTP:Met-tRNAi), and other factors. The 43S complex is recruited to the mRNA 5′-end and scans the mRNA until it finds the initiation AUG codon and can bind the large (60S) ribosomal subunit. Joining of the large (60S) ribosomal subunit completes formation of the 80S ribosome with aminoacylated tRNA in the ribosomal P-site.

Most of the steps of initiation can be regulated. A major regulatory mechanism is triggered by various stress conditions and is called the integrated stress response (ISR, reviewed in (9)). It involves the phosphorylation of the alpha subunit of eIF2 (eIF2a), which reduces the levels of the ternary complex eIF2:GTP:Met-tRNAi. This leads to a downregulation of global translation initiation, to save cellular resources under stress conditions, and the upregulation of specific transcripts, such as Activating transcription factor 4 (ATF4), required to fix stress-related damage (10–12). A number of reports have found that ISR is activated in neurodegenerative diseases, including Alzheimer's and prion disorders (13), amyotrophic lateral sclerosis (14) and cerebellar and retinal degeneration (15).

Recent evidence has shown that the stage of elongation of translation can also be targeted by complex regulatory mechanisms, and that this plays important roles in devel-

*To whom correspondence should be addressed. Tel: +49 30 940 618 50; Email: marina.chekulaeva@mdc-berlin.de

opment and neurologic diseases (reviewed in (16)). Mutation in the ribosome rescue factor GTPBP2, underlying cerebellar and retinal degeneration (17), has been associated with ribosome stalling during elongation (15). Similar effects have been reported for FMRP-linked disorders, Fragile X syndrome and autism (18). Elongation requires two eukaryotic elongation factors (eEFs) and consists of three main steps: (i) the accommodation of the aminoacylated tRNA (aa-tRNA), in complex with eEF1A:GTP, into the A-site of the ribosome, (ii) the formation of the peptide bond, catalyzed by the large ribosomal subunit, during which the growing polypeptide from the P-site is transferred to aa-tRNA in the A-site, (iii) ribosome translocation, catalyzed by eEF2, during which peptidyl-tRNA moves to the P-site and deacylated tRNA is evicted from the P-site. Ribosomes undergo major conformational rearrangements during elongation, and recent works have shown that ribosome profiling can distinguish between two functional states of the ribosome—before and after aa-tRNA binding (19,20).

Here, we dissect the mechanism of translational regulation by CMT2D-causing mutations in GARS (CMT-GARS). Using high-resolution ribosome profiling, we show that CMT-GARS mutant G240R causes ribosomes to stall at glycine codons in open A-sites, due to increased retainment of $tRNA^{Gly}$ on mutant CMT-GARS and a shortage of glycyl-$tRNA^{Gly}$ available for translation. Moreover, ribosome stalling triggers a secondary translational repression mechanism, which involves an increase in the phosphorylation of eIF2α and induction of ISR.

MATERIALS AND METHODS

Cell culture, transfections, and luciferase assay

Human HEK293T cells were grown in Dulbecco's modified Eagle's medium with GlutaMAX™ supplement (DMEM + GlutaMAX, GIBCO) with 10% FBS. Transfections were done in 10 cm, 6-well and 96-well plates with polyethylenimine (PEI) using a 1:3 ratio of DNA:PEI. In reporter experiments, HEK293T cells were transfected with 1–2 ng RL or RL-ATF4, 10 ng FL and 10 ng GARS-myc constructs per well of a 96-well plate. Total amount of transfected DNA was topped up to 50 ng per well of 96-well plate with the empty vector. For other formats, the amounts of plasmids were adjusted proportionally. For myc immunoprecipitation, amounts of GARS-expressing plasmids were adjusted to achieve equal expression levels (1.5 μg WT, 3 μg E71G and 7.5 μg G240R and 10 μg ΔETAQ GARS-myc per 10 cm plate), and amount of transfected DNA was topped up to 10 μg with the empty vector. Cells were lysed 24 h post transfection. Luciferase activities were measured with a homemade luciferase reporter assay system as described earlier (21). For puromycylation assay, cells were treated with 2.5 μg puromycin for 30 min before lysis. Where indicated, thapsigargin was added at 50 nM for 30 min before cell lysis and GCN2-IN-1 at 1 μM at the time of transfection.

Ribosome profiling

Ribosome profiling was performed as earlier described (22), with the following modifications. Monosomes were purified using Microspin S-400 HR columns (GE Healthcare 27-5140-01) and 15–35 nt ribosome-protected fragments were isolated for library generation.

DNA constructs

Reporter plasmids RL and FL have been described previously (23). ATF4-RL reporter was generated by PCR amplifying *ATF4* 5′UTR (ENSMUST00000109605.5) and cloning between SacI and NheI of RL. To generate GARS-myc-expressing plasmid, blasticidin resistance CDS was PCR amplified and cloned between SbfI and SanDI of piggyBac vector pCyl50-MCS (kind gift of Dr Julien Bethune (24)), to generate piggyBac-Blast. GARS CDS (P41250-2) was PCR amplified from human cDNA and cloned between FseI and AgeI sites of piggyBac-Blast. E71G, G240R and ΔETAQ (245-248) mutations were introduced in GARS CDS by site-directed mutagenesis. To generate 3xflag-NSP1-encoding plasmid, a synthetic 3xflag sequence was cloned between BstXI and SbfI sites of pEBG-sic plasmid (25) to produce pEBG-3xflag. CDS of NSP1 was PCR amplified, using SARS-CoV2 cDNA as a template, and cloned between SbfI and NotI sites of pEBG-3xflag.

PAGE and northern blotting

For aminoacylation level experiments, total RNA from 293T cells expressing GARS-myc was isolated with Trizol (Thermo), according to the manufacturer's instructions, and resuspended in 1 mM sodium acetate pH 5.0. A portion of each sample was subjected to deacylation by addition of 0.2 M Tris–HCl pH 9.5 and incubation at 37°C for 30 min. 1 μg of total RNA per sample was further analyzed by acid–urea PAGE and northern blotting as described earlier (26). More specifically, the samples were separated on a 40 cm × 40 cm 10% PAAG (AA:MBA = 19:1) prepared in 0.1 M sodium acetate (pH 5.0) and 8 M urea. The gel was run at 120 V for 18 h at 4°C, until the bromophenol blue dye ran out. For analysis of GARS-myc immunoprecipitates, samples were run on 10% TBE–urea PAAG at 200 V for 1 h, and 400 ng of total RNA were loaded as inputs. RNA was then transferred to a Hybond-N + membrane (Amersham) using semi-dry transfer in 1× TBE buffer at 15 V for 1 h. The membrane was rinsed in 5× SSC buffer and RNA was crosslinked to the mebrane using Stratalinker (265 nm) at 120 000 μJ/cm^2. The membrane was pre-hybridyzed in 6× SSC, 10× Denhardt solution, 0.5% SDS at 42°C for 1 h. Hybridization was done in 6× SSC, 0.1% SDS and 20 pmol of radiolabeled probe at 45°C overnight. The membrane was then washed with 2× SSC three time for 10 min at room temperature and exposed with the phosphorimager screen for 4 h to overnight. The following oligonucleotides were used as probes for northern blotting: TCTACCACTGAACCACCAATGC ($tRNA^{Gly\,(GCC)}$); CAGCCAGATCGCCCTCACATCC, CAGCCAGATCAGCCGAATCAAC, TCTTCGACCG AGCGCGCAGCTT and CTTGAGAGCTTGTTTG GAGGTT (7SK); TAGGTCAGGGTGGTCACGAG, TGGCGGACTTGAAGAAGTCG, CTTGAAGAAG ATGGTGCGCT, TGAACTTGTGGCCGTTTACG (GFP). To prepare the probes, 20 pmol of oligonucleotide

($tRNA^{Gly}$) or oligonucleotide pool (7SK, GFP) was 5′-end labeled with 10 μCi of γ-32P-ATP (3,000 Ci mmol, 10 μCi/μl; PerkinElmer) using T4 PNK.

Immunoprecipitation and western blotting

For anti-myc immunoprecipitations (IP), we used 5 μg of anti-myc antibody (AM1007a Abgent) coupled with 50 μl of protein G Dynabeads (Thermo) per IP. Antibody-coupled beads were incubated with 293T cells lysates overnight at 4°C. Lysates were prepared from 10^7 293T cells, transfected with GARS-myc-expressing constructs, using lysis buffer (50 mM Tris–HCl pH 7.5, 150 mM NaCl, 0.25% NP-40, 2 mM Pefabloc). After IP, the beads were washed three times with the wash buffer (50 mM Tris–HCl pH 7.5, 150 mM NaCl, 0.1% NP-40, 2 mM Pefabloc). 1/20 of the beads were eluted with the SDS-PAGE sample buffer for western blotting analysis with anti-myc antibody, with 3% of inputs and 2.5% of immunoprecipitates loaded on the gel. The rest of the beads were supplemented with 500 ng of GFP spike-in RNA, extracted with Trizol according to the manufacturer's instructions and isolated RNA was analyzed by urea PAGE and northern blotting. For GFP RNA spike-in preparation, a 325-nt fragment of the GFP coding sequence was PCR amplified with the oligos introducing T7 promoter (T7-GFP-fw: TAATACGACTCACTATAGGG ATGGTGAGCAAGGGCGAGGA, GFP-rev: GGGTCT TGTAGTTGCCGTCG), and the resulting PCR fragment was used as a template for T7 *in vitro* transcription reaction.

For western blotting, 20 μg of total protein, unless otherwise indicated, was separated on a 4–12% SDS-PAGE, and proteins were transferred to the PVDF membrane. The membrane was probed with the following primary antibodies: rabbit anti-eIF2a antibody 1:1000 (9722 Cell Signaling), rabbit anti-phospho-eIF2a antibody 1:1000 (9721 Cell Signaling), mouse anti-myc 1:5000 (AM1007a Abgent), mouse anti-beta-actin 1:5000 (A2228 Sigma), mouse anti-puromycin 1:4000 (Kerafast 3RH11).

Bioinformatical data analysis

Analysis of ribosome profiling data was performed using an in-house snakemake based pipeline. First, reads were quality trimmed using trim_galore and filtered for common contaminants (human rRNA sequence (rRNA_U13369.1), tRNA sequences (as predicted by GtRNAdb (27) and selected noncoding RNA sequences from the ENSEMBL ncrna collection). Filtered reads were then analysed using fastqc and mapped to the human genome (GRCh38 version97) using STAR (28). Mapped reads were further analyzed using RiboseQC (https://github.com/ohlerlab/RiboseQC) to obtain P-site cutoffs and counted using a custom htseq-based (29) python script split by annotated gene region, read length and P- and A-site codons. Analysis of codon usage was performed for CDS-mapping reads with 3 nt periodicity (21 nt and 29 nt). For this, counts for each codon in A- or P-site were normalized by the sum of all reads for a given read length, site and sample. Normalized counts were then summed and averaged between different conditions.

RESULTS

Defects in protein production are recapitulated by overexpression of CMT-GARS mutants

CMT2D is caused by the dominant toxic gain-of-function mutations, i.e. mutations that confer a new and toxic activity on GARS protein (3,5,30). This means that the phenotype of the disease, including defects in translation, can be recapitulated by overexpression of mutant GARS. Thus, we set out to recapitulate the global translational repression triggered by CMT-GARS mutations E71G, G240R (7) and deletion of amino acids 245–248 (ΔETAQ) (31) in cultured HEK293T cells. For that, we co-transfected cells with myc-tagged WT or mutant GARS-encoding plasmids and two reporter constructs coding for *Renilla* and firefly luciferase (RL and FL, Figure 1A). An empty vector was used as a negative control. We found that the overexpression of E71G, G240R and ΔETAQ, but not WT GARS, inhibited protein production in the luciferase reporter assay (Figure 1B). Consistently with their role in global translational downregulation and prior work (7), E71G, G240R and ΔETAQ mutant proteins were expressed at lower levels than WT GARS, as revealed by western blotting (Figure 1C). Interestingly, the reporter assay recapitulated the phenotypic strength of the mutations observed in *in vivo* experiments (7,31): the effects of G240R and ΔETAQ were more severe than that of E71G (Figure 1B and C).

To analyze the effects of CMT-GARS on total translation, we used puromycylation assay, which utilizies puromycin-tagging of newly synthesized proteins (32,33). Puromycin is a mimic of the aa-tRNA, which is incorporated into the nascent polypeptide chains, and the levels of resulting puromycin fusion proteins reflect the rate of translation. To compare translation levels between the cells, transfected with either WT or CMT-GARS mutants, we analyzed cell lysate by western blotting with anti-puromycin antibody (Figure 1D). Indeed, CMT-GARS-expressing cells showed lower incorporation of puromycin (anti-puromycin western), in spite of similar protein loading visualized with coomassie staining. These data confirm that the effect of CMT-GARS mutations on translation is global.

CMT-GARS mutant inhibits the accommodation of glycyl-tRNA in the ribosomal A-site and causes ribosome stalling

aa-tRNA synthetases (aaRSs) are required to produce aa-tRNA for the first step of elongation, i.e. accommodation of a cognate aminoacyl-tRNA in the ribosomal A-site (Figure 2A). We decided to test whether this step is affected by CMT-GARS. Our prediction was that, if glycyl-tRNA were deficient in CMT-GARS-expressing cells, ribosomes would stall in a pre-accommodation state once glycine codons entered their A-site. Recent works have shown that high-resolution ribosome profiling can distinguish between different functional states of the ribosome—pre- and post-accommodation of aa-tRNA (20). This technique generates ribosomal footprints on mRNAs; it is achieved by treating cell lysates with RNAse I (34). This degrades most RNA, but leaves ribosome-protected fragments (RPFs) intact; they can then be analyzed by next-generation

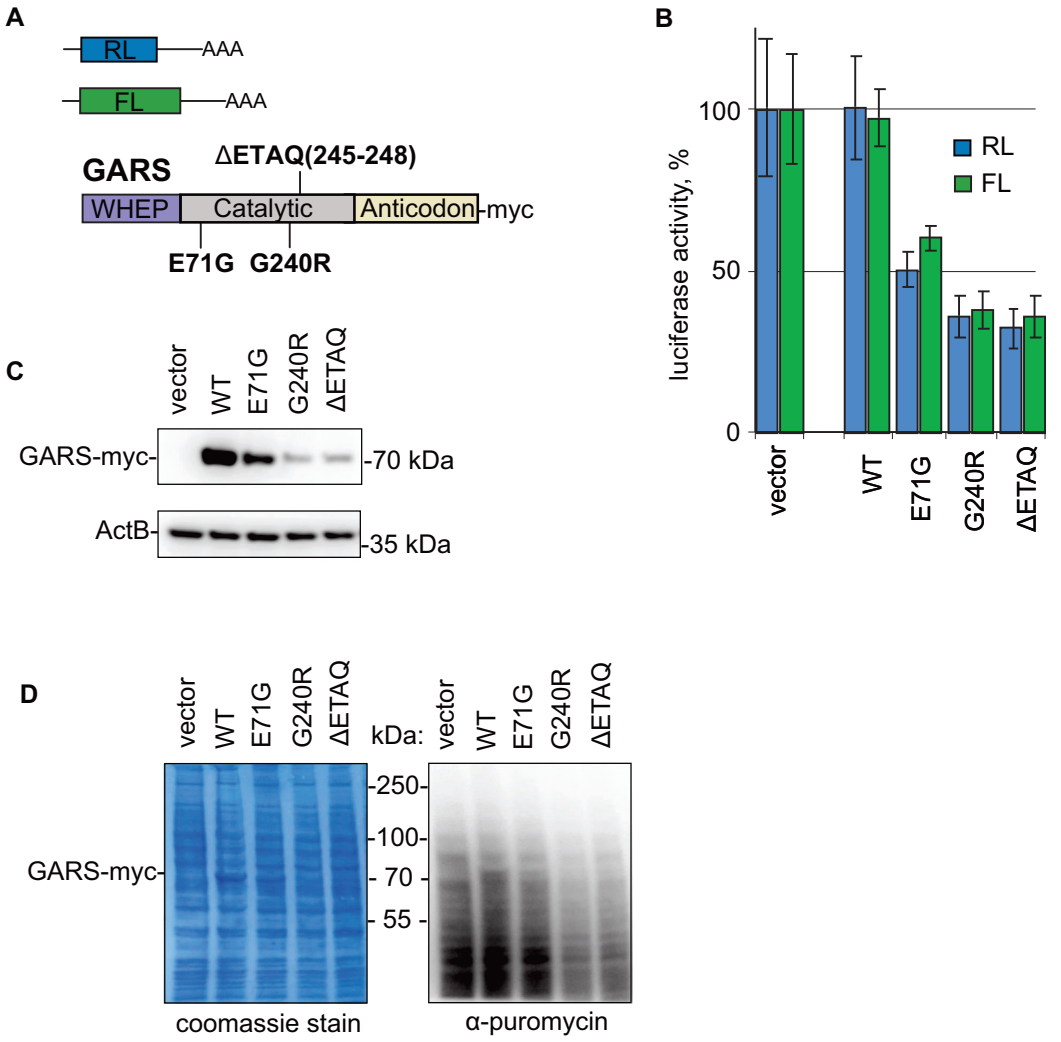

Figure 1. Overexpression of CMT-GARS mutants, E71G, G240R and ΔETAQ, but not WT GARS, represses protein production in cultured cells. (**A**) Schematic representation of constructs used in transfection experiments: RL and FL are reporter constructs encoding *Renilla* and firefly luciferase, correspondingly. Positions of analyzed CMT-GARS mutations in the context of GARS domain structure are shown. (**B**) Repression of RL and FL mRNAs by GARS mutants. Human HEK293T cells were co-transfected with plasmids encoding RL, FL, and myc-tagged GARS, either WT or indicated mutant. As a negative control, empty vector was used instead of GARS-encoding plasmid. RL and FL activities are presented as a percentage of luciferase activity produced in the presence of empty vector. Values represent means ± SD from three experiments. (**C**) Expression levels of myc-fusion proteins were estimated by western blotting with antibodies directed against myc-tag. Beta-actin was used as a loading control. (**D**) Puromycylation assay confirms the role of CMT-GARS in global translational repression. HEK293 cells were transfected with plasmids encoding WT GARS, indicated GARS mutants or an empty vector. After puromycin treatment, cells were lyzed and lysates were analyzed by western blotting with anti-puromycin antibody. PAAG stained with coomassie is provided to visualize equal total protein loading between the samples.

sequencing. Due to substantial conformational rearrangements of the ribosome during elongation, ribosomes lacking tRNA in their A-sites (open A-sites) generate short 21–22 nt RPFs, while ribosomes with occupied A-sites—produce long 27–29 nt RPFs (20). Thus, the lack of a specific aa-tRNA results in ribosomes with open A-sites pausing on the cognate codons, and this can be detected by high-resolution ribosome profiling by enrichment of the corresponding 21–22 nt RPFs (20) (Figure 2A).

To test this hypothesis, we modified the standard ribosome profiling protocol (34) to isolate a wide range (15–35 nt) of RPFs. Triplicate ribosome profiling libraries were prepared from HEK293T cells expressing a strong CMT-GARS mutant G240R or WT GARS (negative control). Most ribosome profiling reads mapped within coding sequences (CDS), reflecting a fraction of translated mRNAs, and showed high correlation between triplicates (Supplementary Figure S1A and B). We observed a bimodal distribution of ribosome footprints, with the peaks corresponding to the ribosomal states with open (21 nt) and occupied (29 nt) A-sites (Figure 2B). Importantly, both short 21 nt and long 29 nt RPFs showed a periodic alignment pattern of 3 nt, which reflects the codon-by-codon movement of translating ribosomes along an mRNA and represents a hallmark of translation (Figure 2C and Supplementary Figure S1C).

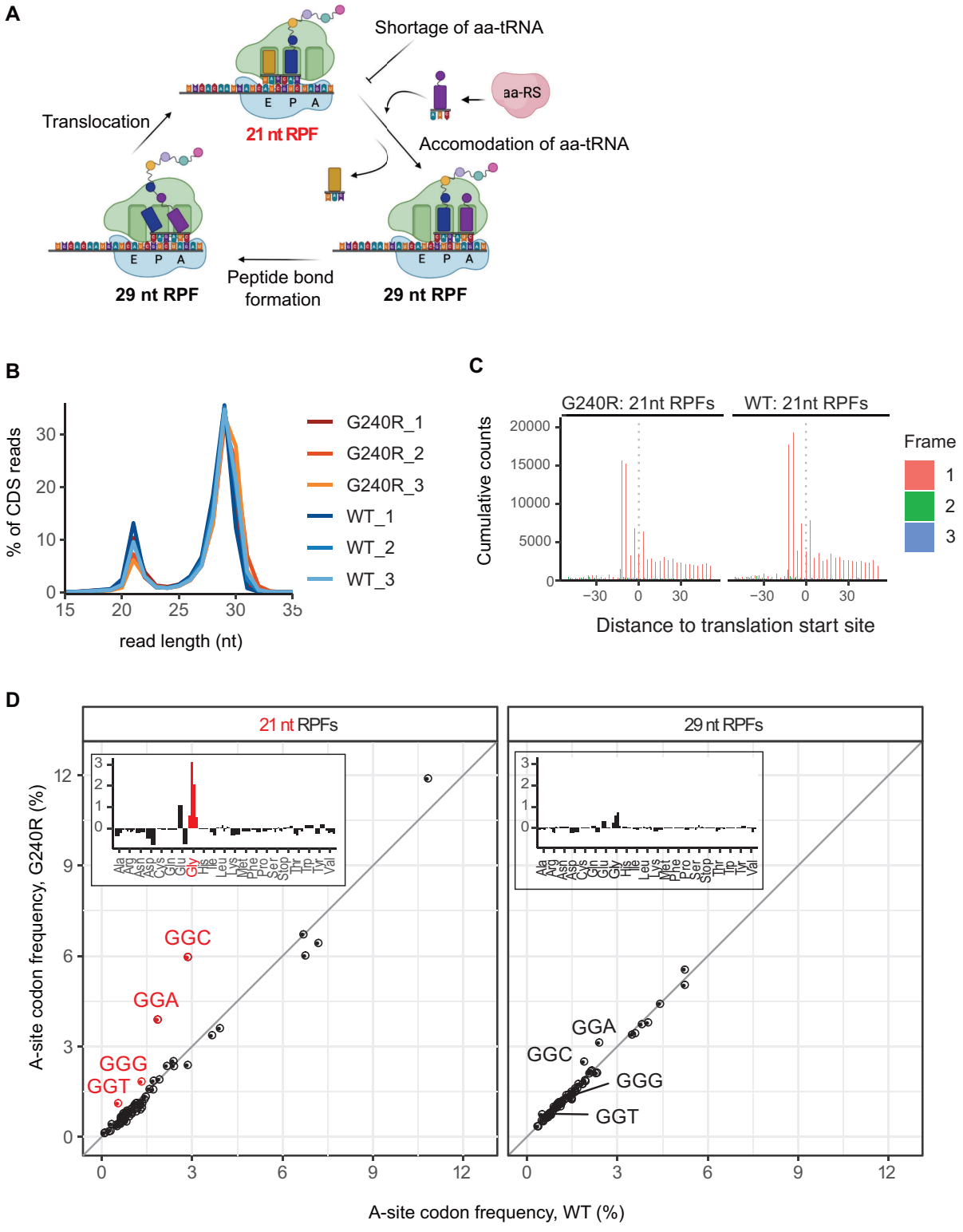

Figure 2. Ribosome profiling detects pausing of ribosome with Gly codons in open A-site in G240R-GARS-expressing cells. (**A**) Scheme showing stages of elongation and the length of ribosome protected fragments (RPFs) generated by each ribosomal state. aa-tRNA: aminoacyl-tRNA, aaRS: aa-tRNA synthetase. (**B**) Length distributions of CDS-mapped ribosome footprints in libraries prepared HEK293T cells expressing either WT or G240R-GARS (in triplicates). (**C**) Metagene aggregate plots displaying distance of 21-nt ribosome footprints from annotated start codon. (**D**) Scatter plots comparing frequencies of 64 codons in the ribosomal A-site between cells expressing WT (X) and G240R-GARS (Y), for 21 nt (left) and 29 nt (right) RPFs. Ribosome frequencies represent the means of triplicates. Glycine codons are labelled and marked in red. Insets show differences between codon frequencies in G240R and WT samples as bar plots.

10012 Nucleic Acids Research, 2021, Vol. 49, No. 17

We next calculated the mean frequencies of 64 codons in the A-sites and P-sites of 21 nt and 29 nt RPFs and compared these values between cells expressing WT and G240R GARS (Figure 2D and Supplementary Figure S1D). The most striking difference in codon frequency between G240R and WT GARS samples was detected for 21 nt RPFs with glycine codons in ribosomal A-site (Figure 2D, left). We found that ribosomes paused on glycine codons (red points, Figure 2D) ∼ 2 times longer in G240R than in WT samples, whereas the values for other codons remained similar (black points). Notably, such pausing was observed in short 21 nt RPFs, corresponding to ribosomes with open A-sites, but not in 29 nt RPFs (<1.3-fold, Figure 2D, right), representing ribosomes with occupied A-sites (20). For comparison, only minor changes in codon frequencies were detected in ribosomal P-sites (<1.5-fold, Supplementary Figure S1D). Thus, our ribosome profiling data demonstrate that CMT-GARS mutant G240R induces a stalling of ribosomes with glycine codons in open A-sites, i.e. in a pre-accommodation state. This mechanism is consistent with a shortage of glycyl-tRNA in G240R-expressing cells.

CMT-GARS mutants have increased capacity to retain bound $tRNA^{Gly}$

Stalling of ribosomes with glycine codons in open A-sites point to a shortage of glycyl-$tRNA^{Gly}$ in G240R-expressing cells. To test if CMT-GARS mutants reduce levels of aminoacylated $tRNA^{Gly}$, we analyzed the levels of Gly-$tRNA^{Gly}$ in CMT-GARS-expressing 293T cells by acid–urea polyacrylamide gel electrophoresis (PAGE) followed by northern blotting. This method allows separation of aminoacylated tRNA from deacylated tRNAs due the mass difference (26). To provide a reference of deacylated $tRNA^{Gly}$, half of each sample was treated with a basic pH buffer, that destabilizes an ester bond between the amino acid carboxyl group and the tRNA terminal 3′-OH group. This analysis showed that most of analyzed $tRNA^{Gly}$ were aminoacylated in 293T cells, and the aminoacylation levels were not substantially altered by expression of either WT or CMT-GARS mutants (Figure 3A). Our results are consistent with the literature data suggesting that CMT-GARS mutations do not disrupt overall aminocylation activity (3–5,7).

Toxic gain-of-function phenotypes can result from increased affinity of the interaction with the natural binders, as observed for example in tauopathies (35). Therefore, we decided to test if a step downstream of aminoacylation, such as the release of $tRNA^{Gly}$ from GARS, is affected by CMT-GARS mutations. To this end, we overexpressed WT GARS and CMT-GARS mutant proteins, tagged with myc-tag, in 293T cells. Given that CMT-GARS mutants are expressed at lower levels than WT (Figure 1C), we adjusted the amounts of transfected plasmids to achieve equal expression of GARS proteins. We followed with immunoprecipitation of GARS-myc fusion proteins with anti-myc antibodies, in duplicates, and analyzed the levels of bound $tRNA^{Gly}$ by PAGE and northern blotting. To control that the efficiency of RNA recovery was the same between the samples, we supplemented the immunoprecipitates with *in vitro* synthesized GFP RNA spike-in before RNA extraction. While efficiency of protein immunoprecipitation (Figure 3B, GARS-myc western) and RNA recovery (RNA spike-in) were similar between the samples, CMT-GARS proteins retained markedly higher amounts of $tRNA^{Gly}$ than WT GARS ($tRNA^{Gly}$). Thus, our data suggest that, due to slow release of $tRNA^{Gly}$, CMT-GARS mutants deplete the pool of glycyl-$tRNA^{Gly}$ available for translation.

CMT-GARS induces eIF2a phosphorylation and integrated stress response

Amino acid starvation and deacylated tRNAs are known to induce ISR by activating the eIF2a kinase GCN2 (36). Recently, ribosome stalling was reported as an an alternative mechanism that can activate ISR via the CGN2-mediated phosphorylation of eIF2a (15,37). Given our evidence for ribosome stalling in CMT-GARS-expressing cells (Figure 2D), we wondered if this also induced the phosphorylation of eIF2a and ISR. As a test, we used western blotting to analyze the levels of phosphorylated eIF2a (P-eIF2a) in cells expressing either mutant or WT GARS (Figure 4A). For a positive control, we treated HEK293T cells with thapsigargin, a drug that induces the PERK-dependent phosphorylation of eIF2a (38). Indeed, we observed that expression of E71G, G240G and ΔETAQ mutant GARS increased the levels of phosphorylated eIF2a, while the total levels of eIF2a remained unaffected.

eIF2a phosphorylation plays an adaptive role during stress, by shutting down global protein synthesis, to save resources, and by upregulating the translation of specific transcripts, such as *ATF4,* required for stress management (10–12). This upregulation occurs through a mechanism involving upstream ORF (uORFs) in *ATF4* 5′UTR. Under normal conditions these uORFs play an inhibitory role, catching scanning ribosomes before they reach the main ORF. The phosphorylation of eIF2a reduces the amount of ternary complex, required for initiation, and therefore increases the chances of scanning ribosomes to reach the main ORF and initiate translation. To test whether this mechanism is activated by CMT-GARS mutations, we generated *Renilla* luciferase reporter bearing *ATF4* 5′UTR (ATF4-RL) and analyzed how CMT-GARS mutants affect its expression (Figure 4B). *Renilla* reporter without *ATF4* 5′UTR (RL) was used as a negative control, and firefly luciferase reporter (FL) was co-transfected with both *Renilla* reporters as a normalization control. We observed that RL and FL reporters were repressed by E71G, G240R and ΔETAQ, as established earlier (Figure 1B and Supplementary Figure S2). Strikingly, ATF4-RL was resistant to CMT-GARS-mediated repression (Supplementary Figure S2, Figure 4C). Indeed, relative RL/FL expression was upregulated by E71G, G240G and ΔETAQ mutants specifically for ATF4-RL, but not RL that served as a negative control (Figure 4C). As a control translational repressor we used SARS-CoV2 nonstructural protein 1 (NSP1), that inhibits global translation initiation by binding and obstructing the mRNA entry tunnel on the small ribosomal subunit (39,40). Indeed, NSP1 repressed all reporters—ATF4-RL, RL and FL—to a similar extent (Supplementary Figure S2 and Figure 4C), pointing that the upregulation of

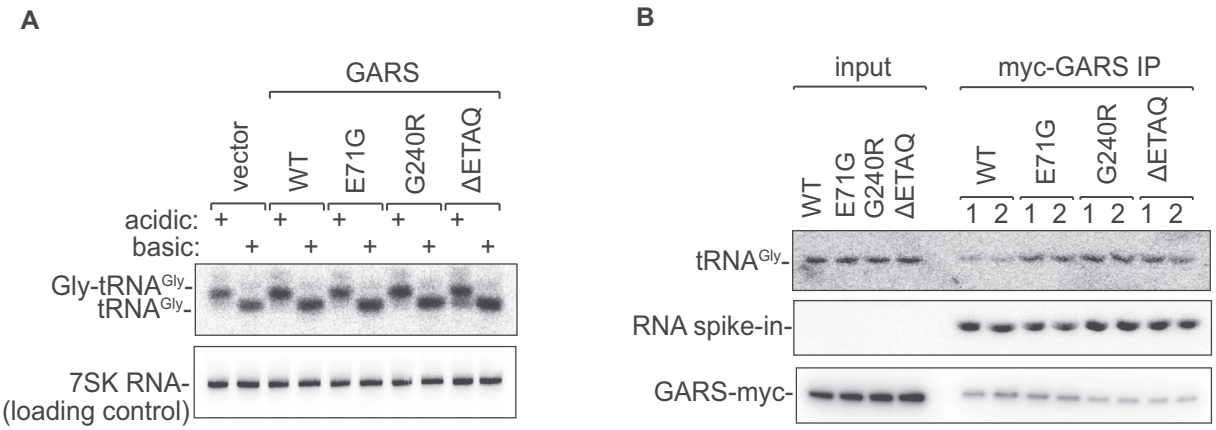

Figure 3. CMT-GARS mutants do not impair overall glycylation activity, but have increased capacity to bind $tRNA^{Gly}$. (**A**) Northern blotting shows that aminoacylation levels of $tRNA^{Gly}$ remain substantially unaffected in the presence of CMT-GARS mutants. HEK293T cells were transfected with plasmids encoding WT, E71G, G240R, ΔETAQ GARS or an empty vector, total RNA was isolated and aminoacylation levels of $tRNA^{Gly}$ were evaluated by acid-urea PAGE and northern blotting. Acidic: lanes showing RNA analysed under acidic pH, that preserves ester bonds linking amino acids to tRNAs. Basic: lanes showing RNA analysed under basic pH, that leads to tRNA deacylation. (**B**) Immunoprecipitation and northern blotting show that CMT-GARS mutants have increased capacity to retain bound $tRNA^{Gly}$. HEK293T cells were transfected with plasmids encoding WT, E71G, G240R or ΔETAQ GARS-myc, with the amounts of plasmid adjusted to achieve equal protein expression. GARS-myc was immunoprecipitated with anti-myc antibody and inputs and immunoprecipitates were analyzed by PAGE and northern blotting to evaluate the levels of GARS-myc-bound $tRNA^{Gly}$. To control for equal efficiency of RNA recovery, immunoprecipitates were supplemented with RNA spike-in before RNA extraction. Duplicates of immunoprecipitates are shown. Western blotting for inputs and immunoprecipitated GARS-myc is shown as a loading control.

ATF4-RL is specific to GARS mutants. Thus, our data show that expression of CMT-GARS mutants induces *ATF4* reporter, a marker of ISR.

We next wondered if phosphorylation of eIF2a substantially contributes to translational repression by CMT-GARS mutants. To this end, we analyzed how CMT-GARS proteins affect translation in the presence of the inhibitor of the eIF2a kinase GCN2, GCN2-IN-1 (41). To evaluate translation levels, we used puromycylation assay introduced in Figure 1D. While addition of GCN2-IN-1 indeed suppressed eIF2a phosphorylation (Figure 4D, P(Ser51)-eIF2a), CMT-GARS mutants continued to repress translation under these conditions (anti-puromycin). Our data suggest that the primary defect caused by CMT-GARS, i.e. ribosome pausing on glycine codons, is sufficient to repress global translation.

DISCUSSION

CMT is the most common inherited neuromuscular disease affecting 1 in 2500 people worldwide (reviewed in (2)). The molecular mechanism of CMT has been obscure. Thus, although CMT-causing heterozygous mutations in the glycyl-tRNA synthetase gene *GARS* affect protein synthesis, loss of aminoacylation activity is neither necessary nor sufficient to cause the disease (3–5,7). Indeed, some of them retain full (E71G) or partial (G240R) aminoacylation activity, and the WT allele of *GARS* produces a fully functional protein (4,5,7). Moreover, the overexpression of CMT-GARS mutants in *Drosophila* caused defects in motor performance, without any reduction in aminoacylation activity and or changes in the ratios between glycylated versus non glycylated tRNAs (7). Additionally, experiments overexpressing WT GARS did not rescue CMT phenotypes in mouse or *Drosophila* models (7,30). These findings suggested that CMT-GARS mutations inhibit translation via some other toxic gain-of-function mechanism which remained enigmatic.

Here, we use high-resolution ribosome profiling to show directly and for the first time that CMT-GARS mutant inhibits the first step of elongation – the accommodation of glycyl-tRNA in the A-site—and thus causes ribosome stalling (Figures 2D and 5). We propose that the degenerative phenotypes observed in CMT can be attributed to this stalling. In other cases, ribosome stalling due to deficiencies in $tRNA^{Arg}$ and ribosome rescue factor GTPBP2 in mouse have been shown to cause neurodegeneration (15).

Our data on ribosome stalling at glycine codons in open A-site point to an insufficiency of glycyl-$tRNA^{Gly}$ in G240R-expressing cells. However, both our results (Figure 3A) and published data (3–5,7) suggest that CMT-GARS mutations do not disrupt aminocylation activity. Toxic gain-of-function mutants can act via different mechanisms, including increased affinity of the interaction with their natural binders, acquiring new abnormal binders or a tendency to aggregate. For example, Alzheimer's disease-associated mutants of a microtubule-binding protein tau bind tubulin heterodimers with enhanced affinity (35). Thus, we considered that a step downstream of aminoacylation, such as the release of glycyl-$tRNA^{Gly}$ from GARS and transfer to eEF1A:GTP for delivery to ribosome, is likely to be affected by CMT-GARS mutations. Indeed, northern blotting of GARS-CMT immunoprecipitates showed that mutant forms of GARS have increased affinity to $tRNA^{Gly}$ (Figure 3B).

While ribosome stalling explains the mechanism of global translational repression by CMT-GARS, we show that it also activates a secondary mechanism of repression at the level of initiation, by inducing ISR via eIF2a phosphorylation (Figure 4A). Reports have shown that stalled

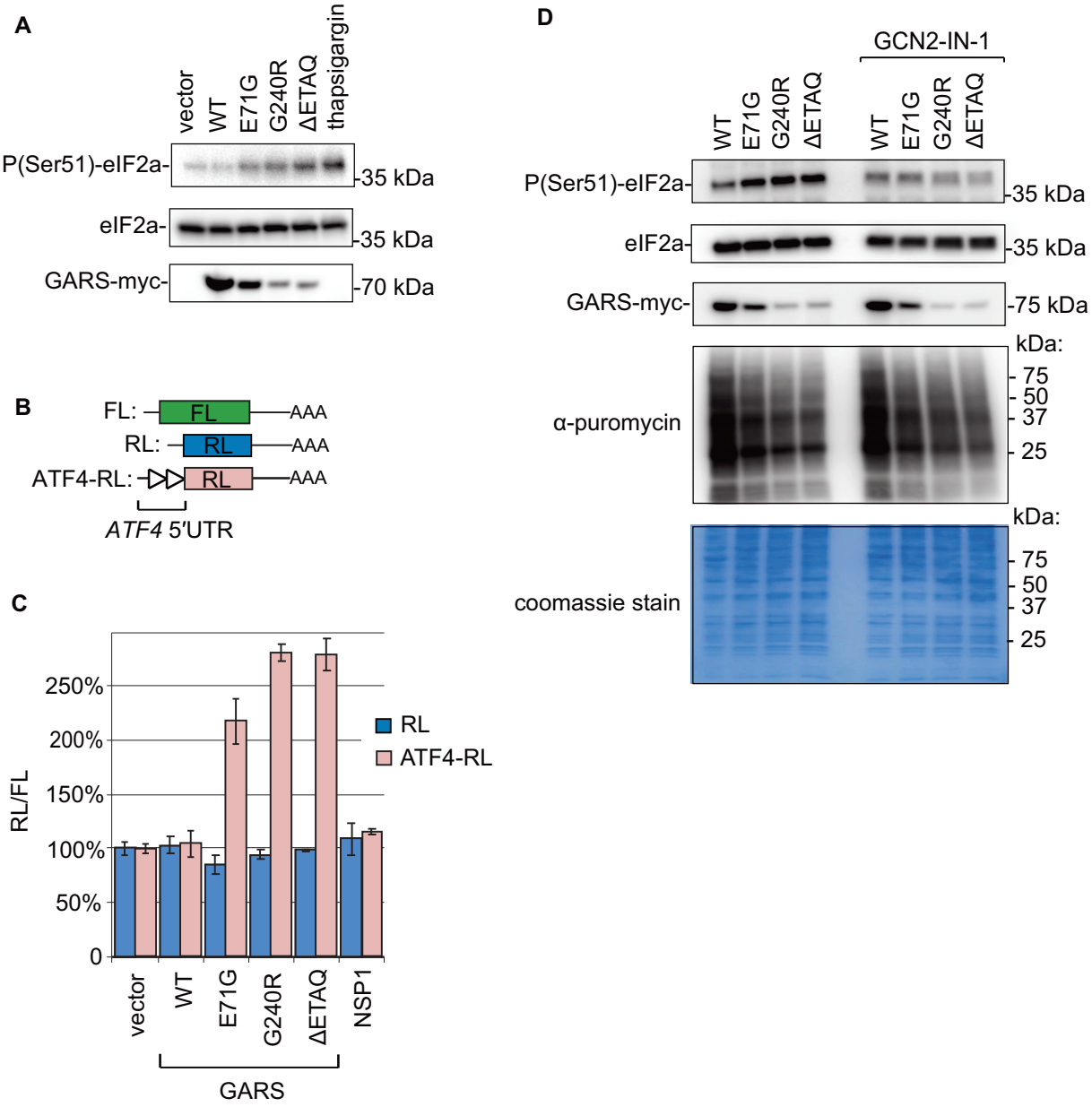

Figure 4. Overexpression of CMT-GARS mutants, E71G, G240R and ΔETAQ, induces integrated stress response (ISR) via phosphorylation of eIF2a. (**A**) Expression of CMT-GARS mutants induces phosphorylation of eIF2a. HEK293T cells were transfected with plasmids encoding WT, E71G, G240R, ΔETAQ GARS or an empty vector. For a positive control of eIF2a phosphorylation, cells were treated with thapsigargin. Cell lysates were analyzed by western blotting using antibodies against phosphorylated eIF2a (P-eIF2a), eIF2a (loading control), and myc (GARS-myc), as indicated on the left. (**B**) Schematic representation of reporter constructs used in transfection experiments: RL and FL are the same as in Figure 2A. ATF4-RL carries 5′UTR of *ATF4* gene. (**C**) E71G, G240R and ΔETAQ GARS mutants activate expression of *ATF4* reporters. Human HEK293T cells were co-transfected with plasmids encoding one of the *Renilla* luciferase reporters (RL, ATF4-RL), FL and myc-tagged GARS, either WT or indicated mutant. As additional controls, empty vector and NSP1-encoding plasmids were used instead of GARS plasmid. RL activity was normalized to that of FL and presented as a percentage of luciferase activity produced in the presence of empty vector for each *Renilla* reporter. Values represent means ± SD from three experiments. (**D**) Puromycylation assay shows that CMT-GARS-mediated translational repression is preserved upon inhibition of eIF2a phosphorylation. HEK293T cells were transfected with plasmids encoding WT, E71G, G240R or ΔETAQ GARS and inhibitor of eIF2a phosphorylation phosphorylation GCN2-IN-1 was added were indicated. After puromycin treatment, cells were lyzed and lysates were analyzed by western blotting with antibodies against phosphorylated eIF2a (P-eIF2a), eIF2a (loading control), myc (GARS-myc) and puromycin, as indicated on the left. PAAG stained with coomassie is provided to show total protein loading.

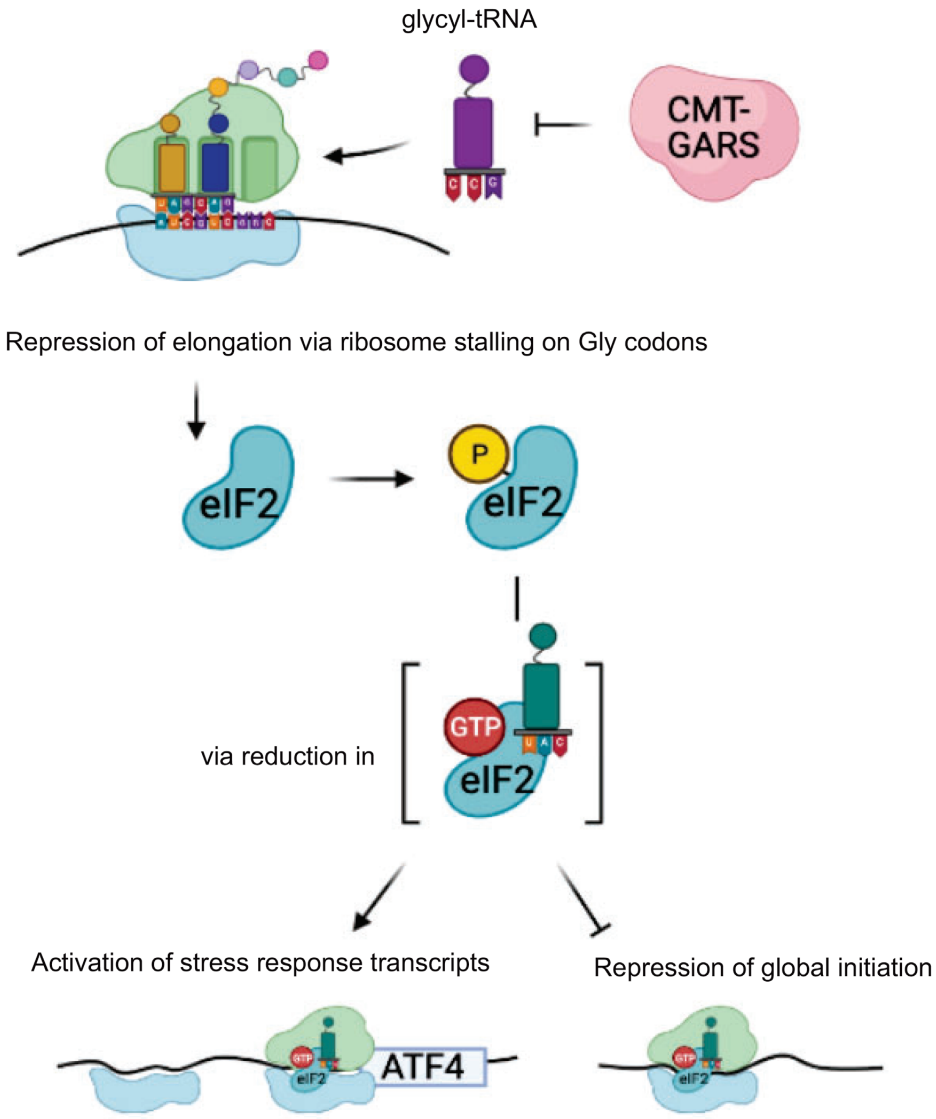

Figure 5. Model illustrating the mechanism of CMT-mutant GARS function in translational regulation. CMT-mutant GARS protein inhibits accommodation of glycyl-tRNA into the ribosomal A-site, possibly via decreasing the pool of available charged glycyl-tRNA, and leads to ribosome stalling on glycine codons. Ribosome stalling results in phosphorylation of eIF2a and activation of integrated stress response. In particular, phosphorylation of eIF2a leads to reduction in the levels of ternary complex eIF2:GTP:Met-tRNAi, which downregulates global translation initiation and upregulates expression of selected transcripts with uORFs, such as *ATF4*. When levels of ternary complex are low, ribosomes bypass uORF, which allows them to initiate translation on the main *ATF4* ORF. ATF4 is a transcription factor that induces stress response genes.

ribosomes are more potent activators of the eIF2a kinase GCN2 than deacylated tRNAs, which result from amino acid starvation (15,37). Interaction with ribosomal P-stalk of stalled ribosomes is suggested to activate GCN2 (37), although the exact mechanism of discrimination between translating and stalled ribosomes remains unclear. The phosphorylation of eIF2a prevents the formation of the ternary complex and thus inhibits global translation initiation, to save cellular resources (Figure 5). Beyond that, it enhances the translation of specific mRNAs, such as *ATF4,* which contains uORFs in it 5′UTRs (10–12). ATF4 promotes the transcription of genes with adaptive functions that can repair damage caused by stress (42,43). However, a chronic activation of ISR can contribute to neurodegenerative phenotypes through the induction of apoptosis, memory impairments due to translational inhibition and other mechanisms (reviewed in (1)). For example, *ATF4* deficiency was shown to alleviate neuronal loss from oxidative stress and amyloid beta peptide (44,45).

It remains unclear why mutations in ubiquitously expressed aaRSs primarily affect peripheral motor and sensory axons. The fact that the expression of CMT-GARS mutants in a heterologous system permits recapitulating the repression of protein production, characteristic of CMT (Figure 1B), suggests that the mechanism *per se* is not unique to a single cell type. One possible explanation for the higher susceptibility of peripheral motor and sensory axons might be that they have low amounts of some of translation

components that are involved in this mechanism (e.g. tRNAs, aaRSs etc.). Further studies aimed at identifying such limiting components are likely to elucidate the cell specificity of this mechanism.

There is no cure for CMT and understanding of the mechanisms of the CMT-GARS function opens new perspectives for development of therapies. Antisense oligos (ASO) are a promising therapeutic strategy to downregulate genes with toxic gain-of-function phenotype (reviewed in (46)). ASO injections produced encouraging results in treatment of several neurological diseases, including spinal muscular atrophy and Huntington's disease. In case of CMT however, this approach would require generation of individualized ASOs recognizing specific CMT-GARS mutations, which in most cases differ from a WT allele in a single nucleotide, making the ASO design complicated. An alternative approach to therapies is targeting different steps of the CMT-GARS-mediated translational repression. Our data on ribosome stalling at glycine codons in open A-site point to the shortage of glycyl-tRNA as a mechanism of CMT. Therefore, providing a supply $tRNA^{Gly}$ could be a therapeutic strategy to alleviate ribosome pausing. Activation of ISR may also contribute to neurodegenerative phenotypes in CMT, supported by data from other neurodegenerative diseases (reviewed in (1)). Indeed, drugs targeting ISR and alleviating translational repression have been shown to efficiently reduce neurodegeneration symptoms in various models (13) and may be a promising approach for treatment of CMT.

DATA AVAILABILITY

RiboseQC tool used for data analysis is available at the github: https://github.com/ohlerlab/RiboseQC. Ribosome profiling data are deposited at the ArrayExpress (accession E-MTAB-10342).

SUPPLEMENTARY DATA

Supplementary Data are available at NAR Online.

ACKNOWLEDGEMENTS

Experiments were performed by S.M. (ribosome profiling, northern blotting, western blotting), M.C. (reporter assays, cloning, IP and northern blotting, western blotting) and L.B. (reporter assays, cloning). N.v.K. performed computational data analysis. M.C. conceptualized and supervised the work, and wrote the paper, with the feedback from all authors. We thank Russ Hodge for the comments of the manuscript. Biorender.com was used in generation of the figures.

FUNDING

The work was supported by the DAAD PhD fellowship to S.M., the MDC PhD fellowship to N.v.K.; the Erasmus fellowship to L.B., the EU-JPND grant (localMND) to M.C. Funding for open access charge: Internal MDC funds.
Conflict of interest statement. None declared.

REFERENCES

1. Bosco,D.A. (2018) Translation dysregulation in neurodegenerative disorders. *Proc. Natl. Acad. Sci. U.S.A.*, **115**, 12842–12844.
2. Moss,K.R. and Hoke,A. (2020) Targeting the programmed axon degeneration pathway as a potential therapeutic for Charcot-Marie-Tooth disease. *Brain Res.*, **1727**, 146539.
3. Seburn,K.L., Nangle,L.A., Cox,G.A., Schimmel,P. and Burgess,R.W. (2006) An active dominant mutation of glycyl-tRNA synthetase causes neuropathy in a Charcot-Marie-Tooth 2D mouse model. *Neuron*, **51**, 715–726.
4. Antonellis,A., Lee-Lin,S.Q., Wasterlain,A., Leo,P., Quezado,M., Goldfarb,L.G., Myung,K., Burgess,S., Fischbeck,K.H. and Green,E.D. (2006) Functional analyses of glycyl-tRNA synthetase mutations suggest a key role for tRNA-charging enzymes in peripheral axons. *J. Neurosci.*, **26**, 10397–10406.
5. Nangle,L.A., Zhang,W., Xie,W., Yang,X.L. and Schimmel,P. (2007) Charcot-Marie-Tooth disease-associated mutant tRNA synthetases linked to altered dimer interface and neurite distribution defect. *Proc. Natl. Acad. Sci. U.S.A.*, **104**, 11239–11244.
6. Storkebaum,E., Leitao-Goncalves,R., Godenschwege,T., Nangle,L., Mejia,M., Bosmans,I., Ooms,T., Jacobs,A., Van Dijck,P., Yang,X.L. *et al.* (2009) Dominant mutations in the tyrosyl-tRNA synthetase gene recapitulate in Drosophila features of human Charcot-Marie-Tooth neuropathy. *Proc. Natl. Acad. Sci. U.S.A.*, **106**, 11782–11787.
7. Niehues,S., Bussmann,J., Steffes,G., Erdmann,I., Kohrer,C., Sun,L., Wagner,M., Schafer,K., Wang,G., Koerdt,S.N. *et al.* (2015) Impaired protein translation in Drosophila models for Charcot-Marie-Tooth neuropathy caused by mutant tRNA synthetases. *Nat. Commun.*, **6**, 7520.
8. Hershey,J.W.B., Sonenberg,N. and Mathews,M.B. (2019) Principles of translational control. *Cold Spring Harb. Perspect. Biol.*, **11**, a032607.
9. Pakos-Zebrucka,K., Koryga,I., Mnich,K., Ljujic,M., Samali,A. and Gorman,A.M. (2016) The integrated stress response. *EMBO Rep.*, **17**, 1374–1395.
10. Blais,J.D., Filipenko,V., Bi,M., Harding,H.P., Ron,D., Koumenis,C., Wouters,B.G. and Bell,J.C. (2004) Activating transcription factor 4 is translationally regulated by hypoxic stress. *Mol. Cell. Biol.*, **24**, 7469–7482.
11. Lu,P.D., Harding,H.P. and Ron,D. (2004) Translation reinitiation at alternative open reading frames regulates gene expression in an integrated stress response. *J. Cell Biol.*, **167**, 27–33.
12. Vattem,K.M. and Wek,R.C. (2004) Reinitiation involving upstream ORFs regulates ATF4 mRNA translation in mammalian cells. *Proc. Natl. Acad. Sci. U.S.A.*, **101**, 11269–11274.
13. Halliday,M., Radford,H., Zents,K.A.M., Molloy,C., Moreno,J.A., Verity,N.C., Smith,E., Ortori,C.A., Barrett,D.A., Bushell,M. *et al.* (2017) Repurposed drugs targeting eIF2α-P-mediated translational repression prevent neurodegeneration in mice. *Brain*, **140**, 1768–1783.
14. Lopez-Erauskin,J., Tadokoro,T., Baughn,M.W., Myers,B., McAlonis-Downes,M., Chillon-Marinas,C., Asiaban,J.N., Artates,J., Bui,A.T., Vetto,A.P. *et al.* (2018) ALS/FTD-Linked mutation in FUS suppresses intra-axonal protein synthesis and drives disease without nuclear loss-of-function of FUS. *Neuron*, **100**, 816–830.
15. Ishimura,R., Nagy,G., Dotu,I., Chuang,J.H. and Ackerman,S.L. (2016) Activation of GCN2 kinase by ribosome stalling links translation elongation with translation initiation. *Elife*, **5**, e14295.
16. Richter,J.D. and Coller,J. (2015) Pausing on polyribosomes: make way for elongation in translational control. *Cell*, **163**, 292–300.
17. Jaberi,E., Rohani,M., Shahidi,G.A., Nafissi,S., Arefian,E., Soleimani,M., Rasooli,P., Ahmadieh,H., Daftarian,N., KaramiNejadRanjbar,M. *et al.* (2016) Identification of mutation in GTPBP2 in patients of a family with neurodegeneration accompanied by iron deposition in the brain. *Neurobiol. Aging*, **38**, 216.
18. Darnell,J.C., Van Driesche,S.J., Zhang,C., Hung,K.Y., Mele,A., Fraser,C.E., Stone,E.F., Chen,C., Fak,J.J., Chi,S.W. *et al.* (2011) FMRP stalls ribosomal translocation on mRNAs linked to synaptic function and autism. *Cell*, **146**, 247–261.
19. Lareau,L.F., Hite,D.H., Hogan,G.J. and Brown,P.O. (2014) Distinct stages of the translation elongation cycle revealed by sequencing ribosome-protected mRNA fragments. *Elife*, **3**, e01257.
20. Wu,C.C., Zinshteyn,B., Wehner,K.A. and Green,R. (2019) High-resolution ribosome profiling defines discrete ribosome

elongation states and translational regulation during cellular stress. *Mol. Cell*, **73**, 959–970.
21. Mauri,M., Kirchner,M., Aharoni,R., Ciolli Mattioli,C., van den Bruck,D., Gutkovitch,N., Modepalli,V., Selbach,M., Moran,Y. and Chekulaeva,M. (2017) Conservation of miRNA-mediated silencing mechanisms across 600 million years of animal evolution. *Nucleic Acids Res.*, **45**, 938–950.
22. Zappulo,A., van den Bruck,D., Ciolli Mattioli,C., Franke,V., Imami,K., McShane,E., Moreno-Estelles,M., Calviello,L., Filipchyk,A., Peguero-Sanchez,E. *et al.* (2017) RNA localization is a key determinant of neurite-enriched proteome. *Nat. Commun.*, **8**, 583.
23. Pillai,R.S., Artus,C.G. and Filipowicz,W. (2004) Tethering of human Ago proteins to mRNA mimics the miRNA-mediated repression of protein synthesis. *RNA*, **10**, 1518–1525.
24. Jain Goyal,M., Zhao,X., Bozhinova,M., Andrade-Lopez,K., de Heus,C., Schulze-Dramac,S., Muller-McNicoll,M., Klumperman,J. and Bethune,J. (2020) A paralog-specific role of COPI vesicles in the neuronal differentiation of mouse pluripotent cells. *Life Sci. Alliance*, **3**, e202000714.
25. Chekulaeva,M., Mathys,H., Zipprich,J.T., Attig,J., Colic,M., Parker,R. and Filipowicz,W. (2011) miRNA repression involves GW182-mediated recruitment of CCR4-NOT through conserved W-containing motifs. *Nat. Struct. Mol. Biol.*, **18**, 1218–1226.
26. Kohrer,C. and Rajbhandary,U.L. (2008) The many applications of acid urea polyacrylamide gel electrophoresis to studies of tRNAs and aminoacyl-tRNA synthetases. *Methods*, **44**, 129–138.
27. Chan,P.P. and Lowe,T.M. (2016) GtRNAdb 2.0: an expanded database of transfer RNA genes identified in complete and draft genomes. *Nucleic Acids Res.*, **44**, D184–D189.
28. Dobin,A., Davis,C.A., Schlesinger,F., Drenkow,J., Zaleski,C., Jha,S., Batut,P., Chaisson,M. and Gingeras,T.R. (2013) STAR: ultrafast universal RNA-seq aligner. *Bioinformatics*, **29**, 15–21.
29. Anders,S., Pyl,P.T. and Huber,W. (2015) HTSeq – a Python framework to work with high-throughput sequencing data. *Bioinformatics*, **31**, 166–169.
30. Motley,W.W., Seburn,K.L., Nawaz,M.H., Miers,K.E., Cheng,J., Antonellis,A., Green,E.D., Talbot,K., Yang,X.L., Fischbeck,K.H. *et al.* (2011) Charcot-Marie-Tooth-linked mutant GARS is toxic to peripheral neurons independent of wild-type GARS levels. *PLos Genet.*, **7**, e1002399.
31. Morelli,K.H., Griffin,L.B., Pyne,N.K., Wallace,L.M., Fowler,A.M., Oprescu,S.N., Takase,R., Wei,N., Meyer-Schuman,R., Mellacheruvu,D. *et al.* (2019) Allele-specific RNA interference prevents neuropathy in Charcot-Marie-Tooth disease type 2D mouse models. *J. Clin. Invest.*, **129**, 5568–5583.
32. Schmidt,E.K., Clavarino,G., Ceppi,M. and Pierre,P. (2009) SUnSET, a nonradioactive method to monitor protein synthesis. *Nat. Methods*, **6**, 275–277.
33. David,A., Dolan,B.P., Hickman,H.D., Knowlton,J.J., Clavarino,G., Pierre,P., Bennink,J.R. and Yewdell,J.W. (2012) Nuclear translation visualized by ribosome-bound nascent chain puromycylation. *J. Cell Biol.*, **197**, 45–57.
34. Ingolia,N.T., Hussmann,J.A. and Weissman,J.S. (2019) Ribosome profiling: global views of translation. *Cold Spring Harb. Perspect. Biol.*, **11**, a032698.
35. Elbaum-Garfinkle,S., Cobb,G., Compton,J.T., Li,X.H. and Rhoades,E. (2014) Tau mutants bind tubulin heterodimers with enhanced affinity. *Proc. Natl. Acad. Sci. U.S.A.*, **111**, 6311–6316.
36. Komar,A.A. and Merrick,W.C. (2020) A Retrospective on eIF2A-and not the alpha subunit of eIF2. *Int. J. Mol. Sci.*, **21**, 2054.
37. Harding,H.P., Ordonez,A., Allen,F., Parts,L., Inglis,A.J., Williams,R.L. and Ron,D. (2019) The ribosomal P-stalk couples amino acid starvation to GCN2 activation in mammalian cells. *Elife*, **8**, e50149.
38. Koumenis,C., Naczki,C., Koritzinsky,M., Rastani,S., Diehl,A., Sonenberg,N., Koromilas,A. and Wouters,B.G. (2002) Regulation of protein synthesis by hypoxia via activation of the endoplasmic reticulum kinase PERK and phosphorylation of the translation initiation factor eIF2alpha. *Mol. Cell. Biol.*, **22**, 7405–7416.
39. Schubert,K., Karousis,E.D., Jomaa,A., Scaiola,A., Echeverria,B., Gurzeler,L.A., Leibundgut,M., Thiel,V., Muhlemann,O. and Ban,N. (2020) SARS-CoV-2 Nsp1 binds the ribosomal mRNA channel to inhibit translation. *Nat. Struct. Mol. Biol.*, **27**, 1094.
40. Thoms,M., Buschauer,R., Ameismeier,M., Koepke,L., Denk,T., Hirschenberger,M., Kratzat,H., Hayn,M., Mackens-Kiani,T., Cheng,J. *et al.* (2020) Structural basis for translational shutdown and immune evasion by the Nsp1 protein of SARS-CoV-2. *Science*, **369**, 1249–1255.
41. Nakamura,A., Nambu,T., Ebara,S., Hasegawa,Y., Toyoshima,K., Tsuchiya,Y., Tomita,D., Fujimoto,J., Kurasawa,O., Takahara,C. *et al.* (2018) Inhibition of GCN2 sensitizes ASNS-low cancer cells to asparaginase by disrupting the amino acid response. *Proc. Natl. Acad. Sci. U.S.A.*, **115**, E7776–E7785.
42. Harding,H.P., Zhang,Y., Zeng,H., Novoa,I., Lu,P.D., Calfon,M., Sadri,N., Yun,C., Popko,B., Paules,R. *et al.* (2003) An integrated stress response regulates amino acid metabolism and resistance to oxidative stress. *Mol. Cell*, **11**, 619–633.
43. Kilberg,M.S., Balasubramanian,M., Fu,L. and Shan,J. (2012) The transcription factor network associated with the amino acid response in mammalian cells. *Adv. Nutr.*, **3**, 295–306.
44. Lange,P.S., Chavez,J.C., Pinto,J.T., Coppola,G., Sun,C.W., Townes,T.M., Geschwind,D.H. and Ratan,R.R. (2008) ATF4 is an oxidative stress-inducible, prodeath transcription factor in neurons in vitro and in vivo. *J. Exp. Med.*, **205**, 1227–1242.
45. Baleriola,J., Walker,C.A., Jean,Y.Y., Crary,J.F., Troy,C.M., Nagy,P.L. and Hengst,U. (2014) Axonally synthesized ATF4 transmits a neurodegenerative signal across brain regions. *Cell*, **158**, 1159–1172.
46. Schoch,K.M. and Miller,T.M. (2017) Antisense oligonucleotides: translation from mouse models to human neurodegenerative diseases. *Neuron*, **94**, 1056–1070.

5. General discussion and outlook

5.1 Neuronal RNA zipcodes and how to find them: Massively parallel reporter assays

Transcriptomic asymmetry in neurons

The first example of a localized mRNA was described in 1983 by Jefferey et al. (Jeffery et al., 1983). They identified the localization or distribution of *β-actin* mRNA to specific cytoplasmic regions within the developing ascidian embryo (Jeffery et al., 1983). This pioneering work paved the way for a whole field of research, studying the different aspects of mRNA localization and its functional contributions within an organism or a cell.

When we mention mRNA localization, we must also discuss asymmetry. Asymmetry is an important factor determining cellular differentiation and development, leading to the polarisation of a cell or organism, including the localization of specific mRNAs. In nearly every cell, asymmetry is a necessity for subsequent function. In oocytes, asymmetric patterning of specific morphogens drives the different cell lineages observed in the embryo (Grünert & St Johnston, 1996). In neurons, neuronal polarity contributes to the directed transmission of signals from the dendrites to the axons. This morphological asymmetry observed in the neuron can be attributed to the differential distribution of proteins within the cell, contributing to the development of specific subcellular compartments. A well accepted mechanism governing this proteomic distribution is the local translation of specifically localized mRNAs within a cell (Sutton & Schuman, 2005).

The detailed mechanisms involved in mRNA localization and cellular compartmentalisation have been constantly investigated since the 90s. However, before we ask the question “how?”, let’s discuss more about the “why?”. Why does mRNA need to be specifically localized in a cell, and what advantages does it have over protein localization? Localization of mRNA has multiple advantages over other means of local protein availability, as described in chapter 1.2.1.1. Briefly, these include: (i) low energy – a single mRNA can produce multiple protein copies, (ii) rapid response of a cell to external cues requiring changes in the local proteome, e.g. production of growth factors or neurotransmitters, (iii) ectopic protein activity is avoided, and (iv) the same transcript can be targeted to different locations within the cell depending on alternative *cis*-elements or *trans*-factors, without affecting structure or functions of the encoded proteins (Cody et al., 2013; Martin & Ephrussi, 2009; Turner-Bridger et al., 2020).

Neurons are the ideal cells to study mRNA localization, due to their strong polarity and length, as well as localized functions that require rapid remodelling of the local proteome in response to external cues. As some neurons in the nervous system, like the motor neurons of the sciatic nerve, can extend their axons up to 1m, there must be some amount of autonomy between the distal axon and the cell body. To this aspect, mRNA localization plays a defining role in modulating local neuronal functions via local translation.

To understand the mechanisms contributing to mRNA localization, we need to know which mRNAs are localized. Multiple studies over the last two decades have contributed to our knowledge of the global analysis of the local transcriptome in neurons, combining cellular fractionation or dissection with microarray or RNA-Seq analyses. The labs of Christine Holt and Erin Schuman were instrumental in expanding our repertoire of the local mouse neuronal transcriptome via laser-capture microdissection combined microarrays or deep sequencing, identifying the mRNAs localized to axonal growth cones, and those in the hippocampal neuropil, respectively (Cajigas et al., 2012; Zivraj et al., 2010). Our lab went a step further, combining local transcriptomics, proteomics, and translatomics from the subcellular compartments of mouse embryonic stem cell differentiated neurons. They showed that nearly half of the neurite-enriched proteome was accounted for by the translation of neurite-localized mRNAs, further highlighting the importance of asymmetric mRNA localization in neurons (Zappulo et al., 2017). At this point, we were privy to multiple datasets from different neurons compiling the various transcripts that are localized to different neuronal compartments, as well as the local proteome. However, one of the questions I wanted to answer during my PhD was “how?”. How do RNAs get transported from the cell body to the distal dendrites and axons, where they perform their localized function?

Since the discovery of the first localization element for *β-actin* mRNA by Kislauskis and Singer in 1994, scientists have been persistently investigating the mechanisms involved in this process (Kislauskis et al., 1994). Many localized mRNAs were discovered to contain *cis*-localization elements called “zipcodes”, that were sequences usually present in their 3’ UTRs. These zipcode sequences were found to be sufficient for mRNA localization, and appeared to be unique, but could also be multiple or variable in length, ranging from long nucleotide stretches to short motifs such as hexamers or structural elements (Carlevaro-Fita & Johnson, 2019; Lubelsky & Ulitsky, 2018; C. J. Shukla et al., 2018). However, these discoveries also highlighted the importance of other factors contributing to transcript localization. *Trans*-acting factors, usually RBPs like ZBP1, which binds to the *β-actin* zipcode (Hüttelmaier et al., 2005; Kim et al., 2015), were identified to recognise and bind these sequences, forming RNP complexes that enable transport of the bound mRNAs and their subsequent regulation of local expression and stability. Although a compilation of local transcriptomic data points to the neurite-localization of hundreds to thousands of mRNAs, the mechanisms and biological functions behind the localization of most transcripts is not understood. Also, all *cis*- and *trans*- elements that were discovered and validated so far, were done so by bioinformatic predictions and/or cell-based screens only for a handful of transcripts at a time. So, we developed a robust assay to identify multiple zipcodes simultaneously within a cellular system.

Establishment and design of the neuronal zipcode identification protocol: N-zip

Even though mRNA localization has been well-documented, the link between sequence and biological function still remains to be fully understood. Without understanding these mechanistic relationships, we lack the ability to model and predict changes in RNA localization dynamics caused by sequence alterations. N-zip was developed with the purpose of bridging this gap in knowledge, providing an experimental approach to map RNA sequence to subcellular neuronal localization. Identification of localization elements allows us the possibility to manipulate localization of specific transcripts, linking their biological roles.

Massively parallel reporter assays (MPRAs) were initially used in the context of mRNAs, to identify the different regulatory elements affecting transcript stability and translation (Elemento et al., 2007; Lubelsky & Ulitsky, 2018; Rabani et al., 2017; Yartseva et al., 2017). Even more recently, Ron and Ulitsky used this approach to study the impact of noncoding RNAs on circular and long RNA localization and stability. (Ron & Ulitsky, 2022) With its multiple applications, we developed an MPRA to study RNA localization elements in primary cortical neurons (PCNs).

The selection of the neurite-localized transcripts was done by my colleague and co-first author, Nicolai von Kügelgen. A major challenge was selecting a representative pool of transcripts that were neurite localized and expressed in multiple published datasets acquired from different types of neurons, and our test system, mouse PCNs. Transcript localization in our case was a measurement akin to transcript enrichment in the neurites in comparison to expression in the soma. This analysis yielded the selection of 99 transcripts, including some well-characterised localized mRNAs, *CaMKIIα* (Mayford et al., 1996; Mori et al., 2000), *Bdnf* (Ma et al., 2010), and *Map2* (Blichenberg et al., 1999; Garner et al., 1988). We also manually added *β-actin* (Kislauskis et al., 1994), and the alternatively spliced neuritically localized *Cdc42* isoform discovered in our lab (Mattioli et al., 2019). The 3' UTRs of all these transcripts were split into overlapping sequences of similar size, 75-110nt, and inserted into the 3' UTR of a lentiviral vector expressing GFP with a Synapsin 1 promoter, to generate a library pool (chapter 3, figure 1a). We chose this design for the N-zip library for specific reasons: (i) the short size of the tiles enabled precise identification of short regulatory sequences, (ii) the short size-range of the tiles allowed easier size selection during library preparation and sequencing of the entire tile, (iii) lentiviral infection of the library pool in PCNs showed the most efficient expression compared to other means of cellular transfection (tested by my other co-first author, Sayaka Dantsuji), and (iv) the Synapsin 1 promoter is neuron specific, controlling for glial contamination, and prevents overexpression of the reporters.

Analysis of the initial N-zip library of 99 transcripts resulted in the identification of 65 neurite-localized tiles belonging to 33 of these selected transcripts. Interestingly, Gene Ontology (GO) term analysis of

these transcripts linked them with local neuronal structures such as synapse and actin cytoskeleton (appendix I, ED figure 3c). Furthermore, motif analysis on the 65 neurite-localized tiles resulted in the identification of multiple motifs, including the *let-7* binding site, and $(AU)_n$ motif (chapter 3, figure 1b; appendix I, ED figure 3a). However, we also performed extensive mutagenesis of 16 fragments that were neurite-localized, introducing every possible single point mutation. Analysis of this mutagenesis N-zip library identified two-specific motifs necessary for neurite-localization (similar to the motif analysis), that when mutated, switched the localization of the tile towards the soma: the *let-7* binding site (CUACCUC), and $(AU)_n$ motif (chapter 3, figure 2).

At this point, we had two motifs that showed up via two different analysis of N-zip. One of the main goals of N-zip is to provide the scientific community with a method that reliably identifies localization elements when designed and analysed in a similar systematic way, as well as provide a basis to further identify the biological function related to this sequence in a cellular system. In our case, it was understanding the role of these motifs and their interacting partners in regulating transcript localization in neurons.

Exploring a new neuronal function for let-7- miRNA

As I already introduced in chapter 1.2.3, miRNAs are small non-coding RNAs expressed across the nervous system, regulating post-transcriptional gene expression by regulating transcript translation and stability (O'Carroll & Schaefer, 2013). Only since 2006, when Schratt et al. discovered the brain-specific function of *miR-134* regulating local *LimK1* translation in dendrites, did scientists start to uncover the contribution of different miRNAs to gene regulation in the brain, and their physiological implications (Schratt et al., 2006).

The *let-7* miRNA family is one of the earliest discovered miRNAs that opened the way for the field of miRNA research. Originally identified in 2000 in C elegans, *let-7* or *lethal-7* was named as such due to its lethality during development on knockout (Ali et al., 2020; Reinhart et al., 2000). It is one of the largest and most conserved miRNA families, with 60% of loci being conserved from mouse to human (Roush & Slack, 2008). *Let-7* miRNAs have been discovered to contribute to multiple physiological functions during development, proliferation, and differentiation, with their aberrant expression implicated in cancer, inflammation, and cerebral and cardiovascular diseases (Bernstein et al., 2021). However, although *let-7* is one of the most abundant miRNAs expressed in the mammalian brain, involved in multiple neuronal processes including synapse formation, it has not yet been implicated in neuronal RNA localization (Lagos-Quintana et al., 2002).

Further reiterating on the mechanisms of RNA localization that I touched upon in chapters 1.2.1.2 and 1.2.3.2, mRNAs can be transported via motor proteins along the cytoskeleton (Bullock, 2011), or can also be selectively degraded in cellular regions where they are not required (Ding et al., 1993). What is

interesting about these two mechanisms, is their contrasting mode of action. While motor proteins transport mRNAs within mRNPs towards their destination, increasing their concentration in a specific region, degradation does exactly the opposite, decreasing mRNA concentration in the target region. Previous studies describe degradation-based RNA localization in the *Drosophila* embryo (Ding et al., 1993), or noncanonical pathways like NMD in neurons (Colak et al., 2013; Notaras et al., 2020). However, although miRNAs have been discovered to locally degrade mRNAs in neuronal processes, they have not been implicated in localization-dependent degradation of their target mRNAs.

When we identified the *let-7* binding site as a neurite-localization motif in N-zip, it seemed likely that it might function based on the above-mentioned mechanisms; degrading its target mRNAs in the soma, thereby increasing their relative expression in the neurites. Compared to other miRNAs, *let-7* sites were enriched in neurite-localized transcripts in PCNs (chapter 3, figure 3e). Along with literature citing *let-7* function in multiple neuronal processes, our result pointed to the discovery of a new neuronal function for *let-7*.

Although we identified the *let-7* binding site as a motif, the question still remained: How exactly does *let-7* contribute to mRNA localization? To systematically answer this question, we started with the most obvious: Is *let-7* expression, and thereby its activity, skewed between the neuronal compartments? Small RNA-Seq of RNA isolated from the neurite and soma compartments showed that *let-7* is the strongest expressed miRNA within each compartment, with similar abundance in the soma and neurites, suggesting another mechanism regulating *let-7* activity in the soma. As miRNAs regulate gene expression via the miRISC, another explanation could be the skewed expression of *let-7* associated regulatory proteins. To confirm this hypothesis, I extracted proteins from the individual compartments for mass spectrometry. Proteomic analysis confirmed this hypothesis, identifying an enrichment of the miRISC protein components such as AGOs and TNRC6s, in the soma (chapter 3, figure 4c).

To validate this *let-7* degradation-based localization and confirm its specificity, I conducted multiple experiments based on targeted depletion of this machinery. Initially, we designed a stably expressed lentiviral *let-7* sponge vector containing six *let-7* binding sites to knockdown *let-7* activity in the PCNs, alleviating its silencing of endogenous transcripts (Petri et al., 2017). The localization shift of *let-7* targets to the soma was significant when compared to the negative control, albeit a minimal shift (Figure S3 (von Kügelgen et al., 2021)). This minimal localization change suggested an incomplete depletion of *let-7* due to limited efficacy of the sponge. Instead, I also analysed the shift in localization of endogenous and N-zip *let-7* target mRNAs and tiles on depletion of AGO2, a major component of the miRISC machinery. AGO2 depletion resulted in a strong shift of *let-7* motif containing transcripts towards the soma, for both, endogenous transcripts, and N-zip tiles (chapter 3, figure 5b,c). Due to the nature of this experimental set-up, these results represented relative rather than absolute changes in expression levels, since AGO2 depletion could have global direct and indirect effects on gene expression. Similarly, absolute

quantification of expression levels of individual N-zip tiles is not possible due to internal normalisation to the entire library.

This result also raised the question of whether this change was actually caused by downregulation of expression in the soma, or upregulation of levels in the neurites. To further support our localization model of transcript destabilisation in the soma, we used the N-zip mutagenesis library to compare expression changes of individual N-zip tiles upon mutation of the *let-7* site(s). We noticed that on mutation of the *let-7* binding sites, specific neurite-localized tiles showed an upregulation in both the soma and neurites, although the effect was significantly higher in the soma (chapter 3, figure 4b). This suggested the destabilisation of *let-7* targets more efficiently in the soma, thereby enriching them in the neurites. This hypothesis was further confirmed when we perturbed mRNA degradation via expression of dnCAF1, a dominant negative catalytic mutant of deadenylase CAF1/CNOT7 that slows down mRNA deadenylation and degradation (D. Zheng et al., 2008). In these neurons, we also observed a soma shift of only *let-7* target mRNAs, further strengthening the hypothesis that *let-7* promotes neurite-enrichment of its targets via regulation of their stability (appendix I, ED figure 6b). My smiFISH experiment comparing distal neurite localization of N-zip reporters containing *let-7* sites on AGO2 depletion nicely correlated with the above results, showing an increase in expression of these reporters at the proximal part of the neurite on *Ago2* knockdown (chapter 3, figure 5d).

As our proposed mechanism of *let-7* mediated mRNA localization is based on soma degradation of mRNAs, how do these mRNAs escape soma *let-7* regulation, enabling their neurite localization? Research on quantifying miRNA regulation has shown that miRNAs have a relatively moderate effect on their target downregulation (~1.3 fold), suggesting the ability of many transcripts to escape soma degradation, and localizing to the neurites (Baek et al., 2008). How is this mRNA localization mediated? This is still an unanswered question that is open for discussion, or rather, the focus of future experiments. Due to the distance an mRNA would need to travel along the neurite to reach the distal terminals, we can speculate the use of active motor-protein directed transport via interactions with RBPs, whereby mRNA inclusion in RBP-mediated mRNP granules facilitates neurite transport, while an mRNA gradient is formed across the cell due to selective degradation. Experiments focused on visualizing specific *let-7* target transcript movement via live-cell imaging in neurons could help elucidate the exact interplay between this degradation-dependent mRNA localization.

Localization of $(AU)_n$ motif containing mRNAs via interacting RBPs

N-zip also identified $(AU)_n$ as another zipcode sufficient for neurite localization (chapter 3, figure 6). Similar to the analysis done for *let-7* targets, analysis of the N-zip mutagenesis library (appendix I, ED figure 8b) and the dnCaf1 perturbation experiment (appendix I, ED figure 8b,c) for $(AU)_n$ containing transcripts also suggested neurite localization mediated via selective destabilisation in the soma.

To address the mechanisms behind $(AU)_n$ transcript localization, we identified the interacting partners mediating this localization via RNA affinity capture. This analysis yielded a few interesting candidates including neuronal ELAVL (nELAVL) proteins and an mRNA decay factor HBS1L (chapter 3, figure 7a), apart from another interesting RBP, RC3H2 (Roquin-2). nELAVL proteins (ELAVL 2, 3, and 4, or HuB, HuC and HuD, respectively) are known to bind AU-rich elements (AREs) (Cook et al., 2011). However, in concordance with the literature, nELAVLs stabilise their bound mRNAs, and on depletion in PCNs, did not affect the neurite localization of $(AU)_n$ containing transcripts (appendix I, ED figure 8g).

In keeping with the theme of degradation-dependent RNA localization, I looked at other interactors that aligned with our hypothesis of a degradation-based mechanism. Roquin-2 is an RBP that mediates the deadenylation-dependent degradation of its target transcripts via the Ccr4-Not complex, and also binds to miRNAs, regulating their homeostasis (Leppek et al., 2013). As it interacts with a constitutive decay element (CDE) rich in A-U pairs, it seemed like a likely candidate (Leppek et al., 2013). However, when I tested localization changes of neurite-localized $(AU)_n$ reporters on depletion of these different RBPs via qPCR (data not shown), I observed a significant shift towards the soma only on depletion of *Hbs1l*.

HBS1L is involved in the No-Go and Nonstop decay mRNA quality control pathways (O'Connell et al., 2019). Due to its homology to the eEF1 and eRF3 translation elongation and termination factors, HBS1L affects translation elongation, followed by the subsequent degradation of stalled mRNAs (Doma & Parker, 2007). Further analysis of the effect of *Hbs1l* depletion on neurite localization of $(AU)_n$ containing endogenous transcripts and N-zip tiles confirmed the role of HBS1L in localization of these transcripts via selective soma degradation (chapter 3, figure 7c,d; appendix I, ED figure 8h).

It still remains to be identified, the exact mechanism by which HBS1L regulates stability, triggering mRNA degradation. As the HBS1L interactome is not well defined, it would be interesting to identify its RNA and protein interactors via CLIP and interactome capture experiments, respectively, that might shed light on the pathway this RBP utilises to mediate selective degradation of $(AU)_n$ containing transcripts.

Diversity in zipcodes and mechanisms of localization

As heavily stated in my thesis, there are hundreds to thousands of neurite-localized transcripts. Although N-zip was decisively able to identify two neuronal zipcodes and a new mechanism of degradation-based localization, there are still many to be identified. Nevertheless, as a proof of principle, we analysed the ability of N-zip to identify previously known zipcodes. As mentioned in chapter 1.2.1.2, the CPE was described to facilitate *Map2* (Y. S. Huang et al., 2003) and *CamkIIα* (Blichenberg et al., 2001; Y. S. Huang et al., 2003; Mori et al., 2000) localization to the dendrites, and was also identified in *bdnf* (Oe & Yoneda, 2010). Using N-zip, we identified the CPE in neurite-localized tiles from *Map2* and *bdnf*, and also identified

a second *bdnf* localization element within the region previously confirmed to direct its dendritic localization (appendix I, ED figure 10). Similarly, we identified a single tile that was sufficient for the localization of the long neurite-localized *Cdc42* isoform (appendix I, ED figure 10) (Mattioli et al., 2019).

Surprisingly, we did not identify the canonical *ß-actin* zipcode (Kislauskis et al., 1994). As N-zip relies on the endogenous cellular mechanisms to regulate localization of the tiles, these tiles must be compatible with binding to their *trans*-factors with respect to secondary structures, and/or transcript modifications such as methylation. A possible explanation for the inability of N-zip to identify the *ß-actin* zipcode could be due to improper m6a depositions on the tile (H. Huang et al., 2018), preventing the binding of its *trans*-binding protein, ZBP1, and subsequent localization of the tile. Another aspect that I will discuss regarding the limitations of this study, is the age of the neurons correlating with different developmental timepoints. Regarding this aspect, ZBP1 is expressed around E12.5 with decreasing levels thereafter. The use of PCNs at P0 might abrogate this interaction due to low levels of ZBP1, preventing the identification of its canonical *cis*-element. Alternatively, a single transcript could have more than one zipcode, that act synergistically or in opposition. Even though we did not identify the canonical *ß-actin* zipcode, we did identify a tile containing the CPE, suggesting the presence of a secondary zipcode (appendix I, ED figure 10).

Another aspect of localization to consider is neuronal activity or depolarisation (Murase et al., 2002). Specialised cells like neurons that require immediate local synaptic remodelling should have the potential to adapt their localized RNA pool when necessary. Especially during states of injury and disease, the local transcriptome and translatome are adapted to the momentary need (Turner-Bridger et al., 2020). Therefore, specific or alternative zipcodes might be differentially recognised and localized depending on the activity state of the neuron, triggering mechanisms of neuronal plasticity and affecting mRNA localization. On depolarisation of the PCNs infected with the N-zip library, we observed the activated localization of some tiles that mapped to transcripts having essential neurite function, including transcripts encoding ribosomal proteins, suggesting a maintenance or generation of neurite ribosomes for local translation (appendix I, ED figure 2).

In parallel to our study, two other labs of Taliaferro (Arora et al., 2022) and Moor (Mikl et al., 2022) also developed a similar approach to identify neuronal zipcodes, while using a test system of neuroblastoma cell lines. Although we did not detect an overlap with the motifs identified in the study of Aurora et al. (Arora et al., 2022), Mikl et al. (Mikl et al., 2022) also discovered the contribution of the $(AU)_n$ motif to RNA localization, suggesting a conserved zipcode in both neuronal systems. These complementary and overlapping results highlight the robustness of MPRAs to understand RNA localization mechanisms. In contrast, the *let-7* binding site zipcode was not identified in the neuroblastoma cell lines. One explanation could be the varying expression of the *trans*-acting factor *let-7* between PCNs and neuronal cell lines

(Cherone et al., 2019). Therefore, as I will elaborate in the next section, the size of the tiles and choice of test system is important in extrapolating the results to more physiological functions.

MPRAs - limitations and future applications

MPRAs allow us to simultaneously analyse thousands of RNA sequences, enabling us to identify multiple zipcodes at the same time. However, the finer details of the assay determine the applicability of the results.

N-zip along with the study by Mikl et al. (Mikl et al., 2022) are limited by the relatively short tile size (≤150nt), allowing for the detection of only short zipcodes. This prevents the identification of longer zipcodes, like the 280nt zipcode of *Mapt*, required for its localization to axons (Behar et al., 1995), or the the 350nt zipcode of Arc (Kobayashi et al., 2005). On the other hand, Arora et al. used 260nt tiles that were densely aligned along the selected 3' UTRs, and were able to identify regulatory elements >100nt. Apart from the length, some zipcodes consist of multiple motifs that act synergistically or in different combinations to mediate localization. A number of studies also indicate the dependence of zipcode dynamics on its secondary structure or modifications, rather than its primary sequence (Serano & Cohen, 1995). These, along with zipcodes dependent on alternative splicing, cannot be identified by the current N-zip design. Another shortcoming of MPRAs is the use of a fixed backbone. On one hand, this ensures that the localization of the reporter is only due to the insert tile. However, different backbones and their specific features like length, GC content, and splicing status could affect the localization potential of individual zipcodes within the tiles. Similarly, the backbone sequence around the tiles could affect the zipcode secondary structure, preventing binding with its *trans*-factor. The use of a mutagenesis library enabled us to detect zipcodes that could be disrupted by single nucleotide mutations or longer kmers. Although we did observe changes in localisation of tiles containing multiple *let-7* seeds when one site was mutated, we cannot exclude other tiles with multiple zipcodes having different behaviours, limiting the detection of redundantly acting zipcodes. Nevertheless, this approach also allowed a high-resolution mapping of the specific motifs required for localization.

As discussed earlier, the choice of test system and developmental stage, as well as neuronal activity, can alter the localization patterns of individual zipcodes. These limitations could explain the lack of localized tiles identified for 66 of the 99 selected N-zip transcripts. Similarly, since the two motifs I characterised in this study were identified in only 15 out of the 33 transcripts having a neurite-enriched tile, this suggests the presence of additional localization mechanisms to the ones discussed above, that would need to be the focus of future studies.

As one might have also noticed, the results of the depletion experiments showed a stronger effect on N-zip reporter localization compared to endogenous transcripts containing *let-7* binding sites and $(AU)_n$

motifs. This could potentially be explained by the presence of additional regulatory elements in the full endogenous 3' UTR, that might act in combination to promote or inhibit localization, thereby contributing to the precise localization of endogenous transcripts. As shown with the CPEs we identified for *Map2* and *bdnf*, the location of the motif in relation to the poly(A) tail might also contribute to its efficiency. The use of N-zip along with other proteomic methods could further contribute to the identification of *cis*- and *trans*-elements governing localization.

As many neuronal diseases like ALS, are associated with cellular degeneration at the distal neuronal ends, it is safe to hypothesise that dysregulation of RNA localization and the subsequent effect on the local proteome could be a viable explanation. Therefore, identification of RNA localization elements via N-zip, followed by a combination of other techniques could help us understand the molecular processes in the different contexts of development, learning, and disease. The most important aspect of this method is its applicability to study RNA localization mechanisms in a variety of polarized cells, including other types of neurons, fibroblasts, epithelial and cancer cells, and oocytes. In summary, my research contributed to the development of a systematic, unbiased, transcriptome-wide assay that enabled us to investigate the *cis*- and *trans*-elements guiding RNA localization, bringing us closer to unravelling the sequence-encoded guidelines targeting RNAs within a polarized cellular system.

5.2 Translating into translation: Profiling translation repression in Charcot-Marie-Tooth disease

Charcot-Marie-Tooth disease (CMT) and its genetic variations

CMT is a heterogenous group of inherited peripheral neuropathies that affect the peripheral nerves of 1 in 2,500 people, resulting in a progressive disability with autonomic, sensory, and motor neuron impairments (Martyn & Hughes, 1997). More than 80 genes have been discovered to associate with the different forms of CMT, affecting the myelin or axons of the peripheral nerves (Martyn & Hughes, 1997). Over the last few decades, progress has been made to identify the various CMT genetic mutations, as well as the pathophysiology linked to these different forms (Beloribi-Djefaflia & Attarian, 2023). However, currently no effective therapy exists. Therefore, scientists have been trying to identify specific genes or pathways affected in the different CMT forms, to discover targets for new therapeutic strategies.

Heterozygous mutations in the genes encoding for six aminoacyl-tRNA synthetases (aaRSs) cause the degeneration of peripheral motor and sensory axons (Storkebaum, 2016; Wei et al., 2019). As described in chapter 1.2.2.1, during translation, amino acids and their cognate tRNAs are ligated by their specific aaRS enzymes (Blanchet et al., 2022; J. Ling et al., 2009). Hence, mutations in these aaRSs suggest impaired translation as a likely disease mechanism. Indeed, to confirm translational defects in these

genetic mutants, Niehues et al. overexpressed mutants of the glycyl- or tyrosyl-tRNA synthetase, encoded by the GARS or YARS gene, respectively, in *Drosophila* (Niehues et al., 2015). However, they observed a decrease in global translation in motor and sensory neurons along with motor defects, that was independent of aaRS enzymatic activity of tRNA charging, i.e. overall aminoacylation activity was not impaired (Niehues et al., 2015). This research added to previous studies using CMT mouse models for dominant GARS mutations, that also showed retained aminoacylation activity (Seburn et al., 2006). However, a loss-of-function allele model did not show the dominant CMT phenotype in the mice, suggesting a gain-of-toxic function of these mutant aaRSs, contributing to translation defects via an unknown mechanism (Seburn et al., 2006).

I was interested in studying the molecular mechanisms of translation inhibition due to dominant mutations in the GARS gene that cause a subtype of CMT, CMT type 2D (CMT2D). As mentioned above, mutations in CMT-GARS possibly results in a toxic gain-of-function, especially since some mutations retain their aminoacylation activity in whole (E71G (Antonellis et al., 2003)), or partially (G240R (Antonellis et al., 2003)), while the WT allele functions as normal (Motley et al., 2011; Niehues et al., 2015). Additionally, recent rescue experiments in *Drosophila* via overexpression of WT GARS were unsuccessful (Motley et al., 2011; Niehues et al., 2015). Therefore, whether translation repression was the result of a gain-of-function or a response to cellular stress caused by another mechanism, was yet to be discovered.

Since overexpression of CMT-GARS mutants was shown to recapitulate motor defects in *Drosophila* (Niehues et al., 2015), we overexpressed different CMT-GARS mutants (E71G, G240R, and ΔETAQ (Morelli et al., 2019)) identified in CMT2D patients, in the human embryonic kidney 293T cell line (HEK293T). Overexpression of CMT-GARS mutants was sufficient to recapitulate global repression of translation, visualized via a puromycelation assay that detects active translation by binding to the nascent peptide (chapter 4, figure 1D). Using this system, I systematically identified the mechanisms contributing to this translation repression, and ultimately CMT2D.

New mechanisms for translation repression in CMT2D

Described in detail in chapter 1.2.2.1, translation is a cyclic complex biological process occurring in three stages (Blanchet et al., 2022). The initiation stage has been considered the primary stage for translational control as it is a rate-limiting step, requiring the interplay of multiple eukaryotic initiation factors (eIFs) (Blanchet et al., 2022). However, the stage of translation elongation is also subject to regulation by various mechanisms and is significant in the context of both development and neurologic diseases. For example, mutation in the ribosome rescue factor, GTPBP2, has been linked to ribosome stalling during elongation and is associated with conditions such as cerebellar and retinal degeneration (Ishimura et al., 2014, 2016).

To briefly recap the intricacies of translation elongation described earlier; it consists of three steps starting with the accommodation of the ternary complex containing aminoacylated tRNA (aa-tRNA) and eEF1A:GTP, into the ribosome A-site, followed by peptide bond formation, and finally, ribosome translocation during which the peptidyl-tRNA is moved to the P-site, evicting the previous deacylated-tRNA (Blanchet et al., 2022). Importantly, during elongation, ribosomes undergo significant conformational changes before and after the binding of aa-tRNAs, and these changes can actually be distinguished via the technique, ribosome profiling (Ribo-Seq) (Blanchet et al., 2022; C. C. C. Wu et al., 2019). Initially, Ribo-Seq was used to only analyse the 29nt ribosome protected fragments (RPFs), a proxy for active translation (Ingolia et al., 2009). However, Wu et al. in 2019, described the presence of the 21nt RPFs which represented the pre-accommodation state of the ribosome, enabling us to zoom-in on the specific stages of translation elongation (C. C. C. Wu et al., 2019). Around the same time as my paper, the labs of Storkebaum (Zuko et al., 2021) and Burgess (Spaulding et al., 2021) were also studying CMT2D. When Zuko et al. manipulated regulatory pathways upstream of translation or translation initiation in *Drosophila* CMT2D models, they did not observe any alleviation of translation repression (Zuko et al., 2021). This data also suggested that translation elongation might be affected in CMT-GARS.

Using high-resolution ribosome profiling from our overexpression CMT-GARS system, I demonstrated the inhibition of the first stage of elongation, the accommodation of glycyl-tRNA in the A-site, leading to ribosome stalling (chapter 4, figure 2). On overexpression of the CMT-GARS G240R mutant, we could clearly observe pausing at the Glycine codon, specifically at the A-site, with a nice correlation to glycine codon usage (chapter 4, figure 2D). Interestingly, but in line with these results, we observed a lower difference in Glycine codon frequency at the P-site (appendix II, figure S1D), confirming the inhibition of the first step of elongation in CMT-GARS. Zuko et al. described similar Ribo-Seq results from mouse CMT-GARS spinal cords, although they observed a minimal effect as they did not independently analyse both 21nt and 29nt RPFs (Zuko et al., 2021). They instead analysed only the 29nt RPFs, preventing the direct analysis of ribosome pausing, and used only one replicate for each condition (Zuko et al., 2021). Additionally, Spaulding et al. reported that eIF2α phosphorylation via activation of the integrated stress response (ISR) in CMT, described in the next sub-chapter, was observed only in alpha motor neurons and in a subset of sensory neurons (Spaulding et al., 2021). This provided an additional explanation to the minimal effect observed by Zuko et al. on using the entire spinal cord. Regardless, both results strongly suggested ribosome stalling as a cause for the degenerative CMT phenotypes.

Under normal conditions, ribosome stalling is usually resolved by rescue pathways. However, Ishimura et al. connected ribosome stalling to neurodegeneration in mutant mice deficient in $tRNA^{Arg}$ and the ribosome rescue factor GTPBP2, pointing towards a similar mechanism in CMT-GARS (Ishimura et al., 2016). Taken together with my Ribo-Seq experiment, it is evident that glycyl-$tRNA^{Gly}$ insufficiency in cells overexpressing G240R contributes to ribosome pausing at glycine codons in the open A-site.

To confirm that aminoacylation activity is not disrupted in the CMT-GARS mutations used in our study and system, we investigated overall glycylation activity using northern blotting. This result further validated published data, showing that aminoacylation levels of $tRNA^{Gly}$ are unaffected in the presence of CMT-GARS mutants (chapter 4, figure 3A). Shifting our focus towards the steps between aminoacylation and translation elongation, we hypothesised that a step downstream of aminoacylation was affected. Northern blotting of GARS-CMT immunoprecipitates showed the release of glycyl-$tRNA^{Gly}$ from GARS was impaired, with the GARS mutants having an increased affinity to $tRNA^{Gly}$ (chapter 4, figure 3B). In this way, there is a deficiency of glycyl-$tRNA^{Gly}$ available for formation of the ternary complex with eEF1A:GTP, and thus, cannot be delivered to the ribosome, resulting in ribosome stalling specifically at Glycine codons. This experiment further validated a toxic gain-of-function for the CMT-GARS mutants, resulting in altered interactions with $tRNA^{Gly}$.

Zuko et al. also observed altered kinetics of $tRNA^{Gly}$ binding and release *in vitro* and by immunoprecipitation of GARS from the brain of *Drosophila* CMT models, validating the sequestration of a large fraction of cellular $tRNA^{Gly}$ by mutant GARS, depleting it for translation (Zuko et al., 2021). Thus, this data along with my results confidently elucidate the mechanism of translation repression in CMT2D caused by ribosome stalling due to slower release of glycyl-$tRNA^{Gly}$ from GARS mutants.

Secondary mechanism acts independently to repress translation

As I mentioned earlier, ribosome stalling during translation was associated with neurodegeneration, however, the signalling pathways affected were unknown. When studying ribosome stalling due to $tRNA^{Arg}$ and GTPBP2 deficiencies in a *Gtpbp2* mutant mouse, Ishimura et al. observed increased levels in phosphorylation of the translation initiation factor eIF2α before the onset of neurodegenerative phenotypes, as well as activation of Activating transcription factor 4 (ATF4), a key component of the ISR (Ishimura et al., 2016). The ISR is a major regulatory mechanism triggered during cellular stress. During ISR, phosphorylation of eIF2α reduces the levels of the initiation ternary complex, eIF2:GTP:Met-tRNAi, resulting in global downregulation of translation initiation. On the other hand, there is an upregulation in translation of specific transcripts required to alleviate and repair stress related damage, such as ATF4, a transcription factor that induces stress response genes. Importantly, chronic ISR activation can lead to neurodegeneration via mechanisms brought on by constant translation inhibition (Bosco, 2018). Therefore, we checked whether the ISR was activated in our CMT-GARS system, contributing to CMT pathophysiology.

Interestingly, we observed increased levels in phosphorylation of eIF2α, as well as enhanced translation of ATF4, in our CMT-GARS system (chapter 4, figure 4A,C). Hence, ribosome stalling also activates a secondary mechanism of repression affecting translation initiation. Although ISR is known to be activated by four distinct kinases, which suppress cap-dependent translation via eIF2α phosphorylation (Pakos-

Zebrucka et al., 2016), Harding et al. contributed the observed eIF2α phosphorylation to the activity of the eIF2α kinase, GCN2 (Harding et al., 2019). They observed an association of GCN2 activation with ribosome stalling caused by amino acid starvation instead of deacylated tRNA levels, proposing a model whereby GCN2 is activated during ribosome pausing due to interactions with the paused ribosome P-stalk (Harding et al., 2019).

To identify the association of ISR activation with translation repression by the CMT-GARS mutants, we analysed global translation changes in the presence of the GCN2 inhibitor, GCN-IN-1. Unsurprisingly, inhibition of GCN2 activity suppressed eIF2α phosphorylation, bringing it to comparable levels between the WT and GARS mutants (chapter 4, figure 4D). However, Puromycylation assay under the same conditions did not show alleviated translation repression, with the mutant GARS showing similar repression levels to pre-treatment (chapter 4, figure 4D), suggesting ribosome pausing as the main repressor of translation, followed by the secondary activation of the ISR.

In a similar study by Spaulding et al. using CMT2D mouse models, they described the activation of ISR related transcripts identified by an *in vivo*, cell-type specific gene expression analysis (Spaulding et al., 2021). They, however, did observe an alleviation in the neuropathic phenotype in CMT-GARS mice on genetic deletion or pharmacological inhibition of GCN2 (Spaulding et al., 2021). Although it did not restore function to levels similar to the littermate controls, improvements were observed ~10 days up to 3 weeks post treatment (Spaulding et al., 2021).

These results demonstrate a secondary molecular mechanism contributing to the CMT phenotype, wherein GCN2 is activated by ribosome pausing caused due to the sequestration of glycyl-tRNA^{Gly} by mutant GARS. The mechanisms described in this chapter underlying CMT-mutant GARS function in translation regulation highlight the critical interplay between the two stages of translation, elongation and initiation, in regulating neuron survival.

Defeating peripheral neuropathies

As I stated in the beginning of this chapter, no cures exist for CMT patients, and most therapy approaches being tested focus on targeting genes that might alleviate CMT symptoms by promoting survival, rather than treating the molecular mechanism causing the disease phenotype (Ozes et al., 2021). Our discovery of the underlying mechanisms contributing to the CMT-GARS phenotype, further strengthened by the correlating data from Zuko et al. (Zuko et al., 2021) and Spauliding et al. (Spaulding et al., 2021), open new avenues for the development of treatments for patients with CMT2D.

Multiple potential strategies could be taken to alleviate the symptoms of CMT2D patients. Starting from the gene itself, as heterozygous mutations are sufficient for the disease onset, downregulation of the

mutated gene might be a promising route. With the development of cell and gene therapies, multiple strategies can be used to selectively downregulate the mutant GARS gene. Antisense oligos (AO) have emerged as a promising therapeutic option to treat diseases with known gene mutations, as observed in spinal muscular atrophy and Huntington's disease, modulating their expression via targeted enzymatic degradation (Kole et al., 2012; Schoch & Miller, 2017). As CMT2D is caused by single nucleotide mutations, specifically targeting the mutant allele would pose some challenges.

Alternatively, therapies could directly target the different steps affected during CMT-GARS translation repression. Indeed, Zuko et al. showed that increasing the levels of $tRNA^{Gly}$ in transgenic animals containing additional copies of the gene encoding $tRNA^{Gly}$, was able to partially rescue peripheral neuropathy in their *Drosophila* CMT models, while completely preventing the phenotype in a CMT mouse model (Zuko et al., 2021). Since this method does not affect GARS mRNA or protein levels, developing another strategy to supply $tRNA^{Gly}$ could alleviate ribosome pausing, and the subsequent neurological phenotype.

ISR can also contribute to the neurodegenerative CMT phenotype. Therefore, drugs targeting ISR to alleviate its initiation-dependent translational repression could reduce CMT symptoms. As mentioned earlier, Spaulding et al. already tested the treatment of a GCN2 inhibitor to reduce activation of the ISR, and did observe a reduction in symptoms in their CMT mouse model, suggesting inhibition of ISR as a promising treatment strategy (Spaulding et al., 2021).

Although CMT primarily affects peripheral motor and sensory axons, our recapitulation of the disease phenotype in HEK293T cells along with the recapitulation of our discovered mechanism of translational repression in other CMT models, suggests the mechanism is not restricted to peripheral neurons but is more aggressive in them. Interestingly, Spaulding et al. did not observe any significant changes in translation repression between their CMT-GARS mutant and control model in liver and heart tissue (Spaulding et al., 2021). This could be explained by the use of 2-week-old mice that were below the age of CMT disease onset, although the motor neurons already showed repression of translation; further reiterating that peripheral neurons are much more susceptible to the mutated GARS compared to other cell types. A potential explanation could be that peripheral neuron axons might be more vulnerable to changes in availability of translational components, progressing their degeneration over other cell types.

With the development of human induced pluripotent stem cell (hiPSC) systems to generate neurons from human fibroblast-derived stem cells, it would be interesting to study the limiting translation components that make these neurons more susceptible to degeneration using actual CMT patient models (Bianchi et al., 2018; Takahashi et al., 2007). These models could also be used to test the different therapeutic strategies, directly extrapolating our findings to the human context.

As the identified mechanisms contributing to CMT2D phenotype explain the gain-of-toxic function of a specific aaRS, GARS, these mechanisms could be generalised for neuropathy-causing mutations in the other five CMT-linked aaRSs. Therefore, similar studies can be conducted to validate our findings in other CMT models, expanding the scope of my research to help a larger cohort of patients suffering from these CMT types.

6. Bibliography

Abudayyeh, O. O., Gootenberg, J. S., Essletzbichler, P., Han, S., Joung, J., Belanto, J. J., Verdine, V., Cox, D. B. T., Kellner, M. J., Regev, A., Lander, E. S., Voytas, D. F., Ting, A. Y., & Zhang, F. (2017). RNA targeting with CRISPR-Cas13. *Nature*, *550*(7675), 280–284. https://doi.org/10.1038/nature24049

Agnes P. Chan, Malgorzata Kloc, & Laurence D. Etkin. (1999). fatvg encodes a new localized RNA that uses a 25-nucleotide element (FVLE1) to localize to the vegetal cortex of Xenopus oocytes. *Development*. https://doi.org/10.1242/dev.126.22.4943

Aitken, C. E., & Lorsch, J. R. (2012). A mechanistic overview of translation initiation in eukaryotes. In *Nature Structural and Molecular Biology* (Vol. 19, Issue 6, pp. 568–576). https://doi.org/10.1038/nsmb.2303

Akiyama, T., Suzuki, N., Ishikawa, M., Fujimori, K., Sone, T., Kawada, J., Funayama, R., Fujishima, F., Mitsuzawa, S., Ikeda, K., Ono, H., Shijo, T., Osana, S., Shirota, M., Nakagawa, T., Kitajima, Y., Nishiyama, A., Izumi, R., Morimoto, S., … Aoki, M. (2019). Aberrant axon branching via Fos-B dysregulation in FUS-ALS motor neurons. *EBioMedicine*, *45*, 362–378. https://doi.org/10.1016/j.ebiom.2019.06.013

Akten, B., Kye, M. J., Hao, L. T., Wertz, M. H., Singh, S., Nie, D., Huang, J., Merianda, T. T., Twiss, J. L., Beattie, C. E., Steen, J. A. J., & Sahin, M. (2011). Interaction of survival of motor neuron (SMN) and HuD proteins with mRNA cpg15 rescues motor neuron axonal deficits. *PNAS*, *108*(25), 10337–10342. https://doi.org/10.1073/pnas.1104928108

Alami, N. H., Smith, R. B., Carrasco, M. A., Williams, L. A., Winborn, C. S., Han, S. S. W., Kiskinis, E., Winborn, B., Freibaum, B. D., Kanagaraj, A., Clare, A. J., Badders, N. M., Bilican, B., Chaum, E., Chandran, S., Shaw, C. E., Eggan, K. C., Maniatis, T., & Taylor, J. P. (2014). Axonal Transport of TDP-43 mRNA Granules Is Impaired by ALS-Causing Mutations. *Neuron*, *81*(3), 536–543. https://doi.org/10.1016/j.neuron.2013.12.018

Alberts B, Johnson A, & Lewis J. (2002). Molecular Motors. In *Molecular Biology of the Cell.* (4th edition.). https://www.ncbi.nlm.nih.gov/books/NBK26888/

Ali, A., Bouma, G. J., Anthony, R. v., & Winger, Q. A. (2020). The role of LIN28-let-7-ARID3B pathway in placental development. *International Journal of Molecular Sciences*, *21*(10). https://doi.org/10.3390/ijms21103637

Andreassi, C., Crerar, H., & Riccio, A. (2018). Post-transcriptional processing of mRNA in neurons: The vestiges of the RNA world drive transcriptome diversity. In *Frontiers in Molecular Neuroscience* (Vol. 11). Frontiers Media S.A. https://doi.org/10.3389/fnmol.2018.00304

Antonellis, A., Ellsworth, R. E., Sambuughin, N., Puls, I., Abel, A., Lee-Lin, S.-Q., Jordanova, A., Kremensky, I., Christodoulou, K., Middleton, L. T., Sivakumar, K., Ionasescu, V., Funalot, B., Vance, J. M., Goldfarb, L. G., Fischbeck, K. H., & Green, E. D. (2003). Glycyl tRNA Synthetase Mutations in Charcot-Marie-Tooth Disease Type 2D and Distal Spinal Muscular Atrophy Type V. In *Am. J. Hum. Genet* (Vol. 72). https://doi.org/10.1086/375039

Aranda-Abreu, G. E., Hernández, M. E., Soto, A., & Manzo, J. (2005). Possible Cis-acting signal that could be involved in the localization of different mRNAs in neuronal axons. *Theoretical Biology and Medical Modelling*, *2*. https://doi.org/10.1186/1742-4682-2-33

Aronov, S., Aranda, G., Behar, L., & Ginzburg, I. (2002). Visualization of translated tau protein in the axons of neuronal P19 cells and characterization of tau RNP granules. *Journal of Cell Science*, *115*(19), 3817–3827. https://doi.org/10.1242/jcs.00058

Arora, A., Castro-Gutierrez, R., Moffatt, C., Eletto, D., Becker, R., Brown, M., Moor, A. E., Russ, H. A., & Taliaferro, J. M. (2022). High-throughput identification of RNA localization elements in neuronal cells. *Nucleic Acids Research*, *50*(18), 10626–10642. https://doi.org/10.1093/nar/gkac763

Aulas, A., & Velde, C. vande. (2015). Alterations in stress granule dynamics driven by TDP-43 and FUS: A link to pathological inclusions in ALS? *Frontiers in Cellular Neuroscience*, *9*(OCTOBER). https://doi.org/10.3389/fncel.2015.00423

Auweter, S. D., Oberstrass, F. C., & Allain, F. H. T. (2006). Sequence-specific binding of single-stranded RNA: Is there a code for recognition? *Nucleic Acids Research*, *34*(17), 4943–4959. https://doi.org/10.1093/nar/gkl620

Aviner, R., Geiger, T., & Elroy-Stein, O. (2013). Novel proteomic approach (PUNCH-P) reveals cell cycle-specific fluctuations in mRNA translation. *Genes and Development*, *27*(16), 1834–1844. https://doi.org/10.1101/gad.219105.113

Bae, B., & Miura, P. (2020). Emerging roles for 3' UTRs in neurons. *International Journal of Molecular Sciences*, *21*(10). https://doi.org/10.3390/ijms21103413

Baek, D., Villén, J., Shin, C., Camargo, F. D., Gygi, S. P., & Bartel, D. P. (2008). The impact of microRNAs on protein output. *Nature*, *455*(7209), 64–71. https://doi.org/10.1038/nature07242

Bagni, C., Mannucci, L., Dotti, C. G., & Amaldi, F. (2000). Chemical Stimulation of Synaptosomes Modulates-Ca 2 /Calmodulin-Dependent Protein Kinase II mRNA Association to Polysomes. *The Journal of Neuroscience*. https://doi.org/10.1523/JNEUROSCI.20-10-j0004.2000

Baj, G., Leone, E., Chao, M. v., & Tongiorgi, E. (2011). Spatial segregation of BDNF transcripts enables BDNF to differentially shape distinct dendritic compartments. *Proceedings of the National Academy of Sciences of the United States of America*, *108*(40), 16813–16818. https://doi.org/10.1073/pnas.1014168108

Balasanyan, V., & Arnold, D. B. (2014). Actin and Myosin-Dependent Localization of mRNA to Dendrites. *PLoS ONE*. https://doi.org/10.1371/journal.pone

Balbo, P. B., & Bohm, A. (2007). Mechanism of Poly(A) Polymerase: Structure of the enzyme-MgATP-RNA ternary complex and kinetic analysis. *Structure*. https://doi.org/10.1016/j.str.2007.07.010

Baleriola, J., Walker, C. A., Jean, Y. Y., Crary, J. F., Troy, C. M., Nagy, P. L., & Hengst, U. (2014). Axonally synthesized ATF4 transmits a neurodegenerative signal across brain regions. *Cell*, *158*(5), 1159–1172. https://doi.org/10.1016/j.cell.2014.07.001

Bassell, G. J., & Warren, S. T. (2008). Fragile X Syndrome: Loss of Local mRNA Regulation Alters Synaptic Development and Function. In *Neuron* (Vol. 60, Issue 2, pp. 201–214). https://doi.org/10.1016/j.neuron.2008.10.004

Bassell, G. J., Zhang, H., Byrd, A. L., Femino, A. M., Singer, R. H., Taneja, K. L., Lifshitz, L. M., Herman, I. M., & Kosik, K. S. (1998). Sorting of β-Actin mRNA and Protein to Neurites and Growth Cones in Culture. *The Journal of Neuroscience*. https://doi.org/10.1523/JNEUROSCI.18-01-00251.1998

Battich, N., Stoeger, T., & Pelkmans, L. (2013). Image-based transcriptomics in thousands of single human cells at single-molecule resolution. *Nature Methods*, *10*(11), 1127–1136. https://doi.org/10.1038/nmeth.2657

Behar, L., Marx, R., Sadot, E., Barg, J., & Ginzburgt, I. (1995). cis-Acting signals and trans-acting proteins are involved in tau mRNA targeting into neurites of differentiating neuronal cells. *Int. J. Devl Neuroscience*, *13*(2), 113–127. https://doi.org/10.1016/0736-5748(95)00001-w

Beloribi-Djefaflia, S., & Attarian, S. (2023). Treatment of Charcot-Marie-Tooth neuropathies. *Revue Neurologique*, *179*(1), 35–48. https://doi.org/https://doi.org/10.1016/j.neurol.2022.11.006

Berleth, T., Burri, M., Thoma, G., Bopp, D., Richstein, S., Frigerio, G., Noll, M., & Nüsslein-Volhard, C. (1988). The role of localization of bicoid RNA in organizing the anterior pattern of the Drosophila embryo. *The EMBO Journal*, *7*(6), 1749–1756. https://doi.org/10.1002/j.1460-2075.1988.tb03004.x

Bernstein, D. L., Jiang, X., & Rom, S. (2021). Let-7 micrornas: Their role in cerebral and cardiovascular diseases, inflammation, cancer, and their regulation. In *Biomedicines* (Vol. 9, Issue 6). MDPI AG. https://doi.org/10.3390/biomedicines9060606

Bertrand, E., Chartrand, P., Schaefer, M., Shenoy, S. M., Singer, R. H., & Long, R. M. (1998). Localization of ASH1 mRNA Particles in Living Yeast. In *Molecular Cell* (Vol. 2). https://doi.org/10.1016/s1097-2765(00)80143-4

Bianchi, F., Malboubi, M., Li, Y., George, J. H., Jerusalem, A., Szele, F., Thompson, M. S., & Ye, H. (2018). Rapid and efficient differentiation of functional motor neurons from human iPSC for neural injury modelling. *Stem Cell Research*, *32*, 126–134. https://doi.org/10.1016/j.scr.2018.09.006

Bingol, B., & Schuman, E. M. (2006). Activity-dependent dynamics and sequestration of proteasomes in dendritic spines. *Nature*, *441*(7097), 1144–1148. https://doi.org/10.1038/nature04769

Bissels, U., Wild, S., Tomiuk, S., Holste, A., Hafner, M., Tuschl, T., & Bosio, A. (2009). Absolute quantification of microRNAs by using a universal reference. *RNA*, *15*(12), 2375–2384. https://doi.org/10.1261/rna.1754109

Blanchet, S., Ranjin, N., & Entian, K.-D. (2022). Translation Phases in Eukaryotes. In *Ribosome Biogenesis. Methods in Molecular Biology* (Vol. 2533). https://doi.org/https://doi.org/10.1007/978-1-0716-2501-9_13

Blichenberg, A., Rehbein, M., Müller, R., Garner, C. C., Richter, D., & Kindler, S. (2001). Identification of a cis-acting dendritic targeting element in the mRNA encoding the alpha subunit of CA2+/calmodul-independent protein kinase II. *European Journal of Neuroscience*, *13*(10), 1881–1888. https://doi.org/10.1046/j.0953-816X.2001.01565.x

Blichenberg, A., Schwanke, B., Rehbein, M., Garner, C. C., Richter, D., & Kindler, S. (1999). Identification of a cis-Acting Dendritic Targeting Element in MAP2 mRNAs. *The Journal of Neuroscience*. https://doi.org/10.1523/JNEUROSCI.19-20-08818.1999

Bodian, D. (1965). A Suggestive Relationship of Nerve Cell RNA with Specific Synaptic Sites. *PNAS*. https://doi.org/10.1073/pnas.53.2.418

Bosco, D. A. (2018). Translation dysregulation in neurodegenerative disorders. In *PNAS* (Vol. 115, Issue 51, pp. 12842–12844). National Academy of Sciences. https://doi.org/10.1073/pnas.1818493115

Bratu, D. P., Cha, B.-J., Mhlanga, M. M., Kramer, F. R., & Tyagi, S. (2003). Visualizing the distribution and transport of mRNAs in living cells. *PNAS*. https://doi.org/https://doi.org/10.1073/pnas.2233244100

Brengues, M., Teixeira, D., & Parker, R. (2005). Movement of Eukaryotic mRNAs Between Polysomes and Cytoplasmic Processing Bodies. In *Science* (Vol. 310, Issue 5747). https://doi.org/10.1126/science.1115791

Bridgman, P. C. (2004). Myosin-Dependent Transport in Neurons. In *Journal of Neurobiology* (Vol. 58, Issue 2, pp. 164–174). https://doi.org/10.1002/neu.10320

Bridgman, P. C., & Elkin, L. L. (2000). Axonal myosins. *Journal of Neurocytology*, *29*. https://doi.org/10.1023/a:1010947525181

Briese, M., Saal, L., Appenzeller, S., Moradi, M., Baluapuri, A., & Sendtner, M. (2015). Whole transcriptome profiling reveals the RNA content of motor axons. *Nucleic Acids Research*, *44*(4). https://doi.org/10.1093/nar/gkv1027

Bullock, S. L. (2011). Messengers, motors and mysteries: Sorting of eukaryotic mRNAs by cytoskeletal transport. In *Biochemical Society Transactions* (Vol. 39, Issue 5, pp. 1161–1165). https://doi.org/10.1042/BST0391161

Burgin, K. E., Waxham, M. N., Rickling, S., Westgate, S. A., Mobley, W. C., & Kelly', P. T. (1990). In situ Hybridization Histochemistry of Ca*+/Calmodulin-Dependent Protein Kinase in Developing Rat Brain. In *The Journal of Neuroscience* (Issue 6). https://doi.org/10.1523/JNEUROSCI.10-06-01788.1990

Buxbaum, A. R., Haimovich, G., & Singer, R. H. (2015). In the right place at the right time: Visualizing and understanding mRNA localization. In *Nature Reviews Molecular Cell Biology* (Vol. 16, Issue 2, pp. 95–109). Nature Publishing Group. https://doi.org/10.1038/nrm3918

Cai, Q., & Sheng, Z. H. (2009). Molecular motors and synaptic assembly. In *Neuroscientist* (Vol. 15, Issue 1, pp. 78–89). https://doi.org/10.1177/1073858408329511

Cajigas, I. J., Tushev, G., Will, T. J., Tom Dieck, S., Fuerst, N., & Schuman, E. M. (2012). The Local Transcriptome in the Synaptic Neuropil Revealed by Deep Sequencing and High-Resolution Imaging. *Neuron*, *74*(3), 453–466. https://doi.org/10.1016/j.neuron.2012.02.036

Campbell, D. S., & Holt, C. E. (2001). Chemotropic Responses of Retinal Growth Cones Mediated by Rapid Local Protein Synthesis and Degradation. In *Neuron* (Vol. 32). https://doi.org/10.1016/s0896-6273(01)00551-7

Cannell, I. G., Kong, Y. W., & Bushell, M. (2008). How do microRNAs regulate gene expression? In *Biochemical Society Transactions* (Vol. 36, Issue 6, pp. 1224–1231). https://doi.org/10.1042/BST0361224

Carlevaro-Fita, J., & Johnson, R. (2019). Global Positioning System: Understanding Long Noncoding RNAs through Subcellular Localization. In *Molecular Cell* (Vol. 73, Issue 5, pp. 869–883). Cell Press. https://doi.org/10.1016/j.molcel.2019.02.008

Castello, A., Fischer, B., Eichelbaum, K., Horos, R., Beckmann, B. M., Strein, C., Davey, N. E., Humphreys, D. T., Preiss, T., Steinmetz, L. M., Krijgsveld, J., & Hentze, M. W. (2012). Insights into RNA Biology from an Atlas of Mammalian mRNA-Binding Proteins. *Cell*, *149*(6), 1393–1406. https://doi.org/10.1016/j.cell.2012.04.031

Chen, A., Liao, S., Cheng, M., Ma, K., Wu, L., Lai, Y., Qiu, X., Yang, J., Xu, J., Hao, S., Wang, X., Lu, H., Chen, X., Liu, X., Huang, X., Li, Z., Hong, Y., Jiang, Y., Peng, J., … Wang, J. (2022). Spatiotemporal transcriptomic atlas of mouse organogenesis using DNA nanoball-patterned arrays. *Cell*, *185*(10), 1777-1792.e21. https://doi.org/10.1016/j.cell.2022.04.003

Chen, K. H., Boettiger, A. N., Moffitt, J. R., Wang, S., & Zhuang, X. (2015). Spatially resolved, highly multiplexed RNA profiling in single cells. *Science*, *348*(6233). https://doi.org/10.1126/science.aaa6090

Cherone, J. M., Jorgji, V., & Burge, C. B. (2019). Cotargeting among microRNAs in the brain. *Genome Research*, *29*(11), 1791–1804. https://doi.org/10.1101/gr.249201.119

Choe, J., Oh, N., Park, S., Lee, Y. K., Song, O. K., Locker, N., Chi, S. G., & Kim, Y. K. (2012). Translation initiation on mRNAs bound by nuclear cap-binding protein complex CBP80/20 requires interaction between CBP80/20-dependent translation initiation factor and eukaryotic translation initiation factor 3g. *Journal of Biological Chemistry*, *287*(22), 18500–18509. https://doi.org/10.1074/jbc.M111.327528

Chu, J. F., Majumder, P., Chatterjee, B., Huang, S. L., & Shen, C. K. J. (2019). TDP-43 Regulates Coupled Dendritic mRNA Transport-Translation Processes in Co-operation with FMRP and Staufen1. *Cell Reports*, *29*(10), 3118-3133.e6. https://doi.org/10.1016/j.celrep.2019.10.061

Chung, S., Eckrich, M., Perrone-Bizzozero, N., Kohn, D. T., & Furneaux, H. (1997). The Elav-like proteins bind to a conserved regulatory element in the 3'- untranslated region of GAP-43 mRNA. *Journal of Biological Chemistry*, *272*(10), 6593–6598. https://doi.org/10.1074/jbc.272.10.6593

Cioni, J. M., Lin, J. Q., Holtermann, A. v., Koppers, M., Jakobs, M. A. H., Azizi, A., Turner-Bridger, B., Shigeoka, T., Franze, K., Harris, W. A., & Holt, C. E. (2019). Late Endosomes Act as mRNA Translation Platforms and Sustain Mitochondria in Axons. *Cell*, *176*(1–2), 56-72.e15. https://doi.org/10.1016/j.cell.2018.11.030

Cody, N. A. L., Iampietro, C., & Lécuyer, E. (2013). The many functions of mRNA localization during normal development and disease: from pillar to post. In *Wiley interdisciplinary reviews. Developmental biology* (Vol. 2, Issue 6, pp. 781–796). https://doi.org/10.1002/wdev.113

Cody, N. A. L., Iampietro, C., & Lécuyer, E. (2013). The many functions of mRNA localization during normal development and disease: from pillar to post. In *Wiley interdisciplinary reviews. Developmental biology* (Vol. 2, Issue 6, pp. 781–796). https://doi.org/10.1002/wdev.113

Colak, D., Ji, S. J., Porse, B. T., & Jaffrey, S. R. (2013). Regulation of axon guidance by compartmentalized nonsense-mediated mRNA decay. *Cell*, *153*(6), 1252. https://doi.org/10.1016/j.cell.2013.04.056

Colgan, D. F., & Manley, J. L. (1997). Mechanism and regulation of mRNA polyadenylation. *Genes Dev.* https://doi.org/10.1101/gad.11.21.2755

Cook, K. B., Kazan, H., Zuberi, K., Morris, Q., & Hughes, T. R. (2011). RBPDB: A database of RNA-binding specificities. *Nucleic Acids Research*, *39*(SUPPL. 1). https://doi.org/10.1093/nar/gkq1069

Cox, L. J., Hengst, U., Gurskaya, N. G., Lukyanov, K. A., & Jaffrey, S. R. (2008). Intra-axonal translation and retrograde trafficking of CREB promotes neuronal survival. *Nature Cell Biology*, *10*(2), 149–159. https://doi.org/10.1038/ncb1677

Coyne, A. N., Siddegowda, B. B., Estes, P. S., Johannesmeyer, J., Kovalik, T., Daniel, S. G., Pearson, A., Bowser, R., & Zarnescu, D. C. (2014). FUTSCH/MAP1B mRNA is a translational target of TDP-43 and is neuroprotective in a Drosophila model of amyotrophic lateral sclerosis. *Journal of Neuroscience*, *34*(48), 15962–15974. https://doi.org/10.1523/JNEUROSCI.2526-14.2014

Cramer, P., Srebrow, A., Kadener, S., Werbajh, S., de La Mata, M., Melen, G., Nogués, G., & Kornblihtt, A. R. (2001). Coordination between transcription and pre-mRNA processing. *FEBS Letters*, *498*(2–3), 179–182. https://doi.org/10.1016/S0014-5793(01)02485-1

Crick, D. F. H. C., Barnetr, L., Brenner, D. S., & Waits-Tobin, D. R. J. (1961). General nature of the genetic code for proteins. *Nature*. https://doi.org/10.1038/1921227a0

Crimella, C., Baschirotto, C., Arnoldi, A., Tonelli, A., Tenderini, E., Airoldi, G., Martinuzzi, A., Trabacca, A., Losito, L., Scarlato, M., Benedetti, S., Scarpini, E., Spinicci, G., Bresolin, N., & Bassi, M. T. (2012). Mutations in the motor and stalk domains of KIF5A in spastic paraplegia type 10 and in axonal Charcot-Marie-Tooth type 2. *Clinical Genetics*, *82*(2), 157–164. https://doi.org/10.1111/j.1399-0004.2011.01717.x

Dajas-Bailador, F., Bonev, B., Garcez, P., Stanley, P., Guillemot, F., & Papalopulu, N. (2012). MicroRNA-9 regulates axon extension and branching by targeting Map1b in mouse cortical neurons. *Nature Neuroscience*, *15*(5), 697–699. https://doi.org/10.1038/nn.3082

Darnell, J. C., Jensen, K. B., Jin, P., Brown, V., Warren, S. T., & Darnell, R. B. (2001). Fragile X Mental Retardation Protein Targets G Quartet mRNAs Important for Neuronal Function. In *Cell* (Vol. 107). https://doi.org/10.1016/s0092-8674(01)00566-9

Darnell, J. C., & Klann, E. (2013). The translation of translational control by FMRP: Therapeutic targets for FXS. In *Nature Neuroscience* (Vol. 16, Issue 11, pp. 1530–1536). https://doi.org/10.1038/nn.3379

Darnell, J. C., van Driesche, S. J., Zhang, C., Hung, K. Y. S., Mele, A., Fraser, C. E., Stone, E. F., Chen, C., Fak, J. J., Chi, S. W., Licatalosi, D. D., Richter, J. D., & Darnell, R. B. (2011). FMRP stalls ribosomal translocation on mRNAs linked to synaptic function and autism. *Cell*, *146*(2), 247–261. https://doi.org/10.1016/j.cell.2011.06.013

Das, S., Singer, R. H., & Yoon, Y. J. (2019). The travels of mRNAs in neurons: do they know where they are going? In *Current Opinion in Neurobiology* (Vol. 57, pp. 110–116). Elsevier Ltd. https://doi.org/10.1016/j.conb.2019.01.016

Dermit, M., Dodel, M., & Mardakheh, F. K. (2017). Methods for monitoring and measurement of protein translation in time and space. In *Molecular BioSystems* (Vol. 13, Issue 12, pp. 2477–2488). Royal Society of Chemistry. https://doi.org/10.1039/c7mb00476a

Dieterich, D. C., Hodas, J. J. L., Gouzer, G., Shadrin, I. Y., Ngo, J. T., Triller, A., Tirrell, D. A., & Schuman, E. M. (2010). In situ visualization and dynamics of newly synthesized proteins in rat hippocampal neurons. *Nature Neuroscience*, *13*(7), 897–905. https://doi.org/10.1038/nn.2580

Dieterich, D. C., Link, A. J., Graumann, J., Tirrell, D. A., Schuman, E. M., & Sharpless, K. B. (2006). Selective identification of newly synthesized proteins in mammalian cells using bioorthogonal noncanonical amino acid tagging (BONCAT). *PNAS*. https://doi.org/https://doi.org/10.1073/pnas.0601637103

Ding, D., Parkhurst, S. M., Halsell, S. R., & Lipshitz, H. D. (1993). Dynamic Hsp83 RNA Localization during Drosophila Oogenesis and Embryogenesis. In *MOLECULAR AND CELLULAR BIOLOGY* (Vol. 15, Issue 14). https://doi.org/10.1128/mcb.13.6.3773-3781.1993

Ding, D., Parkhurst, S. M., Halsell, S. R., & Lipshitz, H. D. (1993). Dynamic Hsp83 RNA Localization during Drosophila Oogenesis and Embryogenesis. *Molecular and Cellular Biology*, *15*(14), 35–37. https://doi.org/10.1128/mcb.13.6.3773-3781.1993

DIng, X., Liu, S., Tian, M., Zhang, W., Zhu, T., Li, D., Wu, J., Deng, H. T., Jia, Y., Xie, W., Xie, H., & Guan, J. S. (2017). Activity-induced histone modifications govern Neurexin-1 mRNA splicing and memory preservation. *Nature Neuroscience*, *20*(5), 690–699. https://doi.org/10.1038/nn.4536

Dolgosheina, E. v., Jeng, S. C. Y., Panchapakesan, S. S. S., Cojocaru, R., Chen, P. S. K., Wilson, P. D., Hawkins, N., Wiggins, P. A., & Unrau, P. J. (2014). RNA Mango aptamer-fluorophore: A bright, high-affinity complex for RNA labeling and tracking. *ACS Chemical Biology*, *9*(10), 2412–2420. https://doi.org/10.1021/cb500499x

Doma, M. K., & Parker, R. (2007). RNA Quality Control in Eukaryotes. In *Cell* (Vol. 131, Issue 4, pp. 660–668). Elsevier B.V. https://doi.org/10.1016/j.cell.2007.10.041

Donlin-Asp, P. G., Polisseni, C., Klimek, R., Heckel, A., Schuman, E. M., Designed, E. M. S., Performed, R. K., & Analyzed, C. P. (2021). Differential regulation of local mRNA dynamics and translation following long-term potentiation and depression. *PNAS*, *118*, 2017578118. https://doi.org/10.1073/pnas.2017578118/-/DCSupplemental

Dörrbaum, A. R., Kochen, L., Langer, J. D., & Schuman, E. M. (2018). Local and global influences on protein turnover in neurons and glia. *ELIFE*. https://doi.org/10.7554/eLife.34202.001

Dunn, J. G., Foo, C. K., Belletier, N. G., Gavis, E. R., & Weissman, J. S. (2013). Ribosome profiling reveals pervasive and regulated stop codon readthrough in Drosophila melanogaster. *ELife*, *2013*(2). https://doi.org/10.7554/eLife.01179

Edbauer, D., Neilson, J. R., Foster, K. A., Wang, C. F., Seeburg, D. P., Batterton, M. N., Tada, T., Dolan, B. M., Sharp, P. A., & Sheng, M. (2010). Regulation of Synaptic Structure and Function by FMRP-Associated MicroRNAs miR-125b and miR-132. *Neuron*, *65*(3), 373–384. https://doi.org/10.1016/j.neuron.2010.01.005

Ederle, H., & Dormann, D. (2017). TDP-43 and FUS en route from the nucleus to the cytoplasm. In *FEBS Letters* (Vol. 591, Issue 11, pp. 1489–1507). Wiley Blackwell. https://doi.org/10.1002/1873-3468.12646

Elemento, O., Slonim, N., & Tavazoie, S. (2007). A Universal Framework for Regulatory Element Discovery across All Genomes and Data Types. *Molecular Cell*, *28*(2), 337–350. https://doi.org/10.1016/j.molcel.2007.09.027

Engel, K. L., Arora, A., Goering, R., Lo, H. Y. G., & Taliaferro, J. M. (2020). Mechanisms and consequences of subcellular RNA localization across diverse cell types. In *Traffic* (Vol. 21, Issue 6, pp. 404–418). Blackwell Munksgaard. https://doi.org/10.1111/tra.12730

Engel, K. L., Lo, H. Y. G., Goering, R., Li, Y., Spitale, R. C., & Matthew Taliaferro, J. (2022). Analysis of subcellular transcriptomes by RNA proximity labeling with Halo-seq. *Nucleic Acids Research*, *50*(4), E24. https://doi.org/10.1093/nar/gkab1185

Erwin van Dijk, Nicolas Cougot, Sylke Meyer, Sylvie Babajko, Elmar Wahle, & Bertrand SeÂraphin. (2002). Human Dcp2 a catalytically active mRNA decapping enzyme located in specific. *The EMBO Journal*. https://doi.org/10.1093/emboj/cdf678

Fallini, C., Bassell, G. J., & Rossoll, W. (2012). Spinal muscular atrophy: The role of SMN in axonal mRNA regulation. In *Brain Research* (Vol. 1462, pp. 81–92). https://doi.org/10.1016/j.brainres.2012.01.044

Fallini, C., Donlin-Asp, P. G., Rouanet, J. P., Bassell, G. J., & Rossoll, W. (2016). Deficiency of the survival of motor neuron protein impairs mrna localization and local translation in the growth cone of motor neurons. *Journal of Neuroscience*, *36*(13), 3811–3820. https://doi.org/10.1523/JNEUROSCI.2396-15.2016

Fallini, C., Rouanet, J. P., Donlin-Asp, P. G., Guo, P., Zhang, H., Singer, R. H., Rossoll, W., & Bassell, G. J. (2014). Dynamics of survival of motor neuron (SMN) protein interaction with the mRNA-binding protein IMP1 facilitates its trafficking into motor neuron axons. *Developmental Neurobiology*, *74*(3), 319–332. https://doi.org/10.1002/dneu.22111

Fallini, C., Zhang, H., Su, Y., Silani, V., Singer, R. H., Rossoll, W., & Bassell, G. J. (2011). The Survival of Motor Neuron (SMN) protein interacts with the mRNA-binding protein HuD and regulates localization of poly(A) mRNA in primary motor neuron axons. *Journal of Neuroscience*, *31*(10), 3914–3925. https://doi.org/10.1523/JNEUROSCI.3631-10.2011

Fazal, F. M., Han, S., Parker, K. R., Kaewsapsak, P., Xu, J., Boettiger, A. N., Chang, H. Y., & Ting, A. Y. (2019). Atlas of Subcellular RNA Localization Revealed by APEX-Seq. *Cell*, *178*(2), 473-490.e26. https://doi.org/10.1016/j.cell.2019.05.027

Feig, S., & Lipton, P. (1993). Pairing the Cholinergic Agonist Carbachol with Patterned Schaffer Collateral Stimulation Initiates Protein Synthesis in Hippocampal CA1 Pyramidal Cell Dendrites via a Muscarinic, NMDA-Dependent Mechanism. *The Journal of Neuroscience*. https://doi.org/10.1523/JNEUROSCI.13-03-01010.1993

Ferguson, A., Wang, L., Altman, R. B., Terry, D. S., Juette, M. F., Burnett, B. J., Alejo, J. L., Dass, R. A., Parks, M. M., Vincent, C. T., & Blanchard, S. C. (2015). Functional Dynamics within the Human Ribosome Regulate the Rate of Active Protein Synthesis. *Molecular Cell*, *60*(3), 475–486. https://doi.org/10.1016/j.molcel.2015.09.013

Fernandopulle, M. S., Lippincott-Schwartz, J., & Ward, M. E. (2021). RNA transport and local translation in neurodevelopmental and neurodegenerative disease. In *Nature Neuroscience* (Vol. 24, Issue 5, pp. 622–632). Nature Research. https://doi.org/10.1038/s41593-020-00785-2

Fiesel, F. C., & Kahle, P. J. (2011). TDP-43 and FUS/TLS: Cellular functions and implications for neurodegeneration. In *FEBS Journal* (Vol. 278, Issue 19, pp. 3550–3568). https://doi.org/10.1111/j.1742-4658.2011.08258.x

Fong, N., & Bentley, D. L. (2001). Capping, splicing, and 3′ processing are independently stimulated by RNA polymerase II: Different functions for different segments of the CTD. *Genes and Development*, *15*(14), 1783–1795. https://doi.org/10.1101/gad.889101

Fornasiero, E. F., Mandad, S., Wildhagen, H., Alevra, M., Rammner, B., Keihani, S., Opazo, F., Urban, I., Ischebeck, T., Sakib, M. S., Fard, M. K., Kirli, K., Centeno, T. P., Vidal, R. O., Rahman, R. U., Benito, E., Fischer, A., Dennerlein, S., Rehling, P., … Rizzoli, S. O. (2018). Precisely measured protein lifetimes in the mouse brain reveal differences across tissues and subcellular fractions. *Nature Communications*, *9*(1). https://doi.org/10.1038/s41467-018-06519-0

Forrest, K. M., & Gavis, E. R. (2003). Live Imaging of Endogenous RNA Reveals a Diffusion and Entrapment Mechanism for nanos mRNA Localization in Drosophila. *Current Biology*, *13*, 1159–1168. https://doi.org/10.1016/S

Forrest, K. M., & Gavis, E. R. (2003). Live Imaging of Endogenous RNA Reveals a Diffusion and Entrapment Mechanism for nanos mRNA Localization in Drosophila. *Current Biology*, *13*, 1159–1168. https://doi.org/10.1016/S

Fukuda, Y., Pazyra-Murphy, M. F., Tasdemir-Yilmaz, O. E., Li, Y., Rose, L., Yeoh, C., Vangos, N. E., Geffken, E. A., Seo, H.-S., Adelmant, G., Walensky, L. D., Marto, J. A., Dhe-Paganon, S., & Segal, R. A. (2020). Fast Transport of RNA Granules by Direct Interactions with KIF5A/KLC1 Motors Prevents Axon Degeneration. *BioRxiv*. https://doi.org/10.1101/2020.02.02.931204

Fusco, D., Accornero, N., Lavoie, B., Shenoy, S. M., Blanchard, J.-M., Singer, R. H., Bertrand, E., & Biol, C. (2003). Single mRNA Molecules Demonstrate Probabilistic Movement in Living Mammalian Cells. In *Curr Biol* (Vol. 13, Issue 2). https://doi.org/10.1016/s0960-9822(02)01436-7

Gamarra, M., de la Cruz, A., Blanco-Urrejola, M., & Baleriola, J. (2021). Local Translation in Nervous System Pathologies. In *Frontiers in Integrative Neuroscience* (Vol. 15). Frontiers Media S.A. https://doi.org/10.3389/fnint.2021.689208

Gao, Y., Tatavarty, V., Korza, G., Levin, M. K., & Carson, J. H. (2008). Multiplexed Dendritic Targeting of Calcium Calmodulin-dependent Protein Kinase II, Neurogranin, and Activity-regulated Cytoskeleton-associated Protein RNAs by the A2 Pathway. *Molecular Biology of the Cell*, *19*, 2311–2327. https://doi.org/10.1091/mbc.E07-09

Gardiol, A., Racca, C., & Triller, A. (1998). Dendritic and Postsynaptic Protein Synthetic Machinery. *The Journal of Neuroscience*. https://doi.org/10.1523/JNEUROSCI.19-01-00168.1999

Garner, C. C., Tucker, R. P., & Matus, A. (1988). Selective localization of messenger RNA for cytoskeletal protein MAP2 in dendrites. *Nature*. https://doi.org/https://doi.org/10.1038/336674a0

Gehring, N. H., & Roignant, J. Y. (2021). Anything but Ordinary – Emerging Splicing Mechanisms in Eukaryotic Gene Regulation. In *Trends in Genetics* (Vol. 37, Issue 4, pp. 355–372). Elsevier Ltd. https://doi.org/10.1016/j.tig.2020.10.008

Giuditta, B. A., Dettbarn, W., & Brzin, Mirosla. (1968). Protein synthesis in the isolated giant axon of the squid. *PNAS*. https://doi.org/https://doi.org/10.1073/pnas.59.4.1284

Glinka, M., Herrmann, T., Funk, N., Havlicek, S., Rossoll, W., Winkler, C., & Sendtner, M. (2010). The heterogeneous nuclear ribonucleoprotein-R is necessary for axonal β-actin mRNA translocation in spinal motor neurons. *Human Molecular Genetics*, *19*(10), 1951–1966. https://doi.org/10.1093/hmg/ddq073

Glock, C., Biever, A., Tushev, G., Nassim-Assir, B., Kao, A., Bartnik, I., Tom Dieck, S., & Schuman, E. M. (2021). The translatome of neuronal cell bodies, dendrites, and axons. *PNAS*. https://doi.org/10.1073/pnas.2113929118/-/DCSupplemental

Glock, C., Heumüller, M., & Schuman, E. M. (2017). mRNA transport & local translation in neurons. In *Current Opinion in Neurobiology* (Vol. 45, pp. 169–177). Elsevier Ltd. https://doi.org/10.1016/j.conb.2017.05.005

Goering, R., Hudish, L. I., Guzman, B. B., Raj, N., Bassell, G. J., Russ, H. A., Dominguez, D., & Taliaferro, J. M. (2020). FMRP promotes RNA localization to neuronal projections through interactions between its RGG domain and g-quadruplex RNA sequences. *ELife*, *9*, 1–31. https://doi.org/10.7554/eLife.52621

Gomes, C., Lee, S. J., Gardiner, A. S., Smith, T., Sahoo, P. K., Patel, P., Thames, E., Rodriguez, R., Taylor, R., Yoo, S., Heise, T., Kar, A. N., Perrone-Bizzozero, N., & Twiss, J. L. (2017). Axonal localization of neuritin/CPG15 mRNA is limited by competition for HuD binding. *Journal of Cell Science*, *130*(21), 3650–3662. https://doi.org/10.1242/jcs.201244

Graf, E. R., Zhang, X., Jin, S. X., Linhoff, M. W., & Craig, A. M. (2004). Neurexins induce differentiation of GABA and glutamate postsynaptic specializations via neuroligins. *Cell*, *119*(7), 1013–1026. https://doi.org/10.1016/j.cell.2004.11.035

Groen, E. J. N., Fumoto, K., Blokhuis, A. M., Engelen-Lee, J. Y., Zhou, Y., van den Heuvel, D. M. A., Koppers, M., van Diggelen, F., van Heest, J., Demmers, J. A. A., Kirby, J., Shaw, P. J., Aronica, E., Spliet, W. G. M., Veldink, J. H., van den Berg, L. H., & Pasterkamp, R. J. (2013). ALS-associated mutations in FUS disrupt the axonal distribution and function of SMN. *Human Molecular Genetics*, *22*(18), 3690–3704. https://doi.org/10.1093/hmg/ddt222

Grünert, S., & St Johnston, D. (1996). RNA localization and the development of asymmetry during Drosophila oogenesis. In *Current Opinion in Genetics & Development* (Vol. 6). https://doi.org/10.1016/s0959-437x(96)80059-1

Ha, M., & Kim, V. N. (2014). Regulation of microRNA biogenesis. In *Nature Reviews Molecular Cell Biology* (Vol. 15, Issue 8, pp. 509–524). Nature Publishing Group. https://doi.org/10.1038/nrm3838

Hancock, M. L., Preitner, N., Quan, J., & Flanagan, J. G. (2014). MicroRNA-132 is enriched in developing axons, locally regulates Rasa1 mRNA, and promotes axon extension. *Journal of Neuroscience*, *34*(1), 66–78. https://doi.org/10.1523/JNEUROSCI.3371-13.2014

Harding, H. P., Ordonez, A., Allen, F., Parts, L., Inglis, A. J., Williams, R. L., & Ron, D. (2019). The ribosomal P-stalk couples amino acid starvation to GCN2 2 activation in mammalian cells. *ELife*, *8*. https://doi.org/10.7554/eLife.50149

Heiman, M., Kulicke, R., Fenster, R. J., Greengard, P., & Heintz, N. (2014). Cell type-specific mRNA purification by translating ribosome affinity purification (TRAP). *Nature Protocols*, *9*(6), 1282–1291. https://doi.org/10.1038/nprot.2014.085

Helder, S., Blythe, A. J., Bond, C. S., & Mackay, J. P. (2016). Determinants of affinity and specificity in RNA-binding proteins. In *Current Opinion in Structural Biology* (Vol. 38, pp. 83–91). Elsevier Ltd. https://doi.org/10.1016/j.sbi.2016.05.005

Hengst, U., Deglincerti, A., Kim, H. J., Jeon, N. L., & Jaffrey, S. R. (2009). Axonal elongation triggered by stimulus-induced local translation of a polarity complex protein. *Nature Cell Biology*, *11*(8), 1024–1030. https://doi.org/10.1038/ncb1916

Holmberg, J., Clarke, D. L., & Frisen, J. (2000). Regulation of repulsion versus adhesion by different splice forms of an Eph receptor. *Nature*. https://doi.org/https://doi.org/10.1038/35041577

Holt, C. E., Martin, K. C., & Schuman, E. M. (2019). Local translation in neurons: visualization and function. In *Nature Structural and Molecular Biology* (Vol. 26, Issue 7, pp. 557–566). Nature Publishing Group. https://doi.org/10.1038/s41594-019-0263-5

Huang, H., Weng, H., Sun, W., Qin, X., Shi, H., Wu, H., Zhao, B. S., Mesquita, A., Liu, C., Yuan, C. L., Hu, Y. C., Hüttelmaier, S., Skibbe, J. R., Su, R., Deng, X., Dong, L., Sun, M., Li, C., Nachtergaele, S., … Chen, J. (2018). Recognition of RNA N6 -methyladenosine by IGF2BP proteins enhances mRNA stability and translation. *Nature Cell Biology*, *20*(3), 285–295. https://doi.org/10.1038/s41556-018-0045-z

Huang, Y. S., Carson, J. H., Barbarese, E., & Richter, J. D. (2003). Facilitation of dendritic mRNA transport by CPEB. *Genes and Development*, *17*(5), 638–653. https://doi.org/10.1101/gad.1053003

Hüttelmaier, S., Zenklusen, D., Lederer, M., Dictenberg, J., Lorenz, M., Meng, X. H., Bassell, G. J., Condeelis, J., & Singer, R. H. (2005). Spatial regulation of β-actin translation by Src-dependent phosphorylation of ZBP1. *Nature*, *438*(7067), 512–515. https://doi.org/10.1038/nature04115

Ingolia, N. T., Brar, G. A., Rouskin, S., McGeachy, A. M., & Weissman, J. S. (2012). The ribosome profiling strategy for monitoring translation in vivo by deep sequencing of ribosome-protected mRNA fragments. *Nature Protocols*, *7*(8), 1534–1550. https://doi.org/10.1038/nprot.2012.086

Ingolia, N. T., Ghaemmaghami, S., Newman, J. R. S., & Weissman, J. S. (2009). Genome-wide analysis in vivo of translation with nucleotide resolution using ribosome profiling. *Science*, *324*(5924), 218–223. https://doi.org/10.1126/science.1168978

Ingolia, N. T., Hussmann, J. A., & Weissman, J. S. (2019). Ribosome profiling: Global views of translation. *Cold Spring Harbor Perspectives in Biology*, *11*(5). https://doi.org/10.1101/cshperspect.a032698

Ingolia, N. T., Lareau, L. F., & Weissman, J. S. (2011). Ribosome profiling of mouse embryonic stem cells reveals the complexity and dynamics of mammalian proteomes. *Cell*, *147*(4), 789–802. https://doi.org/10.1016/j.cell.2011.10.002

Inoue, K., Ohno, M., Sakamoto, H., & Shimura, Y. (1989). Effect of the cap structure on pre-mRNA splicing in Xenopus oocyte nuclei. *Genes & Development*. https://doi.org/10.1101/gad.3.9.1472

Ishimura, R., Nagy, G., Dotu, I., Chuang, J. H., & Ackerman, S. L. (2016). Activation of GCN2 kinase by ribosome stalling links translation elongation with translation initiation. *ELife*. https://doi.org/10.7554/eLife.14295.001

Ishimura, R., Nagy, G., Dotu, I., Zhou, H., Yang, X.-L., Schimmel, P., Senju, S., Nishimura, Y., Chuang, J. H., & Ackerman, S. L. (2014). Ribosome stalling induced by mutation of a CNS-specific tRNA causes neurodegeneration. *Science*, *345*(6195), 451–455. https://doi.org/10.1126/science.1253351

Ishizuka, N., Weber, J., & Amaral, D. G. (1990). Organization of intrahippocampal projections originating from CA3 pyramidal cells in the rat. *Journal of Comparative Neurology*, *295*(4), 580–623. https://doi.org/10.1002/cne.902950407

Jambhekar, A., & Derisi, J. L. (2007). Cis-acting determinants of asymmetric, cytoplasmic RNA transport. In *RNA* (Vol. 13, Issue 5, pp. 625–642). https://doi.org/10.1261/rna.262607

Jan, C. H., Williams, C. C., & Weissman, J. S. (2014). Principles of ER cotranslational translocation revealed by proximity-specific ribosome profiling. *Science*, *346*(6210). https://doi.org/10.1126/science.1257521

Jan, C. H., Williams, C. C., & Weissman, J. S. (2014). Principles of ER cotranslational translocation revealed by proximity-specific ribosome profiling. *Science*, *346*(6210). https://doi.org/10.1126/science.1257521

Jeffery, W. R., & Capco, D. G. (1978). Differential Accumulation and Localization of Maternal Poly(A)-Containing RNA during Early Development of the Ascidian, Styela. In *DEVELOPMENTAL BIOLOGY* (Vol. 67). https://doi.org/10.1016/0012-1606(78)90306-8

Jeffery, W. R., Tomlinson, C. R., & Brodeur, R. D. (1983). Localization of Actin Messenger RNA during Early Ascidian Development. In *DEVELOPMENTAL BIOLOGY* (Vol. 99). https://doi.org/10.1016/0012-1606(83)90290-7

Juven-Gershon, T., Hsu, J. Y., Theisen, J. W., & Kadonaga, J. T. (2008). The RNA polymerase II core promoter - the gateway to transcription. In *Current Opinion in Cell Biology* (Vol. 20, Issue 3, pp. 253–259). https://doi.org/10.1016/j.ceb.2008.03.003

Kaewsapsak, P., Michael Shechner, D., Mallard, W., Rinn, J. L., & Ting, A. Y. (2017). Live-cell mapping of organelle-associated RNAs via proximity biotinylation combined with protein-RNA crosslinking. *ELife*. https://doi.org/10.7554/eLife.29224.001

Kanai, Y., Dohmae, N., & Hirokawa, N. (2004). Kinesin Transports RNA: Isolation and Characterization of an RNA-Transporting Granule. In *Neuron* (Vol. 43). https://doi.org/10.1016/j.neuron.2004.07.022

Kang, H., & Schuman, E. (1996). A Requirement for Local Protein Synthesis in Neurotrophin-Induced Hippocampal Synaptic Plasticity. *Science*. https://doi.org/10.1126/science.273.5280.140

Kao, D. I., Aldridge, G. M., Weiler, I. J., & Greenough, W. T. (2010). Altered mRNA transport, docking, and protein translation in neurons lacking fragile X mental retardation protein. *PNAS*, *107*(35), 15601–15606. https://doi.org/10.1073/pnas.1010564107

Kim, H. H., Lee, S. J., Gardiner, A. S., Perrone-Bizzozero, N. I., & Yoo, S. (2015). Different motif requirements for the localization zipcode element of β-actin mRNA binding by HuD and ZBP1. *Nucleic Acids Research*, *43*(15), 7432–7446. https://doi.org/10.1093/nar/gkv699

Kislauskis, E. H., Zhu, X., & Singer, R. H. (1994). Sequences Responsible for Intracellular Localization of β-Actin Messenger RNA Also Affect Cell Phenotype. *The Journal of Cell Biology*, *127*(2). https://doi.org/10.1083/jcb.127.2.441

Kislauskis, E. H., Zhu, X., & Singer, R. H. (1994). Sequences Responsible for Intracellular Localization of β-Actin Messenger RNA Also Affect Cell Phenotype. *Journal of Cell Biology*. https://doi.org/10.1083/jcb.127.2.441

Kneussel, M., & Wagner, W. (2013). Myosin motors at neuronal synapses: Drivers of membrane transport and actin dynamics. In *Nature Reviews Neuroscience* (Vol. 14, Issue 4, pp. 233–247). https://doi.org/10.1038/nrn3445

Kobayashi, H., Yamamoto, S., Maruo, T., & Murakami, F. (2005). Identification of a cis-acting element required for dendritic targeting of activity-regulated cytoskeleton-associated protein mRNA. *European Journal of Neuroscience*, *22*(12), 2977–2984. https://doi.org/10.1111/j.1460-9568.2005.04508.x

Kole, R., Krainer, A. R., & Altman, S. (2012). RNA therapeutics: Beyond RNA interference and antisense oligonucleotides. In *Nature Reviews Drug Discovery* (Vol. 11, Issue 2, pp. 125–140). https://doi.org/10.1038/nrd3625

Koltun, B., Ironi, S., Gershoni-Emek, N., Barrera, I., Hleihil, M., Nanguneri, S., Sasmal, R., Agasti, S. S., Nair, D., & Rosenblum, K. (2020). Measuring mRNA translation in neuronal processes and somata by tRNA-FRET. *Nucleic Acids Research*, *48*(6), E32–E32. https://doi.org/10.1093/nar/gkaa042

Kornblihtt, A. R., Schor, I. E., Alló, M., Dujardin, G., Petrillo, E., & Muñoz, M. J. (2013). Alternative splicing: A pivotal step between eukaryotic transcription and translation. In *Nature Reviews Molecular Cell Biology* (Vol. 14, Issue 3, pp. 153–165). https://doi.org/10.1038/nrm3525

Kosik, K. S. (2006). The neuronal microRNA system. In *Nature Reviews Neuroscience* (Vol. 7, Issue 12, pp. 911–920). https://doi.org/10.1038/nrn2037

Kozak, M. (1991). Structural Features in Eukaryotic mRNAs That Modulate the Initiation of Translation*. *The Journal of Biological Chemistry*, *266*(30), 19867. https://doi.org/https://doi.org/10.1016/S0021-9258(18)54860-2

Kuehner, J. N., Pearson, E. L., & Moore, C. (2011). Unravelling the means to an end: RNA polymerase II transcription termination. In *Nature Reviews Molecular Cell Biology* (Vol. 12, Issue 5, pp. 283–294). https://doi.org/10.1038/nrm3098

Kuhl, D., & Skehelt, P. (1998). Dendritic localization of mRNAs. *Current Opinion in Neurobiology*. https://doi.org/10.1016/s0959-4388(98)80087-1

Lagos-Quintana, M., Rauhut, R., Yalcin, A., Meyer, J., Lendeckel, W., & Tuschl, T. (2002). Identification of Tissue-Specific MicroRNAs from Mouse. In *Current Biology* (Vol. 12). https://doi.org/10.1016/s0960-9822(02)00809-6

Larcher, J.-C., Gasmi, L., Viranaïcken, W., Eddé, B., Bernard, R., Ginzburg, I., & Denoulet, P. (2004). Ilf3 and NF90 associate with the axonal targeting element of Tau mRNA. *The FASEB Journal*, *18*(14), 1761–1763. https://doi.org/10.1096/fj.04-1763fje

Lawrence, J. B., & Singer, R. F. (1986). Intracellular Localization of Messenger RNAs for Cytoskeletal Proteins. In *Cell* (Vol. 45). https://doi.org/10.1016/0092-8674(86)90326-0

Leppek, K., Schott, J., Reitter, S., Poetz, F., Hammond, M. C., & Stoecklin, G. (2013). Roquin promotes constitutive mrna decay via a conserved class of stem-loop recognition motifs. *Cell*, *153*(4), 869–881. https://doi.org/10.1016/j.cell.2013.04.016

Leung, K. M., van Horck, F. P. G., Lin, A. C., Allison, R., Standart, N., & Holt, C. E. (2006). Asymmetrical β-actin mRNA translation in growth cones mediates attractive turning to netrin-1. *Nature Neuroscience*, *9*(10), 1247–1256. https://doi.org/10.1038/nn1775

Levsky, J. M., Shenoy, S. M., Pezo, R. C., & Singer, R. H. (2002). Single-Cell Gene Expression Profiling. *Science*, *297*, 19. https://doi.org/10.1126/science.1072241

Lin, A. C., & Holt, C. E. (2007). Local translation and directional steering in axons. In *EMBO Journal* (Vol. 26, Issue 16, pp. 3729–3736). https://doi.org/10.1038/sj.emboj.7601808

Ling, J., Reynolds, N., & Ibba, M. (2009). Aminoacyl-tRNA synthesis and translational quality control. In *Annual Review of Microbiology* (Vol. 63, pp. 61–78). https://doi.org/10.1146/annurev.micro.091208.073210

Ling, S.-C., Fahrner, P. S., Greenough, W. T., & Gelfand, V. I. (2004). Transport of Drosophila fragile X mental retardation protein-containing ribonucleoprotein granules by kinesin-1 and cytoplasmic dynein. *PNAS*. https://doi.org/10.1073/pnas.0408114101

Li, Q., Lee, J. A., & Black, D. L. (2007). Neuronal regulation of alternative pre-mRNA splicing. In *Nature Reviews Neuroscience* (Vol. 8, Issue 11, pp. 819–831). https://doi.org/10.1038/nrn2237

Litman, P., Barg, J., Rindzoonski, L., & Cinzburg, I. (1993). Subcellular localization of Tau mRNA in Differentiating Neuronal Cell Culture: Implications for Neuronal Polarity. In *Neuron* (Vol. 10). https://doi.org/10.1016/0896-6273(93)90165-n

Long, R. M., Singer, R. H., Meng, X., Gonzalez, I., Nasmyth, K., & Jansen, R. P. (1997). Mating type switching in yeast controlled by asymmetric localization of ASH1 mRNA. *Science*. https://doi.org/0.1126/science.277.5324.383

López-Erauskin, J., Tadokoro, T., Baughn, M. W., Myers, B., McAlonis-Downes, M., Chillon-Marinas, C., Asiaban, J. N., Artates, J., Bui, A. T., Vetto, A. P., Lee, S. K., Le, A. V., Sun, Y., Jambeau, M., Boubaker, J., Swing, D., Qiu, J., Hicks, G. G., Ouyang, Z., … da Cruz, S. (2018). ALS/FTD-Linked Mutation in FUS Suppresses Intra-axonal Protein Synthesis and Drives Disease Without Nuclear Loss-of-Function of FUS. *Neuron*, *100*(4), 816-830.e7. https://doi.org/10.1016/j.neuron.2018.09.044

Lubeck, E., Coskun, A. F., Zhiyentayev, T., Ahmad, M., & Cai, L. (2014). Single-cell in situ RNA profiling by sequential hybridization. In *Nature Methods* (Vol. 11, Issue 4, pp. 360–361). Nature Publishing Group. https://doi.org/10.1038/nmeth.2892

Lubelsky, Y., & Ulitsky, I. (2018). Sequences enriched in Alu repeats drive nuclear localization of long RNAs in human cells. *Nature*, *555*(7694), 107–111. https://doi.org/10.1038/nature25757

Ludwik, K. A., von Kuegelgen, N., & Chekulaeva, M. (2019). Genome-wide analysis of RNA and protein localization and local translation in mESC-derived neurons. *Methods*, *162–163*, 31–41. https://doi.org/10.1016/j.ymeth.2019.02.002

Lunde, B. M., Moore, C., & Varani, G. (2007). RNA-binding proteins: Modular design for efficient function. In *Nature Reviews Molecular Cell Biology* (Vol. 8, Issue 6, pp. 479–490). https://doi.org/10.1038/nrm2178

Lutz, C. S., & Moreira, A. (2011). Alternative mRNA polyadenylation in eukaryotes: An effective regulator of gene expression. In *Wiley Interdisciplinary Reviews: RNA* (Vol. 2, Issue 1, pp. 22–31). https://doi.org/10.1002/wrna.47

Ma, B., Culver, B. P., Baj, G., Tongiorgi, E., Chao, M. v, & Tanese, N. (2010). Localization of BDNF mRNA with the Huntington's disease protein in rat brain. *Molecular Neurodegeneration*. https://doi.org/https://doi.org/10.1186/1750-1326-5-22

Maday, S., Twelvetrees, A. E., Moughamian, A. J., & Holzbaur, E. L. F. (2014). Axonal Transport: Cargo-Specific Mechanisms of Motility and Regulation. In *Neuron* (Vol. 84, Issue 2, pp. 292–309). Cell Press. https://doi.org/10.1016/j.neuron.2014.10.019

Mao, S., Ying, Y., Wu, R., & Chen, A. K. (2020). Recent Advances in the Molecular Beacon Technology for Live-Cell Single-Molecule Imaging. *IScience* . https://doi.org/10.1016/j.isci

Markworth, R., Bähr, M., & Burk, K. (2021). Held Up in Traffic—Defects in the Trafficking Machinery in Charcot-Marie-Tooth Disease. In *Frontiers in Molecular Neuroscience* (Vol. 14). Frontiers Media S.A. https://doi.org/10.3389/fnmol.2021.695294

Martínez, J. C., Randolph, L. K., Iascone, D. M., Pernice, H. F., Polleux, F., & Hengst, U. (2019). Pum2 Shapes the Transcriptome in Developing Axons through Retention of Target mRNAs in the Cell Body. *Neuron*, *104*(5), 931-946.e5. https://doi.org/10.1016/j.neuron.2019.08.035

Martin, K. C., & Ephrussi, A. (2009). mRNA Localization: Gene Expression in the Spatial Dimension. In *Cell* (Vol. 136, Issue 4, pp. 719–730). Elsevier B.V. https://doi.org/10.1016/j.cell.2009.01.044

Martyn, C. N., & Hughes, R. A. C. (1997). Epidemiology of peripheral neuropathy. In *Journal of Neurology Neurosurgery and Psychiatry* (Vol. 62, Issue 4, pp. 310–318). BMJ Publishing Group. https://doi.org/10.1136/jnnp.62.4.310

Mattioli, C. C., Rom, A., Franke, V., Imami, K., Arrey, G., Terne, M., Woehler, A., Akalin, A., Ulitsky, I., & Chekulaeva, M. (2019). Alternative 3 UTRs direct localization of functionally diverse protein isoforms in neuronal compartments. *Nucleic Acids Research*, *47*(5), 2560–2573. https://doi.org/10.1093/nar/gky1270

Mayford, M., Baranes, D., Podsypanina, K., & Kandel, E. R. (1996). The 3-untranslated region of CaMKII is a cis-acting signal for the localization and translation of mRNA in dendrites. *PNAS*, *93*, 13250–13255. https://doi.org/https://doi.org/10.1073/pnas.93.23.1325

Medioni, C., Mowry, K., & Besse, F. (2012). Principles and roles of mRNA localization in animal development. In *Development (Cambridge)* (Vol. 139, Issue 18, pp. 3263–3276). https://doi.org/10.1242/dev.078626

Mendonsa, S., von Kügelgen, N., Dantsuji, S., Ron, M., Breimann, L., Baranovskii, A., Lödige, I., Kirchner, M., Fischer, M., Zerna, N., Bujanic, L., Mertins, P., Ulitsky, I., & Chekulaeva, M. (2023). Massively parallel identification of mRNA localization elements in primary cortical neurons. *Nature Neuroscience*. https://doi.org/10.1038/s41593-022-01243-x

Merianda, T. T., Lin, A. C., Lam, J. S. Y., Vuppalanchi, D., Willis, D. E., Karin, N., Holt, C. E., & Twiss, J. L. (2009). A functional equivalent of endoplasmic reticulum and Golgi in axons for secretion of locally synthesized proteins. *Molecular and Cellular Neuroscience*, *40*(2), 128–142. https://doi.org/10.1016/j.mcn.2008.09.008

Mikl, M., Eletto, D., Nijim, M., Lee, M., Lafzi, A., Mhamedi, F., David, O., Sain, S. B., Handler, K., & Moor, A. E. (2022). A massively parallel reporter assay reveals focused and broadly encoded RNA localization signals in neurons. *Nucleic Acids Research*, *50*(18), 10643–10664. https://doi.org/10.1093/nar/gkac806

Miller, S., Yasuda, M., Coats, J. K., Jones, Y., Martone, M. E., & Mayford, M. (2002). Disruption of Dendritic Translation of CaMKII Impairs Stabilization of Synaptic Plasticity and Memory Consolidation. In *Neuron* (Vol. 36). https://doi.org/10.1016/s0896-6273(02)00978-9

Milo, R., & Phillips, R. (2015). How fast do molecular motors move on cytoskeletal filaments? In *Cell Biology by the Numbers*. http://book.bionumbers.org/how-fast-do-molecular-motors-move-on-cytoskeletal-filaments/

Mitsumori, K., Takei, Y., & Hirokawa, N. (2017). Components of RNA granules affect their localization and dynamics in neuronal dendrites. *Molecular Biology of the Cell*, *28*(11), 1412–1417. https://doi.org/10.1091/mbc.E16-07-0497

Moazed, D., & Noller, H. F. (1989). Intermediate states in the movement of transfer RNA in the ribosome. *Nature*. https://doi.org/https://doi.org/10.1038/342142a0

Morelli, K. H., Griffin, L. B., Pyne, N. K., Wallace, L. M., Fowler, A. M., Oprescu, S. N., Takase, R., Wei, N., Meyer-Schuman, R., Mellacheruvu, D., Kitzman, J. O., Kocen, S. G., Hines, T. J., Spaulding, E. L., Lupski, J. R., Nesvizhskii, A., Mancias, P., Butler, I. J., Yang, X. L., … Burgess, R. W. (2019). Allele-specific RNA interference prevents neuropathy in Charcot-Marie-Tooth disease type 2D mouse models. *Journal of Clinical Investigation*, *129*(12), 5568–5583. https://doi.org/10.1172/JCI130600

Mori, Y., Imaizumi, K., Katayama, T., Yoneda, T., & Tohyama, M. (2000). Two cis-acting elements in the 3′ untranslated region of α-CaMKII regulate its dendritic targeting. *Nature Neuroscience*, 1079–1084. https://doi.org/10.1038/80591

Motley, W. W., Seburn, K. L., Nawaz, M. H., Miers, K. E., Cheng, J., Antonellis, A., Green, E. D., Talbot, K., Yang, X. L., Fischbeck, K. H., & Burgess, R. W. (2011). Charcot-marie-tooth-linked mutant GARS is toxic to peripheral neurons independent of wild-type GARS levels. *PLoS Genetics*, *7*(12). https://doi.org/10.1371/journal.pgen.1002399

Muddashetty, R. S., Kelić, S., Gross, C., Xu, M., & Bassell, G. J. (2007). Dysregulated metabotropic glutamate receptor-dependent translation of AMPA receptor and postsynaptic density-95 mRNAs at synapses in a mouse model of fragile X syndrome. *The Journal of Neuroscience*, *27*(20), 5338–5348. https://doi.org/10.1523/JNEUROSCI.0937-07.2007

Muddashetty, R. S., Nalavadi, V. C., Gross, C., Yao, X., Xing, L., Laur, O., Warren, S. T., & Bassell, G. J. (2011). Reversible Inhibition of PSD-95 mRNA Translation by miR-125a, FMRP Phosphorylation, and mGluR Signaling. *Molecular Cell*, *42*(5), 673–688. https://doi.org/10.1016/j.molcel.2011.05.006

Mukherjee, C., Patil, D. P., Kennedy, B. A., Bakthavachalu, B., Bundschuh, R., & Schoenberg, D. R. (2012). Identification of Cytoplasmic Capping Targets Reveals a Role for Cap Homeostasis in Translation and mRNA Stability. *Cell Reports*, *2*(3), 674–684. https://doi.org/10.1016/j.celrep.2012.07.011

Murase, S., Mosser, E., & Schuman, E. M. (2002). Depolarization Drives β-Catenin into Neuronal Spines Promoting Changes in Synaptic Structure and Function. In *Neuron* (Vol. 35). https://doi.org/10.1016/s0896-6273(02)00764-x

Muslimov, I. A., Iacoangeli, A., Brosius, J., & Tiedge, H. (2006). Spatial codes in dendritic BC1 RNA. *Journal of Cell Biology*, *175*(3), 427–439. https://doi.org/10.1083/jcb.200607008

Muslimov, I. A., Santi, E., Homel, P., Perini, S., Higgins, D., & Tiedge, H. (1997). RNA Transport in Dendrites: A cis-Acting Targeting Element Is Contained within Neuronal BC1 RNA. *The Journal of Neuroscience*. https://doi.org/10.1523/JNEUROSCI.17-12-04722.1997

Nelles, D. A., Fang, M. Y., O'Connell, M. R., Xu, J. L., Markmiller, S. J., Doudna, J. A., & Yeo, G. W. (2016). Programmable RNA Tracking in Live Cells with CRISPR/Cas9. *Cell*, *165*(2), 488–496. https://doi.org/10.1016/j.cell.2016.02.054

Nicolas, A., Kenna, K., Renton, A. E., Ticozzi, N., Faghri, F., Chia, R., Dominov, J. A., Kenna, B. J., Nalls, M. A., Keagle, P., Rivera, A. M., van Rheenen, W., Murphy, N. A., van Vugt, J. J. F. A., Geiger, J. T., van der Spek, R., Pliner, H. A., Shankaracharya, Smith, B. N., … Traynor, B. J. (2018). Genome-wide Analyses Identify KIF5A as a Novel ALS Gene. *Neuron*, *97*(6), 1268-1283.e6. https://doi.org/10.1016/j.neuron.2018.02.027

Niehues, S., Bussmann, J., Steffes, G., Erdmann, I., Köhrer, C., Sun, L., Wagner, M., Schäfer, K., Wang, G., Koerdt, S. N., Stum, M., RajBhandary, U. L., Thomas, U., Aberle, H., Burgess, R. W., Yang, X. L., Dieterich, D., & Storkebaum, E. (2015). Impaired protein translation in Drosophila models for Charcot-Marie-Tooth neuropathy caused by mutant tRNA synthetases. *Nature Communications*, *6*. https://doi.org/10.1038/ncomms8520

Nikolov, D. B., & Burley, S. K. (1997). RNA polymerase II transcription initiation: a structural view. *Proceedings of the National Academy of Sciences*, *94*(1), 15–22. https://doi.org/10.1073/pnas.94.1.15

Notaras, M., Allen, M., Longo, F., Volk, N., Toth, M., Li Jeon, N., Klann, E., & Colak, D. (2020). UPF2 leads to degradation of dendritically targeted mRNAs to regulate synaptic plasticity and cognitive function. *Molecular Psychiatry*, *25*(12), 3360–3379. https://doi.org/10.1038/s41380-019-0547-5

O'Brien, J., Hayder, H., Zayed, Y., & Peng, C. (2018). Overview of microRNA biogenesis, mechanisms of actions, and circulation. In *Frontiers in Endocrinology* (Vol. 9, Issue AUG). Frontiers Media S.A. https://doi.org/10.3389/fendo.2018.00402

O'Carroll, D., & Schaefer, A. (2013). General principals of miRNA biogenesis and regulation in the brain. In *Neuropsychopharmacology* (Vol. 38, Issue 1, pp. 39–54). https://doi.org/10.1038/npp.2012.87

O'Connell, A. E., Gerashchenko, M. v., O'Donohue, M. F., Rosen, S. M., Huntzinger, E., Gleeson, D., Galli, A., Ryder, E., Cao, S., Murphy, Q., Kazerounian, S., Morton, S. U., Schmitz-Abe, K., Gladyshev, V. N., Gleizes, P. E., Séraphin, B., & Agrawal, P. B. (2019). Mammalian Hbs1L deficiency causes congenital anomalies and developmental delay associated with Pelota depletion and 80S monosome accumulation. *PLoS Genetics*, *15*(2). https://doi.org/10.1371/journal.pgen.1007917

Oe, S., & Yoneda, Y. (2010). Cytoplasmic polyadenylation element-like sequences are involved in dendritic targeting of BDNF mRNA in hippocampal neurons. *FEBS Letters*, *584*(15), 3424–3430. https://doi.org/10.1016/j.febslet.2010.06.040

Ohno, M., Sakamoto, H., & Shimura, Y. (1987). Preferential excision of the 5' proximal intron from mRNA precursors with two introns as mediated by the cap structure. In *Biochemistry* (Vol. 84). https://doi.org/10.1073/pnas.84.15.5187

Ortiz, R., Georgieva, M. v., Gutiérrez, S., Pedraza, N., Fernández-Moya, S. M., & Gallego, C. (2017). Recruitment of Staufen2 Enhances Dendritic Localization of an Intron-Containing CaMKIIα mRNA. *Cell Reports*, *20*(1), 13–20. https://doi.org/10.1016/j.celrep.2017.06.026

Ostroff, L. E., Fiala, J. C., Allwardt, B., & Harris, K. M. (2002). Polyribosomes Redistribute from Dendritic Shafts into Spines with Enlarged Synapses during LTP in Developing Rat Hippocampal Slices. In *Neuron* (Vol. 35). https://doi.org/https://doi.org/10.1016/S0896-6273(02)00785-7

Ozes, B., Moss, K., Myers, M., Ridgley, A., Chen, L., Murrey, D., & Sahenk, Z. (2021). AAV1.NT-3 gene therapy in a CMT2D model: phenotypic improvements in GarsP278KY/ mice. *Brain Communications*, *3*(4). https://doi.org/10.1093/braincomms/fcab252

Pabis, M., Neufeld, N., Steiner, M. C., Bojic, T., Shav-Tal, Y., & Neugebauer, K. M. (2013). The nuclear cap-binding complex interacts with the U4/U6·U5 tri-snRNP and promotes spliceosome assembly in mammalian cells. *RNA*, *19*(8), 1054–1063. https://doi.org/10.1261/rna.037069.112

Paige, J. S., Wu, K. Y., & Jaffrey, S. R. (2011). RNA mimics of green fluorescent protein. *Science*, *333*(6042), 642–646. https://doi.org/10.1126/science.1207339

Pakos-Zebrucka, K., Koryga, I., Mnich, K., Ljujic, M., Samali, A., & Gorman, A. M. (2016). The integrated stress response. *EMBO Reports*, *17*(10), 1374–1395. https://doi.org/10.15252/embr.201642195

Park, H. Y., Lim, H., Yoon, Y. J., Follenzi, A., Nwokafor, C., Lopez-Jones, M., Meng, X., & Singer, R. H. (2014a). Visualization of Dynamics of SingleEndogenous mRNA Labeled in Live Mouse. *Science*, *343*(6169), 419–422. https://doi.org/10.1126/science.1242939

Park, H. Y., Lim, H., Yoon, Y. J., Follenzi, A., Nwokafor, C., Lopez-Jones, M., Meng, X., & Singer, R. H. (2014b). Visualization of Dynamics of Single Endogenous mRNA Labeled in Live Mouse. *Science*, *343*(6169), 422–424. https://doi.org/10.1126/science.1239200

Perry, R. B. T., Doron-Mandel, E., Iavnilovitch, E., Rishal, I., Dagan, S. Y., Tsoory, M., Coppola, G., McDonald, M. K., Gomes, C., Geschwind, D. H., Twiss, J. L., Yaron, A., & Fainzilber, M. (2012). Subcellular Knockout of Importin β1 Perturbs Axonal Retrograde Signaling. *Neuron*, *75*(2), 294–305. https://doi.org/10.1016/j.neuron.2012.05.033

Petri, R., Pircs, K., Jönsson, M. E., Åkerblom, M., Brattås, P. L., Klussendorf, T., & Jakobsson, J. (2017). let-7 regulates radial migration of new-born neurons through positive regulation of autophagy. *The EMBO Journal*, *36*(10), 1379–1391. https://doi.org/10.15252/embj.201695235

Pichon, X., Lagha, M., Mueller, F., & Bertrand, E. (2018). A Growing Toolbox to Image Gene Expression in Single Cells: Sensitive Approaches for Demanding Challenges. In *Molecular Cell* (Vol. 71, Issue 3, pp. 468–480). Cell Press. https://doi.org/10.1016/j.molcel.2018.07.022

Pisarev, A. v., Kolupaeva, V. G., Yusupov, M. M., Hellen, C. U. T., & Pestova, T. v. (2008). Ribosomal position and contacts of mRNA in eukaryotic translation initiation complexes. *EMBO Journal*, *27*(11), 1609–1621. https://doi.org/10.1038/emboj.2008.90

Pisarev, A. v., Skabkin, M. A., Pisareva, V. P., Skabkina, O. v., Rakotondrafara, A. M., Hentze, M. W., Hellen, C. U. T., & Pestova, T. v. (2010). The Role of ABCE1 in Eukaryotic Posttermination Ribosomal Recycling. *Molecular Cell*, *37*(2), 196–210. https://doi.org/10.1016/j.molcel.2009.12.034

Preitner, N., Quan, J., Nowakowski, D. W., Hancock, M. L., Shi, J., Tcherkezian, J., Young-Pearse, T. L., & Flanagan, J. G. (2014). APC is an RNA-binding protein, and its interactome provides a link to neural development and microtubule assembly. *Cell*, *158*(2), 368–382. https://doi.org/10.1016/j.cell.2014.05.042

Proudfoot NJ, & Brownlee GG. (1976). 3′ non-coding region sequences in eukaryotic messenger RNA. *Nature*. https://doi.org/10.1038/263211a0

Rabani, M., Pieper, L., Chew, G. L., & Schier, A. F. (2017). A Massively Parallel Reporter Assay of 3′ UTR Sequences Identifies In Vivo Rules for mRNA Degradation. *Molecular Cell*, *68*(6), 1083-1094.e5. https://doi.org/10.1016/j.molcel.2017.11.014

Ramanathan, A., Robb, G. B., & Chan, S. H. (2016). mRNA capping: Biological functions and applications. In *Nucleic Acids Research* (Vol. 44, Issue 16, pp. 7511–7526). Oxford University Press. https://doi.org/10.1093/nar/gkw551

Rebagliati, M. R., Weeks, D. L., Harvey, F. R., & Melton, D. A. (1985). Identification and Cloning of Localized Maternal RNAs from Xenopus Eggs. In *Cell* (Vol. 42). https://doi.org/10.1016/0092-8674(85)90273-9

Reines, D., Conaway, J. W., & Conaway, R. C. (1996). The RNA polymerase II general elongation factors A role for general elongation factors. *Trends in Biochemical Sciences*. https://doi.org/https://doi.org/10.1016/S0968-0004(96)10045-1

Reinhart, B. J., Slack, F. J., Basson, M., Pasquinelli, A. E., Bettinger, J. C., Rougvie, A. E., Horvitz, R., & Ruvkun, G. (2000). The 21-nucleotide let-7RNA regulates developmental timing in Caenorhabditis elegans. *Nature*. https://doi.org/https://doi.org/10.1038/35002607

Rhee, H. W., Zou, P., Udeshi, N. D., Martell, J. D., Mootha, V. K., Carr, S. A., & Ting, A. Y. (2013). Proteomic mapping of mitochondria in living cells via spatially restricted enzymatic tagging. *Science*, *339*(6125), 1328–1331. https://doi.org/10.1126/science.1230593

Richter, K. N., Wildhagen, H., Helm, M. S., Ußling, J. E., Schikorski, T., & Rizzoli, S. O. (2018). Comparative synaptosome imaging: a semi-quantitative method to obtain copy numbers for synaptic and neuronal proteins. *Scientific Reports*, *8*(1). https://doi.org/10.1038/s41598-018-33130-6

Rihan, K., Antoine, E., Maurin, T., Bardoni, B., Bordonné, R., Soret, J., & Rage, F. (2017). A new cis-acting motif is required for the axonal SMN-dependent Anxa2 mRNA localization. *RNA*. https://doi.org/10.1261/rna.056788

Rodrigues, E. C., Grawenhoff, J., Baumann, S. J., Lorenzon, N., & Maurer, S. P. (2021). Mammalian Neuronal mRNA Transport Complexes: The Few Knowns and the Many Unknowns. In *Frontiers in Integrative Neuroscience* (Vol. 15). Frontiers Media S.A. https://doi.org/10.3389/fnint.2021.692948

Rodriques, S. G., Stickels, R. R., Goeva, A., Martin, C. A., Murray, E., Vanderburg, C. R., Welch, J., Chen, L. M., Chen, F., & Macosko, E. Z. (2019). Slide-seq: A scalable technology for measuring genome-wide expression at high spatial resolution. *Science*. https://doi.org/10.1126/science.aaw121

Ron, M., & Ulitsky, I. (2022). Context-specific effects of sequence elements on subcellular localization of linear and circular RNAs. *Nature Communications*, *13*(1). https://doi.org/10.1038/s41467-022-30183-0

Roush, S., & Slack, F. J. (2008). The let-7 family of microRNAs. In *Trends in Cell Biology* (Vol. 18, Issue 10, pp. 505–516). https://doi.org/10.1016/j.tcb.2008.07.007

Saal, L., Briese, M., Kneitz, S., Glinka, M., & Sendtner, M. (2014). Subcellular transcriptome alterations in a cell culture model of spinal muscular atrophy point to widespread defects in axonal growth and presynaptic differentiation. *RNA*, *20*(11), 1789–1802. https://doi.org/10.1261/rna.047373.114

Sambandan, S., Akbalik, G., Kochen, L., Rinne, J., Kahlstatt, J., Glock, C., Tushev, G., Alvarez-Castelao, B., Heckel, A., & Schuman, E. M. (2017). Activity-dependent spatially localized miRNA maturation in neuronal dendrites. *Science*. https://doi.org/10.1126/science.aaf8995

Saunders, A., Core, L. J., & Lis, J. T. (2006). Breaking barriers to transcription elongation. In *Nature Reviews Molecular Cell Biology* (Vol. 7, Issue 8, pp. 557–567). https://doi.org/10.1038/nrm1981

Savas, J. N., Ma, B., Deinhardt, K., Culver, B. P., Restituito, S., Wu, L., Belasco, J. G., Chao, M. v., & Tanese, N. (2010). A role for Huntington disease protein in dendritic RNA granules. *Journal of Biological Chemistry*, *285*(17), 13142–13153. https://doi.org/10.1074/jbc.M110.114561

Savas, J. N., Makusky, A., Ottosen, S., Baillat, D., Then, F., Krainc, D., Shiekhattar, R., Markey, S. P., & Tanese, N. (2008). Huntington's disease protein contributes to RNA-mediated gene silencing through association with Argonaute and P bodies. *PNAS*. https://doi.org/10.1073/pnas.0800658105

Schmidt, E. K., Clavarino, G., Ceppi, M., & Pierre, P. (2009). SUnSET, a nonradioactive method to monitor protein synthesis. *Nature Methods*, *6*(4), 275–277. https://doi.org/10.1038/nmeth.1314

Schoch, K. M., & Miller, T. M. (2017). Antisense Oligonucleotides: Translation from Mouse Models to Human Neurodegenerative Diseases. In *Neuron* (Vol. 94, Issue 6, pp. 1056–1070). Cell Press. https://doi.org/10.1016/j.neuron.2017.04.010

Schratt, G. M., Tuebing, F., Nigh, E. A., Kane, C. G., Sabatini, M. E., Kiebler, M., & Greenberg, M. E. (2006). A brain-specific microRNA regulates dendritic spine development. *Nature*, *439*(7074), 283–289. https://doi.org/10.1038/nature04367

Schwanhüusser, B., Busse, D., Li, N., Dittmar, G., Schuchhardt, J., Wolf, J., Chen, W., & Selbach, M. (2011). Global quantification of mammalian gene expression control. *Nature*, *473*(7347), 337–342. https://doi.org/10.1038/nature10098

Seburn, K. L., Nangle, L. A., Cox, G. A., Schimmel, P., & Burgess, R. W. (2006). An Active Dominant Mutation of Glycyl-tRNA Synthetase Causes Neuropathy in a Charcot-Marie-Tooth 2D Mouse Model. *Neuron*, *51*(6), 715–726. https://doi.org/10.1016/j.neuron.2006.08.027

Selbach, M., Schwanhäusser, B., Thierfelder, N., Fang, Z., Khanin, R., & Rajewsky, N. (2008). Widespread changes in protein synthesis induced by microRNAs. *Nature*, *455*(7209), 58–63. https://doi.org/10.1038/nature07228

Semotok, J. L., Luo, H., Cooperstock, R. L., Karaiskakis, A., Vari, H. K., Smibert, C. A., & Lipshitz, H. D. (2008). Drosophila Maternal Hsp83 mRNA Destabilization Is Directed by Multiple SMAUG Recognition Elements in the Open Reading Frame . *Molecular and Cellular Biology*, *28*(22), 6757–6772. https://doi.org/10.1128/mcb.00037-08

Sempere, L. F., Freemantle, S., Pitha-Rowe, I., Moss, E., Dmitrovsky, E., & Ambros, V. (2004). Expression profiling of mammalian microRNAs uncovers a subset of brain-expressed microRNAs with possible roles in murine and human neuronal differentiation. *Genome Biology*, *5*(3), 13. https://doi.org/10.1186/gb-2004-5-3-r13

Serano, T. L., & Cohen, R. S. (1995). A small predicted stem-loop structure mediates oocyte localization of Drosophila K10 mRNA. *Development*. https://doi.org/https://doi.org/10.1242/dev.121.11.3809

Shaffer, S. M., Wu, M. T., Levesque, M. J., & Raj, A. (2013). Turbo FISH: A Method for Rapid Single Molecule RNA FISH. *PLoS ONE*, *8*(9). https://doi.org/10.1371/journal.pone.0075120

Sharangdhar, T., Sugimoto, Y., Heraud-Farlow, J., Fernández-Moya, S. M., Ehses, J., Ruiz de los Mozos, I., Ule, J., & Kiebler, M. A. (2017). A retained intron in the 3'- UTR of Calm3 mRNA mediates its Staufen2- and activity-dependent localization to neuronal dendrites . *EMBO Reports*, *18*(10), 1762–1774. https://doi.org/10.15252/embr.201744334

Sheng, M., & Hoogenraad, C. C. (2007). The postsynaptic architecture of excitatory synapses: A more quantitative view. In *Annual Review of Biochemistry* (Vol. 76, pp. 823–847). https://doi.org/10.1146/annurev.biochem.76.060805.160029

Shigeoka, T., Jung, H., Jung, J., Turner-Bridger, B., Ohk, J., Lin, J. Q., Amieux, P. S., & Holt, C. E. (2016). Dynamic Axonal Translation in Developing and Mature Visual Circuits. *Cell*, *166*(1), 181–192. https://doi.org/10.1016/j.cell.2016.05.029

Shigeoka, T., Koppers, M., Wong, H. H. W., Lin, J. Q., Cagnetta, R., Dwivedy, A., de Freitas Nascimento, J., van Tartwijk, F. W., Ströhl, F., Cioni, J. M., Schaeffer, J., Carrington, M., Kaminski, C. F., Jung, H., Harris, W. A., & Holt, C. E. (2019). On-Site Ribosome Remodeling by Locally Synthesized Ribosomal Proteins in Axons. *Cell Reports*, *29*(11), 3605-3619.e10. https://doi.org/10.1016/j.celrep.2019.11.025

Shukla, C. J., McCorkindale, A. L., Gerhardinger, C., Korthauer, K. D., Cabili, M. N., Shechner, D. M., Irizarry, R. A., Maass, P. G., & Rinn, J. L. (2018). High-throughput identification of RNA nuclear enrichment sequences . *The EMBO Journal*, *37*(6). https://doi.org/10.15252/embj.201798452

Shukla, G. C., Singh, J., & Barik, S. (2011). MicroRNAs: Processing, Maturation, Target Recognition and Regulatory Functions. *Mol Cell Pharmacology*.

Sims, R. J., Belotserkovskaya, R., & Reinberg, D. (2004). Elongation by RNA polymerase II: The short and long of it. In *Genes and Development* (Vol. 18, Issue 20, pp. 2437–2468). https://doi.org/10.1101/gad.1235904

Singer, R. H., & Wardt, D. C. (1982). Actin gene expression visualized in chicken muscle tissue culture by using in situ hybridization with a biotinated nucleotide analog. *PNAS*, *79*, 7331–7335. https://doi.org/10.1073/pnas.79.23.7331

Soto, Xe. J. L., Gandal, Xm. J., Gonatopoulos-Pournatzis, Xt., Heller, E. A., Luo, Xd., & Zheng, S. (2019). Mechanisms of neuronal alternative splicing and strategies for therapeutic interventions. *Journal of Neuroscience*, *39*(42), 8193–8199. https://doi.org/10.1523/JNEUROSCI.1149-19.2019

Spaulding, E. L., Hines, T. J., Bais, P., D Tadenev, A. L., Schneider, R., Jewett, D., Pattavina, B., Pratt, S. L., Morelli, K. H., Stum, M. G., Hill, D. P., Gobet, C., Pipis, M., Reilly, M. M., Jennings, M. J., Horvath, R., Bai, Y., Shy, M. E., Alvarez-Castelao, B., … Burgess, R. W. (2021). The integrated stress response contributes to tRNA synthetase-associated peripheral neuropathy. *Science*. https://doi.org/10.1126/science.abb3414

Ståhl PL, Salmén F, Vickovic S, Lundmark A, Navarro JF, Magnusson J, Giacomello S, Asp M, Westholm JO, Huss M, Mollbrink A, Linnarsson S, Codeluppi S, Borg Å, Pontén F, Costea PI, Sahlén P, Mulder J, Bergmann O, … Frisén J. (2016). Visualization and analysis of gene expression in tissue sections by spatial transcriptomics. *Science*, *353*(6294), 74–78. https://doi.org/10.1126/science.aaf4374

Steward, O., & Levy, W. B. (1982). Preferential localization of polyribosomes under the base of dendritic spines in granule cells of the dentate gyrus. *The Journal of Neuroscience*, *2*(3), 284–291. https://doi.org/10.1523/JNEUROSCI.02-03-00284.1982

Storkebaum, E. (2016). Peripheral neuropathy via mutant tRNA synthetases: Inhibition of protein translation provides a possible explanation. *BioEssays*, *38*(9), 818–829. https://doi.org/10.1002/bies.201600052

Sutton, M. A., Ito, H. T., Cressy, P., Kempf, C., Woo, J. C., & Schuman, E. M. (2006). Miniature Neurotransmission Stabilizes Synaptic Function via Tonic Suppression of Local Dendritic Protein Synthesis. *Cell*, *125*(4), 785–799. https://doi.org/10.1016/j.cell.2006.03.040

Sutton, M. A., & Schuman, E. M. (2005). Local translational control in dendrites and its role in long-term synaptic plasticity. In *Journal of Neurobiology* (Vol. 64, Issue 1, pp. 116–131). https://doi.org/10.1002/neu.20152

Takahashi, K., Tanabe, K., Ohnuki, M., Narita, M., Ichisaka, T., Tomoda, K., & Yamanaka, S. (2007). Induction of Pluripotent Stem Cells from Adult Human Fibroblasts by Defined Factors. *Cell*, *131*(5), 861–872. https://doi.org/10.1016/j.cell.2007.11.019

Taliaferro, J. M. (2019). Classical and emerging techniques to identify and quantify localized RNAs. *Wiley Interdisciplinary Reviews: RNA*, *10*(5). https://doi.org/10.1002/wrna.1542

Taliaferro, J. M. (2022). Transcriptome-scale methods for uncovering subcellular RNA localization mechanisms. In *Biochimica et Biophysica Acta - Molecular Cell Research* (Vol. 1869, Issue 4). Elsevier B.V. https://doi.org/10.1016/j.bbamcr.2021.119202

Taliaferro, J. M., Vidaki, M., Oliveira, R., Olson, S., Zhan, L., Saxena, T., Wang, E. T., Graveley, B. R., Gertler, F. B., Swanson, M. S., & Burge, C. B. (2016). Distal Alternative Last Exons Localize mRNAs to Neural Projections. *Molecular Cell*, *61*(6), 821–833. https://doi.org/10.1016/j.molcel.2016.01.020

Taylor, A. M., Berchtold, N. C., Perreau, V. M., Tu, C. H., Li Jeon, N., & Cotman, C. W. (2009). Axonal mRNA in uninjured and regenerating cortical mammalian axons. *Journal of Neuroscience*, *29*(15), 4697–4707. https://doi.org/10.1523/JNEUROSCI.6130-08.2009

Taylor, A. M., Blurton-Jones, M., Rhee, S. W., Cribbs, D. H., Cotman, C. W., & Jeon, N. L. (2005). A microfluidic culture platform for CNS axonal injury, regeneration and transport. *Nature Methods*, *2*(8), 599–605. https://doi.org/10.1038/nmeth777

Thomas, A., Lee, P. J., Dalton, J. E., Nomie, K. J., Stoica, L., Costa-Mattioli, M., Chang, P., Nuzhdin, S., Arbeitman, M. N., & Dierick, H. A. (2012). A versatile method for cell-specific profiling of translated mrnas in Drosophila. *PLoS ONE*, *7*(7). https://doi.org/10.1371/journal.pone.0040276

Tian, B., Hu, J., Zhang, H., & Lutz, C. S. (2005). A large-scale analysis of mRNA polyadenylation of human and mouse genes. *Nucleic Acids Research*, *33*(1), 201–212. https://doi.org/10.1093/nar/gki158

Tian, B., & Manley, J. L. (2016). Alternative polyadenylation of mRNA precursors. In *Nature Reviews Molecular Cell Biology* (Vol. 18, Issue 1, pp. 18–30). Nature Publishing Group. https://doi.org/10.1038/nrm.2016.116

Tiedge, H., & Rgen Brosius, J. (1996). Translational Machinery in Dendrites of Hippocampal Neurons in Culture. *The Journal of Neuroscience*. https://doi.org/10.1523/JNEUROSCI.16-22-07171.1996

Tiruchinapalli, D. M., Oleynikov, Y., Kelič, S., Shenoy, S. M., Hartley, A., Stanton, P. K., Singer, R. H., & Bassell, G. J. (2003). Activity-Dependent Trafficking and Dynamic Localization of Zipcode Binding Protein 1 and-Actin mRNA in Dendrites and Spines of Hippocampal Neurons. *The Journal of Neuroscience*. https://doi.org/10.1523/JNEUROSCI.23-08-03251.2003

Tom Dieck, S., Kochen, L., Hanus, C., Heumüller, M., Bartnik, I., Nassim-Assir, B., Merk, K., Mosler, T., Garg, S., Bunse, S., Tirrell, D. A., & Schuman, E. M. (2015). Direct visualization of newly synthesized target proteins in situ. *Nature Methods*, *12*(5), 411–414. https://doi.org/10.1038/nmeth.3319

Tonna, T., Ozadama, H., Hanb, C., Seguraa, A., Tranc, D., Catoed, D., Salitd, M., & Cenik, C. (2021). Single cell quantification of ribosome occupancy in early mouse development. *BioRxiv*. https://doi.org/10.1101/2021.12.07.471408

Topisirovic, I., Svitkin, Y. v., Sonenberg, N., & Shatkin, A. J. (2011). Cap and cap-binding proteins in the control of gene expression. In *Wiley Interdisciplinary Reviews: RNA* (Vol. 2, Issue 2, pp. 277–298). https://doi.org/10.1002/wrna.52

Trapp, B. D., Pulley, M., & Griffin, J. (1987). Spatial segregation of mRNA encoding myelin-specific proteins. *Proceedings of the National Academy of Sciences of the United States of America*, *84*, 40. https://doi.org/10.1073/pnas.84.21.7773

Tsanov, N., Samacoits, A., Chouaib, R., Traboulsi, A. M., Gostan, T., Weber, C., Zimmer, C., Zibara, K., Walter, T., Peter, M., Bertrand, E., & Mueller, F. (2016). smiFISH and FISH-quant - A flexible single RNA detection approach with super-resolution capability. *Nucleic Acids Research*, *44*(22). https://doi.org/10.1093/nar/gkw784

Turner-Bridger, B., Caterino, C., & Cioni, J. M. (2020). Molecular mechanisms behind mRNA localization in axons: Axonal mRNA Localisation. *Open Biology*, *10*(9). https://doi.org/10.1098/rsob.200177

Turner-Bridger, B., Jakobs, M., Muresan, L., Wong, H. H. W., Franze, K., Harris, W. A., & Holt, C. E. (2018). Single-molecule analysis of endogenous β-actin mRNA trafficking reveals a mechanism for compartmentalized mRNA localization in axons. *PNAS*, *115*(41), E9697–E9706. https://doi.org/10.1073/pnas.1806189115

Tushev, G., Glock, C., Heumüller, M., Biever, A., Jovanovic, M., & Schuman, E. M. (2018). Alternative 3' UTRs Modify the Localization, Regulatory Potential, Stability, and Plasticity of mRNAs in Neuronal Compartments. *Neuron*, *98*(3), 495-511.e6. https://doi.org/10.1016/j.neuron.2018.03.030

van den Hoogenhof, M. M. G., Pinto, Y. M., & Creemers, E. E. (2016). RNA Splicing regulation and dysregulation in the heart. In *Circulation Research* (Vol. 118, Issue 3, pp. 454–468). Lippincott Williams and Wilkins. https://doi.org/10.1161/CIRCRESAHA.115.307872

VanInsberghe, M., van den Berg, J., Andersson-Rolf, A., Clevers, H., & van Oudenaarden, A. (2021). Single-cell Ribo-seq reveals cell cycle-dependent translational pausing. *Nature*, *597*(7877), 561–565. https://doi.org/10.1038/s41586-021-03887-4

Vargas, D. Y., Raj, A., Marras, S. A. E., Kramer, F. R., & Tyagi, S. (2005). Mechanism of mRNA transport in the nucleus. *PNAS*. https://doi.org/https://doi.org/10.1073/pnas.0505580102

von Kügelgen, N., & Chekulaeva, M. (2020). Conservation of a core neurite transcriptome across neuronal types and species. In *Wiley Interdisciplinary Reviews: RNA* (Vol. 11, Issue 4). Blackwell Publishing Ltd. https://doi.org/10.1002/wrna.1590

von Kügelgen, N., Mendonsa, S., Dantsuji, S., Ron, M., Kirchner, M., Zerna, N., Bujanic, L., Mertins, P., #2, I. U., & #1, M. C. (2021). Massively parallel identification of zipcodes in primary cortical neurons. *BioRxiv*. https://doi.org/10.1101/2021.10.21.465275

Walsh, F. S., & Doherty, P. (1997). Neural cell adhesion molecules of the immunoglobulin superfamily: role in axon growth and guidance. In *Annu. Rev. Cell Dev. Biol* (Vol. 13). https://doi.org/10.1146/annurev.cellbio.13.1.425

Wang, B., & Bao, L. (2017). Axonal microRNAs: Localization, function and regulatory mechanism during axon development. In *Journal of Molecular Cell Biology* (Vol. 9, Issue 2, pp. 82–90). Oxford University Press. https://doi.org/10.1093/jmcb/mjw050

Wang, B., Pan, L., Wei, M., Wang, Q., Liu, W. W., Wang, N., Jiang, X. Y., Zhang, X., & Bao, L. (2015). FMRP-Mediated Axonal Delivery of miR-181d Regulates Axon Elongation by Locally Targeting Map1b and Calm1. *Cell Reports*, *13*(12), 2794–2807. https://doi.org/10.1016/j.celrep.2015.11.057

Wang, B., Pan, L., Wei, M., Wang, Q., Liu, W. W., Wang, N., Jiang, X. Y., Zhang, X., & Bao, L. (2015). FMRP-Mediated Axonal Delivery of miR-181d Regulates Axon Elongation by Locally Targeting Map1b and Calm1. *Cell Reports*, *13*(12), 2794–2807. https://doi.org/10.1016/j.celrep.2015.11.057

Wang, P., Tang, W., Li, Z., Zou, Z., Zhou, Y., Li, R., Xiong, T., Wang, J., & Zou, P. (2019). Mapping spatial transcriptome with light-activated proximity-dependent RNA labeling. *Nature Chemical Biology*, *15*(11), 1110–1119. https://doi.org/10.1038/s41589-019-0368-5

Wang, Y., LIU, J., HUANG, B., XU, Y.-M., LI, J., HUANG, L.-F., LIN, J., ZHANG, J., MIN, Q.-H., YANG, W.-M., & WANG, X.-Z. (2015). Mechanism of alternative splicing and its regulation. *Biomedical Reports*, *3*(2), 152–158. https://doi.org/10.3892/br.2014.407

Wei, N., Zhang, Q., & Yang, X. L. (2019). Neurodegenerative Charcot–Marie–Tooth disease as a case study to decipher novel functions of aminoacyl-tRNA synthetases. *Journal of Biological Chemistry*, *294*(14), 5321–5339. https://doi.org/10.1074/jbc.REV118.002955

Weischenfeldt, J., Waage, J., Tian, G., Zhao, J., Damgaard, I., Jakobsen, J. S., Kristiansen, K., Krogh, A., Wang, J., & Porse, B. T. (2012). Mammalian tissues defective in nonsense-mediated mRNA decay display highly aberrant splicing patterns. *Genome Biology*, *13*(5). https://doi.org/10.1186/gb-2012-13-5-r35

Wu, B., Chen, J., & Singer, R. H. (2014). Background free imaging of single mRNAs in live cells using split fluorescent proteins. *Scientific Reports*, *4*. https://doi.org/10.1038/srep03615

Wu, C. C. C., Zinshteyn, B., Wehner, K. A., & Green, R. (2019). High-Resolution Ribosome Profiling Defines Discrete Ribosome Elongation States and Translational Regulation during Cellular Stress. *Molecular Cell*, *73*(5), 959-970.e5. https://doi.org/10.1016/j.molcel.2018.12.009

Wu, K. Y., Hengst, U., Cox, L. J., Macosko, E. Z., Jeromin, A., Urquhart, E. R., & Jaffrey, S. R. (2005). Local translation of RhoA regulates growth cone collapse. *Nature*. https://doi.org/10.1038/nature03885

Wu, L., Fan, J., & Belasco, J. G. (2006). MicroRNAs direct rapid deadenylation of mRNA. *PNAS*. https://doi.org/10.1073/pnas.0510928103

Yanofsky, C. (2007). Establishing the Triplet Nature of the Genetic Code. In *Cell* (Vol. 128, Issue 5, pp. 815–818). Elsevier B.V. https://doi.org/10.1016/j.cell.2007.02.029

Yarmolinsky, M. B., & de La Haba, G. L. (1959). Inhibition by Puromycin of amino acid incorporation into protein. *PNAS*. https://doi.org/10.1073/pnas.45.12.1721

Yartseva, V., Takacs, C. M., Vejnar, C. E., Lee, M. T., & Giraldez, A. J. (2017). RESA identifies mRNA-regulatory sequences at high resolution. *Nature Methods*, *14*(2), 201–207. https://doi.org/10.1038/nmeth.4121

Yin, Y., Edelman, G. M., & Vanderklish, P. W. (2002). The brain-derived neurotrophic factor enhances synthesis of Arc in synaptoneurosomes. *PNAS*, *99*(4), 2368–2373. https://doi.org/https://doi.org/10.1073/pnas.042693699

Yisraeli, J. K., Sokol, S., & Melton, D. A. (1990). A two-step model for the localization of maternal mRNA in Xenopus oocytes: Involvement of microtubules and microfilaments in the translocation and anchoring of Vg1 mRNA. In *Development* (Vol. 108). https://doi.org/10.1242/dev.108.2.289

Yoon, Y. J., Wu, B., Buxbaum, A. R., Das, S., Tsai, A., English, B. P., Grimm, J. B., Lavis, L. D., & Singer, R. H. (2016). Glutamate-induced RNA localization and translation in neurons. *PNAS*, *113*(44), E6877–E6886. https://doi.org/10.1073/pnas.1614267113

Yoo, S., Kim, H. H., Kim, P., Donnelly, C. J., Kalinski, A. L., Vuppalanchi, D., Park, M., Lee, S. J., Merianda, T. T., Perrone-Bizzozero, N. I., & Twiss, J. L. (2013). A HuD-ZBP1 ribonucleoprotein complex localizes GAP-43 mRNA into axons through its 3′ untranslated region AU-rich regulatory element. *Journal of Neurochemistry*, *126*(6), 792–804. https://doi.org/10.1111/jnc.12266

Zappulo, A., van den Bruck, D., Ciolli Mattioli, C., Franke, V., Imami, K., McShane, E., Moreno-Estelles, M., Calviello, L., Filipchyk, A., Peguero-Sanchez, E., Müller, T., Woehler, A., Birchmeier, C., Merino, E., Rajewsky, N., Ohler, U., Mazzoni, E. O., Selbach, M., Akalin, A., & Chekulaeva, M. (2017). RNA localization is a key determinant of neurite-enriched proteome. *Nature Communications*, *8*(1). https://doi.org/10.1038/s41467-017-00690-6

Zhang, H. L., Singer, R. H., & Bassell, G. J. (1999). Neurotrophin Regulation of-Actin mRNA and Protein Localization within Growth Cones. In *The Journal of Cell Biology* (Vol. 147, Issue 1). https://doi.org/10.1083/jcb.147.1.59

Zhang, Y., Liu, L., Qiu, Q., Zhou, Q., Ding, J., Lu, Y., & Liu, P. (2021). Alternative polyadenylation: methods, mechanism, function, and role in cancer. *Journal of Experimental & Clinical Cancer Research*, *40*(1), 51. https://doi.org/10.1186/s13046-021-01852-7

Zhang, Y., Liu, L., Qiu, Q., Zhou, Q., Ding, J., Lu, Y., & Liu, P. (2021). Alternative polyadenylation: methods, mechanism, function, and role in cancer. In *Journal of Experimental and Clinical Cancer Research* (Vol. 40, Issue 1). BioMed Central Ltd. https://doi.org/10.1186/s13046-021-01852-7

Zheng, D., Ezzeddine, N., Chen, C. Y. A., Zhu, W., He, X., & Shyu, A. bin. (2008). Deadenylation is prerequisite for P-body formation and mRNA decay in mammalian cells. *Journal of Cell Biology*, *182*(1), 89–101. https://doi.org/10.1083/jcb.200801196

Zheng, J.-Q., Kelly, T. K., Chang, B., Ryazantsev, S., Rajasekaran, A. K., Martin, K. C., & Twiss, J. L. (2001). A Functional Role for Intra-Axonal Protein Synthesis during Axonal Regeneration from Adult Sensory Neurons. *The Journal of Neuroscience*. https://doi.org/10.1523/JNEUROSCI.21-23-09291.2001

Zheng, S. (2016). Alternative splicing and nonsense-mediated mRNA decay enforce neural specific gene expression. In *International Journal of Developmental Neuroscience* (Vol. 55, pp. 102–108). Elsevier Ltd. https://doi.org/10.1016/j.ijdevneu.2016.03.003

Zheng, S., Gray, E. E., Chawla, G., Porse, B. T., O'Dell, T. J., & Black, D. L. (2012). PSD-95 is post-transcriptionally repressed during early neural development by PTBP1 and PTBP2. *Nature Neuroscience*, *15*(3), 381–388. https://doi.org/10.1038/nn.3026

Zivraj, K. H., Rehbein, M., Ölschläger-Schütt, J., Schob, C., Falley, K., Buck, F., Schweizer, M., Schepis, A., Kremmer, E., Richter, D., Kreienkamp, H. J., & Kindler, S. (2013). The RNA-binding protein MARTA2 regulates dendritic targeting of MAP2 mRNAs in rat neurons. *Journal of Neurochemistry*, *124*(5), 670–684. https://doi.org/10.1111/jnc.12079

Zivraj, K. H., Tung, Y. C. L., Piper, M., Gumy, L., Fawcett, J. W., Yeo, G. S. H., & Holt, C. E. (2010). Subcellular profiling reveals distinct and developmentally regulated repertoire of growth cone mRNAs. *Journal of Neuroscience*, *30*(46), 15464–15478. https://doi.org/10.1523/JNEUROSCI.1800-10.2010

Zuko, A., Mallik, M., Thompson, R., Spaulding, E. L., Wienand, A. R., Been, M., D Tadenev, A. L., van Bakel, N., Sijlmans, C., Santos, L. A., Bussmann, J., Catinozzi, M., Das, S., Kulshrestha, D., Burgess, R. W., Ignatova, Z., & Storkebaum, E. (2021). tRNA overexpression rescues peripheral neuropathy caused by mutations in tRNA synthetase. *Science*. https://doi.org/10.1126/science.abb3356

7. Publication list and contributions

I. **Samantha Mendonsa*,** Nicolai von Kügelgen*, Sayaka Dantsuji*, Maya Ron*, Laura Breimann, Artem Baranovskii, Inga Lödige, Marieluise Kirchner, Meret Fischer, Nadja Zerna, Lucija Bujanic, Philipp Mertins, Igor Ulitsky & Marina Chekulaeva, Massively parallel identification of mRNA localization elements in primary cortical neurons, Nature Neuroscience, January 2023, https://doi.org/10.1038/s41593-022-01243-x
* These authors contributed equally

Own contribution: I designed the experiments with Marina Chekulaeva, and performed the laboratory work for mouse dissections and cell culture, shRNA depletions and library preparations, cloning, and smiFISH staining, imaging and quantification. I contributed to parts of assembly and writing of the manuscript.

II. **Samantha Mendonsa**, Nicolai von Kuegelgen, Lucija Bujanic, Marina Chekulaeva, Charcot–Marie–Tooth mutation in glycyl-tRNA synthetase stalls ribosomes in a pre-accommodation state and activates integrated stress response, Nucleic Acids Research, Volume 49, Issue 17, 27 September 2021, Pages 10007–10017, https://doi.org/10.1093/nar/gkab730

Own contribution: I designed the experiments with Marina Chekulaeva, and performed the laboratory work for cell culture, ribosome profiling, northern blotting, and western blotting. I provided feedback during manuscript writing.

8. Appendix I - Extended Data

Massively parallel identification of mRNA localization elements in primary cortical neurons

Samantha Mendonsa*, Nicolai von Kügelgen*, Sayaka Dantsuji*, Maya Ron*, Laura Breimann, Artem Baranovskii, Inga Lödige, Marieluise Kirchner, Meret Fischer, Nadja Zerna, Lucija Bujanic, Philipp Mertins, Igor Ulitsky & Marina Chekulaeva

* These authors contributed equally

This chapter was published on 16 January 2023:

Nature Neuroscience (2023)

DOI: 10.1038/s41593-022-01243-x

Link: https://doi.org/10.1038/s41593-022-01243-x

 https://doi.org/10.1038/s41593-022-01243-x

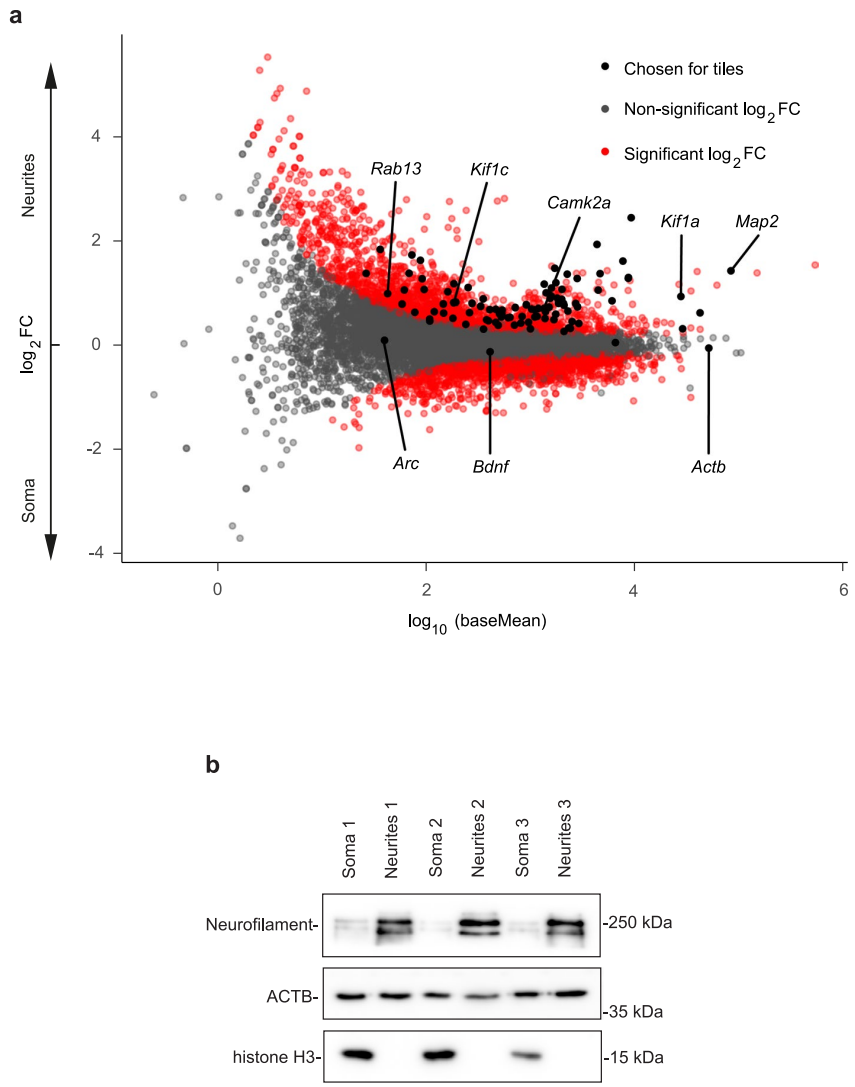

Extended Data Fig. 1 | Analysis of local transcriptome of mouse primary cortical neurons. (**a**) Mean abundance (MA) plot showing enrichment of transcripts in neurites versus soma (Y), plotted against their mean abundance (X). Transcripts are colored by significance (red: adjusted p-value < 0.05) and selection for the N-zip library (black). Selected neuronal mRNAs are labeled. (**b**) Neurites and soma of primary cortical neurons are efficiently separated with the microporous membrane. Neurons were grown on a microporous membrane so that cell bodies stay on the top and neurites grow through the pores on the lower side, as described earlier[25] (see Methods for details). Protein lysates prepared from isolated neurite and soma fractions were analyzed by western blotting with antibodies against histone H3 (soma marker) and Neurofilament (NF, neurite marker). Three independent biological replicates are shown. ACTB was used as a normalization control.

https://doi.org/10.1038/s41593-022-01243-x

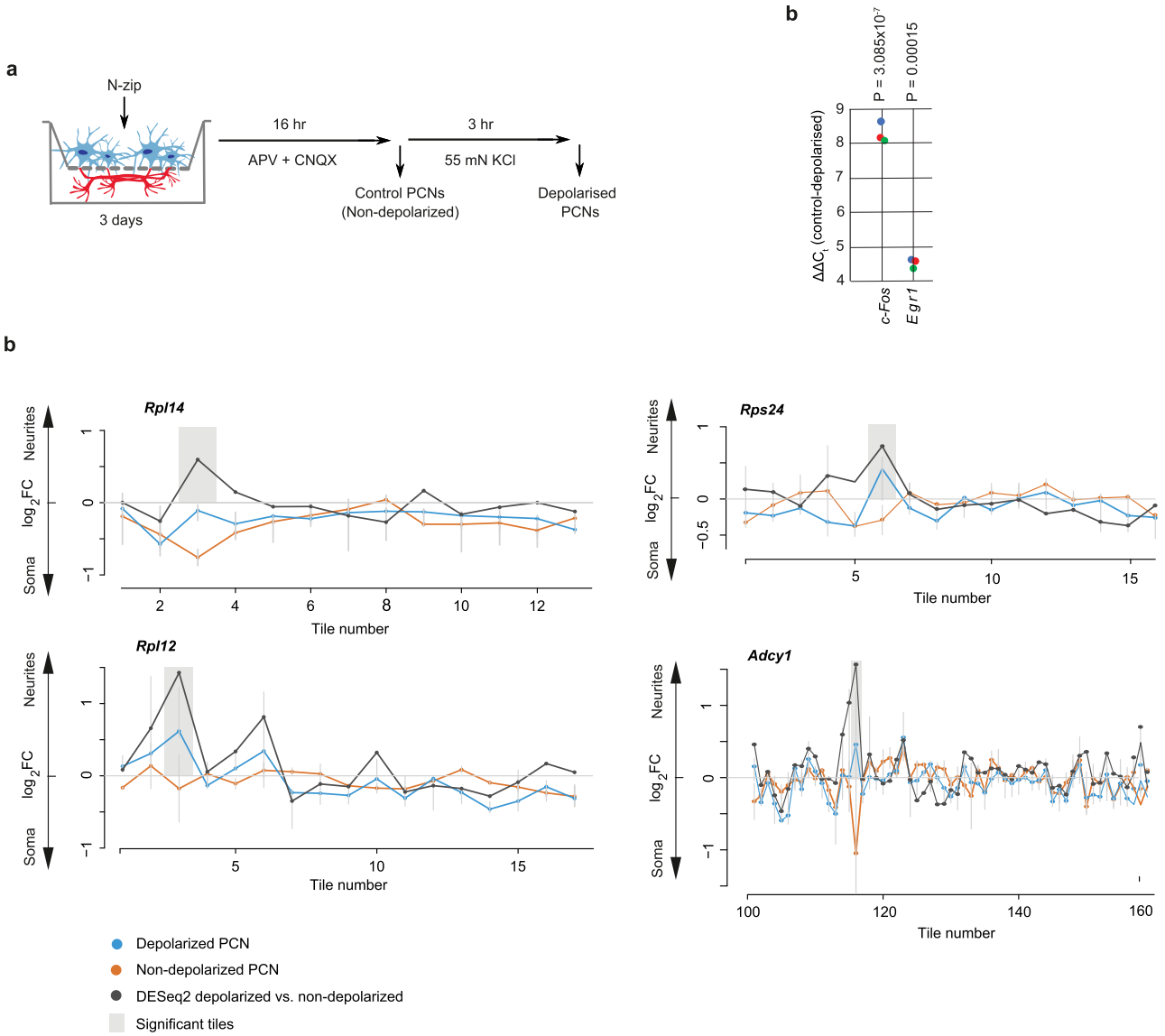

Extended Data Fig. 2 | Depolarization of primary cortical neurons regulates localization of selected 3'UTR fragments to neurites. (**a**) Scheme showing depolarization of primary cortical neurons using KCl. (**b**) RT-qPCR shows an efficient upregulation of depolarisation markers *c-Fos* and *Egr1* in primary cortical neurons upon KCl treatment. Differences in *c-Fos* and *Egr1* expression levels between depolarized and control (non-depolarized) neurons ($\Delta\Delta C_t$) are plotted on (*Y*) as individual biological triplicates (colors dots, n = 3). *Gapdh* was used for normalization. The statistical significance of differences between KCl-treated and control samples was computed by two-sided t-test, and p-values are shown on the plot. (**c**) N-zip identifies 3'UTR fragments driving mRNA localization to neurites of primary cortical neurons upon depolarization. Specific examples of identified tiled fragments that mediate localization to neurites are shown. The data are presented as in Fig. 1b. The gene names are shown above the plot. Localization in depolarized neurons (blue line) and control non-depolarized neurons (orange line) is shown. The differential localization (log_2FC neurites vs. soma) between depolarized and non-depolarized neurons was analyzed with DESeq2 (black line). Shaded in grey are tiles that show a statistically significant shift in localization to neurites upon depolarization.

 https://doi.org/10.1038/s41593-022-01243-x

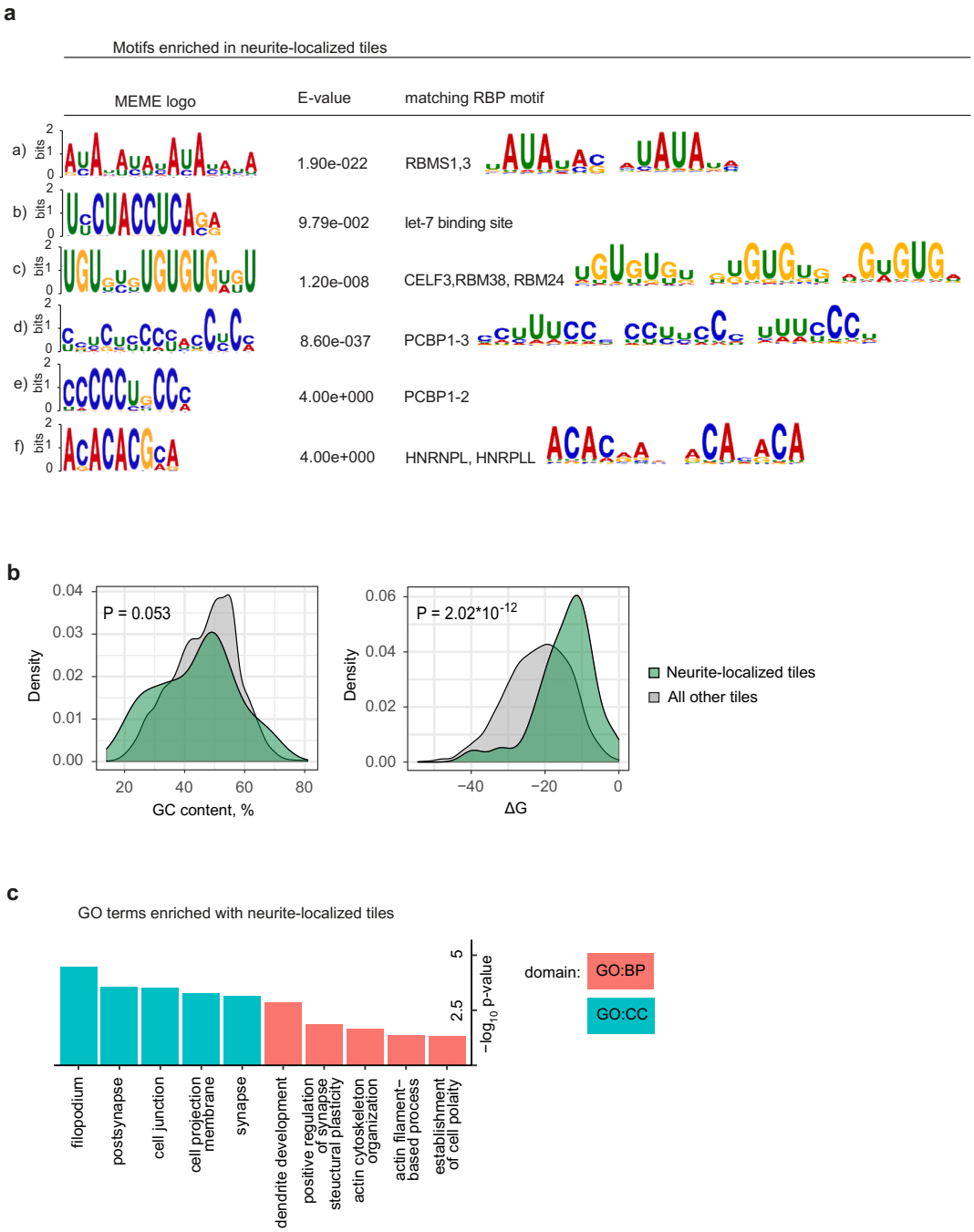

Extended Data Fig. 3 | 3'UTR fragments localized to neurites of primary cortical neurons are enriched in specific motifs and map to the genes associated with synaptic functions and structures. (**a**) Motifs enriched in neurite-localized tiles in primary cortical neurons. Motif discovery was done with XTSREME tool of the MEME suite on all neurite-localized tiles in N-zip (log_2FC neurites/soma ≥ 1, adjusted p-value < 0.1), using all fragments included in N-zip library (Supplementary Table 1) as a background. As a measure of the statistical significance, E-values computed by XTSREME[38] are provided. RBPs with matching motifs are shown. P-values were computed with DEseq2, which uses Wald test; Benjamini-Hochberg procedure was used for correction of p-values for multiple testing. (**b**) Neurite-localized tiles in N-zip have an average CG content and a low tendency to form secondary structures. Histograms showing the CG content (left) and the Gibbs free energy change (ΔG) as a measure of secondary structure formation (right) for neurite-localized tiles (green) and all tiles included in N-zip (grey). For ΔG calculation, we used RNAfold[100]. P-values were computed using two-sided Wilcoxon rank-sum test. (**c**) Transcripts with neurite-localized tiles are linked with synaptic functions, cytoskeleton and cell polarity. Gene Ontology (GO) terms overrepresentation analysis was performed on transcripts with neurite-localized tiles (log_2FC neurites/soma ≥ 1, adjusted p-value < 0.1, Supplementary Table 1), using gProfiler2 (ref. [98]). P-values were computed as in (**a**). All transcripts included in N-zip library were used as a reference. The top 5 GO terms with the lowest p-values are plotted.

https://doi.org/10.1038/s41593-022-01243-x

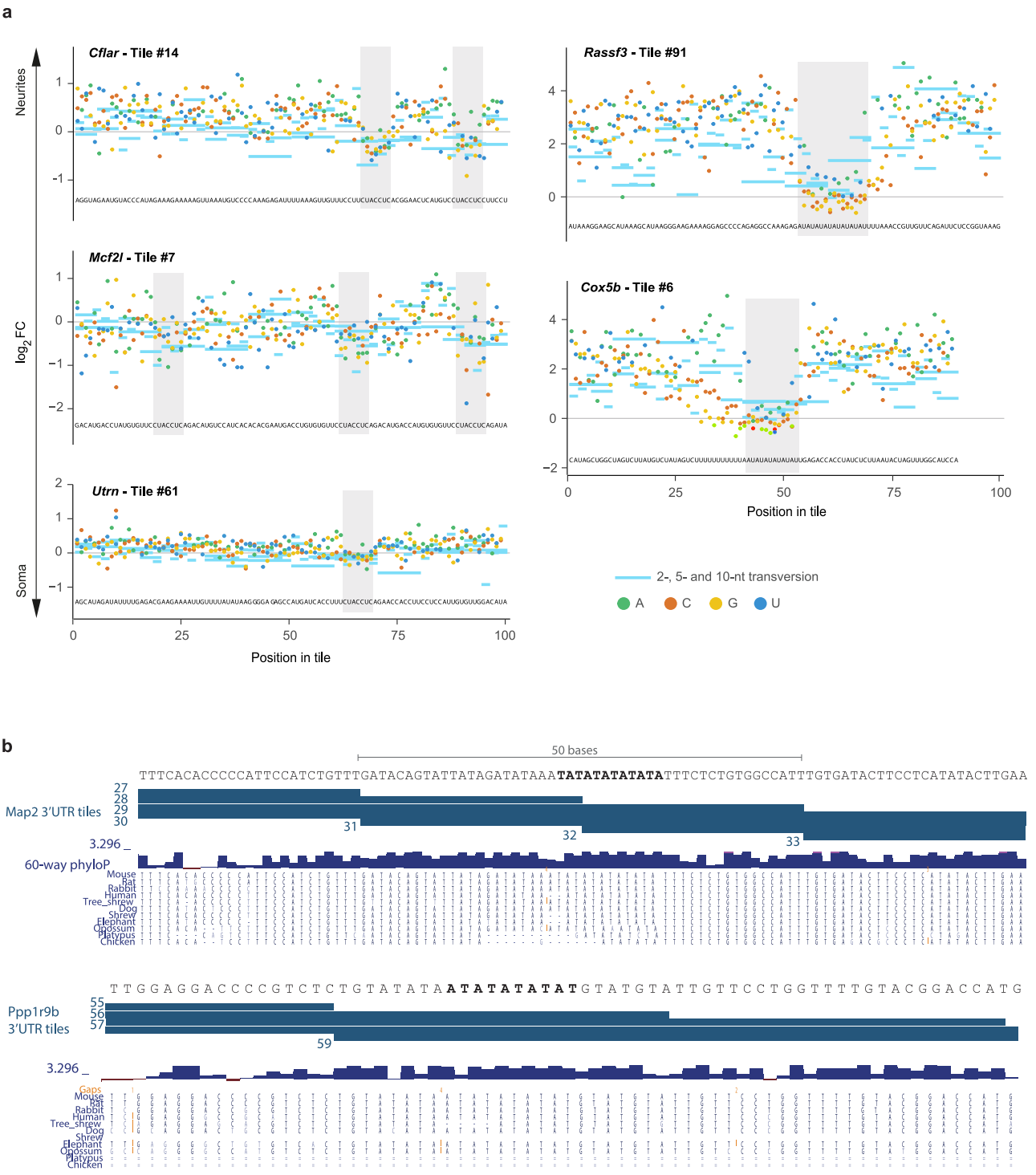

Extended Data Fig. 4 | Elements mediating RNA localization in primary cortical neurons. (**a**) N-zip combined with mutagenesis of 2-nt, 5-nt and 10-nt windows maps motifs driving mRNA localization to neurites of primary cortical neurons. Each horizontal line indicates the window that was mutagenized and the corresponding neurites/soma ratio of the mutated sequence. Within each window, we mutated G ↔ C and A ↔ U. The data are presented as in Fig. 2. The gene name and tile number are shown above the plot. (**b**) Conservation of selected $(AU)_n$ stretches across species. UCSC genome browser view of *Map2* and *Ppp1r9b* 3'UTRs with $(AU)_n$ stretches. The mouse sequence for each stretch and the positions of N-zip tiles are shown on the top. The lower track shows the PhyloP conservation scores and the sequences of the corresponding stretches from other mammals.

https://doi.org/10.1038/s41593-022-01243-x

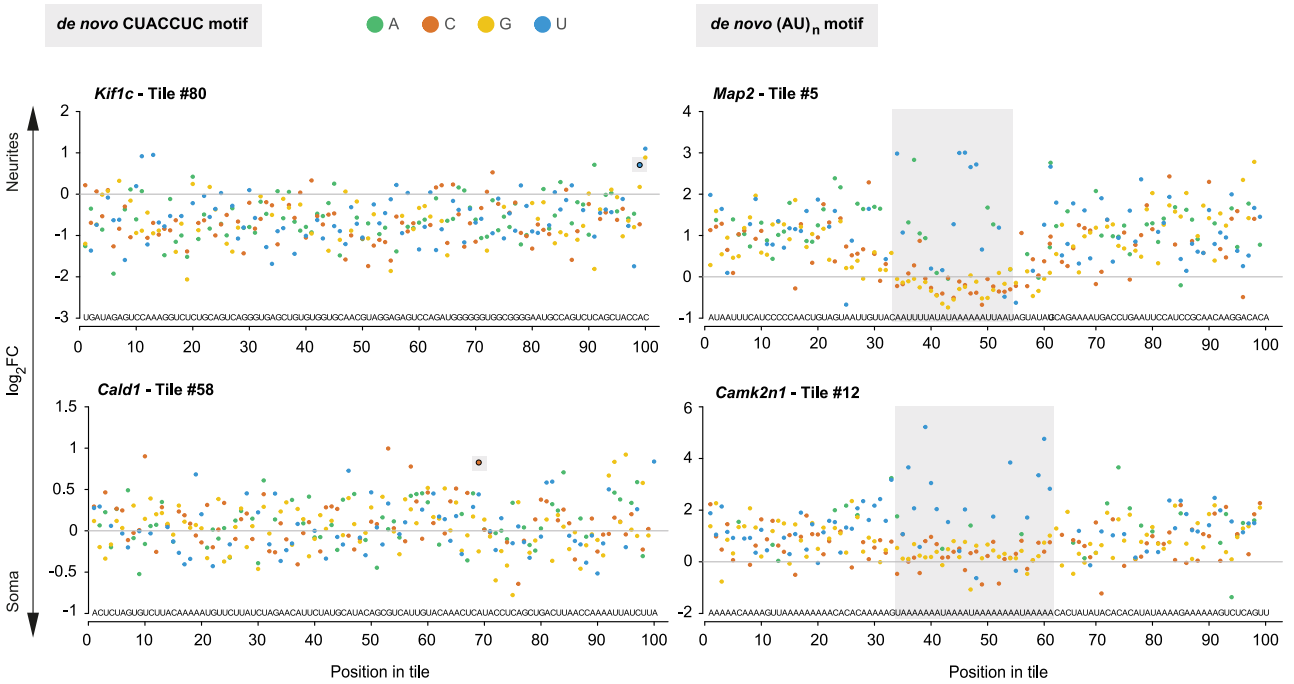

Extended Data Fig. 5 | Introduction of *de novo* identified localization motifs into heterologous context drives their localization to neurites. Specific examples of N-zip fragments where either let-7 binding site or $(AU)_n$ were introduced by chance during the mutagenesis step. The data are presented as in Fig. 2. The gene name and the number of the mutagenized tile are indicated above the plot. Neurite/soma ratios for indicated fragments with single point mutations are shown (Y), with the initial sequence of the mutagenized fragment displayed on (X) and the point mutations indicated with green (A), orange (C), yellow (G) and blue (U) dots. Shaded regions indicate fragments with significant enrichment ($P < 0.05$) in one of the subcellular compartments.

https://doi.org/10.1038/s41593-022-01243-x

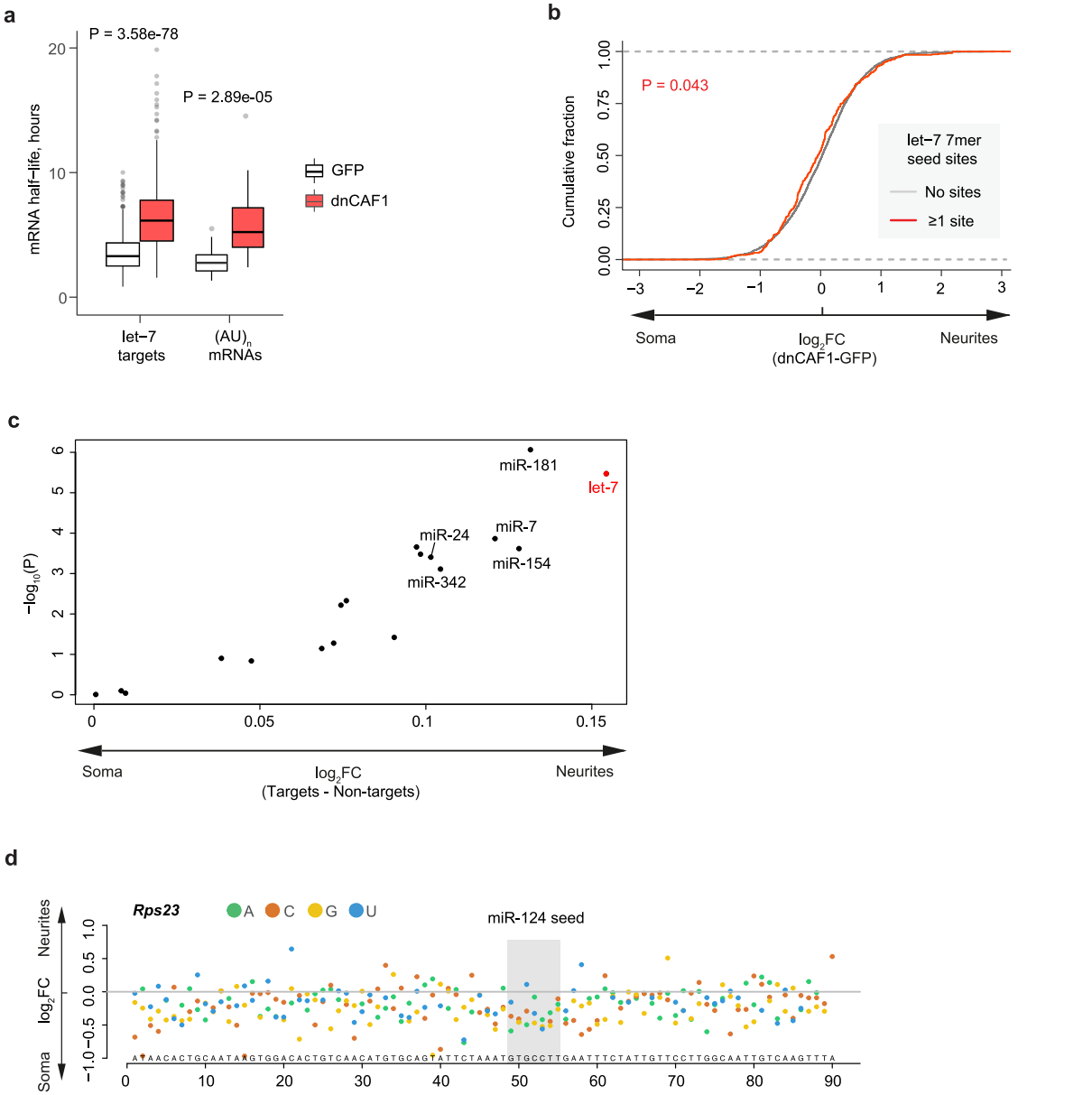

Extended Data Fig. 6 | Effects of miRNAs on mRNA localization in primary cortical neurons. (**a**) Functional depletion of CAF1 via dnCAF1 expression leads to stabilization of let-7 targets and $(AU)_{n\geq6}$-containing mRNAs. Boxplots showing the distribution of half-lives (*Y*), measured by SLAM-seq, for endogenous mRNAs bearing at least one let-7 seed site or $(AU)_{n\geq6}$ stretch in their 3'UTR. The data are shown for primary cortical neurons expressing dnCAF1 (red boxes) or GFP (white boxes, negative control). P-values were computed with two-sided Wilcoxon rank-sum test; n = 3 independent biological replicates. (**b**) mRNA stabilization with dnCAF1 shift localization of let-7 targets towards soma. CDFs showing fractions of endogenous mRNAs with (red) and without let-7 sites (grey), as measured by mRNA-seq (*Y*), plotted against changes in neurite/soma enrichment upon expression of dnCAF1. Two-sided Kolmogorov-Smirnov test was used to estimate the significance. (**c**) The difference in neurites vs. soma enrichment (log_2FC) between targets and non-targets of indicated miRNAs (X) is plotted against $-log_{10}$ of P-values (Y). The data are provided for the top 20 miRNAs expressed in primary cortical neurons, as shown in Fig. 4a. miRNAs with statistically significant enrichment in neurites (P < 0.05, computed by two-sided t-test) are labeled in red. (**d**) Mutation of miR-124 site in *Rps23* tile affects its localization. Enrichment of *Rps23* tile (log_2FC) between subcellular compartments (Y) is plotted for individual point mutants of the tile (X). The initial sequence of the mutagenized fragment is shown above X axis, and the introduced point mutations are indicated with green (A), orange (C), yellow (G) and blue (U) dots. Shaded regions indicate tiles with a significant change in enrichment (P < 0.05). $P = 4.11\times10^{-6}$ between the *Rps23* mutated tiles where the miR-124 seed was mutated and all other mutated *Rps23* tiles (two-sided Wilcoxon rank-sum test).

 https://doi.org/10.1038/s41593-022-01243-x

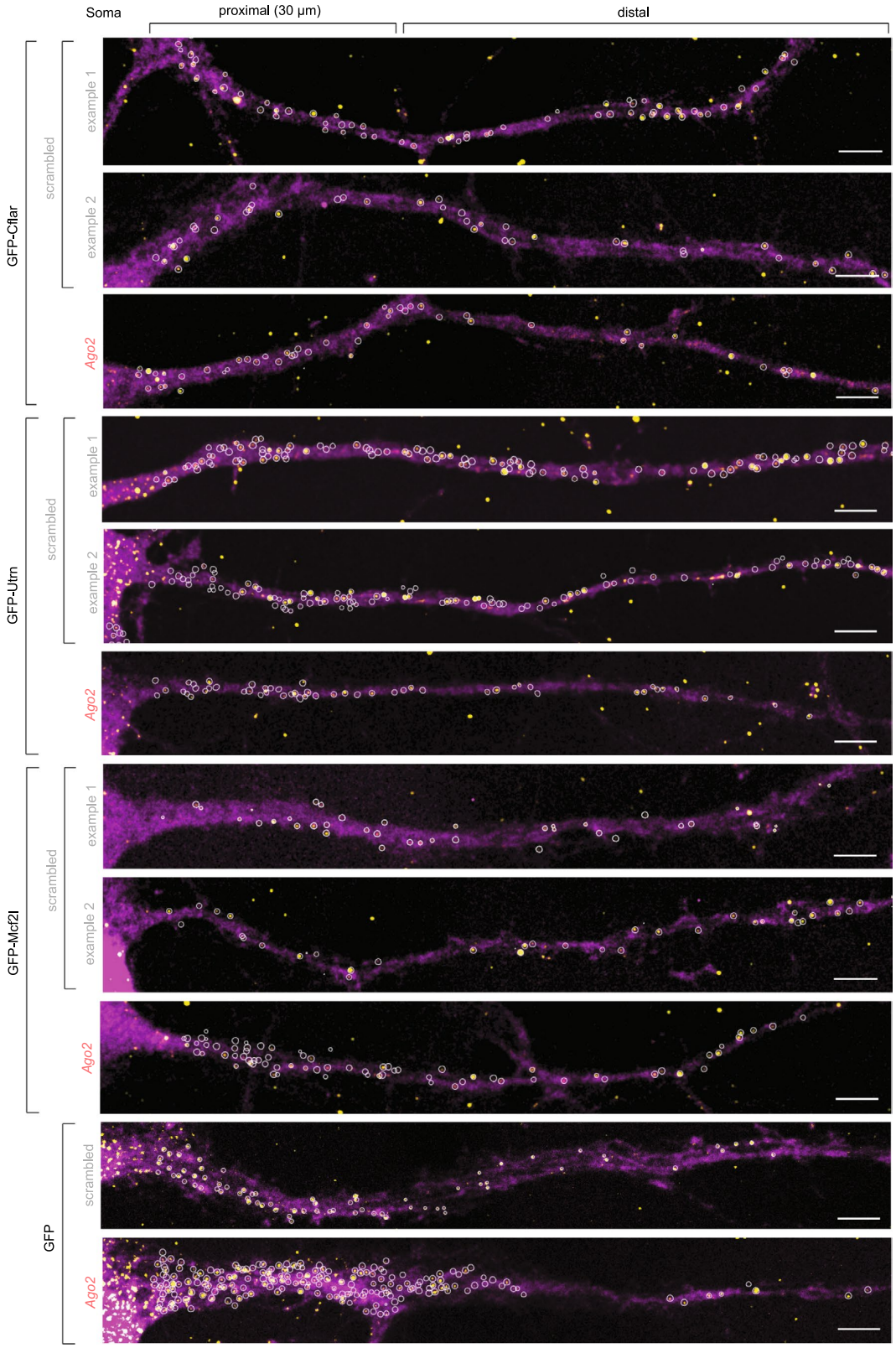

Extended Data Fig. 7 | See next page for caption.

 https://doi.org/10.1038/s41593-022-01243-x

Extended Data Fig. 7 | Additional smiFISH images of let-7 reporters in primary cortical neurons. The experimental setup and quantifications are presented in Fig. 5d. Displayed are representative smiFISH images for GFP-Mcf2l and GFP-Utrn reporters and additional to Fig. 5d examples of images showing neurons with different expression levels of GFP-Cflar (examples 1 and 2). *Gfp* RNA, yellow; GFP protein signal (serving to outline cell borders), magenta; scale bar: 5 µm. Circled (white) are fluorescent *Gfp* RNA spots detected and quantified using the RS-FISH Fiji plugin[81] (see Methods). Each neuron is treated as an independent biological replicate, with 32 to 49 neurons analyzed per each sample. For more details on the number of quantified neurons and statistical analysis of the full dataset, see Fig. 5d.

https://doi.org/10.1038/s41593-022-01243-x

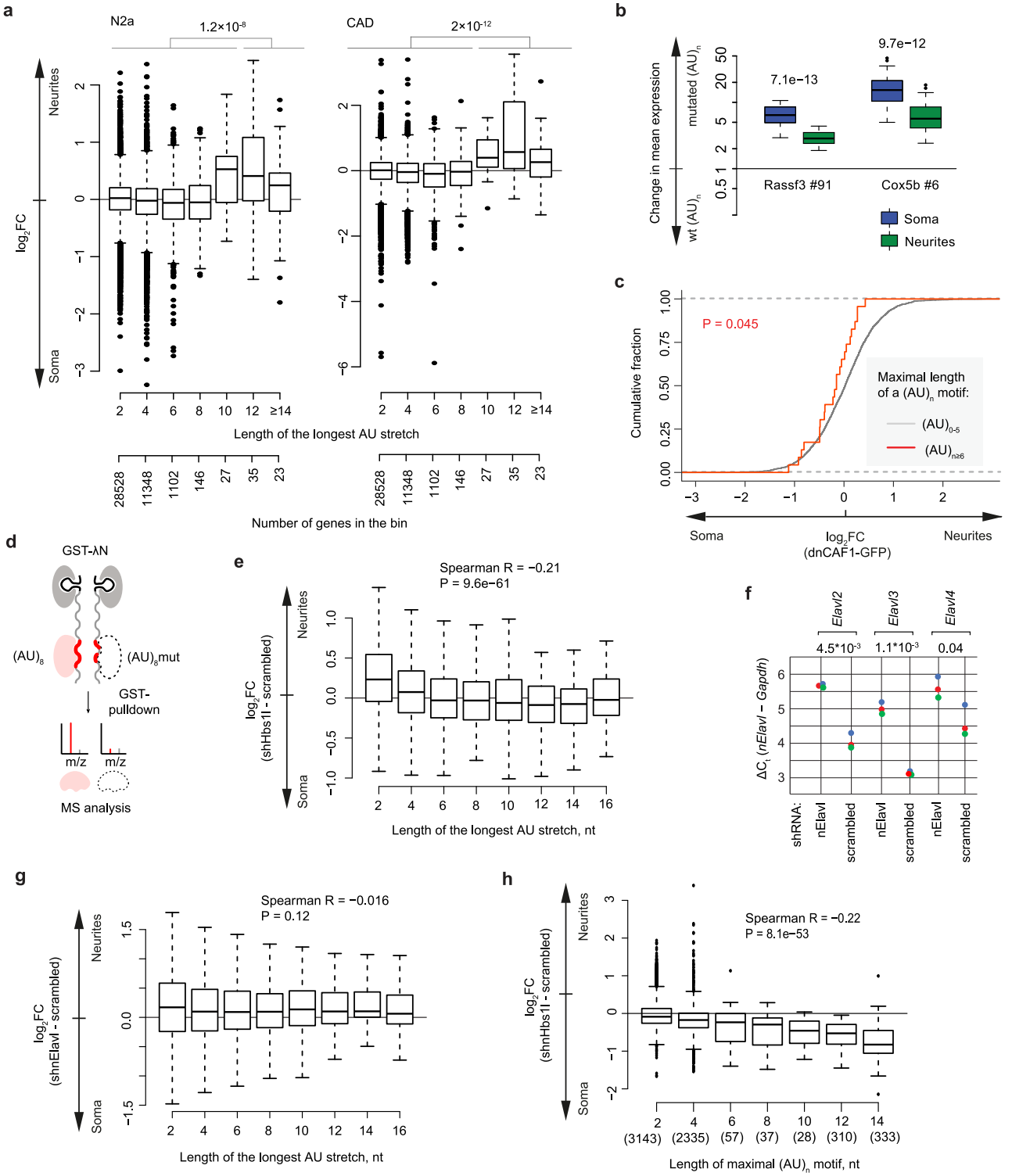

Extended Data Fig. 8 | See next page for caption.

https://doi.org/10.1038/s41593-022-01243-x

Extended Data Fig. 8 | Neurite localization of $(AU)_n$ motif is depedent of the motif length and HBS1L protein. (**a**) $(AU)_n$ motif is enriched in neurites of neuroblastoma N2a and CAD lines. Boxplot showing neurite/soma enrichment (Y) as a function of $(AU)_n$ stretch length (X) in N2a and CAD lines. P-values were computed using two-sided Wilcoxon rank-sum test; n = 3 independent biological replicates. RNA-seq data are from GSE17309838[45]. (**b**) Mutations of $(AU)_n$ motifs led to a stronger increase of N-zip mRNA reporter levels in soma. Boxplots showing changes in the normalized expression levels between tiles that contain intact $(AU)_n$ motifs (wt $(AU)_n$) and tiles in which $(AU)_n$ motifs were mutated (mutated $(AU)_n$). The data are shown separately for each tile (as indicated on X) and each subcellular compartment (green: neurite, blue: soma); n = 3 independent biological replicates. (**c**) mRNA stabilization with dnCAF1 shift localization of mRNAs with a long AU stretch towards soma. CDFs showing fractions of endogenous mRNAs with $(AU)_{0\text{-}5}$ (grey) and $(AU)_{6\text{-}8}$ stretches (red), as measured by mRNA-seq (*Y*), plotted against changes in neurite/soma enrichment upon expression of dnCAF1 (*X*). Two-sided Kolmogorov-Smirnov test was used to estimate the significance. (**d**) Scheme for GRNA chromatography in combination with mass spectrometry to identify RBPs bound to $(AU)_8$-containing RNA. The $(AU)_8$-containing *Rassf3*-91 fragment was tagged with five copies of the boxB sequence, which has a strong affinity to lambda N peptide, and the resulting $(AU)_8$-boxB and a negative control with mutated motif $(AU)_8$mut-boxB were incubated with mouse brain protein lysates. The complexes formed on $(AU)_8$-boxB and $(AU)_8$mut-boxB RNAs were then isolated using lambda N-GST fusion protein immobilized on glutathione beads. Protein binders, eluted with RNAse A, were used for further mass spectrometry. (**e**) Changes in mRNA localization upon *Hsb1l* depletion in primary cortical neurons depend on the length of $(AU)_n$ motif within mRNA 3'UTR. The data are presented as in (**a**), with changes in neurite/soma enrichment upon *Hbs1l* knockdown plotted on (*Y*). In a linear model of the ratios with the shRNA and the $(AU)_n$ motif length as variables, the interaction between the shRNA and the $(AU)_n$ was −0.019 (P = 0.00344, computed with Spearman's correlation test); n = 3 independent biological replicates. (**f**) RT-qPCR showing the efficiency of *Elavl2*, *Elavl3* and *Elavl4* depletion with shRNA in primary cortical neurons. *nElavl* expression levels for *nElavl*-depleted and control scrambled shRNA samples, normalized to *Gapdh* (ΔC_t), are plotted on (*Y*) as individual biological triplicates (colors dots, n = 3). P-values were computed by two-sided t-test and shown on the plot. (**g**) Changes in mRNA localization upon depletion of nElavl in primary cortical neurons do not correlate with the length of $(AU)_n$ motif within mRNA 3'UTR. The data are analyzed and presented as in (**e**); n = 3 independent biological replicates. The interaction in a linear model between the shRNA and the length of the $(AU)_n$ motif is not significant (P = 0.8). (**h**) Depletion of *Hbs1l* in primary cortical neurons shifts $(AU)_n$-containing N-zip reporters towards soma. Boxplots showing changes in neurite/soma enrichment between *Hbs1l*-depleted and control scrambled samples (Y) as a function of the maximal length of the $(AU)_n$ stretch length in the tiles of N-zip mRNA library (X). The number of genes in the bin is shown in parentheses; n = 3 independent biological replicates. Spearman's correlation coefficient and P-value are shown. In a linear model of the ratios with the shRNA and the $(AU)_n$ motif length as variables, the interaction between the shRNA and the $(AU)_n$ was -0.07 ($P < 10^{-16}$).

https://doi.org/10.1038/s41593-022-01243-x

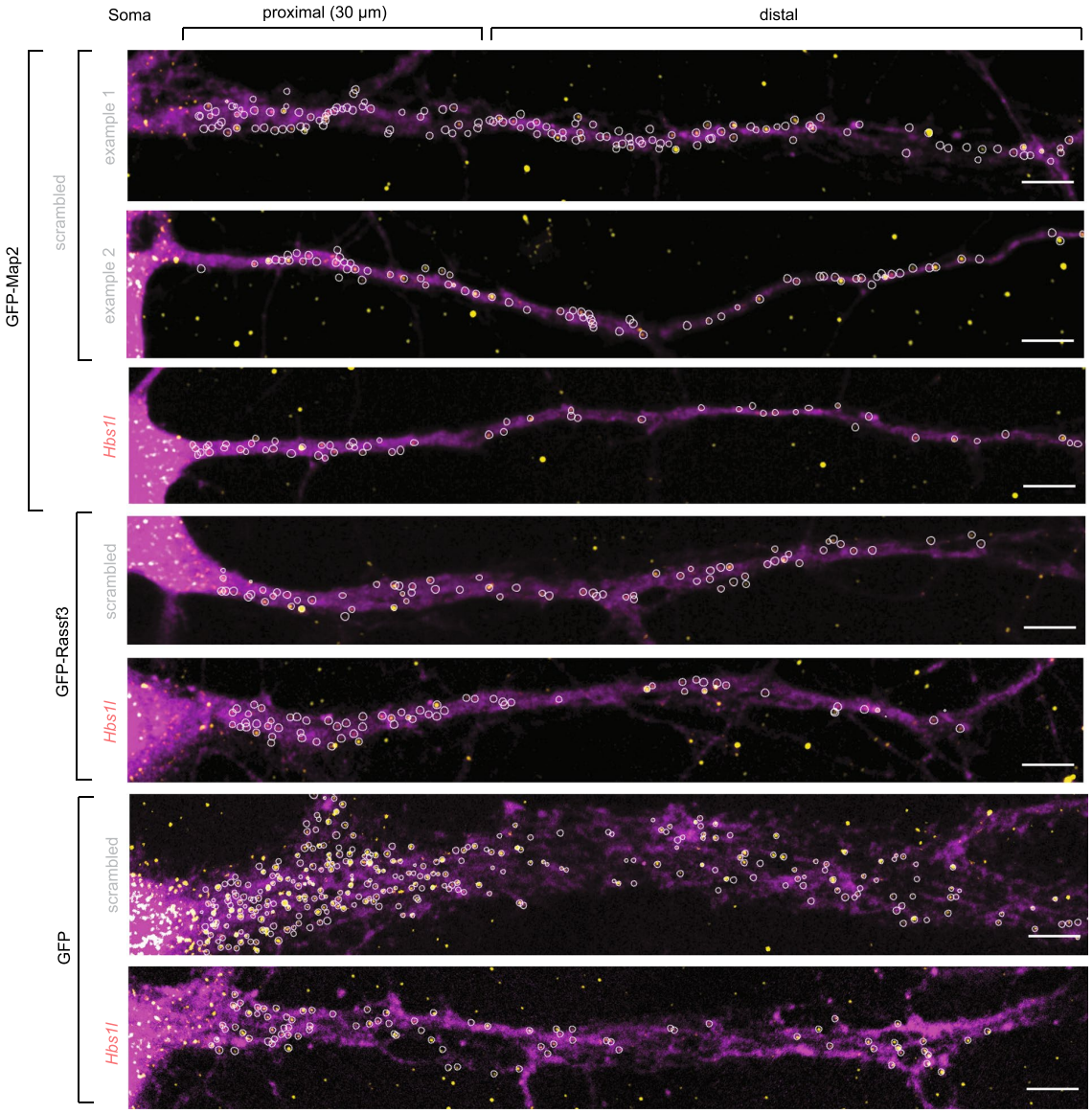

Extended Data Fig. 9 | Additional smiFISH images of $(AU)_n$ reporters in primary cortical neurons. The experimental setup and quantifications are presented in Fig. 7d. Displayed are representative smiFISH images for GFP-Rassf3 reporter and additional to Fig. 7d examples of images showing neurons with different expression levels of GFP-Map2 (examples 1 and 2). *Gfp* RNA, yellow; GFP protein signal (serving to outline cell borders), magenta; scale bar: 5 µm. Circled (white) are fluorescent *Gfp* RNA spots detected and quantified using the RS-FISH Fiji plugin[81] (see Methods). Each neuron is treated as an independent biological replicate, with 33 to 49 neurons analyzed per each sample. For more details on the number of quantified neurons and statistical analysis of the full dataset, see Fig. 7d.

https://doi.org/10.1038/s41593-022-01243-x

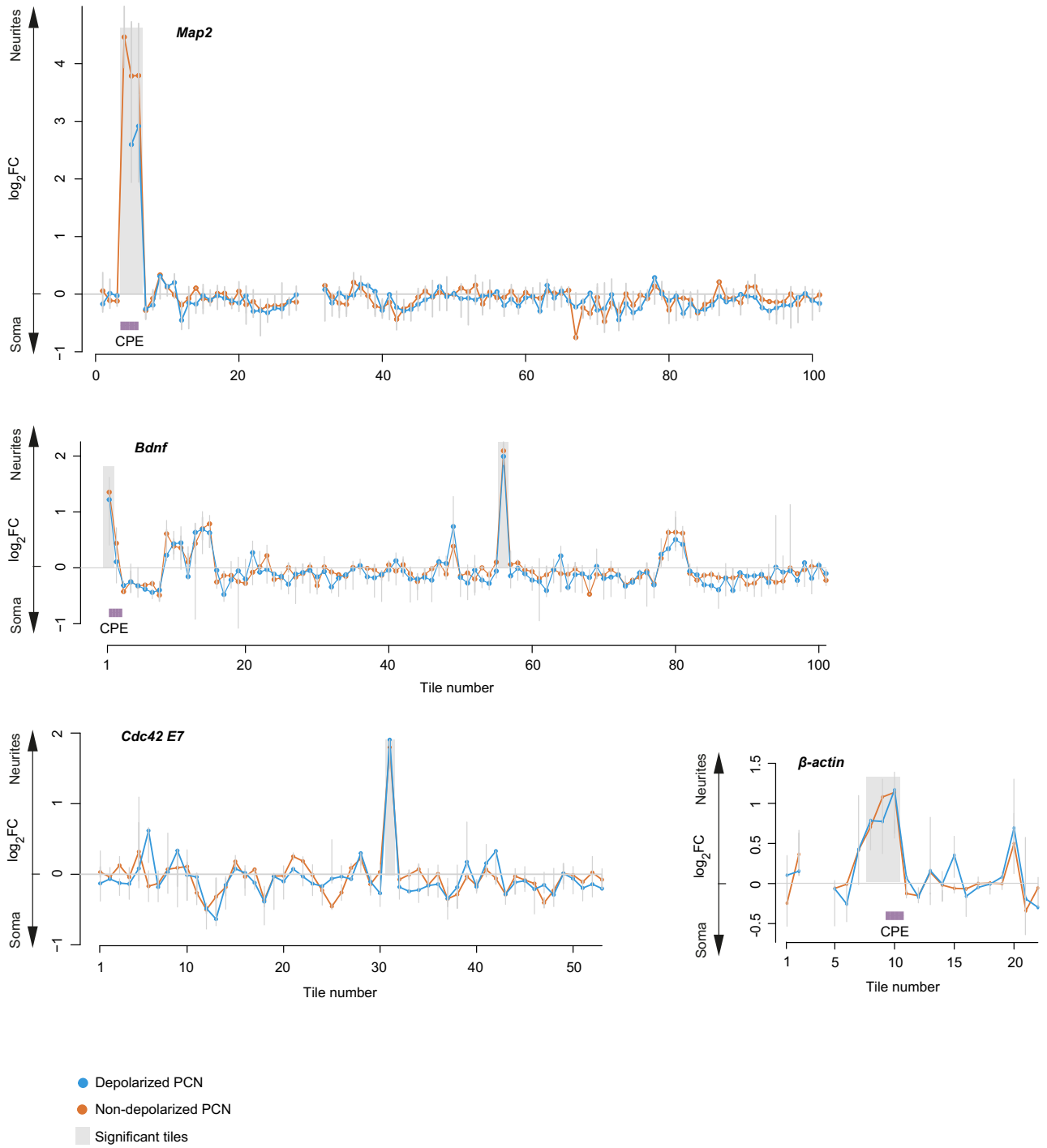

Extended Data Fig. 10 | N-zip identifies and refines known zipcodes in primary cortical neurons. Specific examples of identified tiled fragments that mediate localization to neurites. Enrichment of a given tile (log_2-transformed fold change) between subcellular compartments (*Y*) is plotted against tiled fragment number (*X*). Average neurite/soma ratios for depolarized (blue) and non-depolarized neurons (orange) are plotted. Error bars represent the lowest and the highest measurement for each tile. Shaded regions indicate tiles with significant enrichment ($P < 0.05$) in neurites by more than 2-fold. P-values were computed with DESeq2 two-sided Wald test. In the case of adjacent tiles with significant enrichment, the neighboring tiles with lower than 2-fold enrichment are also shaded. CPE is defined as a stretch of 6 bases including 5 Us. The gene name is shown above each plot.

9. Appendix II - Supplementary Data

Charcot–Marie–Tooth mutation in glycyl-tRNA synthetase stalls ribosomes in a pre-accommodation state and activates integrated stress response

Samantha Mendonsa, Nicolai von Kuegelgen, Lucija Bujanic, Marina Chekulaeva

This chapter was published on 17 August 2021:
Nucleic Acids Research (2021)
DOI: 10.1093/nar/gkab730
Link: https://doi.org/10.1093/nar/gkab730

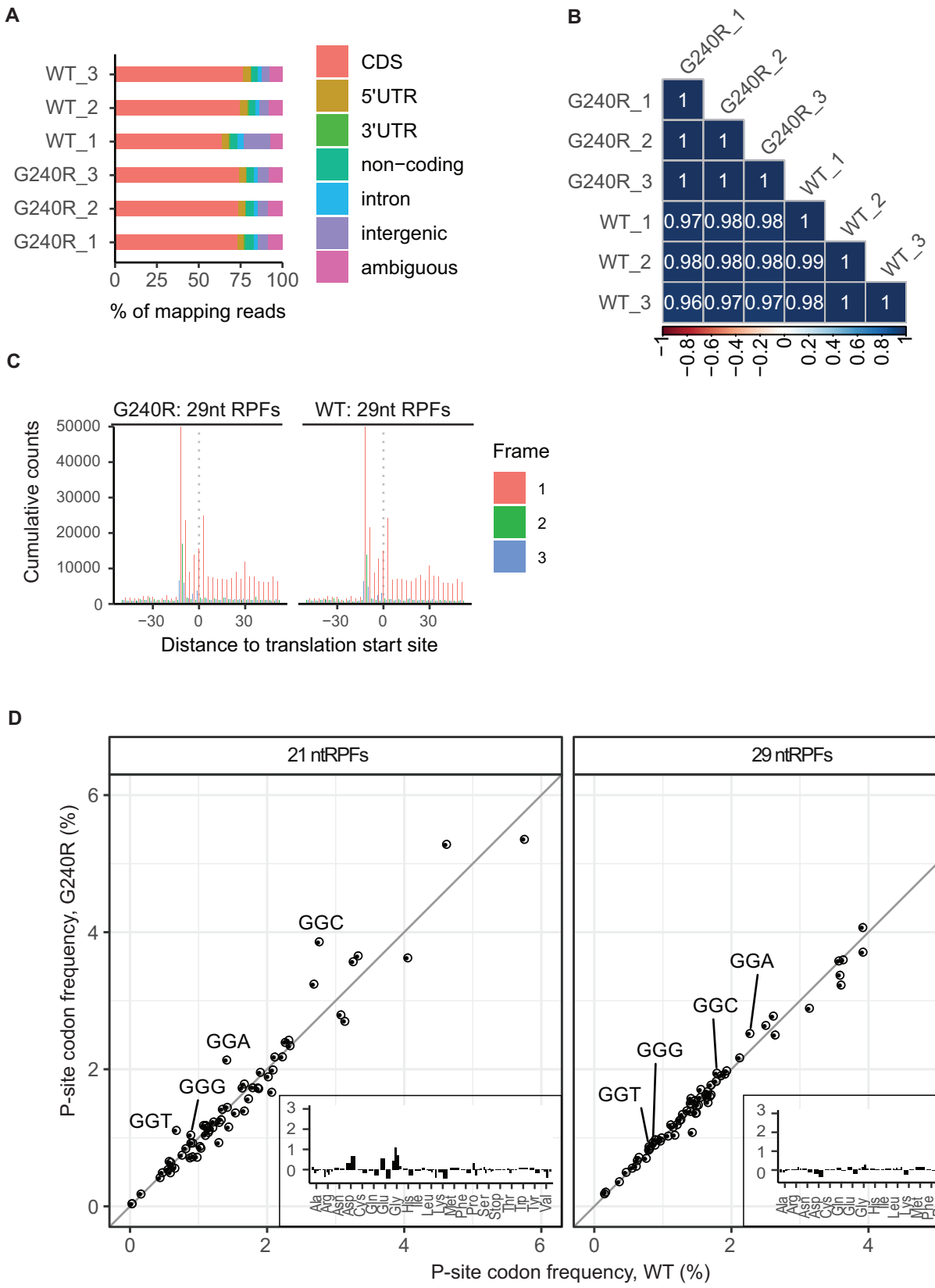

Figure S1. Ribosome profiling of HEK293T cells expressing G240R mutant and WT GARS. (**A**) Bar plot depicting mapping statistics of ribosome profling reads. Most reads map to CDS, as expected from reads derived from translated mRNAs. (**B**) Correlation heatmap of individual ribosome profiling libraries: high correlation is observed between the replicates. The numbers represent Pearson correlation coefficients (reads/gene in CDS). (**C**) Metagene plots showing the percentage of 29-nt ribosome footprints from annotated start codon. (**D**) Scatter plots comparing frequencies of 64 codons in the ribosomal P-site between cells expressing WT (X) and G240R-GARS (Y), for 21 nt (left) and 29 nt (right) RPFs. Ribosome frequencies represent the means of triplicates. Glycine codons are labelled. Insets show differences between codon frequencies in G240R and WT samples as bar plots.

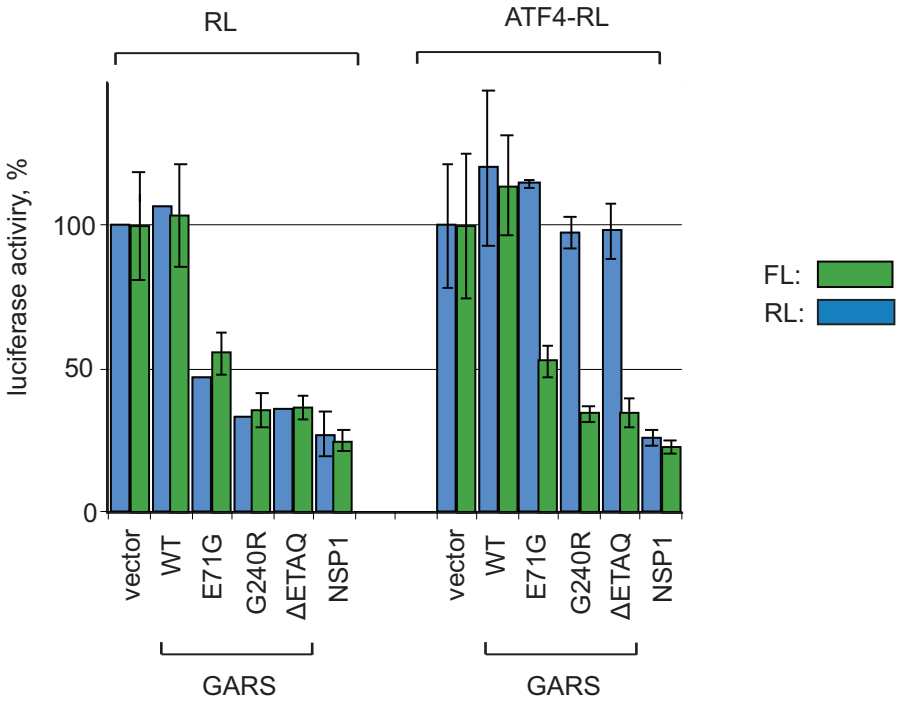

Figure S2. Overexpression of CMT-GARS mutants upregulates ATF4 reporter. The experiment was performed as described in **Figure 3C**, but data are shown separately for RL and FL reporters. In short, HEK293T cells were co-transfected with plasmids encoding one of the Renilla luciferase reporters (blue: RL, ATF4-RL), FL (green), and myc-tagged GARS, either WT or indicated mutant. As additional controls, empty vector and NSP1-encoding plasmids were used instead of GARS plasmid. RL and FL activities are presented as a percentage of luciferase activity produced in the presence of an empty vector. Values represent means +/- SD from 3 experiments.

“Somewhere, something incredible is waiting to be known.”

Carl Sagan